CAF-1 p150 AND Ki-67 REGULATE NUCLEAR STRUCTURE THROUGHOUT THE HUMAN CELL CYCLE

A Dissertation Presented

By

Timothy D. Matheson

Submitted to the Faculty of the
University of Massachusetts Graduate School of Biomedical Sciences, Worcester
in partial fulfillment of the requirements for the degree of

DOCTOR OF PHILOSOPHY

January 9, 2017

Interdisciplinary Graduate Program

CAF-1 p150 AND Ki-67 REGULATE NUCLEAR STRUCTURE THROUGHOUT THE HUMAN CELL CYCLE

A Dissertation Presented
By

Timothy D. Matheson

Dissertation Defense Committee GSBS Members

Job Dekker
Systems Biology

Anthony Imbalzano
Cell and Developmental Biology

Thoru Pederson
Biochemistry and Molecular Pharmacology

Chair of the Dissertation Committee

Thomas Fazzio
Molecular, Cell and Cancer Biology

External Dissertation Committee Member

Michael Blower
Associate Professor, Massachusetts General Hospital

Thesis Advisor

Paul Kaufman
Molecular, Cell and Cancer Biology

Student Program

Interdisciplinary Graduate Program

January 9, 2017

ACKNOWLEDGMENTS

This work would not have been possible without the guidance of my mentor, Dr. Paul Kaufman. Paul's passion for science, ability to give constructive criticism, consistent open-door communication policy, and kind words during tough times allowed me to excel during my graduate career. I would also like to thank the members of my Thesis Research Advisory Committee: Dr. Job Dekker, Dr. Tony Imbalzano, Dr. Thoru Pederson, and Dr. Tom Fazzio. I met individually with each member of my TRAC many times during my graduate career, and their sage counsel and scientific insights were invaluable in my development as a scientist. I would especially like to recognize the chairman of my committee, Dr. Tom Fazzio. My first laboratory rotation in graduate school was in Tom's lab, and Tom was the first to teach me valuable tissue culture skills that would serve me well for the next seven years.

I would also like to thank all past and present members of the Kaufman lab: Dr. Jessica Lopes Da Rosa-Spiegler, Dr. Ahmed Fazly, Dr. Vineeta Bajaj, Dr. Dan Trombly, Dr. Ana Vertii, Dr. Yuichi Ichikawa, Xiaoming Sun, and Aizhan Bizhanova, and Dr. Corey Smith. I would especially like acknowledge Corey for spending countless hours instructing me on the finer molecular biology and cell culture techniques.

Next, I would like to acknowledge everyone who has helped me with technical experimental issues. This includes members of the Lawrence lab, including Dr. Jeanne Lawrence, Dr. Lisa Hall, Dr. Eric Swanson, Dr. Kevin

Creamer, Meg Byron, and Laurie Lizotte, for their help with FISH and IF experiments. I would also like to thank Dr. Judith Sharp for her expertise in fluorescent molecular biology and cell culture, and Dr. Michael Brodsky for the seemingly never-ending use of his Zeiss Axioplan2 fluorescent microscope. Finally, I would like to thank members of the Fazzio lab, including Dr. Andrew Coles, Dr. Sarah Hainer, Lysha Ee, Kurtis McCannell, and Diwash Acharya for their expertise in CRISPR, deep sequencing, RNAi depletion reagent synthesis, and anything else that I am forgetting.

In addition to tremendous support within the UMassMed community, I received a lot of help from my friends and family. In particular, I would like to recognize the amazing, life-long friends that I have made since moving to Massachusetts (in no particular order): Dr. Glen Gallagher, Matt Rosene, Dave Sokolowski, Dan “BOD” Virgil, Dr. Eric Swanson, Dr. Belinda Barbagallo, Dr. Paul Nobrega, Noah Cohen, Kenny Lloyd, Dr. Brendan Hilbert, Mellissa Fulham, Livio Dukaj, Dr. Joseph Yawe, Dr. Djade Soumana, Dr. Caroline Duffey, Dr. Tyler Doughty, Derek and Sarah Lusso, Rhonda and Matthias McFleder, and Nate Gioacchini. There are many other friends, but this section is already a going longer than I planned. I’d also like to thank my parents, Michele and David Matheson, and my brother, Danny Matheson, for their unwavering love and support in everything I have ever done. Finally, I’d like to thank my wife and partner, Dr. Erin Habecker. Erin, your unshaking belief in my ability to succeed is the reason why I am the person that I am today.

ABSTRACT

The three-dimensional organization of the human genome is non-random in interphase cells. Heterochromatin is highly clustered at the nuclear periphery, adjacent to nucleoli, and near centromeres. These localizations are reshuffled during mitosis when the chromosomes are condensed, nucleoli disassembled, and the nuclear envelope broken down. After cytokinesis, heterochromatin is re-localized to the domains described above. However, the mechanisms by which this localization is coordinated are not well understood. This dissertation will present evidence showing that both CAF-1 p150 and Ki-67 regulate nuclear structure throughout the human cell cycle.

Chromatin Assembly Factor 1 (CAF-1) is a highly conserved three-subunit protein complex which deposits histones $(H3/H4)_2$ heterotetramers onto replicating DNA during S-phase of the cell cycle. The N-terminal domain of the largest subunit of CAF-1 (p150N) is dispensable for histone deposition, and instead regulates the localization of specific loci (Nucleolar-Associated Domains, or “NADs”) and several proteins to the nucleolus during interphase. One of the proteins regulated by p150N is Ki-67, a protein widely used as a clinical marker of cellular proliferation. Depletion of Ki-67 decreases the association of NADs to the nucleolus in a manner similar to that of p150. Ki-67 is also a fundamental component of the perichromosomal layer (PCL), a sheath of proteins that surrounds all condensed chromosomes during mitosis. A subset of p150 localizes to the PCL during mitosis, and depletion of p150 disrupts Ki-67

localization to the PCL. This activity was mapped to the Sumoylation Interacting Motif (SIM) within p150N, which is also required for the localization of NADs and Ki-67 to the nucleolus during interphase. Together, these studies indicate that p150N coordinates the three-dimensional arrangement of both interphase and mitotic chromosomes via Ki-67

TABLE OF CONTENTS

ACKNOWLEDGMENTS IV
ABSTRACT VI
TABLE OF CONTENTS VIII
LIST OF FIGURES XII
LIST OF TABLES XIV
LIST OF COPYRIGHTED MATERIALS XV
LIST OF ABBREVIATIONS USED COMMONLY IN THIS WORK XVI

CHAPTER I: INTRODUCTION 1

1.1: ABSTRACT 1

1.2: CHROMATIN ASSEMBLY FACTOR 1 (CAF-1) 2

1.2.1: CAF-1 STRUCTURE 3
1.2.2: CAF-1 COUPLES CHROMATIN ASSEMBLY WITH DNA REPLICATION AND REPAIR 4
1.2.3: CAF-1 REGULATES THE ESTABLISHMENT AND MAINTENANCE OF HETEROCHROMATIN 6
1.2.4: CAF-1 REGULATES CHROMATIN STRUCTURE EARLY IN DEVELOPMENT 8
1.2.5: CLINICAL USES OF CAF-1 9

1.3: THE NUCLEOLUS 10

1.4: ORGANIZATION OF THE GENOME VIA ASSOCIATION WITH SPECIFIC SUB-NUCLEAR REGIONS 11

1.4.1: LAMINA-ASSOCIATED DOMAINS (LADS) 11
1.4.2: NUCLEOLAR ASSOCIATED DOMAINS (NADS) 13
1.4.3: THE PERINUCLEOLAR COMPARTMENT (PNC) OF CANCER CELLS 15

1.5: NAD FUNCTION: PN LOCALIZATION LINKED TO HETEROCHROMATIN SILENCING 16

1.5.1: THE INACTIVE X CHROMOSOME 16
1.5.2: THE 5S RDNA 17
TABLE 1.1: SUMMARY OF KNOWN PERINUCLEOLAR REGION REGULATORS 20
1.6: PROTEIN REGULATORS OF PN STRUCTURE AND FUNCTION 22

1.6.1: CTCF 22
1.6.2: THE NUCLEOPHOSMIN HOMOLOG NLP AND THE NUCLEOLIN HOMOLOG MODULO 23
1.6.3: KI-67 24

1.7: LNCRNAS AS REGULATORS OF PN STRUCTURE AND FUNCTION 26

1.7.1: *KCNQ1OT1* 26
1.7.2: *FIRRE* 27

1.8: CONCLUDING REMARKS 28

1.8.1: WHAT DEFINES THE NADS? 28
1.8.2: WHAT IS THE FUNCTIONAL SIGNIFICANCE OF NADS? 32
VIDEOS 1.1 AND 1.2 THREE-DIMENSIONAL RENDERING OF HELA S3 NUCLEUS WITH AND WITHOUT CAF-1 P150 DEPLETION. 35

CHAPTER II: A SEPARABLE DOMAIN OF THE P150 SUBUNIT OF HUMAN CHROMATIN ASSEMBLY FACTOR-1 PROMOTES PROTEIN AND CHROMOSOME ASSOCIATIONS WITH NUCLEOLI 36

2.1: ABSTRACT 36

2.2: INTRODUCTION 37

2.3: RESULTS 39

2.3.1: P150 INTERACTS WITH NUCLEOLAR PROTEINS 39
2.3.2: P150 INTERACTS WITH NUCLEOLAR DNA 45
2.3.3: P150 REGULATES NUCLEOLAR PROTEIN LOCALIZATION 50
2.3.4: AN N-TERMINAL P150 DOMAIN INCAPABLE OF CAF-1 COMPLEX FORMATION IS SUFFICIENT FOR NORMAL NUCLEOLAR PROTEIN LOCALIZATION. 54
2.3.5: THE P150 N-TERMINUS PROMOTES INTERCHROMOSOMAL INTERACTIONS OF THE 47S RRNA-ENCODING REPEATS. 78

2.4: DISCUSSION 87

2.4.1: A SEPARABLE FUNCTIONAL DOMAIN WITHIN THE CAF-1 P150 N-TERMINUS 87
2.4.2: THE SIM DOMAIN LINKS HUMAN P150N TO NUCLEOLAR STRUCTURES. 88
2.4.3: HIGHER-ORDER INTERACTIONS OF NUCLEOLAR CHROMATIN 95

2.5: MATERIALS AND METHODS 96

2.5.1: PREPARATION OF NUCLEAR EXTRACTS AND AFFINITY CHROMATOGRAPHY FOR MASS SPECTROSCOPY SAMPLES. 96
2.5.2: MASS SPECTROSCOPY 98
2.5.3: SHRNAS 99
2.5.4: P150 DERIVATIVES AND OTHER TRANSGENES 100
2.5.5: ESIRNA METHODS 100
2.5.6: CELL CULTURE METHODS 102
2.5.7: GROWTH ANALYSES 104
2.5.8: ANTIBODIES 104

2.5.9: Immunofluorescence 106
2.5.10: Chromatin immunoprecipitations (ChIP) 107
2.5.11: Visualization of 5-EU-labeled nascent RNA 109
2.5.12: Immuno-FISH and DNA-FISH Experiments 110

CHAPTER III: CAF-1 P150 REGULATES KI-67 LOCALIZATION THROUGHOUT THE CELL CYCLE 113

3.1: Abstract 113

3.2: Introduction 113

3.3: Results 116

3.3.1: Ki-67 regulates alpha satellite localization to the perinucleolar region 116
3.3.2 A subset of p150 co-localizes with Ki-67 foci during mitosis and early G1 phases 121
3.3.3: p150 regulates Ki-67 accumulation on the Perichromosomal Layer 133
3.3.4: p150 regulates the formation of Ki-67 foci in early G1 phase 138
3.3.5: The SIM within the N-terminus of p150 is required for Ki-67 localization to the PCL 141

3.4: Discussion 145

3.5: Materials and Methods 149

3.5.1: Cell culture 149
3.5.2: Depletion Reagents 150
3.5.3: Immunofluorescence and Immuno-FISH 153
3.5.4: Nuclease Digestion 157
3.5.5: Western blotting 158

CHAPTER IV: UTILIZATION OF CRISPR/CAS9 GENE EDITING TECHNOLOGY TO GENERATE CELL LINES EXPRESSING ENDOGENOUS, EPITOPE-TAGGED KI-67 FOR FUTURE STUDIES 159

4.1: Abstract 159

4.2: Introduction 160

4.3: Results 166

4.3.1: Design of repair template 166
4.3.2: Isolation and confirmation of homozygous insert clones 170
4.3.3: Immunoprecipitation of Ki-67 using the V5 epitope 176
4.4: Discussion 179

4.5: Materials and Methods 181

4.5.1: CRISPR/CAS9 DESIGN AND REAGENTS 181
4.5.1: CELL CULTURE 183
4.5.2: IMMUNOFLUORESCENCE AND MICROSCOPY 184
4.5.3: ISOLATION OF GENOMIC DNA AND PCR 185
4.6.3: IMMUNOPRECIPITATION 186

CHAPTER V: DISCUSSION 189

5.1: SCIENTIFIC QUESTIONS ADDRESSED BY THIS DISSERTATION 189

5.2: SUMMARY OF MAJOR RESULTS AND CONCLUSIONS 190

5.2.1: P150 REGULATES THE LOCALIZATION OF SOME NADS 190
5.2.2: THE SIM WITHIN P150N REGULATES NAD LOCALIZATION 193
5.2.3: KI-67 REGULATES NAD LOCALIZATION 195
5.2.4: P150 LOCALIZES TO DISTINCT KI-67 FOCI DURING EARLY G1 OF THE CELL CYCLE 197
5.2.5: P150 LOCALIZES TO THE PCL 199
5.2.6: P150 REGULATES THE FORMATION OF KI-67 FOCI IN EARLY G1 OF THE CELL CYCLE 201
5.2.7: P150 REGULATES KI-67 LOCALIZATION TO THE PCL DURING MITOSIS 203
5.2.8: THE SIM WITHIN P150N IS REQUIRED FOR NORMAL KI-67 LOCALIZATION TO THE PCL 204

5.3: FUTURE DIRECTIONS 205

5.3.1: FURTHER INVESTIGATION INTO NAD STRUCTURE AND FUNCTION 205
5.3.2: WHEN DOES P150 REGULATE KI-67 LOCALIZATION DURING THE CELL CYCLE? 208

5.4: CONCLUDING REMARKS 211

BIBLIOGRAPHY 213

LIST OF FIGURES

FIGURE 1.1: SCHEMATIC OF LNCRNAS FACILITATING TRANS-CHROMOSOMAL INTERACTIONS IN MOUSE. 30

FIGURE 2.1: NUCLEOLAR ASSOCIATIONS OF HUMAN P150. 41

FIGURE 2.2: ADDITIONAL CHARACTERIZATION OF P150 DEPLETION. 48

FIGURE 2.3: P150 DEPLETION DISRUPTS LOCALIZATION OF MULTIPLE NUCLEOLAR PROTEINS. ..52

FIGURE 2.4: P150 DEPLETION ALTERS NUCLEOLAR PROTEIN LOCALIZATION IN HT1080 CELLS. ..58

FIGURE 2.5: DOMAIN ANALYSIS OF HUMAN P150. 60

FIGURE 2.6: THE P150 SUMO-INTERACTION MOTIF (SIM) IS REQUIRED TO MAINTAIN NUCLEOLAR KI67 LOCALIZATION. 62

FIGURE 2.7: THE P150 SIM IS REQUIRED TO MAINTAIN NUCLEOLAR NOPP140 LOCALIZATION. 64

FIGURE 2.8: ANALYSIS OF KI67 LOCALIZATION IN ADDITIONAL CELL LINES, PERFORMED AS IN FIGURE 2.7 66

FIGURE 2.9: DENSITOMETRIC ANALYSIS OF KI67 LOCALIZATION. 68

FIGURE 2.10: ANALYSIS OF NOPP140 LOCALIZATION IN ADDITIONAL CELL LINES, PERFORMED AS IN FIGURE 2.7 (PANELS A-E) 70

FIGURE 2.11: DENSITOMETRIC ANALYSIS OF NOPP140 LOCALIZATION. 72

FIGURE 2.12: ANALYSIS OF TTF-1 LOCALIZATION PERFORMED AS IS FIGURES 2.7 AND 2.8. 74

FIGURE 2.13: DENSITOMETRIC ANALYSIS OF TTF-1 LOCALIZATION. 76

FIGURE 2.14: HIGHER ORDER INTERACTIONS OF RDNA CHROMATIN ARE ALTERED UPON P150 DEPLETION. 81

FIGURE 2.15: THE P150 N-TERMINUS IS NECESSARY AND SUFFICIENT FOR NUCLEOLAR INTERCHROMOSOMAL ASSOCIATIONS. 83

FIGURE 2.16: THE P150 SIM AND SUMOYLATION PROTEINS ARE REQUIRED FOR NUCLEOLAR INTERCHROMOSOMAL ASSOCIATIONS. 85

FIGURE 2.17: RAPID INHIBITION OF RNA POLYMERASE I DOES NOT AFFECT ASSOCIATION OF ALPHA-SATELLITE DNA TO THE NUCLEOLAR PERIPHERY....91
FIGURE 2.18: CONSERVATION OF THE TYPE B SIM DOMAIN IN P150 HOMOLOGS....93
FIGURE 3.1: ALPHA-SATELLITE ASSOCIATIONS WITH NUCLEOLI ARE REDUCED UPON DEPLETION OF KI-67 BUT NOT NUCLEOLIN....119
FIGURE 3.2: A SUBSET OF P150 LOCALIZES TO THE PCL DURING PROMETAPHASE....123
FIGURE 3.3: A SUBSET OF P150 LOCALIZES TO THE PCL DURING METAPHASE....125
FIGURE 3.4: A SUBSET OF P150 LOCALIZES TO THE PCL DURING ANAPHASE....127
FIGURE 3.5: RNASE A MEDIATED DEGRADATION AND WESTERN BLOT OF DNASE I TREATED PCL PREPARATION....129
FIGURE 3.6: A SUBSET OF P150 LOCALIZES TO KI-67 FOCI DURING EARLY G1 OF INTERPHASE...131
FIGURE 3.7: P150 REGULATES KI-67 LOCALIZATION DURING MITOSIS....136
FIGURE 3.8: P150 REGULATES KI-67 LOCALIZATION DURING EARLY G1 PHASE OF INTERPHASE....139
FIGURE 3.9: THE SIM WITHIN THE N-TERMINAL DOMAIN OF P150 IS SUFFICIENT TO MAINTAIN KI-67 LOCALIZATION TO THE PCL....143
FIGURE 3.10: P150 REGULATES KI-67 LOCALIZATION THROUGHOUT THE CELL CYCLE: A SUMMARY OF DEPENDENCY RELATIONSHIPS....147
FIGURE 4.1: DIAGRAM OF ISOFORM 1 (395 KDA) OF KI-67....164
FIGURE 4.2: DIAGRAM OF MCHERRY_V5 INSERT....168
FIGURE 4.3: ISOLATION AND VALIDATION OF HOMOZYGOUSLY REPAIRED CLONE....172
FIGURE 4.4: KI-67_MCHERRY_V5 LOCALIZES TO THE PCL DURING MITOSIS....174
FIGURE 4.5: IMMUNOPURIFICATION OF KI-67_MCHERRY_V5....177

LIST OF TABLES

TABLE 1.1 SUMMARY OF KNOWN PERINUCLEOLAR REGION REGULATORS 21

TABLE 2.1: MASS SPECTROMETRY DATA FOR NTAP-P150 ASSOCIATED PROTEINS. 43

TABLE 3.1: PRIMERS FOR ESIRNA SYNTHESIS 151

TABLE 3.2: ANTIBODIES USED FOR IMMUNOFLUORESCENCE AND WESTERN BLOTTING 155

LIST OF COPYRIGHTED MATERIALS

Chapter I is reprinted with permission from the journal, Chromosoma (License # 3993800179964)

Chapters II and III are reprinted from the journal Molecular Biology of the Cell (permission not required)

LIST OF ABBREVIATIONS USED COMMONLY IN THIS WORK

3C: Chromosome conformation capture

aa: Amino acids

AID: Auxin-inducible degron

bp: base pairs

CAF-1: Chromatin Assembly Factor 1

ChIP: Chromatin immunoprecipitation

ChIP-seq: Chromatin immunoprecipitation coupled with high throughput deep sequencing

Co-IP-MS: Coimmunoprecipitation combined with mass spectrometry

CRISPR: Clustered regularly interspaced short palindromic repeats

DNA: Deoxyribonucleic acid

DSB: Double stranded break

esiRNAs: Endoribonuclease-prepared siRNAs

FBL: Fibrillarin

FISH: Fluorescence in-situ hybridization

H3K27me3: Histone H3, lysine 27 trimethylation

H3K9me3: Histone H3, lysine 9 trimethylation

H4K20me3: Histone H4, lysine 20 trimethylation

HDR: Homology directed repair

Hi-C: Chromosome conformation capture coupled with high-throughput deep

sequencing

HP1: Heterochromatin Protein 1

IF: Immunofluorescence

kDA: Kilodalton

LADs: Lamina Associated Domains

Luc: Luciferase

NADs: Nucleolar Associated Domains

NCL: Nucleolin

NHEJ: Non-homologous end joining

NL: Nuclear Lamina

NOR: Nucleolus organizer region

NPM: Nucleophosmin

p150C: C-terminal domain of CAF-1 subunit p150

p150N: N-terminal domain of CAF-1 subunit p150

PCL: Perichromosomal Layer

PCR: Polymerase Chain Reaction

PIP: PCNA interacting peptide

PN: Perinucleolar

PNC: Perinucleolar compartment

PP1: Protein phosphatase 1

RNA: Ribonucleic acid

rRNA: ribosomal RNA

RT-qPCR: Reverse Transcription quantitative PCR

Scr: Scramble sequence

sgRNA: short guide RNA

shRNAs: Short hairpin RNAs

SIM: Sumoylation interacting motif

siRNAs: Small interfering RNAs

TADs: Topologically associating domains

CHAPTER I: INTRODUCTION

1.1: Abstract

This dissertation is focused on the interplay of two proteins that contribute the structure and function of the human cell nucleus. Chromatin Assembly Factor 1 (CAF-1) is an evolutionary conserved three-subunit complex responsible for depositing histone $(H3/H4)_2$ heterotetramers onto newly-replicated DNA. As a result, CAF-1 contributes to the maintenance of histone modifications related to heterochromatic gene silencing. Ki-67 is a protein that has long been used as a clinical marker of cell replicative activity for grading neoplastic growths. Ki-67 also affects heterochromatin structure; however, the molecular mechanisms of Ki-67 action remain poorly understood. My thesis work described in the later chapters in this dissertation will provide evidence that the largest subunit of CAF-1, p150, and Ki-67 both regulate the 3-dimensional localization of the human genome.

My studies showed that CAF-1 and Ki-67 are especially important at genomic regions that interact directly and frequently with the nucleolus. These loci are termed Nucleolar Associated Domains (NADs), and are enriched in repetitive elements, the inactive X chromosome (Xi), and several different RNA polymerase III-transcribed genes. NADs are often marked by chromatin modifications characteristic of heterochromatin, including H3K27me3, H3K9me3, and H4K20me3, and artificial targeting of genes to this area is correlated with

reduced expression. Therefore, it has been postulated that NAD localization to the perinucleolar region contributes to the establishment and maintenance of heterochromatic silencing at these loci. Recently published studies from several multicellular eukaryotes have begun to reveal the trans-acting factors involved in NAD localization, including the insulator protein CTCF, several nucleolar proteins, and two long non-coding RNAs (lncRNAs). The mechanisms by which these factors coordinate with one another in regulating NAD localization and/or silencing are still unknown. This chapter will summarize recently published studies, discuss where additional research is required, and speculate about the mechanistic and functional implications of genome organization around the nucleolus.

1.2: Chromatin Assembly Factor 1 (CAF-1)

In eukaryotic cells, DNA is bound by histones and other proteins in a complex macromolecular assembly known as chromatin. The fundamental subunit of chromatin is the nucleosome, comprised of 146 bases of DNA wrapped around a heterotetramer of Histones H3 and H4, flanked by H2A/H2B heterodimers (Luger et al., 1997). The structure of chromatin can dictate both the localization of the DNA within the nucleus and the transcriptional activity of the associated DNA. Elucidating the mechanism and regulation of chromatin assembly has been a primary interest of biology as it is invariably tied to global nuclear structure. In 1986, Bruce Stillman discovered that nuclear extracts from

human 293T cells induced *in vitro* chromatin assembly of SV40 viral plasmid DNA (Stillman, 1986). Three years later, the chromatin assembly activity of the nuclear fraction was traced back to a three subunit complex named Chromatin Assembly Factor 1 (CAF-1) (Smith and Stillman, 1989). Since its initial discovery as a factor required for replication-dependent chromatin assembly, CAF-1 has been shown to play a role in regulating DNA damage repair (Gaillard et al., 1996; Green and Almouzni, 2003; Polo et al., 2006), heterochromatin silencing (Houlard et al., 2006; Huang et al., 2010; Loyola et al., 2009; Murzina et al., 1999; Quivy et al., 2004, 2008; Roelens et al., 2016), stem cell identity (Cheloufi et al., 2015; Hatanaka et al., 2015; Ishiuchi et al., 2015), and multicellular organism development (reviewed in (Yu et al., 2015). These roles, in addition to novel roles outlined in later chapters, will demonstrate that CAF-1 is a major regulator of human nuclear structure.

1.2.1: CAF-1 Structure

CAF-1 is an evolutionarily conserved complex comprised of three subunits in 1:1:1 stoichiometric ratio (Verreault et al., 1996). Smith and Stillman first named the human subunits p150, p60, and p48, after the approximate molecular weight of each subunit (Smith and Stillman, 1989) (Kaufman et al., 1995). The 2 smaller subunits, p60 and p48, are both members of the tryptophan-aspartate (WD) repeat family of proteins (Kaufman et al., 1995; Verreault et al., 1996). This family of proteins contains repeats of approximately 40 amino acids rich in

WD residues, and both p60 and p48 contain 7 distinct WD repeat domains. The largest subunit of the complex, p150, is 938 amino acids in length and acts a binding scaffold for the other subunits of the CAF-1 complex (Kaufman et al., 1995). p150 contains a highly charged KER domain rich in lysine (K), glutamic acid (E), and arginine (R) within amino acids 311-445, and a negatively charged ED domain rich in E and aspartic acid (D) within amino acids 564-641 (Kaufman et al., 1995). Both p150 and p60 contain a canonical PEST domain (Kaufman et al., 1995) which is involved in regulating the half-life of many proteins *in vivo* (Rogers et al., 1986). While p48 has been implicated as a subunit in other nuclear complexes such as the NURF remodeling complex (Martínez-Balbás et al., 1998), the NuRD remodeling/deacetylase complex (Zhang et al., 1999), and polycomb repressor complex PRC2 (Anderson et al., 2011), no evidence exists that p60 or p150 are constituents of chromatin-associated complexes other than CAF-1. However, the fly homolog of p60 has a CAF-1 independent role during sperm chromatin formation (Doyen et al., 2013), and my studies described below have elucidated a CAF-1 independent role for p150 in organization of nucleolar proteins and associated NADs.

1.2.2: CAF-1 Couples Chromatin Assembly with DNA Replication and Repair

The primary function of CAF-1 is to deposit histone $(H3/H4)_2$ heterotetramers onto replicating DNA during S-phase of the cell cycle (Krude,

1995; Shibahara and Stillman, 1999; Smith and Stillman, 1989). During DNA replication, proliferating cell nuclear antigen (PCNA) forms a ring-like homotrimer around replication forks, to which DNA polymerases and other components required for DNA replication and chromatin assembly are tethered (reviewed in (Moldovan et al., 2007)). CAF-1 associates with replication forks via direct interaction between PCNA and a PCNA interaction peptide (PIP) box located within the KER domain of p150 (Rolef Ben-Shahar et al., 2009; Shibahara and Stillman, 1999). A 2nd PIP box also exists within the N-terminus of p150 that features greater binding affinity to PCNA *in vitro*. However, the N-terminal PIP is dispensable for *in vivo* chromatin assembly activity, and thus its true function remains unknown (Rolef Ben-Shahar et al., 2009). CAF-1 acquires newly synthesized H3/H4 heterodimers from histone chaperone Asf1, which directly interacts with a C-terminal region of the p60 subunit (Mello et al., 2002; Tyler et al., 2001). Asf1 has the ability to interact with H3/H4 dimers comprised of all histone 3 variants: H3.1, H3.2, and H3.3 (Latreille et al., 2014). Despite this, CAF-1 preferentially binds to dimers containing histone variants H3.1 (Tagami et al., 2004) or 3.2 (Latreille et al., 2014). Variants H3.1 and H3.2 are nearly identical, as both are primarily synthesized during S-phase and differ structurally by a single cysteine – serine residue at amino acid 96 (Franklin and Zweidler, 1977). In contrast, variant H3.3 is continuously synthesized throughout the cell cycle (Ahmad and Henikoff, 2002; Wu et al., 1982), and differs in structure from H3.1 by 5 residues (Volk and Crispino, 2015). H3.3 is primarily associated with

actively transcribed chromatin (Ahmad and Henikoff, 2002) and deposited onto DNA by the histone chaperone HIRA (Tagami et al., 2004). Evidence that CAF-1 interacts with histone H3 variants synthesized during S-phase further supports the hypothesis that the primary function of CAF-1 is to establish chromatin structure in a replication-dependent manner. However, several studies have demonstrated that CAF-1 does have at least some chromatin assembly activity outside of S-phase. For example, CAF-1 localizes to sites of UV-induced DNA damage outside of S-phase, and deposits H3.1 onto repaired DNA (Gaillard et al., 1996; Green and Almouzni, 2003; Polo et al., 2006). It is hypothesized that replication-independent CAF-1 mediated chromatin assembly occurs mechanistically similar to replication-dependent chromatin assembly, as PCNA and Asf-1 are also present at sites of UV-induced DNA damage (Green and Almouzni, 2003; Mello et al., 2002).

1.2.3: CAF-1 Regulates the Establishment and Maintenance of Heterochromatin

The discovery that CAF-1 does not chaperone the H3.3 variant, which is deposited largely at transcriptionally active euchromatin outside of S phase, is consistent with data from multiple organisms implicating CAF-1 in maintaining transcriptionally silent heterochromatin. The first evidence of this was found in *S. cerevisiae* lacking CAF-1 subunit gene homologs, which display less stable silencing of genes adjacent to heterochromatic telomeric regions (Enomoto et al.,

1997; Kaufman et al., 1997). This derepression was later correlated with a loss of enrichment of heterochromatin-associated SIR (Silent Information Regulator) proteins (Huang et al., 2007). In multicellular organisms, two hallmarks of transcriptionally inactive heterochromatin are the presence of tri-methylation on lysine 9 of histone 3 (H3K9me3) and the association of heterochromatin protein 1 (HP1). CAF-1 directly regulates the association of HP1 to silenced regions within the genome during both replication-dependent and independent chromatin assembly (Houlard et al., 2006; Huang et al., 2010; Murzina et al., 1999; Quivy et al., 2004, 2008; Roelens et al., 2016). This is accomplished through direct interaction between HP1 and the N-terminus of p150 (Murzina et al., 1999). p150 also interacts with the sumoylated form of the methyl-CpG binding protein MBD1, which is commonly enriched on pericentric heterochromatin (Sarraf and Stancheva, 2004; Uchimura et al., 2006). HP1 and/or MBD1 facilitates the recruitment of histone methyltransferase SETDB1 into a complex containing CAF-1 during replication-coupled chromatin assembly (Loyola et al., 2009; Sarraf and Stancheva, 2004; Uchimura et al., 2006). Through this complex, SETDB1 mono-methylates lysine 9 on non-nucleosomal H3 (Loyola et al., 2009), presumably in preparation for further bi- and tri-methylation by the Suv39H1/H2 (Loyola et al., 2006). Consistent with these processes being particularly important during multicellular organism development, CAF-1 is required for normal development of diverse eukaryotes, including both plants and animals

(Fischer et al., 2007; Houlard et al., 2006; Kaya et al., 2001; Quivy et al., 2001; Song et al., 2007; Yu et al., 2013).

1.2.4: CAF-1 Regulates Chromatin Structure Early in Development

Chromatin structure begins to change as soon as the sperm and oocyte genomes fuse to form the novel zygote genome, which begins the process of spatial and temporal regulation of development (reviewed in (Maeso et al., 2016)). After the zygote divides and enters the 2-cell (2C) stage, each daughter cell retains the ability to differentiate into any cell type, a property known as totipotency. While embryonic stem cells (ESCs) retain the ability to differentiate into most cell types (pluripotency), very few retain totipotency. However, a recent study found that partial depletion of p150 and p60 in mouse ESCs resulted in a reacquisition of characteristics inherent to cells at the 2C stage (Ishiuchi et al., 2015). Some of these characteristics include the derepression of genes transcribed during the 2C stage, including the heterochromatic repeat elements MERVL and the major satellite repeat. Depletion of CAF-1 subunits in early mouse embryos also resulted in derepression of retrotransposon elements, a decrease in enrichment of heterochromatic silencing marks such as H3K9me3, and an increase in H3.3 enrichment on endogenous retrotransposons (Hatanaka et al., 2015). This suggests that in the absence of CAF-1, the transcriptionally active histone variant H3.3 is deposited onto endogenous retrotransposon elements, resulting in a failure to replicate epigenetic histone silencing marks and

reactivation of expression. To further emphasize the importance of CAF-1 in mouse development, deletion of p150 results in developmental arrest at the 16 cell stage and ablation of the heterochromatic chromocenters characteristic of differentiating mouse cells (Houlard et al., 2006). Cells in the 2C stage lack chromocenters and feature endogenous retrotransposon activity, further suggesting that CAF-1 is important in maintaining the chromatin structure required of differentiated cells. Additionally, depletion of either p150 or p60 in mouse increased the efficiency of reprogramming fibroblasts to induced pluripotent stem cells (iPSCs) by several orders of magnitude (Cheloufi et al., 2015). While these discoveries are important in terms of advancing the ability to study early stages of development, they also demonstrate that CAF-1 is critical in regulating chromatin structure early in development.

1.2.5: Clinical uses of CAF-1

Cancer cells often feature accelerated proliferation rates negatively correlated with clinical prognosis (reviewed in (Evan and Vousden, 2001)). One of the most reliable methods to grade the proliferation rate of neoplastic tissue is to probe the tissue for a marker associated with cellular proliferation. The expression of a proliferation marker is positively correlated to the growth rate of the neoplastic tissue, and thus negatively correlated with the clinical prognosis. In 2004 Almouzni and colleagues proposed using the subunits of CAF-1 as proliferation markers, as both p150 and p60 are expressed throughout the cell

cycle and minimally expressed during senescence (Polo et al., 2004). Expression of p150 and p60 strongly correlated with other established proliferation markers, including PCNA and Ki-67 (Polo et al., 2004), and several studies have successfully used CAF-1 subunits in grading cancer growth rates in prostate cancer, melanoma, and several types of oral cancers (Mascolo et al., 2010, 2012a, 2012b; Polo et al., 2010; Staibano et al., 2007). One study even showed that expression of p60 is statistically the best independent predictor of cancer development in benign salivary gland growths and metastasis in malignant salivary gland tumors (Staibano and Mascolo, 2011). Despite the promise that these studies have shown, CAF-1 subunits have not been widely adopted as proliferation markers in grading neoplastic growths. However, the increased usage of tissue microarrays (Mascolo et al., 2012b) may encourage the expanded use of novel proliferation markers, including CAF-1 subunits, and further facilitate the clinical study of cancer.

1.3: The Nucleolus

The nucleolus was first described by Wagner (1835) and Valentin (1836) through light microscopy observations, highlighting the prominence of the nucleolus as a sub-nuclear body visible under crude light microscopy conditions (Valentin, 1836, 1839; Wagner, 1835). In the early 1930s, Heitz and McClintock independently discovered that the nucleoli are organized around specific genomic loci, which were later termed nucleolus organizer regions (NORs)

(Heitz, 1931; McClintock, 1934). An explosion of discoveries were made in the mid 1960's, culminating in the landmark discovery that nucleoli are the sites of ribosomal biogenesis (reviewed in (Pederson, 2011)). In addition to its primary role as the site of ribosomal transcription and maturation, the nucleolus hosts many other biological processes, including replication of various viruses (Boyne and Whitehouse, 2006; Li, 1997; Sonntag et al., 2010), signal recognition particle biosynthesis (Ciufo and Brown, 2000; Grosshans et al., 2001; Jacobson and Pederson, 1998; Pederson and Politz, 2000; Politz et al., 2000), sequestration of cell cycle regulators such as p53 and mdm2 (Weber et al., 1999), and sequestration of the transcription factor Hand1 prior to stem cell differentiation (Martindill et al., 2007). This section of this chapter will focus on how the periphery of the nucleolus contacts particular regions of the genome and will outline what is known about the functionality of these interactions.

1.4: Organization of the Genome via Association with Specific Sub-Nuclear Regions

1.4.1: Lamina-Associated Domains (LADs)

With the advent of high-throughput sequencing, scientists have devised several genome-scale methods to test whether nuclear structures associate with the genome in a random or non-random manner. One important method, termed Dam-ID, was developed by Bas van Steensel and Steven Henikoff (van Steensel and Henikoff, 2000). Dam-ID involves the fusion of selected proteins with *E. coli*

DNA adenine methyltransferase (Dam), followed by isolation and deep sequencing-based identification of DNA containing methylated adenine. Eukaryotes lack adenine methylation; therefore genome-scale mapping of this orthologous mark reveals genomic loci that were in close proximity to the fused protein of interest. Studies in a *D. melanogaster* embryonic cell line (Pickersgill et al., 2006) and human fibroblasts (Guelen et al., 2008) fused B-type lamins with Dam to detect peripherally-localized genomic regions, which were termed lamina-associated domains (LADs). LADs tend to be gene-poor and enriched for heterochromatic silencing marks such as H3K9me2 (Kind et al., 2013). Mouse and human genomes contain up to 1,400 LADs encompassing approximately 40% of the genome, ranging in size from 40 kilobases to over 30 megabases (Kind and van Steensel, 2010; Peric-Hupkes et al., 2010).

The mechanisms that govern tethering of LADs to the nuclear periphery are still largely unclear, but recent studies suggest this tethering may be crucial in regulating the transcriptional status of the LADs. This was tested by using a LacO array proximal to a reporter gene and expressing a LacI fused to a protein which directly interacts with the inner nuclear membrane, such as EMD or Lap2β (Dialynas et al., 2010; Finlan et al., 2008; Reddy et al., 2008). In these experiments, targeting various reporter genes to the nuclear lamina (NL) resulted in decreased reporter expression. Likewise, in a comparison of LADs in mouse embryonic stem cells (ESCs) and neural precursor cells (NPCs), an increase in NL association was correlated with a decrease in expression level. Conversely,

gene ontology (GO) analysis revealed that ~20% of genes that featured decreased association with the NL during ESC→NPC differentiation were required for neural physiology. These neural physiology genes generally displayed increased expression during neural differentiation, suggesting that release from the NL is an important step during the induction of lineage-specific gene expression (Peric-Hupkes et al., 2010). In summation, these studies suggest that positioning of LADs at the NL is an important method for physically and functionally compartmentalizing eukaryotic genomes.

1.4.2: Nucleolar Associated Domains (NADs)

In 2010, two independent studies isolated and sequenced the genomic DNA associated with purified nucleoli (van Koningsbruggen et al., 2010; Németh et al., 2010). Both studies found that these nucleolar-associated domains (NADs) are relatively gene-poor compared to the rest of the genome and are highly enriched for satellite DNA repeats. Additionally, both studies also found enrichment for specific types of genes including those coding for the 5S rRNA, immunoglobulins, olfactory receptors, and zinc-finger proteins. These gene classes often exist as multigene arrays, however it remains unknown to what extent primary sequences contribute to perinucleolar localization (see concluding remarks below).

Along with these similarities in the two NAD datasets, there are several notable differences that may be attributable to the different cell types or

experimental procedures used (notably, the use of crosslinking). The Längst group isolated nucleoli from formaldehyde-crosslinked HeLa cells and observed that NADs were significantly enriched for tRNA genes, which are transcribed by RNA polymerase III (Németh et al., 2010). This finding is compatible with previous observations that RNA polymerase III is especially active around the nucleolar periphery (Haeusler and Engelke, 2006; Matera et al., 1995; Thompson et al., 2003). The Lamond group analyzed NADs in non-crosslinked HT-1080 fibrosarcoma cells and emphasized that the majority of the NAD peaks overlap with previously published LADs (van Koningsbruggen et al., 2010). To explore this overlap, the Lamond group photoactivated a GFP-tagged histone around the periphery of the nucleolus and then tracked the localization of that chromatin through the cell cycle. It was found that after mitosis, the photoactivated chromatin could localize to either the perinucleolar (PN) region or the NL, indicating that the PN and the NL may be interchangeable addresses for some loci. These data are consistent with other studies which found that LADs often re-localize to the PN region after mitosis (Kind et al., 2013). LADs can also redistribute to either the PN or pericentromeric (PC) heterochromatin regions upon a short treatment with actinomycin D at a dose that selectively inhibits transcription by RNA polymerase I (Ragoczy et al., 2015). However, the transcriptional activity of the relocalized loci were not altered during this treatment, suggesting that the PN and NL serve as dynamic, functionally

overlapping regions for genome organization and silencing (reviewed in (Padeken and Heun 2014)).

1.4.3: The Perinucleolar Compartment (PNC) of Cancer Cells

The HeLa and HT-1080 cells used by the Lamond and Längst laboratories (van Koningsbruggen et al., 2010; Németh et al., 2010) both contain a cancer-specific sub-nuclear structure known as the perinucleolar compartment (PNC) (Norton et al., 2008). The PNC is localized on a portion of the nucleolar surface (Huang et al., 1997) and thus may copurify with nucleoli. This suggests that some of the NADs described in the previous section may be cancer cell-specific. The presence of the PNC is correlated with metastasis and inversely correlated with patient survival and relapse (Kamath et al., 2005). The PNC is enriched in proteins that regulate the splicing and polyadenylation of RNA polymerase II transcripts (Ghetti et al., 1992; Hall et al., 2004; Matera et al., 1995; Timchenko et al., 1996). This compartment also contains specific RNA polymerase III transcripts, including RNase P, RNAse MRP, Y RNAs (Matera et al., 1995), Alu RNAs, and signal recognition particle RNA (Wang et al., 2003). These RNA species are not actively transcribed within the PNC (Matera et al., 1995; Wang et al., 2003) and the compartment is devoid of most RNA polymerase III transcripts, notably tRNAs (Matera et al., 1995). The function of the PNC is still unknown, but is of great interest to the field of cancer biology (reviewed in (Pollock and

Huang, 2010)). In the interest of space, the remainder of this section will focus on NAD associations which occur in both primary and cancer cells.

1.5: NAD Function: PN Localization Linked to Heterochromatin Silencing

1.5.1: The Inactive X Chromosome

In 1949 Barr and Bertram described a “nucleolar satellite” which protruded from the nucleolus of female cat motor neurons (Barr and Bertram, 1949). This structure was later identified as the inactive X chromosome. During embryonic development of female mammalian cells, one of the X chromosomes is silenced in order to provide dosage compensation, ensuring that female cells with two X chromosomes do not overexpress X-linked genes (Lyon, 1961). During gastrulation and after most of the DNA methylation imprints from the parents are erased, the two X-chromosomes pair and each chromosome is randomly assigned to become active (Xa) or inactive (Xi). The designated Xi then transcribes a long non-coding RNA (lncRNA) known as Xist (Brown et al., 1991), which spreads across the Xi in *cis* (Clemson et al., 1996). Xist recruits Polycomb Repressive Complexes 1 and 2 (PRC1 and PRC2), which induce methylation of histone H3 lysine 27 and silence the transcriptional activity of most of the genes on the Xi ((Plath et al., 2003, 2004); reviewed in (Lee, 2012; Lucchesi et al., 2005; Thorvaldsen et al., 2006)). Thus, X inactivation is a prominent example of gene regulation via alteration of chromatin state.

Several studies have shown that the Xi can associate with either the NL or PN regions of the nucleus (Barton et al., 1965; Bourgeois et al., 1985). A study by the Lee laboratory found that Xi association with nucleoli is most prevalent during mid-late S-phase of the cell cycle (Zhang et al., 2007). This study also showed that the interaction is dependent upon the X inactivation center (*Xic*), the region encoding the Xist locus, because autosomes bearing Xic translocations also preferentially associate with nucleoli. Conversely, deletion of Xist reduces nucleolar association, H3K27 methylation, and derepression of Xic-proximal genes in some cell lines analyzed. This PN localization occurs during mid-late S-phase when heterochromatin is replicated, suggesting that replication in the PN region helps to maintain the silent state of the Xi. Additional tools to perturb Xi-nucleolar associations without having to delete central silencing factors such as Xist will be important to further test this hypothesis. However, it seems likely that the Xi-PN association by itself is not essential for maintaining the bulk of Xi silencing, consistent with previous observations of a large degree of functional overlap between Xist and other factors (Csankovszki et al., 2001).

1.5.2: The 5S rDNA

Eukaryotic ribosomes are comprised of large (60S) and small (40S) subunits. The major RNA species found in mature ribosomes (28S, 18S, and 5.8S rRNA) are encoded within the 47S rRNA primary transcripts that are produced from repeated templates on the short arms of the five acrocentric

chromosomes in humans (reviewed in (Boisvert et al., 2007; Németh and Längst, 2011; Sirri et al., 2008)). An additional rRNA species is encoded by an array of approximately 100 RNA polymerase III-transcribed 5S rDNA genes located on Chromosome 1 (Steffensen et al., 1974; Stults et al., 2008). As noted above, several studies have found that RNA polymerase III transcribed genes, including the 5S rDNA, are enriched in the PN region in a variety of different species and cell types (van Koningsbruggen et al., 2010; Matera et al., 1995; Németh et al., 2010; Thompson et al., 2003). For example, the 5S array-nucleolar association in humans was described in HeLa cells, and its localization was noted as being outside of the PNC region (Matera et al., 1995). One possible rationale for the close proximity of the 5S array to nucleoli would be to increase the efficiency of ribosome assembly (Haeusler and Engelke, 2006). However, a study by the Magnuson lab suggests instead that nucleolar localization of 5S rDNA repeats may facilitate transcriptional silencing. In this study, the 119-bp 5S rDNA and a reporter gene were randomly inserted into the genome of mouse ES cells, and these transgenes frequently associated with nucleoli. This association was correlated with reduced reporter gene expression and increased H3K9me3 enrichment. Furthermore, endogenous mouse 5S pseudogenes, which maintain internal RNA polymerase III transcription factor binding sites but do not produce a functional transcript, also frequently associate with the PN region. ChIP-qPCR analysis demonstrated that many of these pseudogenes feature low RNA polymerase III transcription factor occupancy, suggesting that the 5S rDNA

sequence and not the RNA Polymerase III transcription machinery is responsible for PN localization (Fedoriw et al., 2012a). The cis-acting sequences and trans-acting factors required for these types of higher-order genome interactions are of major interest, and specific examples related to nucleoli are discussed below (Table 1.1).

Table 1.1: Summary of Known Perinucleolar Region Regulators

This table lists all known proteins and lncRNAs which regulate the structure or localization of known NAD elements. References for each item given in parenthesis.

Table 1.1 Summary of Known Perinucleolar Region Regulators

Protein or RNA	Known Interphase Nuclear Localization	Regulation Target (Species)
CTCF	Insulator Elements (Kim et al., 2007)	Insulators (*H. sapiens*)(Yusufzai et al., 2004) Clustered Centromeres (*D. melanogaster*) (Padeken et al., 2013) Xi (*M. musculus*) (Yang et al., 2015)
NLP (NCL)	Nucleolar Fibrillar Centers(Lischwe et al., 1981; Spector et al., 1984) Nucleolar Dense Fibrillar Component (Escande et al., 1985; Spector et al., 1984) Nucleolar Granular Component (Escande et al., 1985)	Clustered Centromeres (*D. melanogaster*)(Padeken et al., 2013)
Modulo (NPM1)	Nucleolar Granular Component (Spector et al., 1984)	Clustered Centromeres (*D. melanogaster*) (Padeken et al., 2013)
Ki-67	Satellite DNA (Bridger et al., 1998) Nucleolar Dense Fibrillar Component (Kill, 1996)	47S rDNA (*H. sapiens*) (Chromosome 13p) (Booth et al., 2014)
Kcnq1ot1	*Kcnq1* Locus (Pandey et al., 2008)	Kcnq1 locus (*H. sapiens, M. musculus*) (Mohammad et al., 2008; Pandey et al., 2008)
Firre	6 gene-containing loci (*Firre, Slc25a12, Ypel4, Eef1a1, Atf, Ppp1r10*), and 34 non-gene loci (Hacisuleyman et al., 2014)	Xi (*M. musculus*) (Yang et al., 2015)

1.6: Protein Regulators of PN Structure and Function

Tethering of NADs to the PN region is now known to require several trans-acting factors, which presumably directly or indirectly bind to NAD DNA. These NAD-bound factors must either interact with the ribosomal DNA of the nucleolus or with nucleolar proteins in order to facilitate nucleolar localization. The following sections will briefly introduce the protein and RNA factors thus far discovered to be involved in NAD localization.

1.6.1: CTCF

The CCCTC-Binding Factor (CTCF) is a DNA-binding protein with between 55,000-65,000 sites of enrichment throughout the human genome (Chen et al., 2012b). CTCF is particularly enriched on insulator elements (DeMare et al., 2013; Kim et al., 2007; Song et al., 2011), which block interaction between promoters and enhancers. Importantly, CTCF regulates the three-dimensional interaction of these regulatory elements with distal promoters, thereby regulating transcription (Sanyal et al., 2012; Shen et al., 2012). Insulator occupancy by CTCF is cell-type specific (Barski et al., 2007; Chen et al., 2008; Cuddapah et al., 2009; Kim et al., 2007; Shen et al., 2012), suggesting that CTCF contributes to regulatory networks responsible for changes in cell-lineage specific nuclear architecture.

One study in human leukemia cells showed that CTCF binding sites within an exogenous insulator conferred a higher propensity to associate with nucleoli.

This study further showed that CTCF interacts with the nucleolar protein nucleophosmin (NPM1/B23), and that NPM1 enrichment on the exogenous insulator was dependent on the presence of CTCF binding sites (Yusufzai et al., 2004). One plausible model to explain this tethering would be that CTCF links insulator elements to the nucleoli via interaction with the nucleolar protein NPM1. Later sections in this review will discuss the role of CTCF in regulating the nucleolar localization of clustered centromeres and the Xi.

1.6.2: The Nucleophosmin Homolog NLP and the Nucleolin Homolog Modulo

Nucleolin (NCL/C23) is a multifunctional protein that primarily localizes to the nucleolus (Bugler et al., 1982), interacts with snoRNAs (Sáez-Vasquez et al., 2004), regulates the folding and assembly of ribosomes (Ginisty et al., 1998), and regulates 47S rDNA transcription (Rickards et al., 2007; Roger et al., 2002). NPM1 is also a multifunctional nucleolar protein (Michalik et al., 1981) that interacts with several ribosomal proteins (Lindström and Zhang, 2008; Yu et al., 2006) and has multiple roles in nucleolar biology including acting as a pre-rRNA endoribonuclease (Herrera et al., 1995; Savkur and Olson, 1998) and facilitating 40S and 60S nuclear export (Maggi et al., 2008). NPM1 interact with a wide variety of proteins, including the centromere-specific histone variant CENP-A (Foltz et al., 2006). Centromeres often cluster together and localize to the nucleolus in many species and cell types (Weierich et al., 2003). The Heun

laboratory showed that depletion of NLP, a Drosophila homolog of NPM1, or the Drosophila CTCF insulator protein resulted in de-clustering of centromeres and a decrease in centromere association with nucleoli. Depletion of Modulo, the Drosophila homolog of NCL, also resulted in de-clustering of centromeres and disruption of nucleolar structure, making it difficult to determine whether Modulo is required for PN positioning. NLP or Modulo depletions also resulted in de-repression of several classes of transposable elements and cells showed signs of genomic instability, including increased double stranded breaks and lagging chromosomes during mitosis (Padeken et al., 2013). These data are consistent with the idea that the frequent nucleolar localization of centromeres is functionally important for maintaining a chromatin structure optimal for proper chromosome segregation.

1.6.3: Ki-67

Ki-67 was first identified as an epitope recognized by a monoclonal antibody raised against nuclei from a Hodgkin lymphoma cell line (Gerdes et al., 1983). Since its initial discovery, Ki-67 has been used as a cell proliferation marker in thousands of clinical studies in order to grade the proliferative rates of various types of cancers. Despite this, relatively little is known about the molecular functions of Ki-67. In interphase cells Ki-67 primarily localizes to the nucleolus (Cheutin et al., 2003; Kill, 1996), is enriched on the 47S rDNA gene (Bullwinkel et al., 2006), and is required for normal levels of 47S rDNA

transcription (Booth et al., 2014; Rahmanzadeh et al., 2007). In early G1, Ki-67 localizes to distinct foci which co-localize with several different classes of repeats enriched within the NADs, including centromeric alpha satellite, telomeric repeats, and Sat III (Bridger et al., 1998). Several studies have found that Ki-67 is required for the formation of the human perichromosomal layer (Booth et al., 2014; Sobecki et al., 2016), a proteinaceous sheath that coats condensed chromosomes during mitosis (reviewed in (Van Hooser et al., 2005)). While the function of the PCL is still being explored, one recent study suggests that the presence of Ki-67 at the PCL may serve to create a surfactant layer to keep mitotic chromosomes dispersed (Cuylen et al., 2016). Two recent studies have also found evidence that Ki-67 is important in regulating the PN localization of two different classes of NADs. The first showed that Ki-67 is required for normal nucleolar association of an rDNA-proximal NAD sequence containing a LacO reporter array (Booth et al., 2014). This is especially intriguing because nucleoli are constructed around the rDNA repeat arrays, and so this evidence suggests Ki-67 may also regulate the reconstruction of the nucleoli at the beginning of G1. A second study found that Ki-67 is required for nucleolar association of the centromeric histone variant CENP-A (Sobecki et al., 2016). CENP-A is enriched on all centromeres within the human genome, therefore this suggests that Ki-67 is required for the localization centromeric satellite repeat elements to the PN region. While there are now two examples of Ki-67 regulating NAD localization, future studies should take an unbiased approach and perform NAD-seq upon Ki-

67 depletion in order to determine which classes of NADs are specifically regulated by Ki-67. Future studies should examine whether Ki-67's role in regulating PCL structure and NAD localization are interrelated.

1.7: lncRNAs as Regulators of PN Structure and Function

1.7.1: *Kcnq1ot1*

The *Kcnq1* locus in mouse and human cells is regulated through maternal imprinting. While genes within this locus are expressed on the maternal chromosome, the paternal chromosome expresses an antisense lncRNA known as *Kcnq1*ot1 in order to facilitate silencing of the paternal genes (Mancini-DiNardo et al., 2006; Pandey et al., 2004, 2008; Thakur et al., 2004). In contrast to the paternally-derived chromosome, *Kcnq1*ot1 expression on the maternal chromosome is inhibited due to imprinted methylation of the *Kcnq1*ot1 promoter (Fitzpatrick et al., 2002). The Kanduri laboratory discovered that the *Kcnq1*ot1 locus is often enriched for heterochromatic histone silencing marks in mouse placenta cells, but not in fetal liver cells. In placenta cells, the *Kcnq1*ot1 locus is also associated with nucleoli twice as frequently as observed in fetal liver cells (Pandey et al., 2008), supporting the correlation between nucleolar localization and the establishment and/or maintenance of heterochromatin. Another study found that an 890-bp region near the 5'-end of the human *Kcnq1*ot1 transcript is required for silencing of the other Kcnq1 locus genes. Furthermore, when this silencing domain was inserted into an episomal vector, the vector localized to

nucleoli during mid S-phase and a flanking reporter gene was silenced. When the silencing domain was inserted in reverse orientation, the vector failed to localize to nucleoli and the reporter gene was expressed (Mohammad et al., 2008). These results support the hypothesis that the transcribed *Kcnq1ot1* lncRNA and not the DNA sequence encoding it is required for localization to the PN region and silencing of the vector reporter genes.

1.7.2: *Firre*

One of the X-linked genes which escapes silencing during X-inactivation encodes the lncRNA *Firre* (Yang et al., 2010). *Firre* is important for long-range chromosomal interactions, interacting with the RNA-binding protein hnRNPU to facilitate localization of the Xi to regions from five different chromosomes (Hacisuleyman et al., 2014). *Firre* is also required for normal association of the mouse Xi with nucleoli, as the frequency of PN localization of the X-linked *Firre* and DXZ4 macrosatellite loci decrease upon depletion of the *Firre* lncRNA (Yang et al., 2015). *Firre* depletion also decreases the enrichment of the heterochromatic silencing mark H3K27me3 on the Xi without decreasing the expression levels of Xist. However, depletion of *Firre* did not result in significant transcriptional changes on the Xi. Future experiments will be required to distinguish whether these data result from functional redundancy among repressive factors which govern Xi silencing, or because transcriptional regulation is not a major functional consequence of NAD localization.

The *Firre* and DXZ4 loci also feature enrichment of the insulator protein CTCF (Hacisuleyman et al., 2014; Yang et al., 2015). CTCF depletion decreased PN association of both the *Firre* and DXZ4 loci, reduced expression of the *Firre* lncRNA, and diminished levels of H3K27me3 on the Xi (Yang et al., 2015). Therefore, CTCF may regulate PN localization and silencing of the Xi as both a direct interaction factor and as a transcriptional regulator of *Firre* expression. Additional studies should explore whether the trans-chromosomal interactions regulated by *Firre* also localize to the periphery of the nucleolus and are regulated by CTCF.

1.8: Concluding Remarks

1.8.1: What defines the NADs?

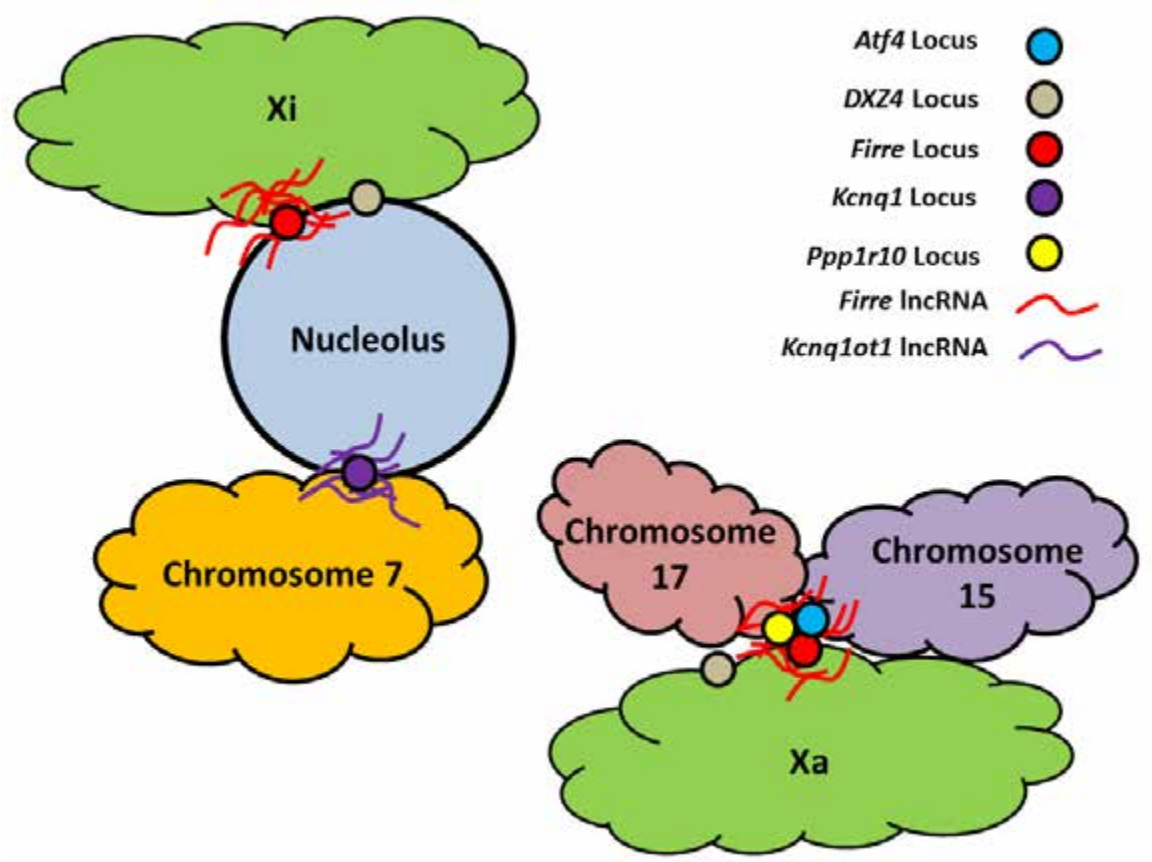
One possible determinant of NAD localization is genomic DNA sequence. Primary DNA sequence is likely critical for some classes of NADs, as is the case for 5S pseudogenes, which can associate with the nucleoli independently of RNA polymerase III machinery (Fedoriw et al., 2012a). However, primary DNA sequence cannot be the only determinant of all nucleolar localization. For example, in the case of *Firre*-dependent PN localization of the inactive Xi chromosome (Figure 1.1)(Yang et al., 2015), the primary sequences of the Xi must be insufficient for nucleolar association because the Xa chromosome does not localize to the PN region. The discovery that lncRNAs are required for some NAD associations is an exciting development, as over 100,000 lncRNAs have

been annotated in the human genome (Volders et al., 2013), and the functions of most of these molecules remain unknown. Additional research is required to elucidate how proteins and lncRNAs coordinate NAD-PN interactions. One likely possibility is that the lncRNAs directly interact with nucleolar targeting proteins, and recent advances in high throughput RNA-binding protein identification will be instrumental in determining the binding partners for *Kcnq1ot1*and *Firre* (Chu et al., 2015; McHugh et al., 2015). In the case of *Firre*, a particularly relevant interacting protein is the RNA binding protein hnRNPU. hnRNPU binds to *Firre* and is required for the inter-chromosomal interactions mediated by *Firre* (Hacisuleyman et al., 2014). Another protein of interest, CTCF, binds to both the *Firre* RNA and DNA (Hacisuleyman et al., 2014; Yang et al., 2015) and this interaction may be mediated by hnRNPU. Many more contributing factors are likely to be discovered as investigations of these higher-order interactions continue.

Figure 1.1: Schematic of lncRNAs Facilitating Trans-Chromosomal Interactions in Mouse.

The *Kcnq1ot1* lncRNA tethers the *Kcnq1* locus to the nucleolus (Mohammad et al., 2008), while the lncRNA *Firre* mediates nucleolar association of the *Firre* and *DXZ4* loci (Yang et al., 2015). *Firre* also mediates transchromosomal interactions of the *Firre* locus with 5 other loci, including the *Atf4* locus on chromosome 15 and the *Ppp1r10* locus on chromosome 17 (Hacisuleyman et al., 2014).

Figure 1.1: Schematic of lncRNAs Facilitating Trans-Chromosomal Interactions in Mouse.



1.8.2: What is the functional significance of NADs?

The major question to be answered is whether nucleolar localization affects the biological activities of NAD sequences. Multiple studies have correlated localization of NADs to the PN region with heterochromatin formation and transcriptional silencing (Fedoriw et al., 2012a, 2012b; Mohammad et al., 2008; Pandey et al., 2008; Yang et al., 2015; Zhang et al., 2007). In the example of the Xi, failure to localize to the PN region during S-phase results in decreased heterochromatic silencing marks (Yang et al., 2015; Zhang et al., 2007) without changes in gene expression at most Xi loci (Zhang et al., 2007). Likewise, loci which failed to associate with the nucleolus often re-localize to the NL or PC regions and transcriptional silencing is maintained (van Koningsbruggen et al., 2010; Ragoczy et al., 2015). Together, these data are consistent with the idea that PN localization is one of several functionally overlapping mechanisms for transcriptional repression, although there is a lack of data for a unique role of NAD localization in regulating gene expression. It should be considered that transcriptional regulation may not be the only or even a major outcome of NAD localization to the PN region. In contrast, the data from the Heun laboratory in the Drosophila system points to genome stability as a critical outcome of proper NLP (NPM1) and Modulo (NCL) function (Padeken et al., 2013). There is precedent for deleterious hyper-recombination phenotypes within the rDNA upon chromatin perturbation in budding yeast (Cesarini et al., 2012; Ide et al., 2013; Lindstrom et

al., 2011), but these types of events have not been examined in conjunction with NAD analysis in metazoans.

We do not presently understand how NADs migrate among different repressive nuclear regions, nor is it likely that we know all of the proteins and/or RNA factors involved in these transitions. Further study is needed to determine whether and how association of NADs with the nucleolus affects nucleolar structure and function. These questions will be especially challenging to explore because many of the proteins required for NAD localization also regulate rDNA transcription and/or nucleolar structure. For example, CTCF (Huang et al., 2013; van de Nobelen et al., 2010), NCL (Cong et al., 2012; Rickards et al., 2007; Roger et al., 2002), NPM1 (Murano et al., 2008), and Ki-67 (Booth et al., 2014; Rahmanzadeh et al., 2007) all regulate rDNA transcription. Likewise, depletion of Modulo (NCL) in flies disrupts nucleolar structure as demonstrated by immunofluorescence (Padeken et al., 2013), and Ki-67 depletion in human cells results in fewer and smaller nucleoli (Booth et al., 2014). However, not all perturbations necessarily affect all structural aspects of the nucleolus. For example, depletion of CAF-1 p150 causes mislocalization of multiple nucleolar proteins (Smith et al., 2014) but does not appear to alter the macrostructure of the rDNA (videos 1.1 and 1.2). Therefore, it remains to be determined whether the structure or function phenotypes observed in the depletion of these proteins is caused by mislocalization of NADs or merely correlated with it, and mutations that separate these functions will be required to assess this.

Understanding the structure of the genome is critical for understanding human disease, as many diseases are dependent upon genomic three-dimensional structure (reviewed in (Misteli, 2010)). For example, translocations are associated with a variety of different cancers, and these translocation events occur most frequently between genomic elements in close proximity to one another (Zhang et al., 2012). This has been particularly well documented in the case of ABL-BCR translocations that drive chronic myeloid leukemia, because the *BCR* gene on chromosome 9 is often found in close proximity to the *ABL* gene on chromosome 22 in hematopoietic cells (Lukášová et al., 1997; Neves et al., 1999). Although the periphery of the nucleolus is a small fraction of nuclear volume, many higher order chromosomal interactions occur there. Discovering the extent to which this organizational hub is coordinated with other nuclear elements will be critical in comprehending the three-dimensional structures of metazoan genomes, and how these structures are perturbed in disease states.

Videos 1.1 and 1.2 Three-Dimensional Rendering of HeLa S3 Nucleus with and without CAF-1 p150 Depletion.

Video 1.1 shows a HeLa S3 nucleus after 72 hours of expression of a control shRNA directed against luciferase. DAPI staining is in blue (A), the nucleolar and Cajal body protein Nopp140 in green (B) and the ribosomal rDNA in red (C). Video 1.2 shows a HeLa S3 nucleus after 72 hours of expression of an shRNA directed against CAF-1 p150 with the same channels as in Video 1. Note that Nopp140 does not localize to the nucleolus in video 2C, but does maintain localization to two different Cajal bodies. In contrast, the morphology of the nucleolus visualized by rDNA hybridization is not significantly different. (Methods, probes, and antibodies described in (Smith et al., 2014) . The Nopp140 antibody (RS8) was a generous gift of U. Thomas Meier, Albert Einstein College of Medicine, New York, NY (Kittur et al., 2007). Z-stack images were taken on a Leica TCS SP5 II Laser Scanning Confocal Microscope and videos were generated using the Leica Application Suite AF version 2.5.1.6757)
Please visit http://link.springer.com/article/10.1007/s00412-015-0527-8 to view the videos.

CHAPTER II: A SEPARABLE DOMAIN OF THE P150 SUBUNIT OF HUMAN CHROMATIN ASSEMBLY FACTOR-1 PROMOTES PROTEIN AND CHROMOSOME ASSOCIATIONS WITH NUCLEOLI

Note about authorship:

This chapter was previously published (Smith et al., 2014) as a collaboration between the following authors: Corey L. Smith, Timothy D. Matheson, Daniel J. Trombly, Xiaoming Sun, Eric Campeau, Xuemei Han, John R. Yates III, and Paul D. Kaufman. I was personally responsible for Figures 2.14-2.17, methods sections 2.5.11-2.5.12, and for editing the manuscript. I chose to include the entire manuscript within this chapter because the presented evidence is imperative in understanding chapters III, IV, and the molecular mechanism of p150 in regulating nuclear structure.

2.1: Abstract

Chromatin Assembly Factor-1 (CAF-1) is a three-subunit protein complex conserved throughout eukaryotes that deposits histones during DNA synthesis. In this chapter we present a novel role for the human p150 subunit in regulating nucleolar macromolecular interactions. Acute depletion of p150 causes redistribution of multiple nucleolar proteins and reduces nucleolar association with several repetitive element-containing loci. Notably, a point mutation in a

SUMO-interacting motif (SIM) within p150 abolishes nucleolar associations, whereas PCNA or HP1 interaction sites within p150 are not required for these interactions. Additionally, acute depletion of SUMO-2 or the SUMO E2 ligase Ubc9 reduces alpha-satellite DNA association with nucleoli. The nucleolar functions of p150 are separable from its interactions with the other subunits of the CAF-1 complex, because an N-terminal fragment of p150 (p150N) that cannot interact with other CAF-1 subunits is sufficient for maintaining nucleolar chromosome and protein associations. Therefore, these data define novel functions for a separable domain of the p150 protein, regulating protein and DNA interactions at the nucleolus.

2.2: Introduction

In eukaryotes, histones are deposited onto DNA by nucleosome assembly proteins, including Chromatin Assembly Factor-1 (CAF-1) (reviewed in (Ransom et al., 2010)). CAF-1 is a three-subunit protein complex conserved throughout eukaryotes. In humans, the three CAF-1 subunits are named based on their gel migration (Smith and Stillman, 1989). The largest subunit, p150, is the platform that binds the other two subunits, the WD-40 repeat proteins p60 and p48; all three subunits are required for *in vitro* nucleosome assembly activity (Kaufman et al., 1995; Verreault et al., 1996). CAF-1 deposits histones during DNA synthesis, and interacts with DNA replication protein proliferating cell nuclear antigen (PCNA) and the replication-linked histone isoform H3.1 (Shibahara and Stillman,

1999; Tagami et al., 2004). Throughout the eukaryotes, CAF-1 is required for normal S phase progression, heterochromatin formation (Houlard et al., 2006; Klapholz et al., 2009; Quivy et al., 2008; Takami et al., 2007), and chromatin restoration after DNA repair (Gaillard et al., 1996; Green and Almouzni, 2003). Consistent with its role in chromosome duplication, CAF-1 protein levels correlate with cell proliferation and cancer prognosis (Mascolo et al., 2010; Polo et al., 2004; Staibano et al., 2009).

In all eukaryotes, a dedicated polymerase, RNA polymerase I (Pol I), transcribes the large ribosomal RNAs (rRNAs; 18S and 28S in humans) as long precursor species (47S in humans) from repeated ribosomal DNA (rDNA) templates. The 47S rRNA-encoding repeats cluster to form the nucleolus, a specialized, non-membrane-bound sub-nuclear compartment (McStay and Grummt, 2008). Pol I transcription constitutes the majority of RNA synthesis in cells and is regulated by cell growth and energy supply, differentiation, cell cycle progression, tumor suppressors (p53 and Rb) and oncoproteins (c-myc) (McStay and Grummt, 2008; Murayama et al., 2008). Additionally, the nucleolus is a dynamic hub where many nuclear proteins (Emmott and Hiscox, 2009) and genomic loci (van Koningsbruggen et al., 2010; Németh et al., 2010) are tethered (Padeken et al., 2013). Notably, nucleolar alterations can be important for cancer diagnoses (Maggi and Weber, 2005). However, our understanding of the structure and function of nucleolar macromolecular networks remains incomplete. Here, mass spectrometric analysis of the human CAF-1 p150 subunit led us to

discover previously unrecognized roles in regulating macromolecular interactions at the nucleolus.

2.3: Results

2.3.1: p150 interacts with nucleolar proteins

To find novel protein interaction partners, we generated a human HeLa S3 cell line expressing an N-terminal tandem affinity tagged-CAF-1 p150 subunit (NTAP-p150). NTAP-p150 localizes normally to PCNA-labeled DNA replication foci during S phase (Campeau et al., 2009), indicating functionality *in vivo*. Nuclear extracts from asynchronous HeLa S3 cells either containing or lacking the NTAP-tagged p150 gene were subjected to affinity purification under mild (200 mM NaCl) buffer conditions that included 50 μg/ml ethidium bromide to avoid co-precipitation of proteins via bridged nucleic acid interactions (Lai and Herr, 1992). Gel analysis of the purified proteins demonstrated that NTAP-p150 complexed with the other two CAF-1 subunits, p60 and p48 (Figure 2.1, B), and that this tagged complex was recovered in a tag-dependent manner. Proteins from two independent preparations were identified by mass spectrometry (Figure 2.1, A, and Table 2.1). In the tagged but not untagged samples, we detected all three CAF-1 subunits, as well as known CAF-1-binding proteins such as core histones, histone deposition factor Asf1 (Sharp et al., 2001; Tang et al., 2006; Tyler et al., 2001), and HP1 (Murzina et al., 1999; Quivy et al., 2004). Additionally, the tagged samples contained multiple nucleolar proteins that were

not previously known to associate with p150. These included Ki67, a large, proteolytically sensitive protein that is commonly used to mark proliferative cells in pathology studies (Yerushalmi et al., 2010). Notably, Ki67 prominently localizes to nucleoli (Espada et al., 2007; MacCallum and Hall, 1999; Takagi et al., 2001) (Figure 2.1, C) This interaction is functionally important, because inactivation of Ki67 inhibits rRNA synthesis (Rahmanzadeh et al., 2007). The p150-associated proteins also included NPM (also known as B23), and NCL, which are both nucleolar histone chaperones that assist Pol I transcription (Angelov et al., 2006; Murano et al., 2008; Rickards et al., 2007). Our affinity-purified NTAP-p150 preparations additionally included Nucleolar Protein 58 (Nop5/Nop58), a snoRNA-binding protein whose nucleolar localization is regulated by SUMOylation (Westman et al., 2010), DDX17, a DEAD-box protein that contributes to rRNA processing and nucleolar protein localization (Jalal et al., 2007), and RRP1B, a nucleolar targeting protein implicated in metastasis susceptibility (Chamousset et al., 2010; Crawford et al., 2007). Additionally, we detected DNAJC9, a DnaJ homolog that was previously isolated as a binding partner of RRP1B, as were the nucleolar proteins NCL, NPM, and Ki67 (Crawford et al., 2009) that we identified here (Table 2.1). Finally, we note that p150 was identified in an independent proteomic analysis of purified nucleoli (Ahmad et al., 2009), supporting our findings.

Figure 2.1: Nucleolar associations of human p150.

(**A**) Novel nucleolus-related p150-interacting proteins identified by mass spectrometry are summarized. Proteins listed were not previously known to interact with p150 and had multiple peptides detected in two different experiments (E1 and E2). Full lists are in Table S1. Number of peptides (#Pep) and spectral counts (SpC) are indicated. (**B**) Purified p150-associated proteins prepared for mass spectrometry. Affinity-purified samples from untagged HeLa S3-Trex (lane 1) and HeLa S3-Trex-NTAP-p150 (lane 2) cells were analyzed on a silver-stained 5-20% SDS-PAGE gel. CAF-1 subunits p150, p60 and p48 are indicated. (**C**) Confocal microscopy analysis of p150 (red) and Ki67 (green) in HeLa S3 cells detects partial colocalization at nucleoli in the merged image (yellow). Fields of cells were photographed with a 63x objective. Cells had either been blocked in G1 phase by double thymidine treatment or released into S phase for 2 hours. Scale bars are 10 μm. (**D**) Location of ChIP primer pairs on the human 47S rRNA-encoding rDNA locus. (**E**) p150 occupancy at rDNA genes in asynchronous HeLa S3-Trex-shRNA cells. Also assayed were the pol II gene *RPS20* and a gene desert from chromosome 16. Cells expressing either a control shRNA (sh-Luc) or the shRNA targeting p150 (sh-p150) were compared. Chromatin was precipitated with either non-immune rabbit sera (IgG) or anti-p150 sera (α-p150) as indicated. The mean percentages of input chromatin precipitated from three biological replicates are presented, with error bars representing standard deviations. Asterisks indicate loci at which sh-p150 caused a statistically significant decrease in p150 occupancy ($p < 0.05$). Dotted line shows p150 signal at the gene desert. (**F**) p150 occupancy in asynchronous HeLa cells compared with cells blocked with a double thymidine treatment. Asterisks indicate loci at which thymidine arrest caused a statistically significant increase in p150 occupancy ($p < 0.05$).

Figure 2.1: Nucleolar associations of human p150.

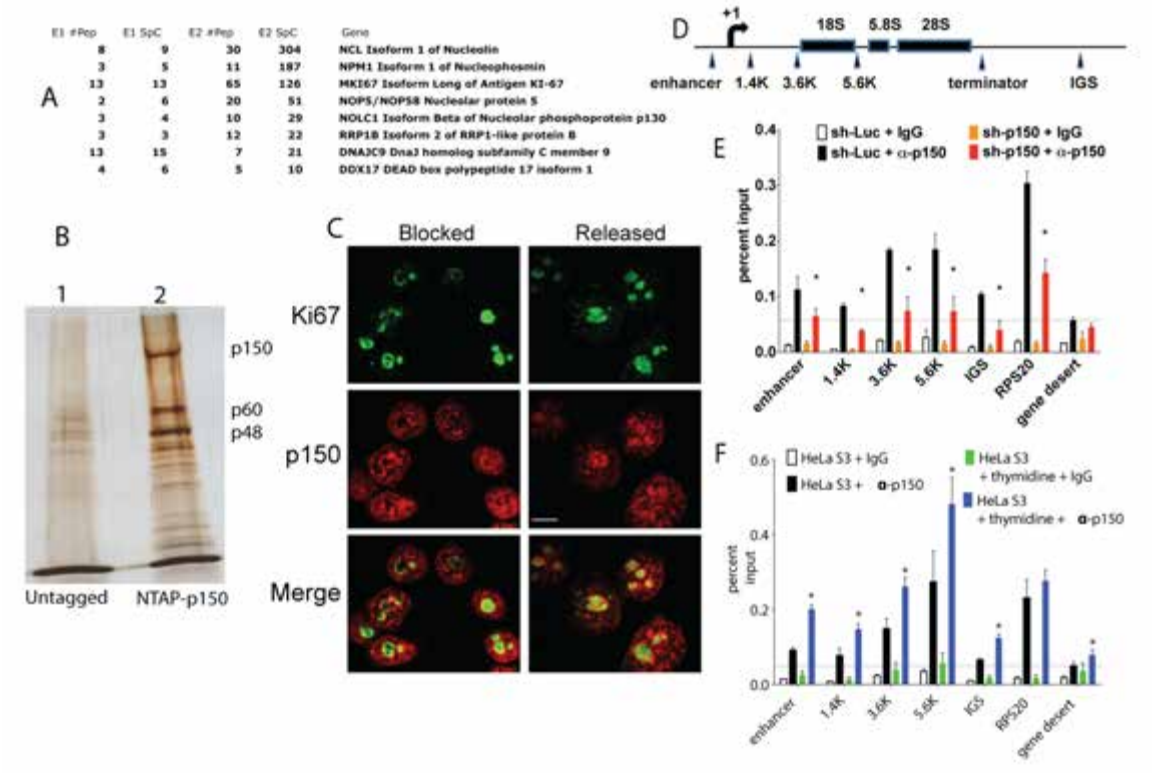


Table 2.1: Mass spectrometry data for NTAP-p150 associated proteins.

Two independent affinity purifications (“exp1” and “exp2”) were performed with NTAP-p150 and untagged control cells in parallel. Proteins listed were detected in both NTAP-p150 preparations, with no more than a single peptide detected in either of the untagged control preparations. Number of distinct peptides detected (#peptides), total number of spectral counts (#spectral cts), sequence coverage (seq. coverage) and spectral counts per kD of molecular weight (cts/kD) are shown for both experiments. Genes identified in red encode CAF-1 subunits or previously known interaction partners. Genes identified in black are novel interaction partners, and those in black with bold font encode proteins that are localized to the nucleolus (NCL, NPM, MKI67, NOP58, NOLC1, RRP1B), participate in rRNA maturation (DDX17), or interact with RRP1B (DNAJC9).

Table 2.1: Mass spectrometry data for NTAP-p150 associated proteins.

exp1# peptides	exp1# spectral cts	exp1. seq. coverage	exp 1 cts/kD	exp2# peptides	exp2# spectral cts	exp2. seq. coverage	exp 2 cts/kD	Length (#aa)	MW	Gene
8	**9**	**14.20%**	**0.117470469**	**30**	**304**	**27.00%**	**3.967891405**	**710**	**76615**	**NCL Isoform 1 of Nucleolin**
44	145	44.20%	1.356078035	33	225	38.40%	2.10425902	956	106926	CHAF1A chromatin assembly factor 1, subunit A
3	**5**	**21.10%**	**0.153491942**	**11**	**187**	**50.90%**	**6.346512812**	**294**	**32575**	**NPM1 Isoform 1 of Nucleophosmin**
13	**13**	**4.50%**	**0.03624249**	**65**	**126**	**25.60%**	**0.351273366**	**3256**	**358695**	**MKI67 Isoform Long of Antigen KI-67**
25	58	47.80%	0.943196787	17	123	45.40%	2.000227668	559	61493	CHAF1B Chromatin assembly factor 1 subunit B
21	51	63.50%	1.070169548	14	61	60.20%	1.280006715	425	47656	RBBP4 Histone-binding protein RBBP4
2	**6**	**4.90%**	**0.100708315**	**20**	**51**	**42.70%**	**0.856020679**	**529**	**59578**	**NOP5/NOP58 Nucleolar protein 5**
3	**4**	**5.50%**	**0.053513853**	**10**	**29**	**9.40%**	**0.387975437**	**709**	**74747**	**NOLC1 Isoform Beta of Nucleolar phosphoprotein p130**
6	7	53.40%	0.615817718	9	23	53.40%	2.023401073	103	11367	Histone H4
3	**3**	**7.30%**	**0.036514119**	**12**	**22**	**24.20%**	**0.267770204**	**740**	**82160**	**RRP1B Isoform 2 of RRP1-like protein B**
13	**15**	**47.70%**	**0.501504514**	**7**	**21**	**34.20%**	**0.702106319**	**260**	**29910**	**DNAJC9 DnaJ homolog subfamily C member 9**
12	19	47.00%	0.912978713	7	19	47.00%	0.912978713	183	20811	CBX3;LOC653972 Chromobox protein homolog 3
1	1	14.60%	0.070816514	6	13	52.30%	0.922312877	130	14121	Histone H2A
10	11	28.50%	0.230029276	6	12	26.40%	0.250941029	425	47820	RBBP7 Histone-binding protein RBBP7
1	1	23.50%	0.064985703	2	11	31.60%	0.714842735	136	15388	Histone H3.2
27	30	19.00%	0.13243279	9	10	9.90%	0.044144263	1960	226530	MYH9 Myosin-9
4	**6**	**7.00%**	**0.074744933**	**5**	**10**	**8.80%**	**0.124574888**	**729**	**80273**	**DDX17 DEAD box polypeptide 17 isoform 1**
5	6	38.70%	0.269966254	3	5	21.50%	0.224971879	191	22225	CBX5 Chromobox protein homolog 5
2	4	4.10%	0.036810042	3	5	4.40%	0.046012552	955	108666	THRAP3 Thyroid hormone receptor-associated protein 3
3	3	17.30%	0.133725595	2	4	17.30%	0.178300793	202	22434	ASF1B Histone chaperone ASF1B

2.3.2: p150 interacts with nucleolar DNA

Based on the abundance of nucleolar proteins detected, we assessed whether p150 resides in the nucleolus by performing immunolocalization studies. Because CAF-1 localization is regulated by cell cycle progression, and is prominently redistributed to DNA replication foci during S phase of the cell cycle (Krude, 1995), we examined synchronized populations, comparing cells blocked at the G1/S phase border via a double thymidine block (Whitfield et al., 2002) and those released into S phase. We used Ki67 as a marker for nucleoli, as described previously (Figure 2.1, C) (MacCallum and Hall, 1999). In these confocal microscopy images, p150 was detected throughout the nucleoplasm, and in the G1/S-arrested cells a subset of p150 was colocalized with Ki67 at the surface of the nucleoli (Figure 2.1, C). More p150 was observed inside nucleoli in the cells released into mid-S phase. We conclude that a subset of cellular p150 colocalized with the nucleolar protein Ki67, even when DNA replication is inhibited.

To assess functional roles of p150, we generated human HeLa S3 cells with a doxycycline-inducible shRNA targeting p150 (p150shRNA-1). A time course after shRNA induction was analyzed by immunoblotting, confirming p150 depletion (Figure 2.2). Upon p150 depletion we observed partial co-depletion of CAF-1 p60, as expected from other studies (Hoek and Stillman, 2003; Ye et al., 2003). In contrast, nucleolar protein levels appeared unaltered during this time course,

with the exception of a mild increase in UBF1 levels at late time points (Figure 2.2, A). Over the first 72 hours there was a mild increase in the doubling time of the p150-depleted cells (from 26 to 33 hr), but no dramatic alteration of the cell cycle profile until 96 hours, when S/G2 phase cells accumulated (Figure 2.2, B-C). Our acute depletion experiments were therefore limited to the first 72 hours after shRNA inductions to minimize the mild growth differences. We also detected no DNA damage checkpoint-mediated phosphorylations (Ciccia and Elledge, 2010) or apoptosis-related PARP cleavage (Duriez and Shah, 1997) during acute depletion of p150 (Figure 2.2, D). These data are consistent with previous studies in which depletion of p150 via RNAi did not activate DNA damage checkpoints (Hoek and Stillman, 2003; Quivy et al., 2008). Likewise, no PARP cleavage was observed in experiments using an alternative depletion reagent, *in vitro* diced “esiRNA” (Surendranath et al., 2013) molecules targeting the 3’UTR of the p150 mRNA (Figure 2.2, E).

We then tested whether p150 is closely associated with 47S rRNA-encoding chromatin via chromatin immunoprecipitation (ChIP) assays (Figure 2.1, D-F), comparing cells expressing a control shRNA targeting luciferase with those expressing p150shRNA-1. In control experiments with pre-immune sera (IgG), no specific enrichments were observed in either cell line. In contrast, using anti-p150 polyclonal sera, we detected enrichments at the rDNA enhancer, at multiple sites within the pol I transcription unit, and within the rDNA intergenic spacer (IGS) (Figure 2.1, E). Additionally, we examined a gene desert region, which displayed

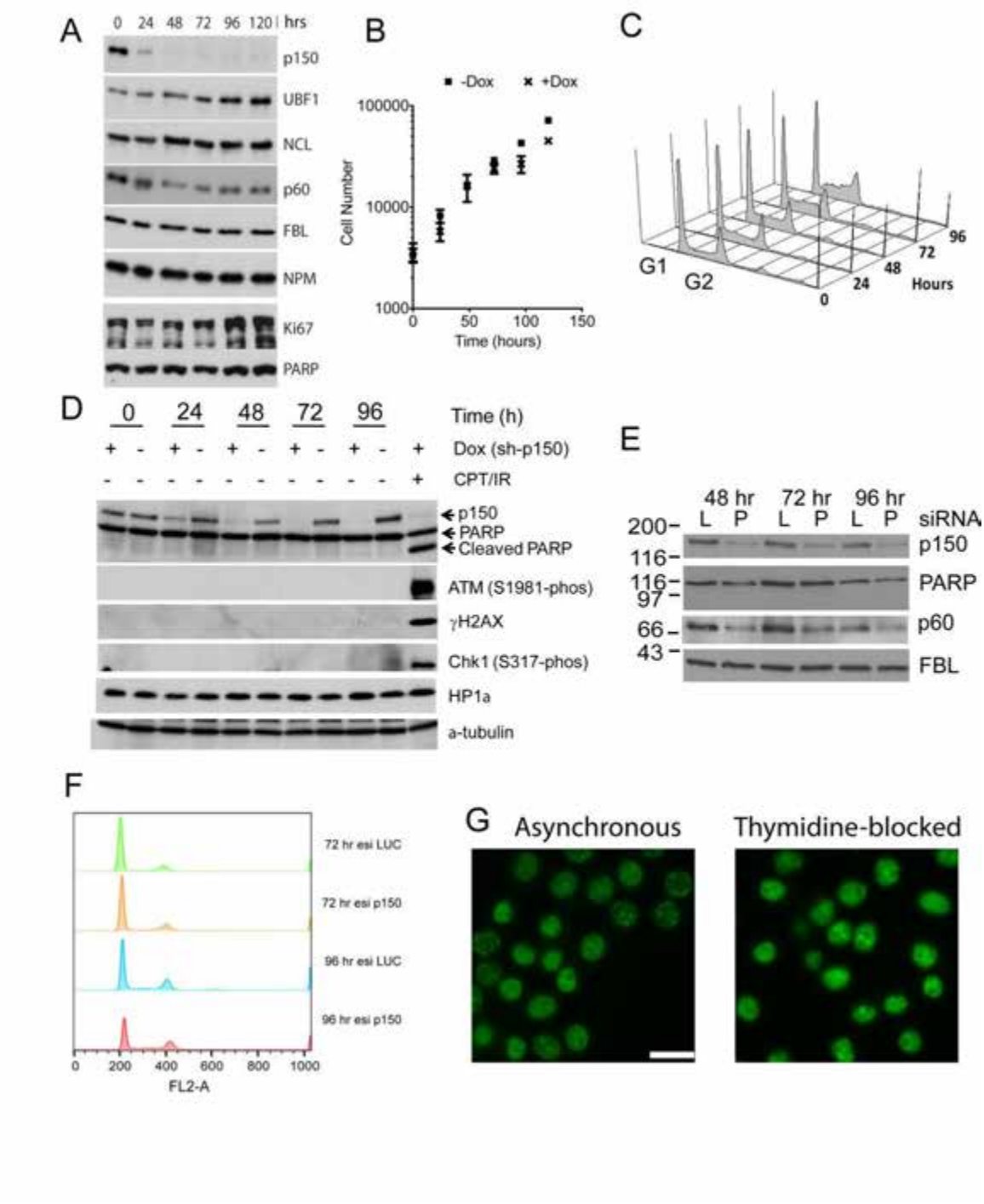
a low level of p150 enrichment. Unlike the other loci tested, the levels of p150 at the gene desert were not significantly reduced upon p150 depletion, suggesting that this represents experimental background. Additionally, because p150 contributes to genome-wide nucleosome deposition during DNA synthesis, we did not expect rDNA to be the only site of enrichment. Indeed, a RNA polymerase II-transcribed gene, *RPS20*, also displayed p150 enrichment, as did other Pol II genes (unpublished observations). We conclude that the 47S rRNA-encoding repeats are one of many sites of p150 localization, consistent with the confocal microscopy data (Figure 2.1, C) showing a subset of p150 localized to nucleoli.

The experiments above were performed with populations of asynchronous cells, so that the observed signals could include contributions from CAF-1 complexes associated with loci transiently during genome duplication in S phase of the cell cycle. Our confocal microscopy images suggested that p150's association with nucleoli would not be limited to S phase (Figure 2.1, C). To explore this via ChIP, we arrested cells at the G1/S phase border via double thymidine treatment. In the arrested cells, p150 was still associated with 47S rRNA-encoding repeats (Figure 2.1, F), but punctate PCNA foci characteristic of mid- and late-S phase were absent (Figure 2.2, G). Indeed, at each of the locations within the rDNA analyzed, but not at the *RPS20* gene, p150 occupancy was significantly increased in the thymidine-arrested cells (Figure 2.1, F). We conclude that p150 is associated with 47S rRNA-encoding repeats, and that these associations are not dependent on ongoing DNA replication.

Figure 2.2: Additional characterization of p150 depletion.

(**A**) Immunoblot analysis of nucleolar and other proteins during a time course of p150 depletion in HeLa S3-Trex cells harboring doxycycline-inducible p150-shRNA1. (**B**) Growth curve of HeLa S3-Trex-p150-shRNA1 cells with or without doxycycline-mediated induction of shRNA. (**C**) Fluorescence-activated cell sorting (FACS) of propidium iodide-stained HeLa S3-Trex-p150-shRNA1 cells during the time course in panel B. (**D**) Checkpoint activation is not observed upon p150 depletion. Western blot analysis of the indicated stress and cell cycle checkpoint proteins in HeLa S3-Trex-p150-shRNA cells. Extracts from cells were collected at the indicated time points with or without doxycycline induction (-/+ Dox). The last lane contains samples that were gamma irradiated (5 Gy, IR) and treated with 6 μM camptothecin (CPT) for 4 hours as a positive control. Cleaved PARP, phosphorylated ATM, γH2AX and phosphorylated Chk1 were only observed in the positive control sample. **(E)** Immunoblot analysis of a time course of p150 depletion in HeLa cells with siRNAs targeting either luciferase (L) or p150 (P). (**F**) FACS analysis of siRNA-treated cells from panel E. (**G**) PCNA staining of asynchronous or thymidine-blocked cells used for the ChIP analysis in Figure 2.1, F. Scale bar is 20 μm.

Figure 2.2 Additional characterization of p150 depletion.



2.3.3: p150 regulates nucleolar protein localization

One of the nucleolar proteins identified in our mass spectrometry data is NPM (Figure 2.1, A), which is a nucleocytoplasmic shuttling protein important for the localization of multiple proteins to the nucleolus (Korgaonkar et al., 2005; Li and Hann, 2013). We therefore tested whether p150 depletion would also affect the localization of nucleolar proteins. We began this analysis with HeLa-derived cells, and we observed that p150 depletion indeed altered the steady-state localization of multiple nucleolar interaction partners we identified by mass spectrometry (Figures 2.3, A-B): NPM, Ki67, and nucleolar phosphoprotein Nopp140 (also known as Nopp130; encoded by the *NOLC1* gene) (Isaac et al., 1998). Additionally, the Pol I transcription factor UBF1(Bell et al., 1988), the Pol I transcription termination/activation protein TTF1 (Längst et al., 1997; Németh et al., 2008), and NCL, which binds rDNA and stimulates Pol I transcription (Rickards et al., 2007) were also redistributed upon p150 depletion. In contrast, the localization of fibrillarin, a rRNA 2'-O-methyltransferase and histone H2A glutamine methyltransferase involved in RNA polymerase I transcription and pre-rRNA processing (Reichow et al., 2007; Tessarz et al., 2014) remained unchanged by p150 depletion, indicating that nucleolar structure was not completely disrupted (Figure 2.3, C). Consistent with the unaltered distribution of fibrillarin, the overall appearance of the 47S rRNA-encoding repeats is not altered upon p150 depletion (see Figures 2.14 and 2.15). We note that in each of the cases we tested (e.g. UBF1, NCL/C23, NPM/B23, Ki67), none of the

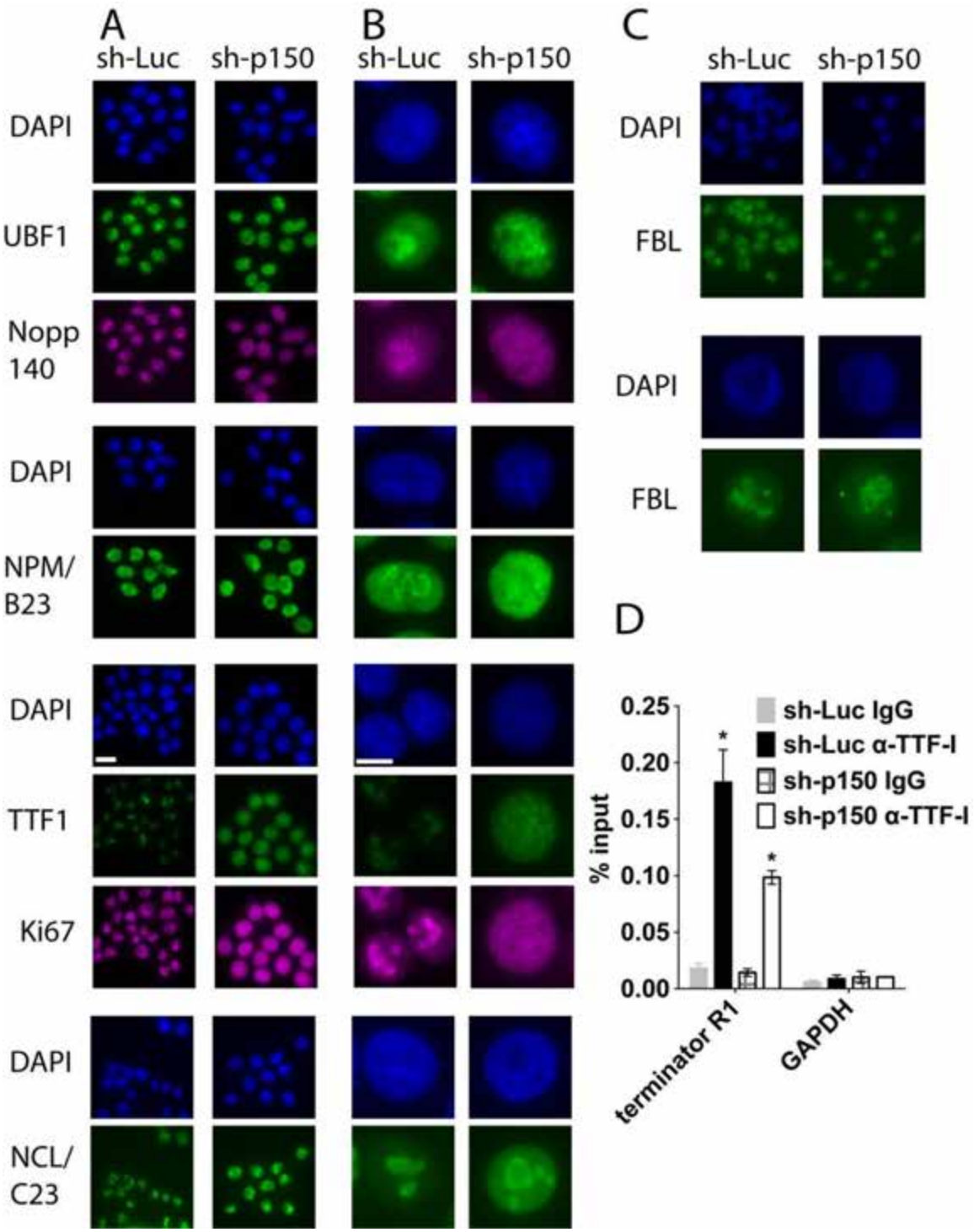
relocalized proteins displayed reduced total protein levels (Figure 2.2). Protein relocalizations were not limited to HeLa S3 cells, because similar results were observed in HT1080 cells (Figure 2.4).

We further explored our finding that TTF-1 is among several nucleolar proteins dispersed upon p150 depletion. TTF-1 is a DNA-binding protein that interacts with the enhancer, promoter, and terminator regions in the rDNA repeats, and stimulates both rDNA transcription and Pol I transcriptional termination (McStay and Grummt, 2008). Furthermore, TTF-1 promotes loop formation between the promoter and terminator regions (Németh et al., 2008), and this three-dimensional interaction is thought to be of central importance to rDNA gene activation (Mayer et al., 2011). We therefore hypothesized that p150 might contribute to localization of TTF-1 to rDNA. Indeed, ChIP analyses demonstrated that p150 depletion reduced the level of TTF-1 at the rDNA terminator (Figure 2.3, D). We conclude that p150 regulates the nucleolar localization of multiple proteins.

Figure 2.3: p150 depletion disrupts localization of multiple nucleolar proteins.

(**A**) HeLa S3-Trex-p150-shRNA1 (“sh-p150”) or Luciferase-shRNA cells (“sh-Luc”) were treated with doxycycline for 72 hours to induce shRNA expression and then prepared for indirect immunofluorescence, staining up to two nucleolar proteins simultaneously in each experiment as indicated. Fields of cells photographed with a 63x objective. Scale bar is 20 μm. (**B**) Representative individual cells from panel (A) were enlarged. Scale bar is 10 μm. (**C**) As in panels A and B, showing the localization of fibrillarin, which remains unchanged upon p150 depletion. (**D**) ChIP analysis of TTF-1 in HeLa S3 cells expressing the indicated shRNAs. Chromatin was precipitated with either non-immune rabbit sera (IgG) or anti-TTF-1 antibodies as indicated and occupancy at the rDNA terminator R1 and the GAPDH gene was measured. The mean amounts of precipitated chromatin from three biological replicates are presented as percentages of input. Error bars represent standard deviations. Asterisks indicate $p < 0.01$ comparing TTF-1 occupancy at R1 in the sh-Luc and sh-p150 samples; $p \geq 0.25$ for all other pairs shown.

Figure 2.3: p150 depletion disrupts localization of multiple nucleolar proteins.



2.3.4: An N-terminal p150 domain incapable of CAF-1 complex formation is sufficient for normal nucleolar protein localization.

To determine whether the entire p150 protein is important for nucleolar protein localizations, we generated cloned, stable cell lines that each express a different V5-epitope-tagged, shRNA-resistant p150-derived transgene (Figure 2.5, A). These cell lines were then subjected to acute RNA-mediated protein depletion experiments. These complementation experiments allowed us to define functional domains and to determine whether p150 depletion phenotypes could be directly attributed to p150 loss rather than indirect effects. Immunoblot analyses of these cells confirmed expression of the expected protein species and demonstrated that we could achieve efficient depletion of endogenous p150 in these cells (Figure 2.5, B). We note that many of these cell lines upregulated transgene-encoded protein levels in response to depletion of endogenous p150, perhaps suggesting a compensatory mechanism.

We tested the ability of the transgene-encoded proteins to interact with the CAF-1 p60 subunit via immunoprecipitation. Consistent with published data (Kaufman et al., 1995; Takami et al., 2007), amino acids 245-938 contained the p60-binding domain (Figure 2.5, C, compare lanes 4 and 10), and deletion of the C-terminal third of p150 (amino acids 642-938) eliminated co-precipitation of p60 (Figure 2.5, C, compare lanes 4 and 6). We also tested transgenes for their ability to maintain cell proliferation over a seven-day period (Figure 2.5, D). Consistent with data from chicken cells (Takami et al., 2007), the C-terminal

region (amino acids 245-938) containing the p60 binding site was required for maintaining cell growth upon loss of endogenous p150. We conclude that these cell lines are useful tools for studying human p150 functional domains.

We then tested the transgene-expressing cells in immunolocalization assays, comparing cells infected with shRNA-encoding lentiviruses to deplete endogenous p150, or luciferase as a control. Immunolocalization of the V5 epitope-tagged proteins confirmed that the majority of cells in these lines expressed detectable transgene products (Figures 2.6 and 2.7). We first confirmed that negative control cells expressing a V5-luciferase transgene and an shRNA targeting luciferase displayed normal nucleolar localization of Ki67 and Nopp140, and that depletion of p150 in the same cells delocalized these proteins (Figures 2.6, A and 2.7, A; see also Figures 2.8-2.13). Conversely, in positive control cells expressing an shRNA-resistant cDNA encoding full-length p150 (aa 1-938), nucleolar localization of Ki67 and Nopp140 was unaltered upon depletion of endogenous p150, indicating functional complementation. We conclude that p150 depletion and not untargeted alterations caused mislocalization of Ki67 and Nopp140.

We also observed that C-terminally deleted p150 transgenes (e.g. 1-641 and 1-310) maintained Ki67 and Nopp140 localization upon depletion of endogenous p150 (Figures 2.6-2.13). Thus, amino acids 1-310 of p150 sufficed for Ki67 and Nopp140 localization, even though this domain is incapable of p60 binding (Figure 2.5, C, compare lanes 4 and 8), These data indicate that the N-terminal

310 amino acids of p150 constitute a domain which is functionally separable from the CAF-1 complex, that we will term p150N.

To test for functionally important regions within p150N, we mutated previously described interaction motifs. These included a non-canonical PIP(Moggs et al., 2000; Rolef Ben-Shahar et al., 2009), a HP1 binding site (Murzina et al., 1999), and a SIM that binds sumoylated proteins (Sun and Hunter, 2012; Uwada et al., 2010). Deletion of the PCNA- or HP1-binding sites resulted in transgenes that supported less robust growth than the wild-type full-length transgene, whereas a point mutation within the SIM did not appear to reduce growth (Figure 2.5, D).

In protein localization experiments analogous to those described above, cells expressing p150 transgenes with mutations in either the PCNA- or HP1-binding motifs displayed no defects in localizing Ki67, Nopp140, or TTF-1 (Figures 2.6-2.13). In contrast, a single I99A amino acid substitution within the SIM reduced the ability of the p150 transgene to maintain Ki67, Nopp140 and TTF-1 localization upon depletion of endogenous p150 (Figures 2.6-2.13). We conclude that the SIM domain within p150N is a key factor for the normal localization of several nucleolar proteins.

Analysis of additional transgenes showed that Ki67 and Nopp140 localization display some difference in the regulation of their localization. Nucleolar localization of Ki67 was largely diminished in cells expressing a large C-terminal fragment of p150 (amino acids 245-938) upon depletion of endogenous p150 (Figures 2.8 and 2.9). Therefore, p150N was necessary and sufficient for Ki67

localization. In contrast, nucleolar localization of Nopp140 was not only maintained by p150N, but by the C-terminus as well (Figures 2.10 and 2.11). Nevertheless, the Nopp140 localizing function within p150N depended on the SIM motif (Figure 2.7), and mutation of the SIM motif reduced nucleolar localization of Nopp140 even within the context of the full-length p150 transgene (Figure 2.10). These data indicate that the SIM is an important, but not unique domain for localizing Nopp140. Additionally, a localization pattern similar to Nopp140 was observed for TTF-1 (Figures 2.12 and 2.13).

Figure 2.4: p150 depletion alters nucleolar protein localization in HT1080 cells.

(A) HT1080-Trex-sh-Luciferase (“sh-Luc”) or HT1080-Trex-p150-shRNA1 (“sh-p150”) cell lines were treated with doxycycline for 72 hours to induce shRNA expression and then prepared for indirect immunofluorescence, staining for two different proteins in each experiment as indicated. Images were taken with a 63x objective. **(B)** Immunoblot analysis of p150 depletion by p150-shRNA1 in HT1080-Trex cells. Internal loading control was alpha-tubulin (TUBA).

Figure 2.4: p150 depletion alters nucleolar protein localization in HT1080 cells.

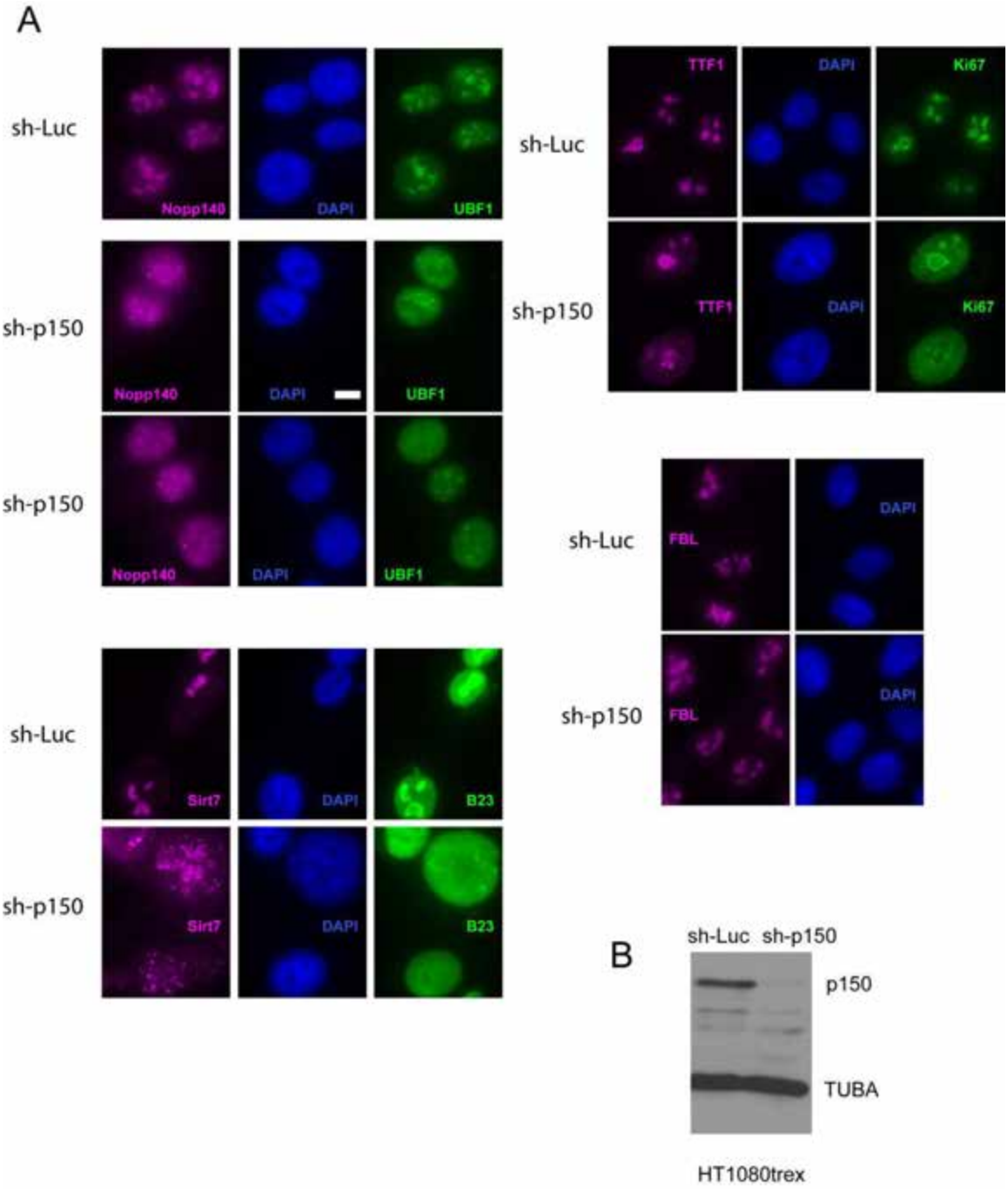


Figure 2.5: Domain analysis of human p150.

(**A**) Diagram of transgenes introduced into HeLa cells. Colored boxes indicate the V5 epitope tags (yellow), PEST region (red), low complexity regions KER (blue) and ED (green), dimerization region (D, orange), the N-terminal PCNA interaction peptide (PIP, cyan), and the HP1 binding site (pink). The I99A point mutation that inactivates the SUMO-interaction motif (SIM, red asterisk) and silent mutations rendering the transgenes resistant to RNAi (shR, black asterisks) are indicated. Regions previously shown to be sufficient for *in vitro* chromatin assembly and p60 interaction are drawn below the top diagram. (**B**) Immunoblot analysis of V5-tagged transgene-expressing cell lines, in two independent experiments (lanes 1-10 and 11-28). Cells were infected for 72 hours with lentiviruses expressing either sh-Luciferase (L, odd numbered lanes) or sh-p150 (P, even numbered lanes) and whole cell extracts were separated on 10% SDS-PAGE gels. After transfer, blots were probed with anti-p150 to detect endogenous p150, anti-V5 to detect transgene products, and anti-tubulin (TUBA) or anti-fibrillarin (FBL) antibodies as loading controls. Arrowheads indicate full-length p150 protein. **(C)** Interaction between p150 transgene products and p60. Extracts from the indicated V5-tagged transgene-expressing cell lines were immunoprecipitated with anti-V5 antibodies. Input extracts (In, odd numbered lanes) and immunoprecipitates (IP, even numbered lanes) were resolved on 10% SDS-PAGE gels, transferred to membranes and probed with anti-p150, V5, and p60 antibodies. Arrowhead indicates full-length p150 protein; asterisks indicate anti-V5 IgG bands in IP samples detected by the anti-mouse secondary antibody. Note that the 1-310 transgene co-migrates with the IgG heavy chain. **(D)** V5-tagged RNAi-resistant p150 transgenes were tested for the ability to maintain cell proliferation in the presence of either sh-Luciferase (”sh-Luc”) or p150-shRNA1 (“sh-p150”) in HeLa cells. Cells (4500) were plated in 6-well dishes and infected with the indicated lentivirus, and selection for infected cells began 48 hours post infection. Seven days post infection, cell proliferation was assessed by crystal violet staining.

Figure 2.5: Domain analysis of human p150.

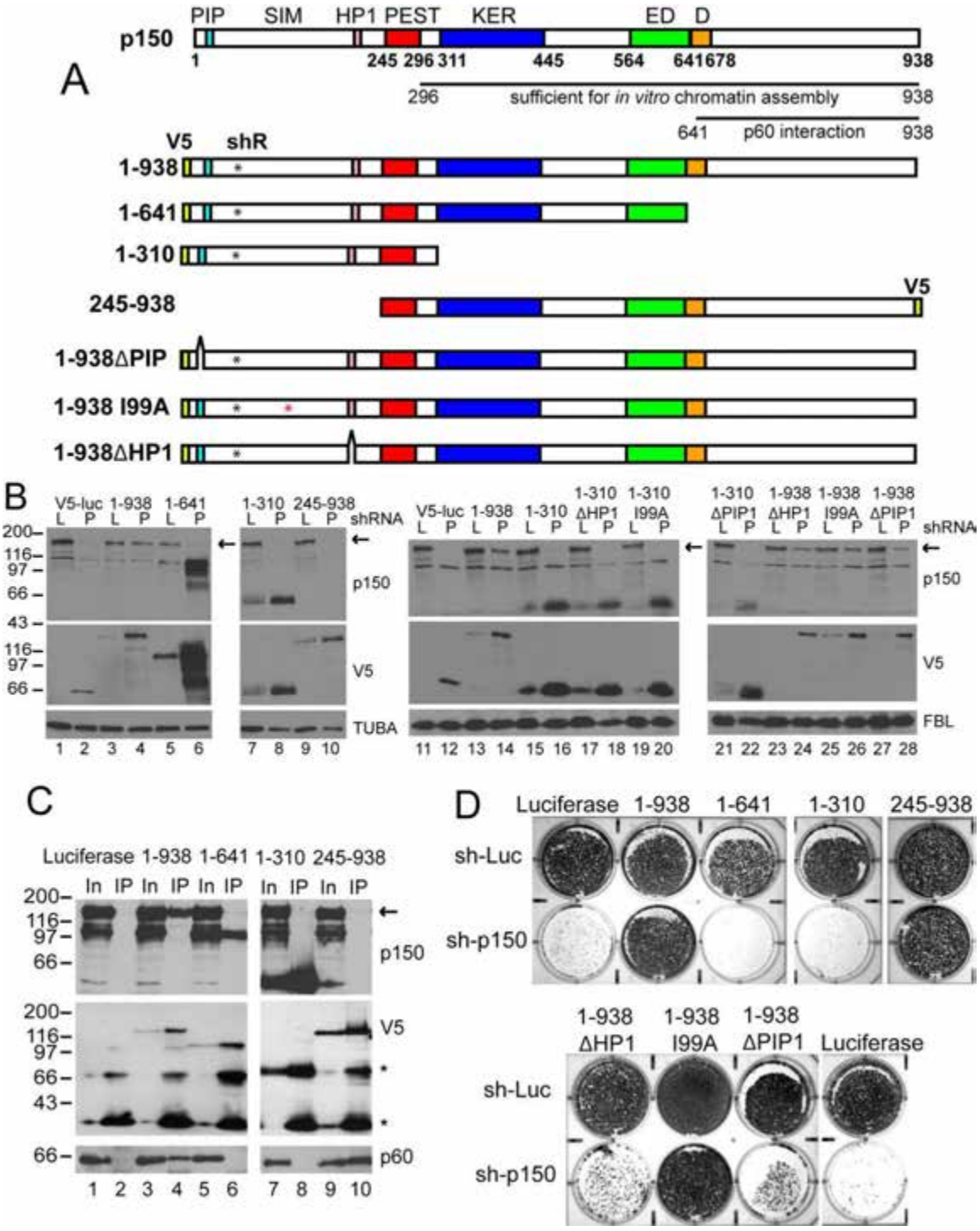


Figure 2.6: The p150 SUMO-interaction motif (SIM) is required to maintain nucleolar Ki67 localization.

HeLa cell lines expressing the indicated V5-tagged transgenes (A, luciferase; B, 1-938; C, 1-310; D, 1-310-ΔHP1; E, 1-310-I99A; F, 1-310-ΔPIP1; see Figure 2.5, A) were infected with lentiviruses encoding the indicated shRNAs (sh-luciferase or sh-p150) and prepared for indirect immunofluorescence 72 hours later. Scale bar is 20 μm.

Figure 2.6: The p150 SUMO-interaction motif (SIM) is required to maintain nucleolar Ki67 localization.

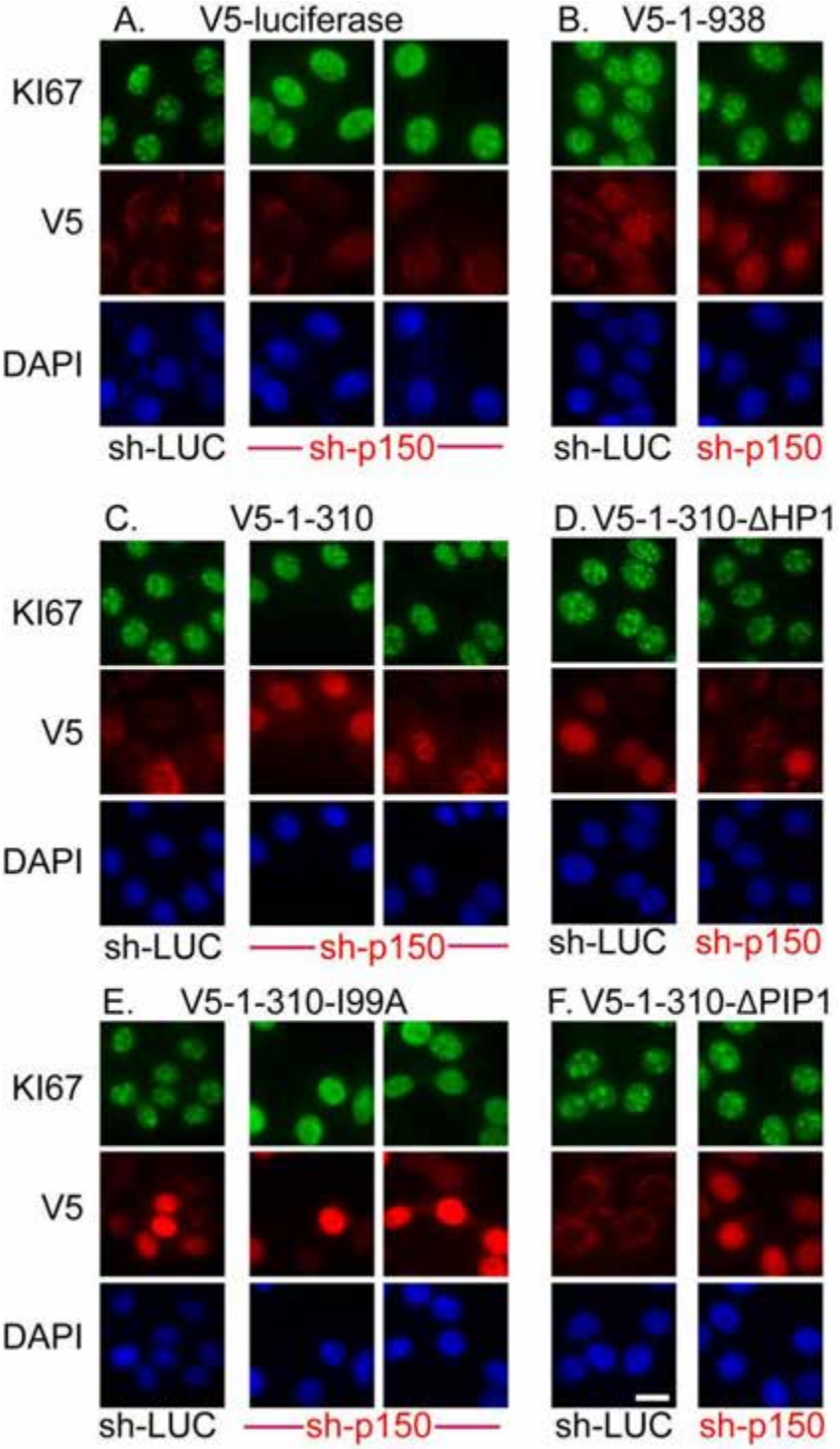


Figure 2.7: The p150 SIM is required to maintain nucleolar Nopp140 localization.

As in Figure 2.6, HeLa cell lines expressing the indicated V5-tagged transgenes were infected with lentiviruses encoding the indicated shRNAs (sh-luciferase or sh-p150) and prepared for indirect immunofluorescence 72 hours later. Scale bar is 20 μm.

Figure 2.7: The p150 SIM is required to maintain nucleolar Nopp140 localization.

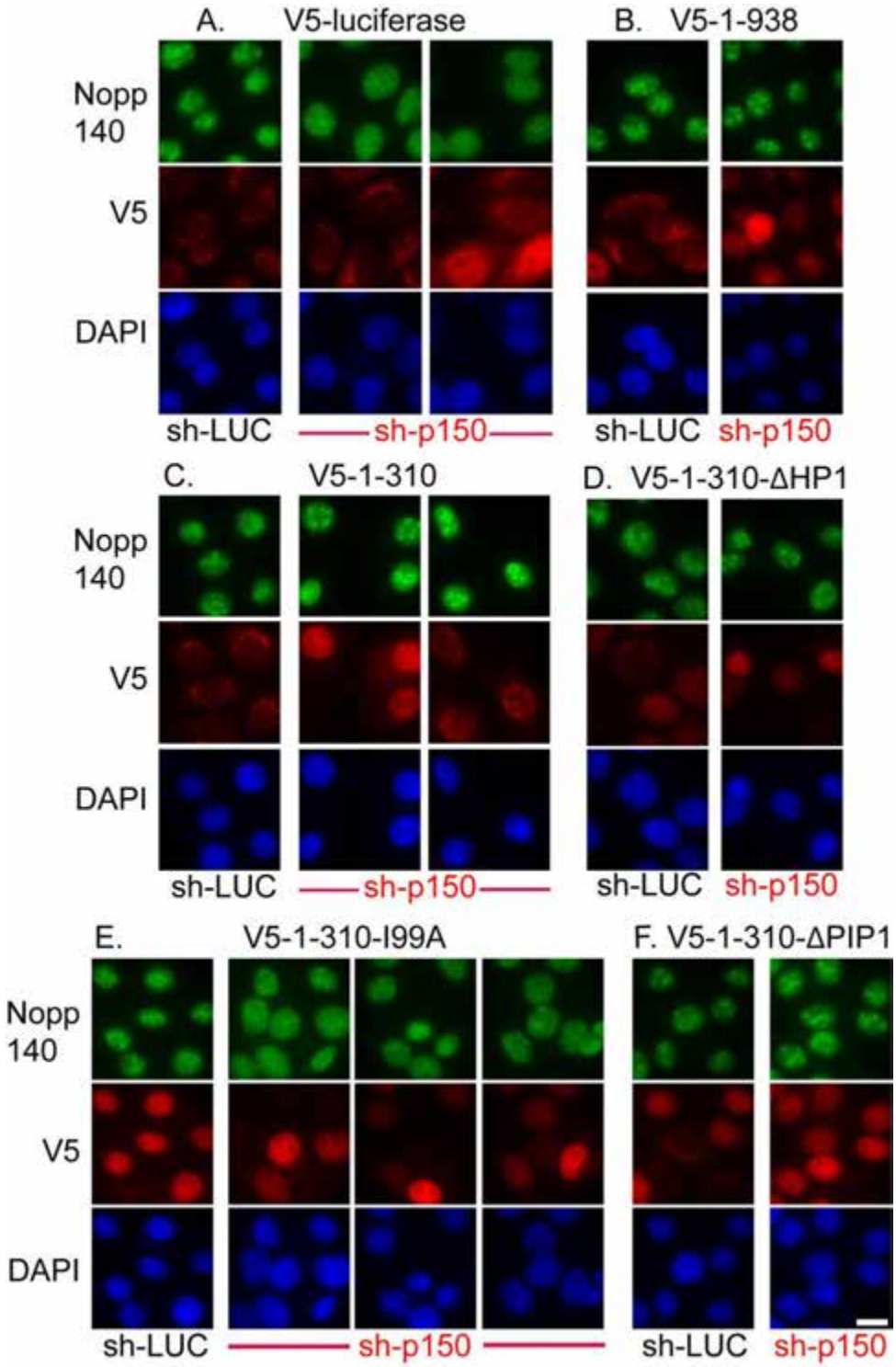


Figure 2.8: Analysis of Ki67 localization in additional cell lines, performed as in Figure 2.7

Additional HeLa cell lines expressing the indicated p150 transgene were depleted of endogenous p150 as performed in Figure 2.7. Scale bar is 20 μm.

Figure 2.8: Analysis of Ki67 localization in additional cell lines, performed as in Figure 2.7

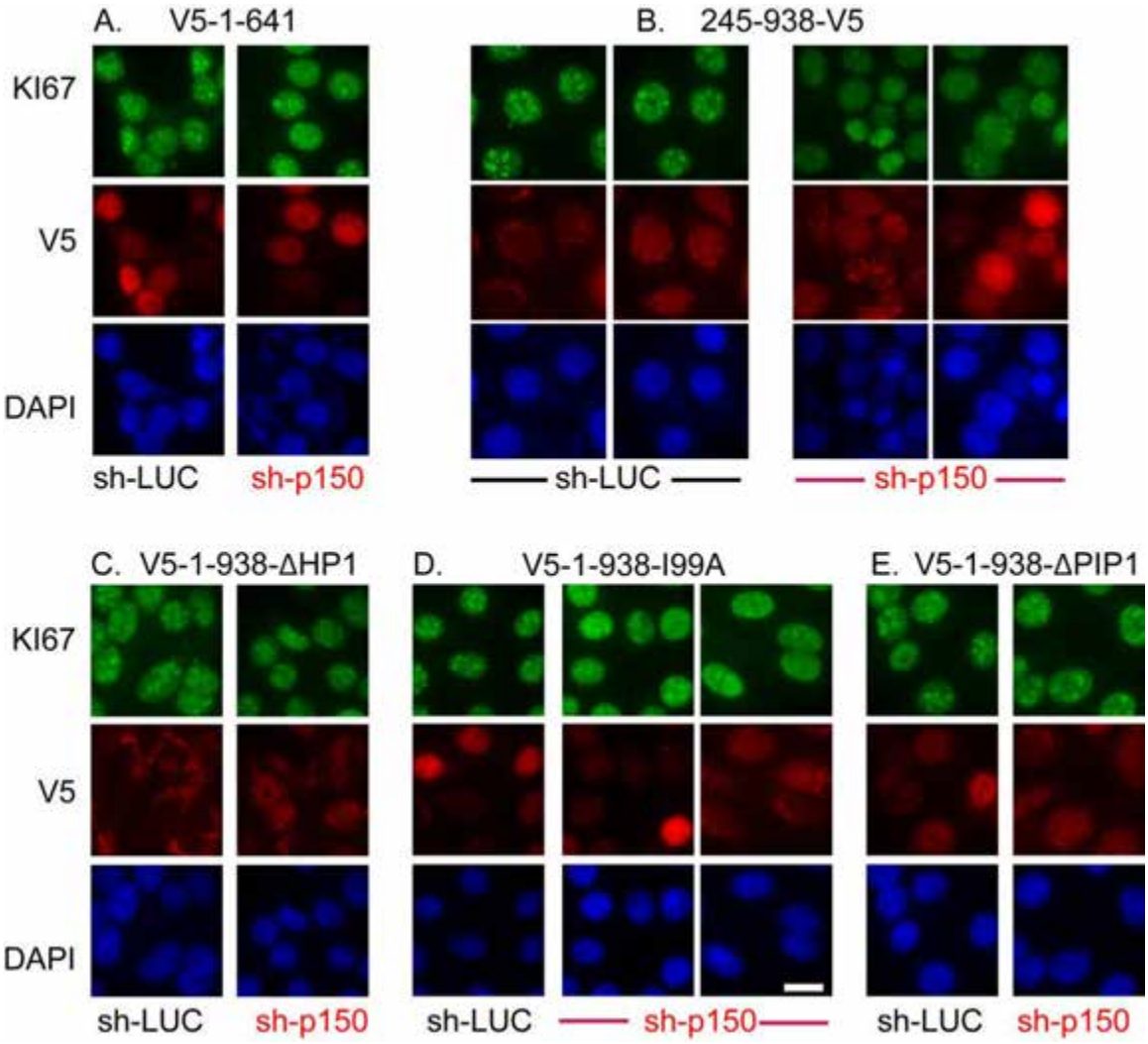


Figure 2.9: Densitometric analysis of Ki67 localization.

Fluorescence images of individual cells from the panels in Figure 2.6 and Figure 2.8 were scanned as shown on the left, and fluorescence intensity was plotted (right). Cells displaying reduced focal accumulation of Ki67 upon p150 depletion have plots highlighted in red. Scale bar is 10 μm.

Figure 2.9: Densitometric analysis of Ki67 localization.

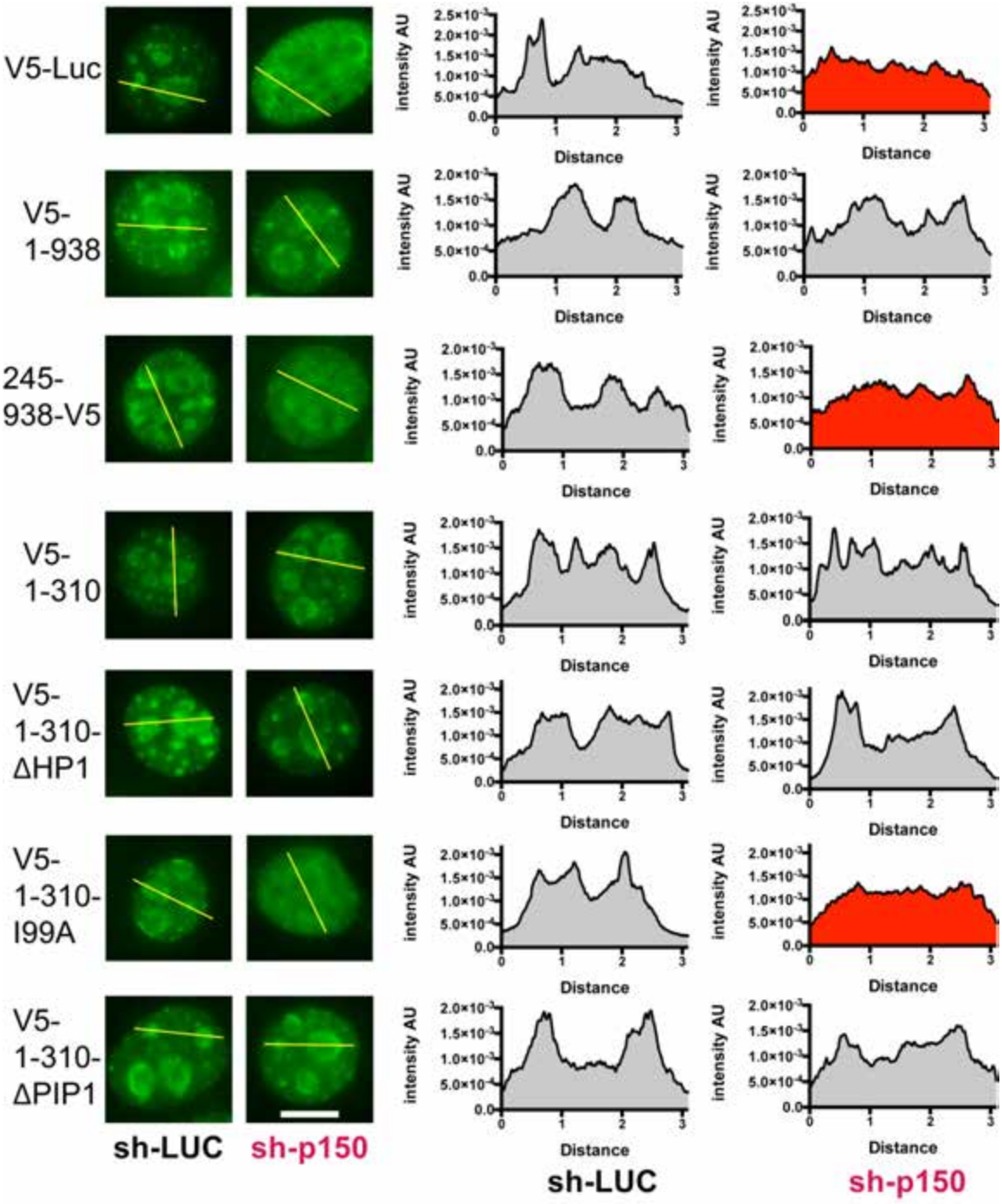


Figure 2.10: Analysis of Nopp140 localization in additional cell lines, performed as in Figure 2.7 (panels A-E).

Additional HeLa cell lines expressing the indicated p150 transgene were depleted of endogenous p150 as performed in Figure 2.7. In panel F, we performed a control immunofluorescence experiment in uninfected cells to determine whether the anti-V5 antibody recognized any cellular structures in the absence of a transgene. Scale bar is 20 μm.

Figure 2.10: Analysis of Nopp140 localization in additional cell lines, performed as in Figure 2.7 (panels A-E).

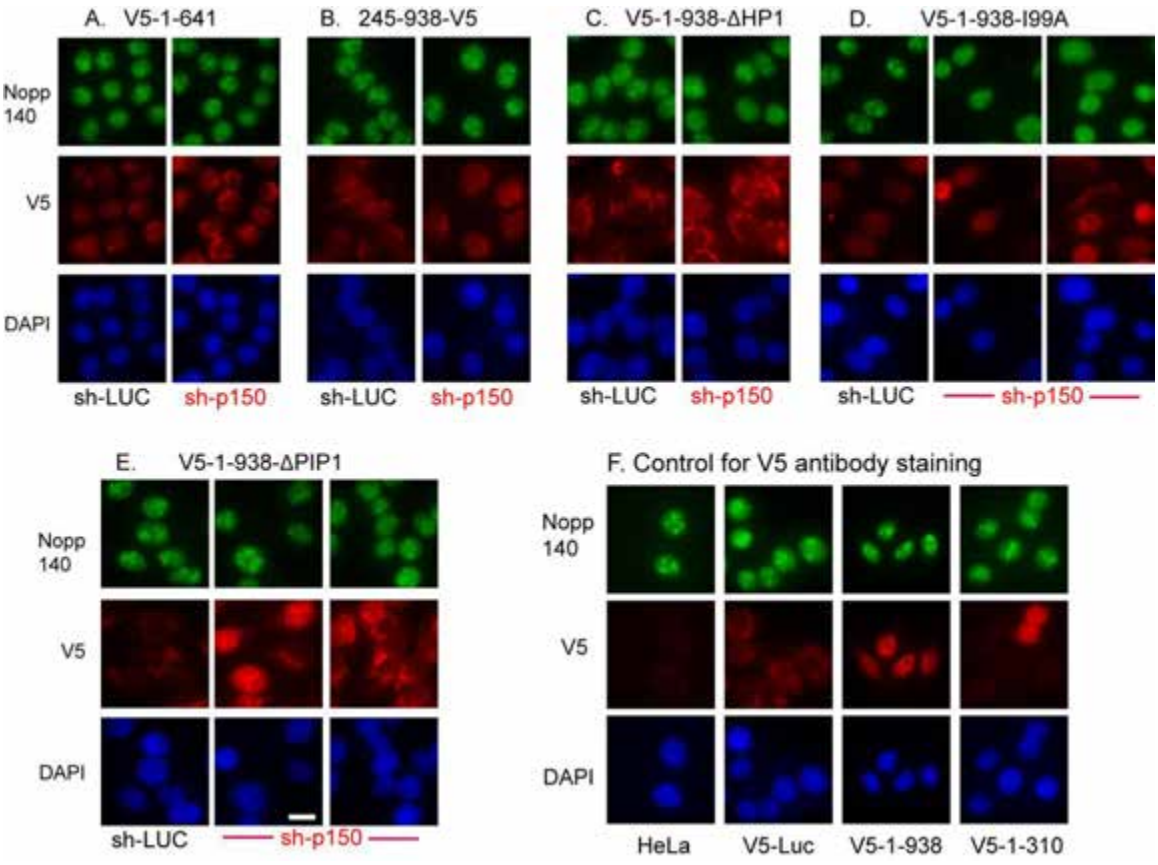


Figure 2.11: Densitometric analysis of Nopp140 localization.

Fluorescence images of individual cells from the panels in Figure 2.7 and Figure 2.10 were scanned as shown on the left, and fluorescence intensity was plotted (right). Cells displaying reduced focal accumulation of Nopp140 upon p150 depletion have plots highlighted in red. Scale bar is 10 μm.

Figure 2.11: Densitometric analysis of Nopp140 localization.

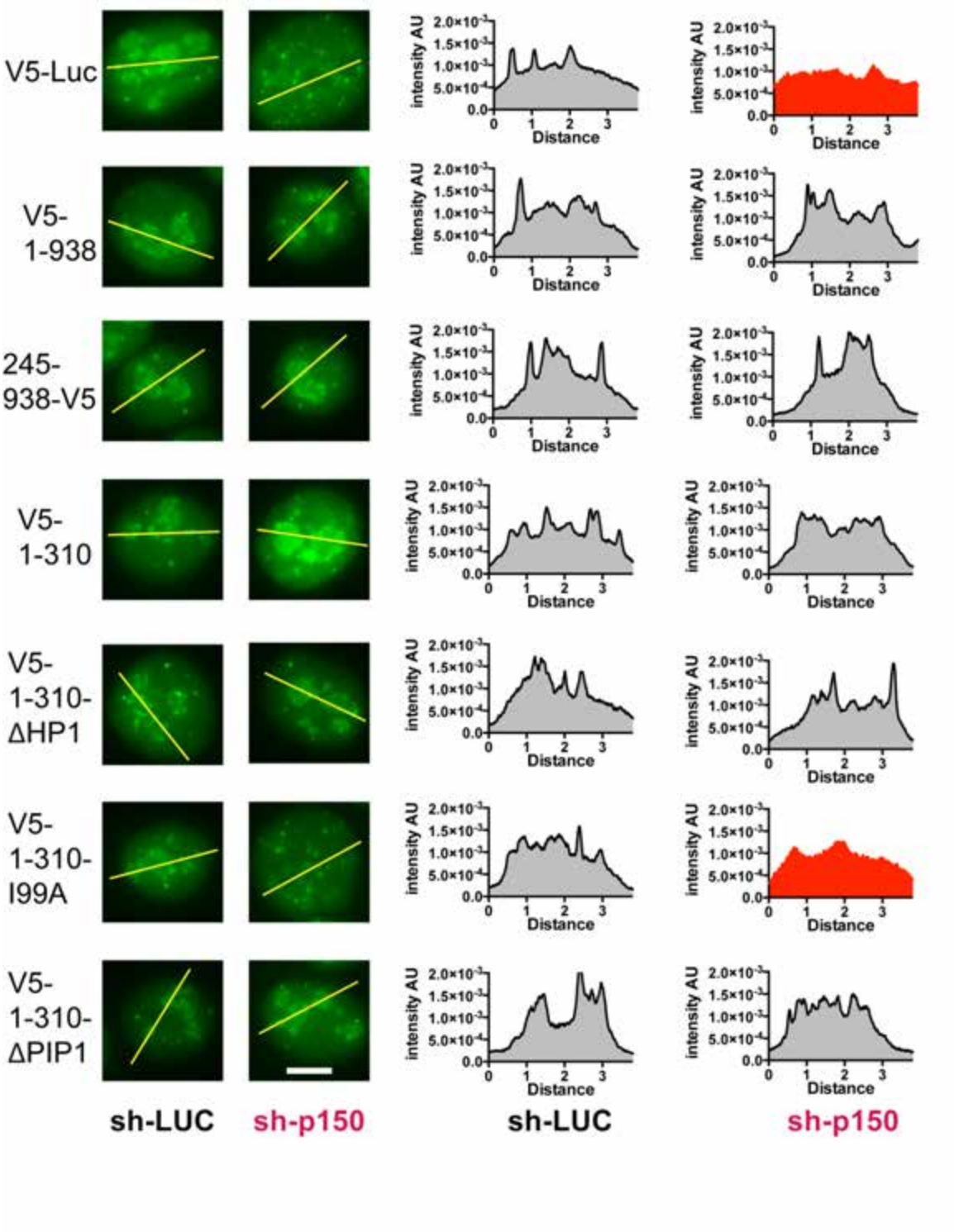


Figure 2.12: Analysis of TTF-1 localization performed as is figures 2.7 and 2.8.

Scale bar is 20 μm.

Figure 2.12: Analysis of TTF-1 localization performed as is figures 2.7 and 2.8.

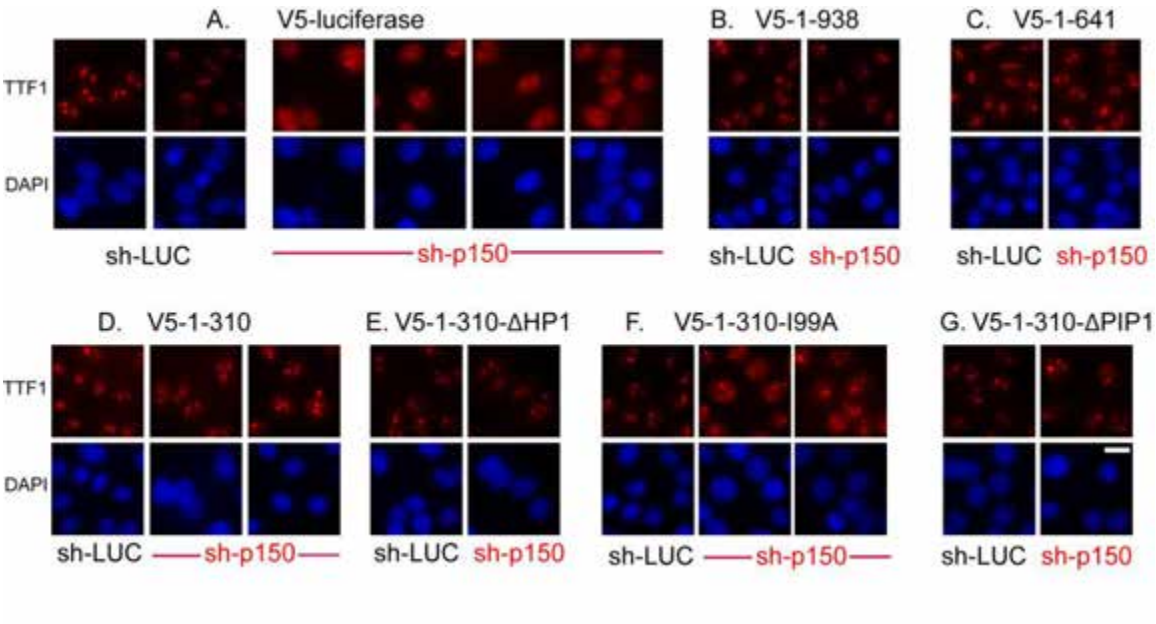
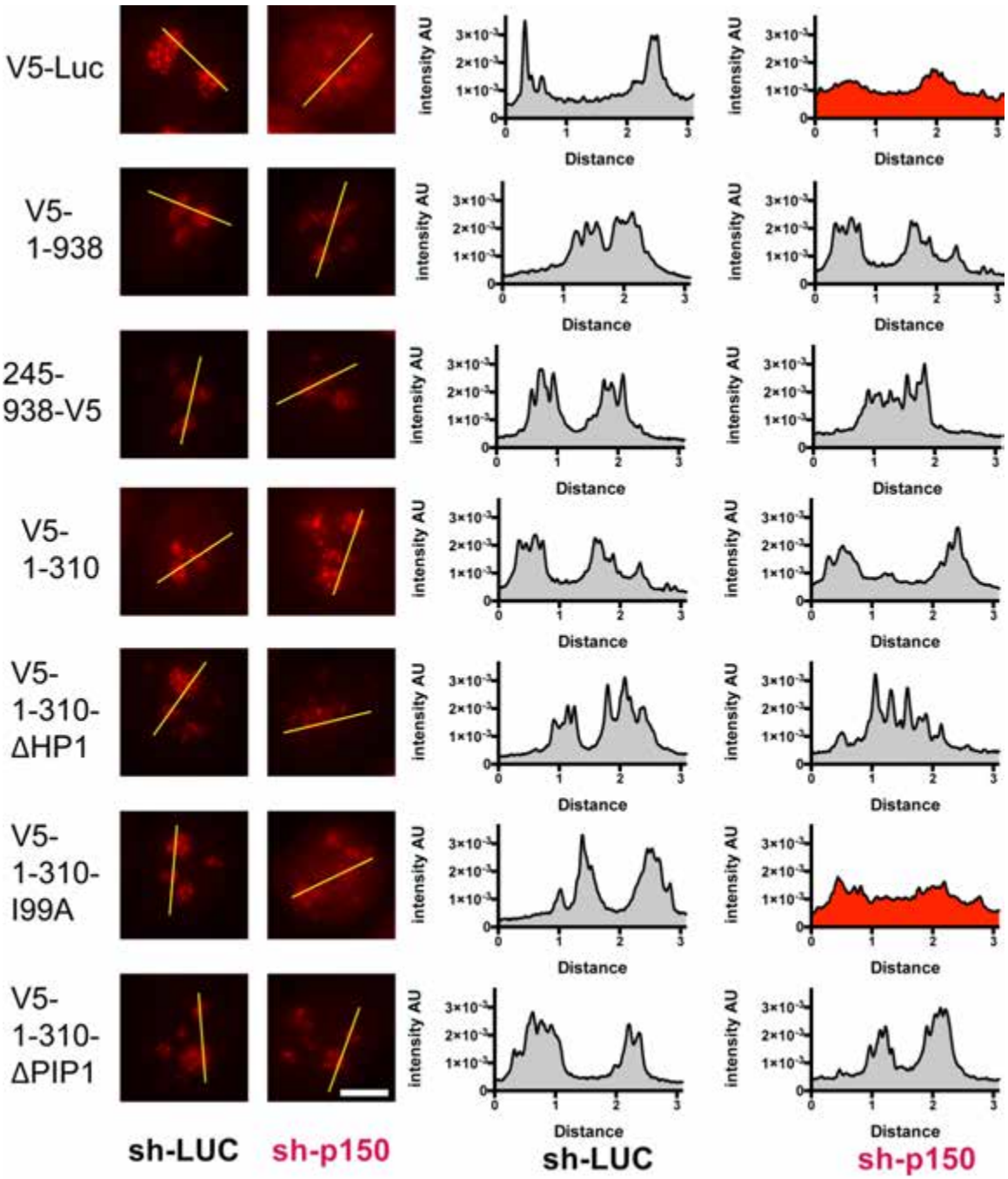


Figure 2.13: Densitometric analysis of TTF-1 localization.

Fluorescence images of individual cells from the panels in Figure 2.12 were scanned as shown on the left, and fluorescence intensity was plotted (right). Cells displaying reduced focal accumulation of TTF-1 upon p150 depletion have plots highlighted in red. Scale bar is 10 μm.

Figure 2.13: Densitometric analysis of TTF-1 localization.



2.3.5: The p150 N-terminus promotes interchromosomal interactions of the 47S rRNA-encoding repeats.

Deep sequencing experiments have detected genomic regions preferentially associated with nucleoli (van Koningsbruggen et al., 2010; Németh et al., 2010). Among the NADs discovered were several types of repetitive DNA including centromeric satellite DNA, D4Z4 repetitive DNA elements from the telomeric regions of chromosomes 4q and 10q, and the array of 5S rDNA genes from chromosome 1q. Therefore, using two-color DNA FISH experiments, we tested whether these long-range interchromosomal associations with 47S rRNA-encoding repeats were affected by p150 depletion. FISH experiments were initially performed in MCF-10A cells, because these have a flattened morphology we found more conducive to rDNA hybridization. In MCF10A cells expressing a control sh-Luciferase hairpin RNA, we observed that ~30-40% of 10q telomere, 5S rDNA array, and alpha satellite alleles associated with 47S rRNA-encoding repeats (Figures 2.14, A-C). In contrast, a negative control BAC probe lacking NAD sequences displayed the expected background of ~10% association (Németh et al., 2010). In cells expressing sh-p150, we observed a statistically significant decrease in nucleolar associations for all three loci NAD-containing loci tested, but no change was observed for the negative control. To extend this finding beyond immortalized cell lines, we then tested whether p150-dependent nucleolar associations could be detected in primary human cells. Using foreskin fibroblasts, we observed that the association of alpha satellite DNA with nucleoli

was indeed significantly reduced upon depletion of p150 (Figure 2.14, D-G). In these cells, detection of nucleoli was more robust using an anti-fibrillarin antibody rather than a 47S rRNA-encoding repeat probe. We conclude that p150 is important for nucleolar association of several repetitive DNAs in both primary and transformed human cells.

We then tested whether the p150N protein fragment would suffice for maintaining these chromosomal interactions. In HeLa cells expressing the control V5-luciferase transgene, we again observed frequent associations of alpha satellite DNA with the 47S rRNA-encoding repeats, which were reduced upon p150 depletion (Figure 2.15, A-B). A similar loss of alpha satellite-rDNA associations was observed in cells expressing a large C-terminal p150 fragment (amino acids 245-938; Figures 2.15, A and 7C). In contrast, cells expressing p150N (amino acids 1-310) maintained these associations upon depletion of endogenous p150, measured either as the total number of allele associations (Figure 2.15, A), or the number of alleles associated per cell (Figure 2.15, D). Taken together, our data indicate that the p150N domain of p150 is sufficient for promoting efficient nucleolar protein localizations and interchromosomal associations.

We next tested how point mutations within p150N affected alpha satellite interactions with the nucleolus. As observed in the protein localization experiments (Figures 2.6 and 2.7), the I99A but not the PCNA- or HP1-binding site mutations reduced the nucleolar associations (Figures 2.16, A-D). To test

whether SUMO conjugation itself is important for nucleolar chromosome interactions, we used siRNAs to transiently deplete p150, or Ubc9, the E2 enzyme required for all SUMO conjugation events in human cells (Jentsch and Psakhye, 2013), or SUMO2 itself. RT-PCR analysis confirmed reduction of UBC9 and SUMO2 mRNA levels (Figure 2.16, G). The p150 depletion confirmed that siRNA-mediated targeting of the p150 mRNA via a different sequence than recognized in shRNA-mediated depletions still significantly reduced alpha satellite-nucleolar interactions. Additionally, we observed significantly reduced interactions upon either UBC9 or SUMO2 depletion. We conclude that both a SUMO interaction motif within the p150N domain and the SUMO conjugation machinery contribute to efficient nucleolar protein localizations and interchromosomal interactions.

Figure 2.14: Higher order interactions of rDNA chromatin are altered upon p150 depletion.

(**A**) DNA FISH analysis of MCF10A-tetkrab cells expressing the indicated shRNAs. Three biological replicate experiments were performed, with mean % nucleolar association and standard deviations graphed. Probes analyzed were a chromosome 10q BAC (10q, n (total alleles assayed) = 332 for sh-Luc, 262 for sh-p150), a 5S rDNA-containing BAC (5S, n = 312 for sh-Luc, 352 for sh-p150), alpha satellite DNA from chromosome 17 (αSat 17, n = 288 for sh-Luc, 306 for sh-p150), and negative control BAC (- Control, n=314 for sh-Luc, 306 for sh-p150) that was previously reported to be unassociated with nucleoli (Nemeth *et al.*, 2010). The p-values comparing the sh-Luc and sh-p150 samples for each probe are indicated, with p values < 0.05 indicated in red, demonstrating statistical significance. (**B**) Fluorescence microscopy images of representative cells from an experiment from panel (A). rDNA is colored red, the 10q BAC is green and DAPI is blue. Scale bar is 5 μm. (**C**) Immunoblot of representative whole cell extracts from an experiment in panel A, with tubulin as the loading control. (**D**) Immuno-FISH analysis of primary human foreskin fibroblasts treated either with Luciferase control or p150-targeted sh-RNAs. Cells were treated with anti-fibrillarin antibodies followed by hybridization with a αSat 17 probe. N (total alleles assayed) = 324 for sh-Luc, 308 for sh-p150. (**E**) Data from panel (D), plotting the percentage of cells displaying the indicated numbers of αSat 17 alleles associated with fibrillarin. n (total cells assayed) = 162 for sh-Luc, 154 for sh-p150. (**F**) Fluorescence microscopy images of representative cells from an experiment from panel (D). Fibrillarin is in green and the αSat 17 probe is red. Scale bar is 5 μm. (**G**) Immunoblot of representative whole cell extracts from an experiment in panel D, with fibrillarin as the loading control.

Figure 2.14: Higher order interactions of rDNA chromatin are altered upon p150 depletion.

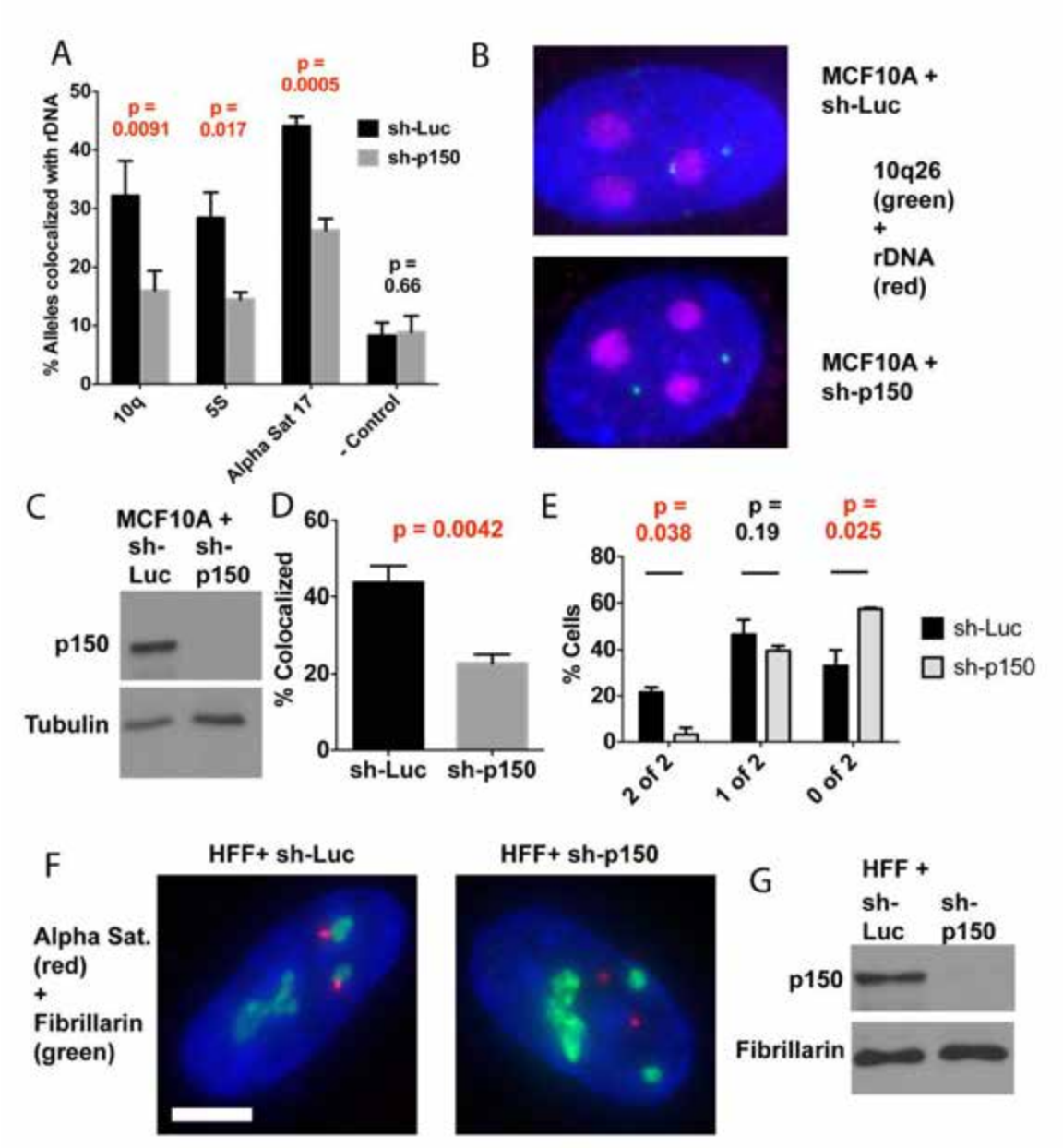


Figure 2.15: The p150 N-terminus is necessary and sufficient for nucleolar interchromosomal associations.

(**A**) DNA FISH analysis of the association between αSat 17 and rDNA in HeLa cells expressing the indicated V5-tagged transgenes (Luciferase, p150N (amino acids 1-310), or p150C (amino acids 245-938)). The percentage of αSat 17 alleles colocalized with the rDNA is indicated, with mean and standard deviations from three experiments. For V5-Luciferase cells, n (total alleles assayed) = 471 for sh-Luc, 480 for sh-p150. For V5-p150N cells, n = 525 for sh-Luc, 489 for sh-p150. For V5-p150C cells, n = 450 for sh-Luc, 468 for sh-p150. p values comparing the sh-Luc and sh-p150 samples are indicated, demonstrating statistically significant rescue by the p150N but not the p150C transgene. (**B-D**) Data from the experiment in panel (A) was replotted to display the number of αSat 17 alleles per cell associated with the rDNA. Note that these HeLa-derived lines have three copies of chromosome 17. For V5-Luciferase cells, n (total cells examined) = 157 for sh-Luc, 160 for sh-p150. For V5-p150N cells, n = 175 for sh-Luc, 163 for sh-p150. For V5-p150C cells, n = 150 for sh-Luc, 156 for sh-p150. Comparisons for which $p \leq 0.05$ are indicated by asterisks, and a number sign indicates $p \leq 0.01$. (**E**) Fluorescence microscopy images of representative cells from an experiment from panel (A). rDNA is colored red, the αSat 17 is green and DAPI is blue. Scale bar is 5 μm.

Figure 2.15: The p150 N-terminus is necessary and sufficient for nucleolar interchromosomal associations.

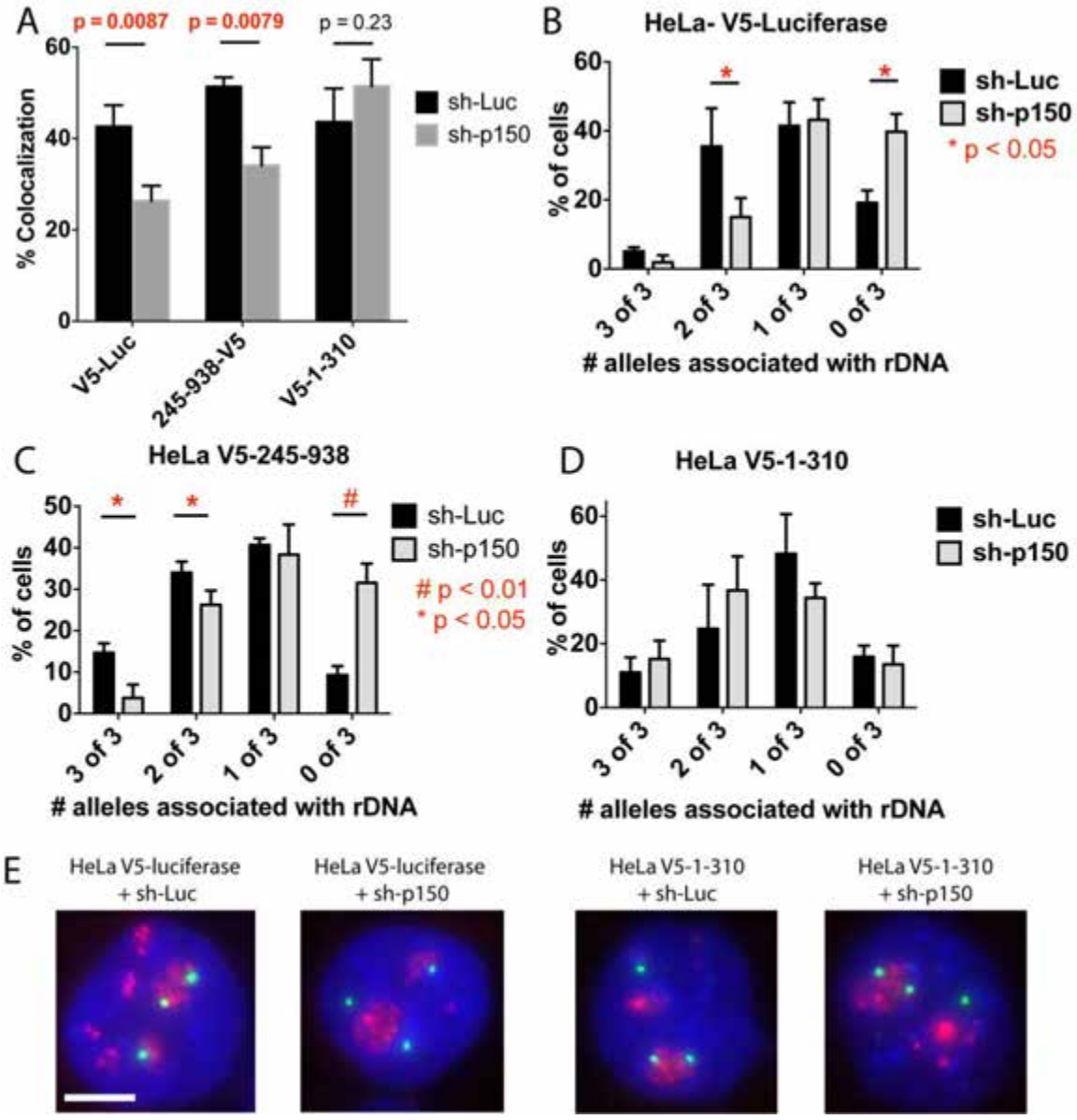
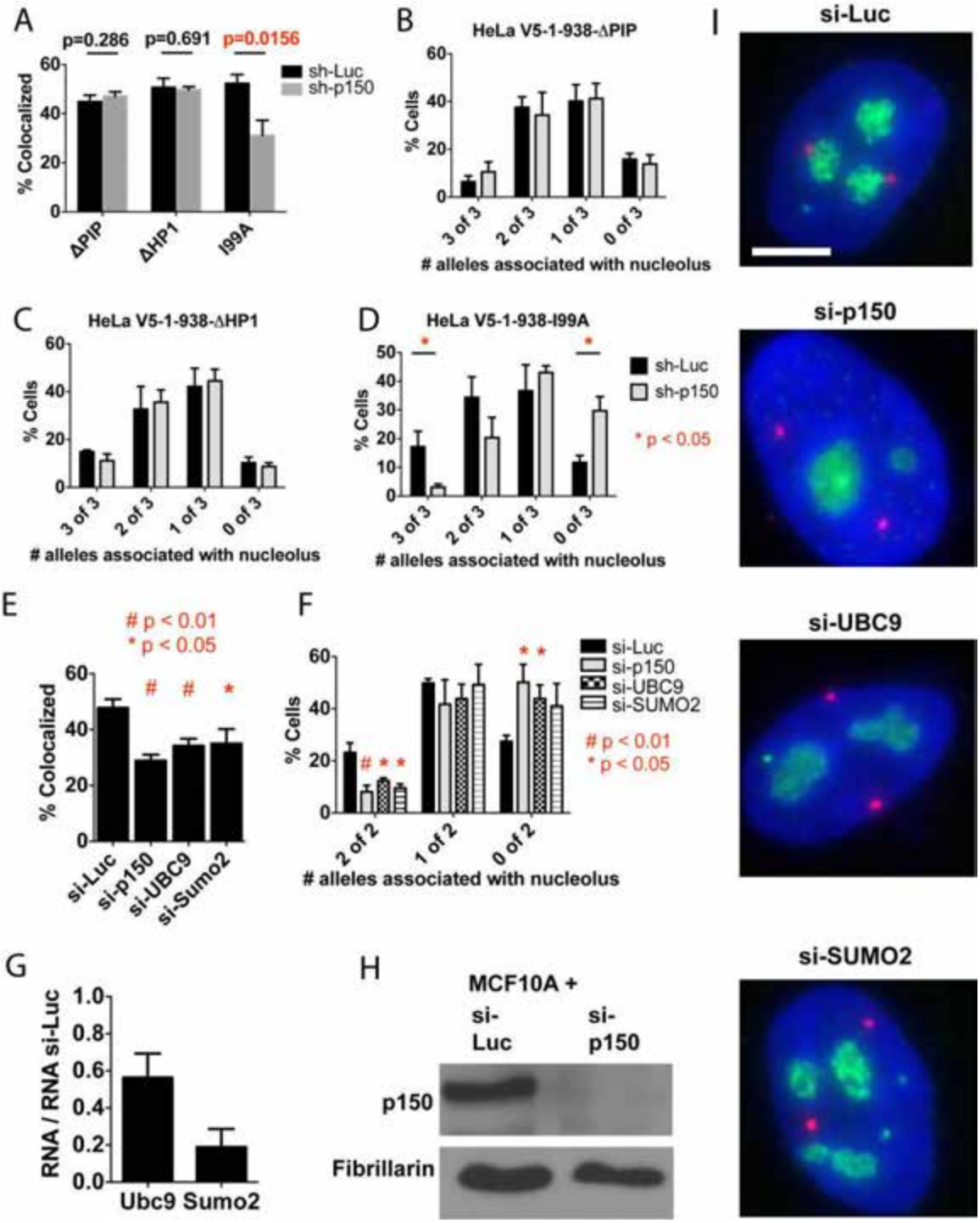


Figure 2.16: The p150 SIM and sumoylation proteins are required for nucleolar interchromosomal associations.

(**A**) ImmunoFISH analysis of the association between αSat 17 and fibrillarin in HeLa cells expressing the indicated V5-tagged transgene derivatives of full-length p150. The percentage of αSat 17 alleles colocalized with fibrillarin is indicated, with mean and standard deviations from three experiments. For ΔPIP cells, n (total alleles assayed) = 510 for sh-Luc, 477 for sh-p150. For ΔHP1 cells, n = 522 for sh-Luc, 513 for sh-p150, and for I99A cells, n = 486 for sh-Luc, 480 for sh-p150. p values comparing the sh-Luc and sh-p150 samples are indicated, demonstrating statistically significant rescue by the ΔPIP and ΔHP1 but not the I99A transgenes. (**B-D**) Data from the experiment in panel (A) was replotted to display the number of αSat 17 alleles per cell associated with the rDNA. Note that these HeLa-derived lines have three copies of chromosome 17. For ΔPIP cells, n (total cells examined) = 170 for sh-Luc, 159 for sh-p150. For ΔHP1 cells, n = 174 for sh-Luc, 171 for sh-p150. For I99A cells, n = 162 for sh-Luc, 160 for sh-p150. Comparisons for which $p \leq 0.05$ are indicated by asterisks. (**E**) ImmunoFISH analysis of MCF10A cells treated with the indicated siRNAs. The percentage of αSat 17 alleles colocalized with fibrillarin is indicated, with mean and standard deviations from three experiments. n (total alleles assayed) = 328 for si-Luciferase-treated cells, n = 346 for si-p150-treated cells, n = 324 for si-UBC9-treated cells, and n = 342 for si-SUMO2-treated cells. p values comparing the sh-Luc and other samples are indicated, demonstrating statistically significant reductions in association by each of the three test depletions, with p values indicated. (**F**) Data from the experiment in panel (E) was replotted to display the number of αSat 17 alleles per cell associated with fibrillarin. Note that these MCF10A-derived lines have two copies of chromosome 17. (**G**) qPCR analyses of esiRNA treatments demonstrating reduced steady-state mRNA levels in the targeted cells. (**H**) Immunoblot of representative whole cell extracts from an experiment in panel E, with fibrillarin as the loading control. (**I**) Fluorescence microscopy images of representative cells from an experiment from panels E-F. Fibrillarin is colored green, the αSat 17 is red and DAPI is blue. Scale bar is 5 μm.

Figure 2.16: The p150 SIM and sumoylation proteins are required for nucleolar interchromosomal associations.



2.4: Discussion

2.4.1: A separable functional domain within the CAF-1 p150 N-terminus

We show here that the N-terminal domain of p150 (amino acids 1-310) is sufficient to maintain nucleolar protein and interchromosomal associations, and thereby constitutes a distinct and separable functional domain. Because p150 residues 1-310 cannot bind the CAF-1 p60 subunit, and lacks the previously described dimerization motif within p150 (Quivy et al., 2001) (Figure 2.5), these data suggest that the canonical three-subunit CAF-1 complex is not required for these novel functions. We note that previous proteomic analysis of nucleoli detected p150 but not p60 (Ahmad et al., 2009), consistent with the idea of nucleolar functions for p150 separate from CAF-1. We also note that a previous proteomic analysis of p150 detected interacting proteins largely non-overlapping with those reported here (Hoek et al., 2011), raising the possibility that differences in the epitope tags used or other experimental details can favor retention of distinct subsets of the protein interactions of p150.

In all eukaryotic species, CAF-1 is a complex of three conserved subunits, all of which are required for *in vitro* nucleosome assembly activity (Kaufman et al., 1995; Verreault et al., 1996). Additionally, roles outside of the CAF-1 complex have been described for individual subunits. For example, p60 was recently shown to act as a protamine deposition factor independent of CAF-1 during fruit fly spermatogenesis (Doyen et al., 2013). p48 is a histone H4-binding (Murzina et al., 2008; Song et al., 2008) subunit of many complexes involved in chromosome

biology (Kuzmichev et al., 2002; Martínez-Balbás et al., 1998; Zhang et al., 1999). Two functions for p150 independent of CAF-1 have been described. First, p150, but not p60, is required for efficient replication of HP1-rich pericentric heterochromatin in mouse cells, and this activity requires the canonical HP1-binding site on p150 (Quivy et al., 2008). Second, p150 but not p60 stimulates transcription from the major immediate early promoter (MIEP) of human cytomegalovirus (Lee et al., 2009). In the latter studies, the p150 N-terminal 310 amino acids (p150N) were shown to be an activation domain for MIEP transcription (Lee et al., 2009). Although subregions within p150N were not tested in that system, those findings are consistent with our conclusion that p150N can act as a separable domain with distinct functions. Here, we show that human p150N has important structural roles outside of the context of viral infection, maintaining normal nucleolar protein localization and interchromosomal interactions. Therefore, the C-terminal two-thirds of human p150 essential for formation of the nucleosome assembly complex CAF-1 are appended to a separable domain that regulates the structure of the nucleolus and the interconnectivity of the human genome.

2.4.2: The SIM domain links human p150N to nucleolar structures.

Our studies show the p150 SIM domain is required for nucleolar macromolecular associations. This p150 SIM domain was previously shown to bind the highly homologous SUMO-2 and SUMO-3 proteins, but not SUMO-1

(Uwada et al., 2010). Furthermore, mutational analysis of the p150 SIM was shown to alter association of SUMO-2 and SUMO-3 with DNA replication foci. However, the converse was not true, because acute depletion of SUMO2/3 did not affect p150 association with replication foci. These data suggested that p150 recruits SUMO2/3 to DNA replication foci via the SIM domain. We do not yet know whether those observations are related to those reported here. Our data suggest that the interaction of p150 with the rDNA is not limited to S phase of the cell cycle (Figures 2.1 and 2.2), and the p150 SIM domain appears dispensible for p150's contribution to cell proliferation (Figure 2.5, D). Also, we observe that strong inhibition of rDNA transcription with actinomycin D does not impair the alpha satellite-nucleolar interaction (Figure 2.17), although in other studies different NAD-nucleolar interactions were variably reduced upon similar treatments (Németh et al., 2010). Therefore, we are currently investigating how these chromosome interactions are dynamic with regards to transcription and growth control, and whether they are cell cycle regulated. We also note that a large number of sumoylated proteins reside in the nucleolus (Finkbeiner et al., 2011; Westman et al., 2010), and we are currently exploring whether particular protein interactions depend on the p150 SIM domain.

A previously published protein alignment suggested that Cac1, the budding yeast homolog of human p150, also contains a putative SIM (Uwada et al., 2010). Subsequent analysis in the Hunter laboratory showed that the SIM in the N-terminus of human p150 is a "type B" or "VIDLT" class of SIM that is often found

as a dominant SIM in multi-SIM proteins (Sun and Hunter, 2012). The p150 N-terminal SIMs are also of the canonical type B in other animals, including mammals and the sea urchin *S. purpuratus* (Figure 2.18). In contrast, this SIM is altered from the type B consensus in frogs, zebrafish and chickens, and insects. The budding yeast SIM sequence lacks the characteristic aspartate at position 3 that is critical for high affinity binding, and no apparent type B SIM sequences could be identified in fission yeast, worms, or the plants *Arabidopsis thaliana* or *Triticum urartu*. Future studies will be required to clarify whether and how nucleolar associations are mediated by p150 homologs in other organisms.

In that regard, it is of particular interest that recent papers have shown a progressive loss of 45S rDNA copies in *Arabidopsis thaliana* mutants in lacking the CAF-1 p150 or p60 subunits (Mozgova *et al.*, 2010). Further, these mutants display a loss of partitioning of silent 45S rDNA copies into the nucleoplasm (Pontvianne et al., 2013), while 5S rDNA remains stable in its copy number and localization. We do not observe altered DNA-FISH signals with a 47S-encoding rDNA probe in human cells (Figures 2.14 and 2.15), so we do not presently have evidence for a similar mechanism in humans. Also, as mentioned above, there is no discernable SIM in *A. thaliana* p150. However, we cannot rule out less dramatic reorganization of 47S rDNA that would have escaped detection in our FISH experiments, and the full range of contributions of p150 to the structure and function of nucleolar chromatin in human cells remains an open an interesting avenue for exploration.

Figure 2.17: Rapid inhibition of RNA polymerase I does not affect association of alpha-satellite DNA to the nucleolar periphery.

(A) Fluorescent microscopy images detecting a pulse of incorporation of the UTP analog 5-ethynyl uridine (EU) (15 minutes) during treatment with the RNA Pol II inhibitor alpha-amanitin (20 μg/mL for 4 hours), actinomycin D (50 ng/mL for 15 minutes, which selectively inhibits RNA polymerase I), or both. Scale bar is 20 μm. (**B**) Graphical representation of 3 biological replicate DNA-FISH experiments, comparing the association of chromosome 17 alpha-satellite with rDNA during incubation with actinomycin D or no treatment.

Figure 2.17: Rapid inhibition of RNA polymerase I does not affect association of alpha-satellite DNA to the nucleolar periphery.

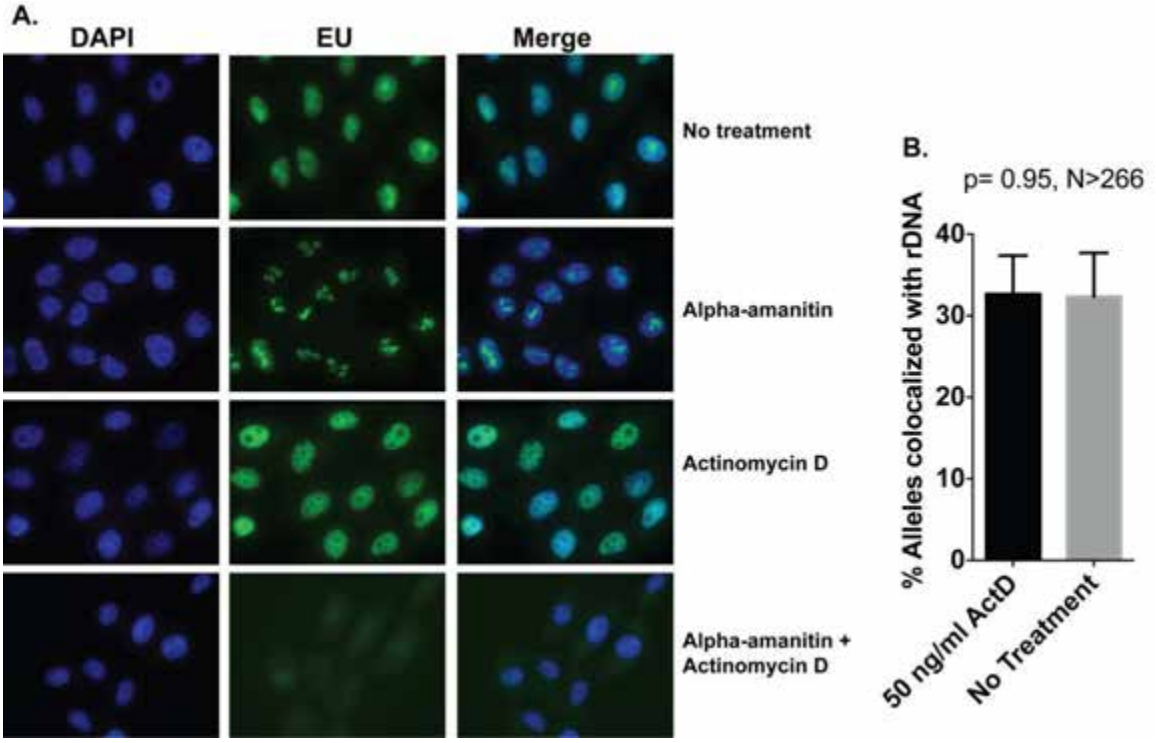
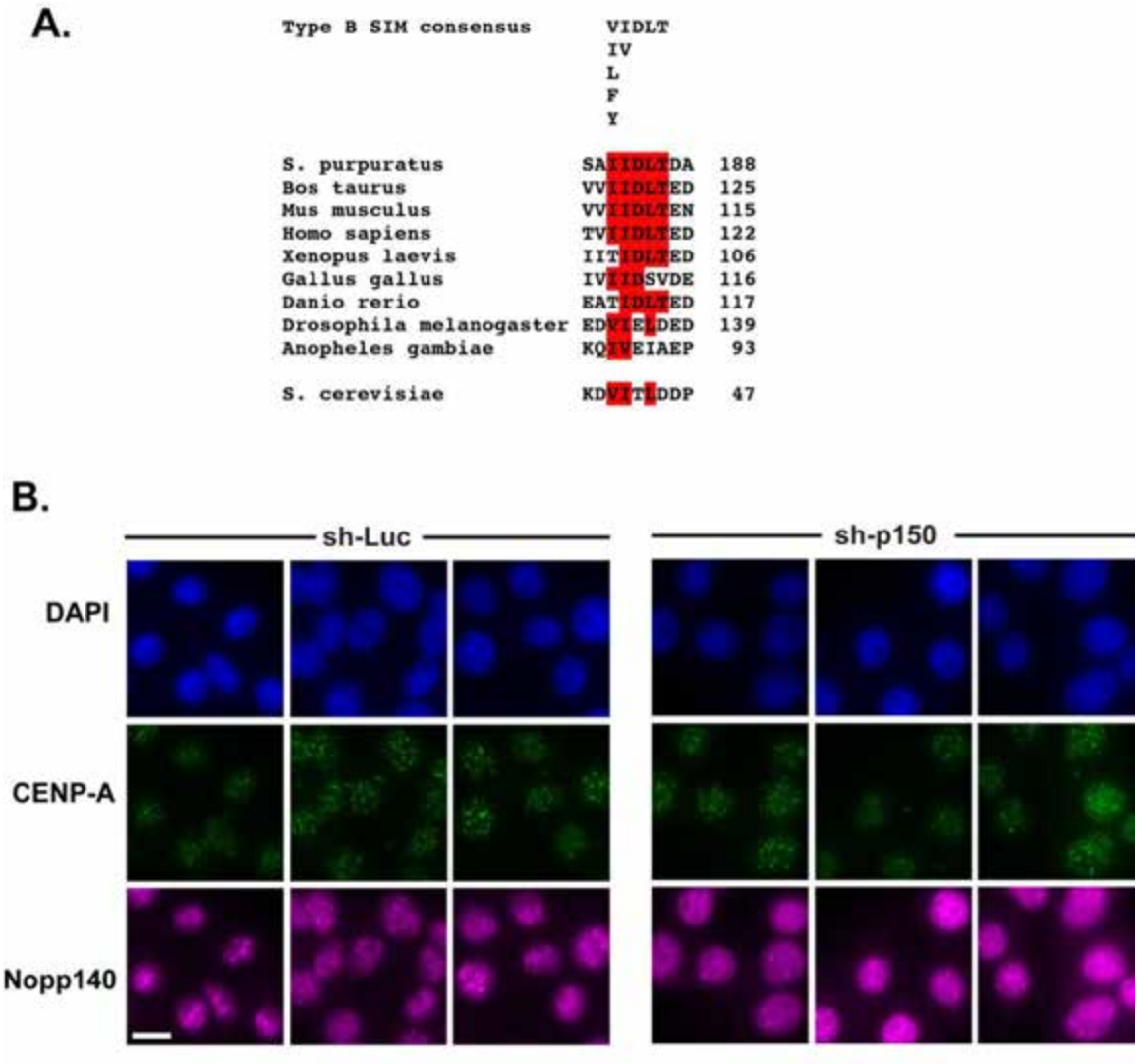


Figure 2.18: Conservation of the type B SIM domain in p150 homologs.

(A) The consensus sequence is from (Sun and Hunter, 2012). Residues conforming to the consensus are highlighted in red. Numbers at the end of each sequence indicate amino acid position. **(B) CENPA localization does not change upon p150 depletion.** Indirect immunofluorescence localization of CENPA (green) in HeLa cells infected with lentiviruses expressing either sh-Luciferase or sh-p150 for 72 hours, as indicated. Cells were costained with anti-Nopp140 antibodies (magenta) to confirm nucleolar protein relocalization in cells depleted of p150. Fields of cells were imaged with a 63x objective.

Figure 2.18: Conservation of the type B SIM domain in p150 homologs.



2.4.3: Higher-order interactions of nucleolar chromatin

Several connections between heterochromatin, centromeric DNA, and the nucleolus have been described previously. For example, in Drosophila, the nucleolar protein Modulo, a NCL homolog, affects formation of centromeric chromatin (Chen et al., 2012). Conversely, depletion of Drosophila HP1 causes dispersal of the rDNA and nucleolar proteins, including fibrillarin (Peng and Karpen, 2007). We note that vertebrate p150 homologs include an HP1-binding domain (Murzina et al., 1999) that is within the p150N domain, although we do not observe fragmentation of rDNA upon depletion of p150 in human cells (Figure 2.15). Other links between the nucleolus and centromeric DNA in Drosophila include recent studies showing that nucleoplasmin (NLP), a nucleophosmin-related protein, is required is required for centromere clustering and anchoring of centromeric DNA to nucleoli (Padeken et al., 2013). Also, both Drosophila NLP (Padeken et al., 2013) and human NPM (Foltz et al., 2006) interact with the centromere-specific histone CENP-A. Biochemical interactions between CENP-C and UBF1 (Pluta and Earnshaw, 1996) and colocalization of centromeric proteins with the nucleolus (Ochs and Press, 1992; Wong et al., 2007) have also been described. Together, these data, and other data reviewed recently (Padeken and Heun, 2014), suggest conserved links among nucleoli, heterochromatin, and centromeres. However, we do not observe changes in the distribution of CENP-A upon p150 depletion in human cells (Figure 2.18, B). Therefore, the extent of p150N's contributions to heterochromatin and

centromere function remains to be determined. Experiments are underway to determine which partner proteins are involved in the ability of p150N to stimulate the higher order chromatin interactions of nucleoli, and to determine if these interactions are specific to repetitive sequences.

2.5: Materials and Methods

2.5.1: Preparation of nuclear extracts and affinity chromatography for mass spectroscopy samples.

HeLa S3 Trex (untagged) and HeLa S3 Trex-NTAP-p150 cells were maintained as monolayers and then expanded to suspension cultures for large-scale preparations. Suspension cultures were started at a cell density of 3 x 10^5/ml and maintained between 1.5 x 10^5-6 x 10^5/ml. NTAP-p150 synthesis was induced by addition of doxycycline (1 µg/mL) for 16-18 hrs. Untagged samples were also treated with doxycycline in the same fashion. Routinely 6-8 liters of suspension cells were grown for each harvest. Suspension cultures were harvested by centrifugation at 1000x g at 4°C. Pellets were used to generate nuclear extracts by dounce homogenization. Briefly, suspension cells were collected by centrifugation at 1000 x g for 5 minutes. Cells were washed with ice cold PBS, then homogenization buffer (20 mM Hepes-KOH, pH 8.0, 5 mM KCl, 1.5 mM $MgCl_2$), then resuspended in 1 mL of homogenization buffer per mL of packed cell volume. Cells were disrupted by 28 strokes of a B pestle (Wheaton, loose) by dounce homogenization and nuclei were pelleted by centrifugation (5

mins at 1000 x g) and washed with nuclei wash buffer (10 mM $NaCO_3$, 150 mM NaCl). Nuclear extracts were made by incubating nuclei with extraction buffer (15 mM Tris-HCl, pH 7.8, 1 mM EDTA, 400 mM NaCl, 10% sucrose, 0.1 mM PMSF, 1 mM DTT) for 30 mins, rotating at 4°C. Extracts were then clarified by ultracentrifugation at 100,000 x g for 60 mins and then frozen in aliquots and stored at -80°C. For samples analyzed by mass spectroscopy, 12.5 mg (exp. 1) or 25 mg (exp 2) of nuclear extract was used for affinity purification.

Affinity purifications were performed with Streptavidin-sepharose (GE healthcare). All steps were performed at 4°C. 300 µl resin was used per 25 mg of nuclear extract. Extracts were diluted two-fold with Buffer A (25 mM Tris-HCl pH 7.5, 1 mM EDTA, 10% glycerol, 0.01% NP40) to reduce the NaCl concentration from 400 mM to 200 mM and rotated with the resin for 3 hours. Beads were washed twice for 20 mins with MS200 (100 mM Tris pH 8.5, 200 mM NaCl) + 50 µg/mL ethidium bromide (EtBr). Beads were then washed twice more with MS200 without EtBr and twice with MS50 (100 mM Tris pH 8.5, 50mM NaCl). Proteins were then eluted from the beads with ME buffer (100 mM Tris pH 8.5, 8 M Urea). Samples were precipitated with 20% trichloracetic acid on ice for 30 minutes and centrifuged for 10 minutes at 16,000 x g at 4°C. The supernatants were removed and the pellets were washed twice with -20 °C acetone and air-dried.

2.5.2: Mass spectroscopy

The NTAP-p150 and untagged samples were first denatured in 8M urea and then reduced and alkylated with 10 mM Tris(2-carboxyethyl)phosphine hydrochloride [Roche Applied Science] and 55 mM iodoacetamide [Sigma-Aldrich] respectively. The sample was then digested over-night with trypsin [Promega] according to the manufacturer's specifications.

The protein digest was pressure-loaded onto a 250 micron i.d. fused silica capillary [Polymicro Technologies] column with a Kasil frit packed with 3 cm of 3 micron C18 resin [Phenomenex]. After desalting, this column was connected to a 100 micron i.d. fused silica capillary [Polymicro Technologies] analytical column with a 5 micron pulled-tip, packed with 10 cm of 3 micron C18 resin [Phenomenex].

The column was placed inline with a 1200 quaternary HPLC pump [Agilent Technologies] and the eluted peptides were electrosprayed directly into an LTQ mass spectrometer [Thermo Scientific]. The buffer solutions used were 5% acetonitrile/0.1% formic acid (buffer A) and 80% acetonitrile/0.1% formic acid (buffer B). The 180 minute elution gradient had the following profile: 10% buffer B beginning at 15 minutes to 40% buffer B at 105 minutes, to 70% buffer B at 150 minutes, to 100% buffer B from 155 minutes to 165 minutes. A cycle consisted of one full scan mass spectrum (400-1600 m/z) followed by 5 data-dependent collision induced dissociation (CID) MS/MS spectra. Application of

mass spectrometer scan functions and HPLC solvent gradients were controlled by the Xcalibur data system [Thermo Scientific].

MS/MS spectra were extracted using RawXtract (version 1.9.9) (McDonald et al., 2004). MS/MS spectra were searched with the Sequest algorithm (Eng et al., 1994) against an EBI International Protein Index (IPI) protein database version 3.30 (June 2007) concatenated to a decoy database in which the sequence for each entry in the original database was reversed (Peng et al., 2003). The Sequest search was performed using full enzyme specificity, including static modification of cysteine due to carboxyamidomethylation (57.02146). Up to two missed cleavages were considered. Sequest search results were assembled and filtered using the DTASelect (version 2.0) algorithm (Tabb et al., 2002)). The peptide identification false positive rate was kept below one percent.

2.5.3: shRNAs

shRNA expression constructs were made using the system we described previously (Campeau et al., 2009). The shRNA for depletion of p150 (p150shRNA-1) had the following targeting sequence: AGGGGAAAGCCGATGACAT. Destination vectors for expressing p150shRNA-1 were created by recombining pENTR1A/pTER p150shRNA-1 (435-1) into pLenti RNAi X2 neo (w18-1) to create pLenti RNAi X2 Neo/pTER p150shRNA-1 (w23-2) and pLenti RNAi X2 Puro (w16-1) to create pLenti RNAi X2 Puro/pTer

p150shRNA-1 (pPK655). The luciferase shRNA-expressing construct pLenti X2 Neo/pTER shLUC (w181-1) was previously described (Campeau et al., 2009).

2.5.4: p150 derivatives and other transgenes

The p150 amino acid numbers used here are based on the published literature (Kaufman et al., 1995; Lee et al., 2009). Various p150 constructs were altered by site-directed mutagenesis to make them resistant to p150shRNA-1. First, we used oligonucleotides ECA552 and ECA553 to alter the p150 cDNA in plasmid pPK8 (Kaufman et al., 1995), generating plasmid pPK649 which carries the "sh^{R}" version of the p150 cDNA. RNAi-resistant V5-tagged p150 C-terminal or internal deletion Gateway entry constructs were generated by cloning fragments of pPK649 into pENTR-V5 (w71-3). Lentiviral expression vectors were made by LR recombination of the pENTR-based entry constructs into pLenti CMV Hygro (w117-1). The negative control transgene, V5-tagged luciferase, was generated by LR recombination of 468-1 (pENTR vector + V5-Luciferase) into w117-1 to generate pPK678 (pLenti CMV V5-luciferase).

2.5.5: esiRNA methods

siRNAs were generated using the DEQOR method (Surendranath et al., 2013), with primers designed using the DEQOR database (http://deqor.mpi-cbg.de/deqor_new/input.html) to generate T7-tailed dsDNA templates from human cDNA in two rounds of PCR. In the case of the luciferase esiRNA, RNA

from a HeLa cell line expressing V5-luciferase was used to generate cDNA; all other esiRNAs derived from cDNA from normal HeLa cells. In the 1st round of PCR, primers specific to the gene of interest (p150, Luciferase, UBC9, or SUMO2) were used in the following program: 95 °C for 3 mins, 16 cycles of (95 °C for 1 min, 65 °C -1 °C/cycle for 1 min, and 72 °C for 1 min) followed by an additional 15 cycles of (95 °C for 1 min, 60 °C for 1 min, and 72 °C for 1 min) and one final cycle at 72 °C for 5 mins. In the 2nd round of PCR, a T7 promoter-tailed primer was used to amplify the product of the 1st round with the following program: 95 °C for 2 mins, 4 cycles of (95 °C for 30 seconds, 42 °C for 45 seconds, and 72 °C for 1 min) followed by an additional 29 cycles of (95 °C for 30 seconds, 60 °C for 45 seconds, and 72 °C for 1 min) and one final cycle at 72 °C for 5 mins. The product of the 2nd round of PCR is used to transcribe ds esiRNA using T7 RNAP in presence of 25 mM NTPs and 40 mM Tris pH 7.9, 6 mM $MgCl_2$, 2 mM spermidine and 10 mM NaCl using the following thermocycler program: 37 °C for 5 hours 30 mins, 90 °C for 3 mins, Ramp 0.1 °C/second to 70 °C, 70 °C for 3 mins, Ramp 0.1 °C/second to 50 °C, 50 °C for 3 mins, Ramp 0.1 °C/second to 25 °C, 25 °C for 3 mins. After transcription and annealing, products were digested with 2U of RQ1 DNAseI for 15 minutes at 37 °C. esiRNAs were then generated by digesting dsRNAs with RNAse III (Fazzio et al., 2008) and purified as described using Invitrogen RNA Mini Kits.

2.5.6: Cell culture methods

For inducible expression of transgenes, a HeLa S3-Trex cell line expressing the tetracycline repressor was established by infecting HeLa S3 cells with lentiviruses containing pLenti CMV TetR Blast (716-1) and selecting for blasticidin-resistant cells. HeLa S3-Trex cells were maintained either on plates or in suspension in RPMI medium with 5% tetracycline-free fetal bovine serum (FBS). HeLa-S3-Trex cells were infected with lentiviruses carrying CMV/TO promoters driving expression of NTAP-tagged p150 (pPK560) or p150-directed shRNAs. Individual drug-resistant clones were picked for each of these cell lines. The NTAP-p150-expressing clone was chosen because it expressed tagged protein levels similar to endogenous p150 levels, and is described previously (Campeau et al., 2009). p150 shRNA clones were selected based on the extent of p150 depletion. Inducible expression of transgenes was achieved by supplementing media with 1 µg/mL (NTAPp150) or 2 µg/mL (shRNAs) doxycycline.

RNAi-resistant V5-tagged transgene expression constructs were introduced into the HeLa S3 Trex-p150shRNA-1 cell line via lentiviral infection, followed by hygromycin selection. Cloned MCF10A-tet-krab cell lines (Cohet et al., 2010) harboring p150shRNA-1 or sh-Luciferase were generated and grown in DMEM/F12 media (Lonza) supplemented with 5% horse serum, 20 ng/mL EGF, 10 µg/mL Insulin, 0.5 µg/mL hydrocortisone, 100 ng/mL cholera toxin, and antibiotic/antimycotic solution (Life Technologies). HT1080 cells (ATCC) were

maintained in DMEM with 5% tet-free FBS, and Trex and sh-RNA expressing cells lines were made as above.

For double thymidine block experiments, HeLa S3 cells were blocked in RPMI + 5% FBS media supplemented with 2 mM thymidine for 18 hours, released into thymidine-free media four 9 hours and blocked again with media containing 2 mM thymidine for 17 hours (Whitfield et al., 2002). For serum starvation studies, MCF10A-tet-krab cells were cultured in complete DMEM/F12 media as described above, or in DMEM/F12 containing only 1 mg/ml BSA and antibiotic/antimycotic with no additional growth factors for 96 hours. The shRNAs were induced by adding 2 µg/mL doxycycline to the media during the last 48 hours.

Human foreskin fibroblasts (HFF; a kind gift of Jennifer Benanti, (Benanti and Galloway, 2004)) were grown in DMEM supplemented with 10% FBS and antibiotic/antimycotic solution (Life Technologies). HFF cells were maintained above 25% confluence at all times and were split 1:4 every 2 days. HFF cells used for the immuno-FISH and DNA-FISH experiments were grown on poly-lysine coated coverslips between PD22-30. MCF-10A and HeLa cells were cultured as described above on non-treated coverslips for immuno-FISH and DNA-FISH experiments.

2.5.7: Growth analyses

To measure growth rates during p150 depletion, HeLa S3 Trex-p150shRNA-1 and HeLa S3 Trex-shRNA-Luciferase cells were plated at 1500 cells per well in 48-well plates. Triplicate wells for each time point (0 to 120 hours) were assayed with CellTiter 96 AQueous One (Promega) per manufacturer's instructions. For growth analysis of cells expressing V5-tagged p150 or luciferase transgenes, 9000 cells per well in 6-well dishes were infected with lentiviruses expressing either shRNA-luciferase or p150shRNA-1 at an MOI of 2. After 48 hrs, drug selection for infected cells was begun (1 mg/ml G418 or 0.5 µg/mL puromycin, respectively). After 7 days post infection, cells were stained with crystal violet (Campeau et al., 2009) and photographed.

2.5.8: Antibodies

For p150, mouse monoclonals ss1 and ss48 (Smith and Stillman, 1991) were used for immunoblots and immunofluorescence. Additionally, rabbit polyclonal anti-p150 antibodies (Santa Cruz, sc-10772 and sera specifically generated for this study) were used for immunoblotting and ChIP. To generate polyclonal antibodies, a codon-optimized version of the first 200 amino acids of the p150 cDNA was cloned into pGEX6 (GE Healthcare) to generate pPK621. The codon numbering for this construct is based on the full-length p150 ORF that contains an additional 18 amino acids at the N-terminus not present in the original cDNAs (accession # NM_005483). Synthesis of the GST-p150(1-200)

fusion protein was induced in BL21(DE3)pLysS *E. coli* cells grown in LB with 35 µg/mL chloramphenicol and 100 µg/mL ampicillin at 37 ^{o}C by addition of 0.5 mM IPTG at OD_{600} 0.4 for 2 hrs. Pellets were collected, washed in ice-cold PBS, frozen in liquid nitrogen and stored at -80^{o}C. Glutathione affinity chromatography on Glutathione Sepharose 4 Fast Flow and separation of GST from p150(1-200) by PreScission Protease digestion were performed in PBS at 4°C per manufacturer's instructions (GE Healthcare). Additional purification of p150(1-200) was performed by ion exchange chromatography on a 1 mL Poros 20 HQ column (Life Technologies). Soluble protein collected from the PreScission digestion was loaded onto a HQ column pre-equilibrated in HQ buffer (25 mM Tris pH 7.5, 1 mM EDTA, 1 mM DTT) with 100 mM NaCl and eluted using a gradient from 100 mM to 1 M NaCl. p150(1-200) eluted near the beginning of the gradient. This purified antigen was used to immunize rabbits for antisera production (at Pocono Rabbit Farm and Laboratory, Inc., under the approval of the UMASS Medical School IACUC Off-Site Animal Protocol A-1692-12). Antibodies to CBP (ICL, RCBP-45A), Ki67 (Novus, NB500-170), CAF1-p60 (ss96; (Smith and Stillman, 1991)), CENPA (Abcam, ab13939), phospho(S1981)-ATM (Rockland 200-301-400), phospho(S317)-Chk1 (Bethyl, A300-163A), phospho(S139)-γH2AX (Upstate, 05-636), HP1α (Millipore 05-689), nucleophosmin (NPM/B23, Santa Cruz, sc-32256), nucleolin (NCL/C23, Santa Cruz, sc-9893), Nopp140 (RS8, generous gift of U. Thomas Meier, Albert Einstein College of Medicine (Kittur *et al.*, 2007)), fibrillarin (FBL, Abcam,

ab5821), UBF1 (Santa Cruz, sc-13125), PARP (BD Pharmingen, 556362), TTF1 (Santa Cruz, sc-136371), Tubulin (DM1a), and V5 (Life Technologies, R96025) were used for immunofluorescence and immunoblots. Anti-BrdU (USBiologicals, B2850-01G) was used to detect BrUTP-labeled RNAs. Secondary antibodies were obtained from either Jackson Laboratory (FITC, Cy5) or from Life Technologies (AlexaFluor 488, 594, and 647).

2.5.9: Immunofluorescence

Cells grown on Labtek cc2 8-chamber slides were fixed either in methanol (10 minutes) or 4% paraformaldehyde (5 minutes) as indicated, and then permeabilized with 0.5% Triton X-100 (5 min) at room temperature. Samples were blocked in 0.5% BSA, 0.2% fish skin gelatin for 1 hour. Samples were then incubated with primary antibodies (1:500-1:1000) in blocking buffer (1 hour) followed by 3 PBS washes and then secondary antibody incubation (1:800 FITC and Cy5, 1:2000 Alexa Fluor 488 and Alexa Fluor 647). Immunofluorescence images were taken on a Zeiss Axioplan2 microscope using Axiovision v4.6 with a 63x objective connected to a Hamamatsu 1394 ORCA-ER HD camera. Confocal images were taken on a Leica SP2 microscope with a 100x objective using Leica imaging software, utilizing 405, 488, and 561 nm laser lines. Colocalization images were generated using Imaris x64 v6.1.3. Densitometry of individual immunostained cells were performed using TIFF files in ImageJ 1.48r (National Institute of Health) by constructing histograms across nucleoli of shRNA treated

cell lines. Pixel values were normalized to the total pixel density of the histogram and plotted in Prism (Graphpad software).

2.5.10: Chromatin immunoprecipitations (ChIP)

HeLa S3-Trex-p150shRNA-1 or sh-Luciferase cells were treated with 2 µg/ml of doxycycline for 72 hours. For each sample, approximately 3 x 10^7 cells were fixed with 1% formaldehyde for 10 minutes at room temperature and subsequently quenched with 0.125 M glycine. After two washes in PBS, cells were collected by scraping, centrifuged and then flash frozen in liquid nitrogen. Thawed pellets were resuspended in ChIP lysis buffer (50 mM HEPES-KOH pH 7.5, 150 mM NaCl, 1 mM EDTA, 0.5% SDS, 0.1% sodium deoxycholate, 1% Triton X-100) and sonicated using a Branson Sonifier 450. After six 20 second pulses (power 3, 30% duty cycle), fractionated chromatin was ultracentrifuged at 100,000 x g for 45 minutes, and the supernatant was recovered. Bradford assays (BioRad) were used to determine protein content in the soluble chromatin preparations. All samples were pre-cleared with 100 µl of Recombinant Protein G – Sepharose® 4B beads (Life Technologies, Grand Island, NY) pre-blocked with 0.5 mg/ml BSA and 0.2 mg/ml sheared salmon sperm DNA in ChIP lysis buffer overnight at 4°C. For p150 and TTF-I analyses, 500 µg chromatin was incubated overnight with 5 µg of our own anti-p150 antisera or 2.5 µg of anti-TTF-I (SC-136371, Santa Cruz Biotechnology, Inc, Santa Cruz, CA) antibody. Rabbit pre-immune serum or mouse IgG (SC-2025, Santa Cruz Biotechnology, Inc, Santa

Cruz, CA) served as negative immunoprecipitation controls. Following an overnight incubation with 100 µl of Protein G beads, beads were washed twice with ChIP lysis buffer, once with high salt buffer (50 mM HEPES-KOH pH 7.5, 1M NaCl, 1 mM EDTA, 0.5% SDS, 0.1% sodium deoxycholate, 1% Triton X-100), 3 times with RIPA buffer (50 mM Tris-HCl pH 8.0, 250 mM LiCl, 1 mM EDTA, 0.5% NP40, 0.5% sodium deoxycholate), and once with TE buffer containing 50 mM NaCl. Protein-DNA complexes were extracted from beads at 65°C in elution buffer (0.1 M $NaHCO_3$, 1% SDS) for 15 minutes, followed by centrifugation at 16,000 x g for one minute and collection of supernatants. To reverse crosslinking, eluted chromatin and corresponding input samples were rotated overnight at 65ºC. Samples were then subjected to RNAse A (80 µg for 2 hours at 37 °C) and proteinase K (80 µg for 2 hours at 55°C) digestions. Samples were extracted with phenol:chloroform:isoamyl alcohol (25:24:1) and precipitated with 2.5 volumes of ethanol in 0.2 M NaCl plus 30 µg of glycogen. Precipitated DNA was resuspended in 10 mM Tris-HCl, pH 8.0. The Fast SYBR Green reagent (Life Technologies, Grand Island, NY) was used in ChIP-PCR studies to quantify p150 and TTF-1 occupancies. Primer sequences are in Table S2. The PCR reactions were performed using a StepOnePlus machine (Life Technologies) with the following program: hold 95°C for 20 minutes, followed by 40 cycles of 95 °C for 3 seconds, 60°C for 30 seconds. To calculate the percentage of bound DNA, unimmunoprecipated input chromatin from each sample was analyzed simultaneously. $\Delta\Delta$CT was calculated from the following formula (Life

Technologies): Adjusted input = Ct input – 6.644. Percent input = 100*2^ (Adjusted input – Ct(IP)). Three biological replicates for each experiment were performed, and comparisons between samples were analyzed by two-tailed, unpaired Student's t-tests with equal variance (homoscedastic).

2.5.11: Visualization of 5-EU-labeled nascent RNA

MCF-10A cells were grown in 4-well chamber slides (Fisher) overnight and then in some cases incubated with the RNA polymerase II inhibitor alpha-amanitin (Sigma), the inhibitor of RNA polymerase I transcription actinomycin D (Sigma), or both. Alpha-amanitin was added at 20 µg/mL for 4 hours and actinomycin D was added at 50 ng/mL for 15 minutes. Pre-warmed MCF-10A media containing the indicated drug(s) and 500 µM of the UTP analog 5-ethynyl-uridine (5-EU, Invitrogen) was added for 15 minutes, followed by washing with 1X PBS. Cells were then fixed with 3.7% formaldehyde/ 1X PBS for 15 minutes at room temperature. Following another 1X PBS wash, the cells were permeabilized in 0.5% Triton-X100/ 1X PBS for 15 minutes at room temperature. Cells were then washed again in 1X PBS before incubation with the click chemistry cocktail (50 mM carboxyrhodamine 110-Azide (Click Chemistry Tools), 100 mM ascorbic acid (Sigma), and 1 mM $CuSO_4$ (Sigma) in 100 mM Tris-Cl pH 8.5) for 30 minutes at room temperature in the dark. The cells were then washed 3 times in 0.5% Triton-X100/ 1X PBS for 5 minutes in the dark and then incubated in 130 ng/mL DAPI in 1X PBS for 1 minute. The chamber was then

manually removed and a few drops of Vectashield (Vector Labs) was added before a coverslip was placed on top and sealed with nail polish. Images were taken on a Zeiss Axioplan2 microscope with a 63x objective.

2.5.12: Immuno-FISH and DNA-FISH Experiments

The bacterial artificial chromosomes RP5-915N17 (1q42.13; '5S rDNA'), RP11-413F20 (10q26.3; 'D4Z4 array') and RP11-123G19 (10q24.1; 'Negative Control', which was previously shown to lack nucleolar localization (Németh et al., 2010) were obtained from the BACPAC Resource Center of Children's Hospital Oakland Research Institute (CHORI). The plasmid pB containing a 5.6 Kb EcoRI fragment of human 47S rRNA-encoding repeat was a gift from Sui Huang (Northwestern University School of Medicine). The chromosome 17 alpha satellite probe was prepared as previously described (Warburton et al., 1991). BAC probes were labeled using the Bioprime Labeling Kit (Invitrogen), and the rDNA and alpha satellite probes were labeled using the Nick Translation Mix Kit (Roche).

Expression of either sh-luciferase or sh-p150 in MCF10A-tet-krab cells was induced with 2 μg/mL doxycycline for 72 hours, followed by fixation and storage in 1X PBS at 4^{o}C for up to a week. For all transgene experiments involving lentivirus-encoded shRNAs, cells were infected at MOI = 7.5 with 6 μg/mL polybrene. 72 hours post-infection, cells were fixed and stored for up to a week in 1X PBS at 4^{o}C. For other depletions, siRNAs were constructed as previously

described (Fazzio et al., 2008) and 500 ng of siRNAs were transfected in 1 mL Opti-MEM (Gibco) with 6 μL oligofectamine (Life Technologies). Transfections were performed in 6-well dishes containing coverslips, and after 6.5 hours 2.5 mLs of appropriate media were added on top of the transfection cocktail. At 72 hours after transfection, cells were fixed and stored for up to a week in 1X PBS at 4ºC.

Immuno-FISH and DNA FISH experiments in MCF-10A, HFF, and HeLa cells were performed using previously published methods (Byron et al., 2013) with some modification. Briefly, cells were grown on cover slips, permeabilized in 0.5% Triton X-100 in CSK buffer on ice for 5 minutes, and fixed in 4% paraformaldehyde in 1X PBS at room temperature for 10 minutes. For Immuno-FISH experiments, cells were then processed using the immunofluorescence protocol described in these methods using an anti-fibrillarin antibody (Abcam). The cells were then fixed again in in 4% paraformaldehyde in 1X PBS at room temperature for 10 minutes before proceeding to DNA denaturation. For DNA-FISH experiments, after initial fixation RNA was removed by incubating the cells in 0.2 N NaOH in 70% ethanol for 5 minutes at room temperature before proceeding to genome denaturation. The genome was denatured by placing the coverslips in 70% formamide (Sigma)/2X SSC heated to 80ºC for 2-3 minutes. Denaturation was quenched in ice-cold 70% ethanol for 5 minutes, followed by washing with ice-cold 100% ethanol and air-drying. 50 μg of labeled probe was mixed with 1 μg of Cot-1 (Roche), 1 μg *E. Coli* tRNA (Sigma), and 1 μg single

stranded salmon sperm DNA (Sigma) in 50% formamide (Sigma) and 50% hybridization buffer. Hybridization buffer is comprised of 20% dextran sulfate (Sigma) and 1% BSA in 4X SSC. The probe was denatured at 80^{o}C for 10 minutes and then incubated underneath the coverslips in a 37^{o}C humid chamber overnight. Cells were washed for 20 minutes in 50% fromamide in 2X SSC at 37^{o}C, then for 20 minutes in 2X SSC at 37^{o}C, and for 20 minutes in 1X SSC at room temperature. The probe was detected using either FITC conjugated to an anti-digoxigenin antibody (Roche) or an Alexa Fluor conjugated to streptavidin (Invitrogen) in 1% BSA/ 4X SSC for 60 minutes in a 37 ^{o}C humid chamber. Cells were washed again in 4X SSC three times for 10 minutes at room temperature in the dark. Coverslips were mounted with Vecta Shield (Vector Labs) and Z-stack images were taken on a Zeiss Axioplan2 microscope with a 63x objective. Z-steps of 200 nM were taken and the maximum intensity projections generated using Axiovision v4.6. Association percentages for each of the three biological replicates were transformed into arcsine units and the unpaired Student's t-test was used (with Welch's correction) to generate p-values. P-values < 0.05 were considered statistically significant.

CHAPTER III: CAF-1 P150 REGULATES KI-67 LOCALIZATION THROUGHOUT THE CELL CYCLE

3.1: Abstract

Chromatin Assembly Factor 1 (CAF-1) deposits histones during DNA synthesis. The p150 subunit of human CAF-1 contains an N-terminal domain (p150N) that is dispensable for histone deposition but which promotes the localization of specific loci (Nucleolar-Associated Domains, or “NADs”) and proteins to the nucleolus during interphase. One of the p150N-regulated proteins is proliferation antigen Ki-67, whose depletion also decreases the nucleolar association of NADs. Ki-67 is also a fundamental component of the perichromosomal layer (PCL), a sheath of proteins surrounding condensed chromosomes during mitosis. We show here that a subset of p150 localizes to the PCL during mitosis, and that p150N is required for normal levels of Ki-67 accumulation on the PCL. This activity requires the Sumoylation Interacting Motif (SIM) within p150N, which is also required for the nucleolar localization of NADs and Ki-67 during interphase. In this manner, p150N coordinates both interphase and mitotic nuclear structures via Ki67.

3.2: Introduction

Eukaryotic chromosomes must condense for segregation during mitosis, and then decondense and re-adopt interphase configurations in the next cell

cycle. However, mechanisms that link higher-order mitotic and interphase genome organization remain poorly understood. Notably, cellular heterochromatin is highly enriched at specific sites in interphase nuclei, at the nuclear lamina, in pericentric foci, and in perinucleolar regions (reviewed in (Politz et al., 2016). Therefore, a major question is how these loci are relocalized after each mitosis, and what mitotic molecules might aid in this.

Nucleolar Associated Domains (NADs) are genomic loci that interact frequently with the nucleolar periphery (van Koningsbruggen et al., 2010; Matheson and Kaufman, 2015; Németh et al., 2010; Padeken and Heun, 2014; Pontvianne et al., 2016). NADs are highly enriched for repetitive DNA satellites and histone modifications associated with heterochromatic silencing such as H3K27me3, H3K9me3, and H4K20me3 (Németh et al. 2010; Politz et al. 2016). One protein recently shown to regulate NAD localization is the p150 subunit of Chromatin Assembly Factor 1 (CAF-1) (Smith et al., 2014). CAF-1 is a highly conserved three-subunit protein complex which deposits histone $(H3/H4)_2$ tetramers onto replicating DNA during S-phase of the cell cycle (Kaufman et al., 1995; Krude, 1995; Smith & Stillman, 1989), and is particularly important for DNA replication and maintenance of histone marks at heterochromatic loci (Baldeyron et al., 2011; Dohke et al., 2008; Houlard et al., 2006; Huang et al., 2010; Quivy et al., 2004, 2008; Reese et al., 2003; Sarraf and Stancheva, 2004). In addition to these functions, the N-terminal domain of p150 (p150N) regulates the association

of NADs to the perinucleolar region, and also regulates the nucleolar localization of several proteins, including the proliferation antigen Ki-67 (Smith et al., 2014).

Ki-67 also regulates heterochromatin modification (Sobecki et al., 2016) and affects its condensation (Kametaka et al., 2002; Takagi et al., 1999). Ki-67 is highly expressed in proliferating cells, minimally expressed in quiescent cells (Gerdes et al., 1984; Gerdes et al., 1983), and meta-analyses of numerous clinical studies have validated Ki-67 as a prognostic marker in grading tumors (Luo et al., 2015; Pezzilli et al., 2016; Pyo et al., 2016; Richards-Taylor et al., 2016). Similar to Ki-67, p150 is also highly expressed in proliferating cells, minimally expressed in quiescent cells, and has been proposed as an alternative cellular proliferation marker in clinical studies (Polo et al., 2004).

Recent studies have demonstrated that Ki-67 is required for formation of the perichromosomal layer (PCL) (Booth et al., 2014; Sobecki et al., 2016), a layer of proteins that surrounds all condensed chromosomes during mitosis (reviewed in (Van Hooser 2005). At the PCL, Ki-67's status as a large, charged protein that possesses "surfactant"-like properties keeps individual mitotic chromosomes dispersed rather than aggregated upon nuclear envelope disassembly, thereby ensuring normal kinetics of anaphase progression (Cuylen et al., 2016). Likewise, acute depletion experiments show that Ki-67 is important for maintaining mitotic chromosome structure and function (Takagi et al., 2016). Since p150N regulates interphase Ki-67 localization, we investigated whether p150N also affects Ki-67 localization during mitosis.

3.3: Results

3.3.1: Ki-67 regulates alpha satellite localization to the perinucleolar region

Recent studies have suggested Ki-67 regulates repetitive DNA localization to the nucleolus. Ki-67 depletion decreased the nucleolar association of a LacO array proximal to the rDNA repeats on chromosome 13 (Booth et al., 2014), and the centromeric histone variant CENP-A (Sobecki et al., 2016). To determine if Ki-67 also regulates satellite repeat association with the nucleolus, we transfected siRNAs into HeLa cells and performed immuno-FISH to visualize the position of alpha satellite DNA from chromosome 17 (αSat 17) relative to the nucleolar protein fibrillarin. HeLa cells transfected with siRNAs directed against luciferase or a scramble control displayed ~45% of αSat 17 alleles associated with nucleoli, which represents a high-frequency interaction characteristic of a NAD locus (Németh et al., 2010; Smith et al., 2014; van Koningsbruggen et al., 2010). In contrast, cells transfected with two different siRNA reagents directed against distinct regions of the Ki-67 mRNA displayed αSat 17 association frequencies to ~25% (Figure 3.1, A and B).

We also depleted HeLa cells of nucleolin (NCL), a nucleolar protein which primarily localizes to the perinucleolar region (Bugler et al., 1982) and regulates transcription, folding, and assembly of ribosomal RNA (Ginisty et al., 1999; Ginisty et al., 1998; Rickards et al., 2007; Roger et al., 2002). Depletion of NCL altered nucleolar morphology (Figure 3.1, B) as previously reported (Ma et al., 2007; Ugrinova et al., 2007) but did not affect the association of αSat 17 with

fibrillarin (Figure 3.1, A). We conclude that in human cells Ki-67 is required for efficient localization of NADs to nucleoli, and that NCL is not required at least for alpha satellite-nucleolar interactions.

Our results with human nucleolin depletion are somewhat different from those obtained in a recent study of nucleolin's contribution to NAD localization in the plant *A. thaliana* (Pontvianne et al., 2016). As in our experiments (Fig. 1B), cells from nucleolin mutant (*nuc1*) plants also showed altered nucleolar morphology. However, deep sequencing of purified nucleoli revealed altered NAD profiles in *nuc1* cells, including decreased nucleolar association of telomeric heterochromatin, coinciding with a 30% loss of telomere length on all chromosomes. It is possible that there are altered NAD associations in nucleolin-depleted human cells that we could not have detected using an alpha-satellite probe specific for chromosome 17. Alternatively, there is precedence for species-specific interactions mediated by nucleolin. For example, depletion of nucleolin increases centromere-nucleolar interactions in Arabidopsis (Pontvianne et al., 2016), but decreases such interactions in Drosophila (Padeken et al., 2013).

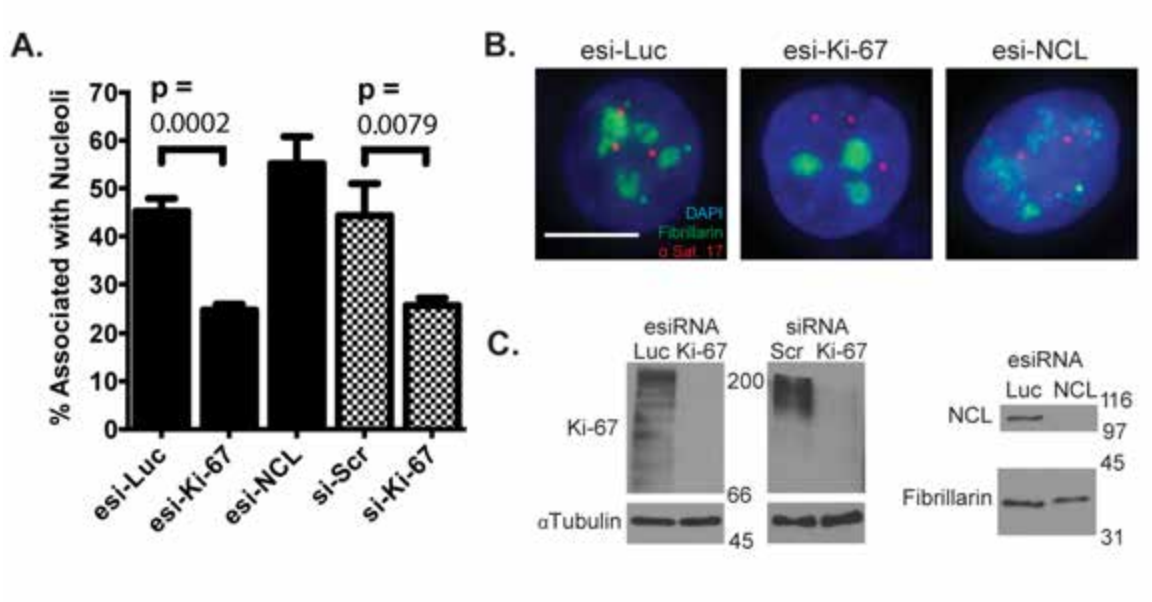
Interestingly, decreased telomere lengths were also observed in Arabidopsis *fas1* and *fas2* mutants (Pontvianne et al., 2016), which lack the homologs of the human p150 and p60 subunits of CAF-1. Another study found that *fas1* and *fas2* mutants also display decreased copy number of the 45S rRNA genes, along with increased nucleolar association of the remaining 45S rRNA genes (Pontvianne et al., 2013). We note that human p150 and *Arabidobsis* Fas1

share 29.8% amino acid identity, but Fas1 completely lacks the p150N domain, the N-terminal 310 amino acids of p150 previously shown to regulate human nucleolar structure (Smith et al., 2014). Together, these data suggest that p150/Fas1 regulate nucleolar structure in both plants and mammals, but also that there are marked mechanistic differences in how this regulation occurs in different organisms. We also note that a higher percentage of the genome is nucleolar-associated in human cells (Dillinger et al., 2016) when compared to plant cells (Pontvianne et al., 2016).

Figure 3.1: Alpha-satellite associations with nucleoli are reduced upon depletion of Ki-67 but not nucleolin.

(A): Immuno-FISH analyses of the association between alpha satellite DNA from chromosome 17 (αSat 17, red) and fibrillarin (green) was performed in HeLa cells transfected for 72 hours with in vitro-diced “esiRNAs” targeting luciferase, Ki-67, or nucleolin (NCL) (black bars), or with synthetic duplex siRNAs (checked bars) targeting Ki-67 or a scrambled sequence control (si-Scr). The percentage of αSat 17 alleles co-localized with fibrillarin is indicated, with means and standard deviation error bars from three replicate experiments. p values comparing association frequencies in cells treated with esi-Luc (N=669 alleles) vs. esi-Ki-67 (573 alleles), and si-SCR (N=540 alleles) with si-Ki-67 (N=567 alleles) are indicated. (B): Representative FISH images of cells analyzed in panel (A). Scale bar is 10 μm. (C): Immunoblot analyses of cells from panel (A). Blots were probed with antibodies recognizing Ki-67, α-Tubulin (loading control), NCL, or fibrillarin (loading control), as indicated.

Figure 3.1: Alpha-satellite associations with nucleoli are reduced upon depletion of Ki-67 but not nucleolin.



3.3.2 A subset of p150 co-localizes with Ki-67 foci during mitosis and early G1 phases

Ki-67 has three distinct nuclear localization patterns, which appear at distinct cell-cycle periods. First, Ki-67 localizes to the nucleolus during interphase (Cheutin et al., 2003; Traut et al., 2002; Verheijen et al., 1989), and a subset co-localizes with p150 at the perinucleolar region (Smith et al., 2014). Second, Ki-67 localizes to the PCL during mitosis (Gerdes et al., 1984; Gerdes et al., 1983; Verheijen, et al., 1989). In contrast to the chromosome-associated state of mitotic Ki-67, mitotic phosphorylation evicts the majority of CAF-1 from mitotic chromosomes and inhibits its nucleosome assembly activity (Keller and Krude, 2000; Marheineke and Krude, 1998; Matsumoto-Taniura et al., 1996; Murzina et al., 1999). However, mass spectrometric analyses suggested that a mitotic chromosome-associated subset of p150 exists (Ohta et al., 2010), but its relationship to the PCL had not been directly tested. To analyze this we took advantage of the fact that Ki-67 localization to the PCL remains visibly unchanged even after extraction with 2 M NaCl and treatment with either RNase A or DNase I (Sheval and Polyakov, 2008), indicating the structural stability of the PCL is independent of the chromatin it surrounds. We performed immunofluorescence on RPE1-hTERT cells that were digested with either RNase A, DNase I, or mock digested, and then high-salt extracted. As previously reported, Ki-67 remained on the PCL throughout mitosis even after DNA or RNA digestion, as shown for prophase (Figure 3.2), metaphase (Figure 3.3), and

anaphase (Figure 3.4). As expected, p150 as well as Ki67 could be easily detected on anaphase chromosomes presumably because at that stage the mitotic phosphorylations of CAF-1 are removed, triggering bulk re-association with chromatin and reactivation of nucleosome assembly activity (Keller and Krude, 2000). In contrast, during prophase or metaphase a large amount of p150 evicted into the nucleoplasm made it difficult to determine whether p150 localized to the PCL. The combination of high-salt extraction and DNase I digestion however revealed that a subset of p150 localized to the PCL during all phases of mitosis.

The third Ki-67 localization pattern occurs after cytokinesis and early in G1 phase. At this stage, Ki-67 localizes to hundreds of distinct foci (du Manoir et al., 1991; Isola et al.,1990) that co-localize with heterochromatic satellite repeats (Bridger et al., 1998). These foci are transient and appear to be intermediates in the process of reformation of nucleoli as cells transition from mitosis to interphase (Saiwaki et al., 2005). Because a subset of p150 is in the mitotic PCL (Figures 3.2-3.4), we sought to determine if p150 also co-localized with early G1 Ki-67 foci. To do this, we performed immunofluorescence on early G1 RPE1-hTERT cells digested with nucleases or mock digested as previously described (Figure 3.6). In all three conditions, a subset of p150 foci in early G1 cells co-localized with Ki-67 foci, as indicated by line scan analyses. These data suggest that a subset of p150 travels together with Ki67 during exit from mitosis, as PCL components transit towards reforming nucleoli.

Figure 3.2: A subset of p150 localizes to the PCL during prometaphase

RPE1-hTERT cells in prometaphase were either untreated or digested with RNase A or DNase I as indicated, and then high-salt extracted. Cells were stained with DAPI to detect DNA (blue), and with antibodies recognizing p150 (green), and Ki-67 (red). Note the DNase I-treated cells lack DAPI staining. Scale bar is 10 μm.

Figure 3.2: A subset of p150 localizes to the PCL during prometaphase

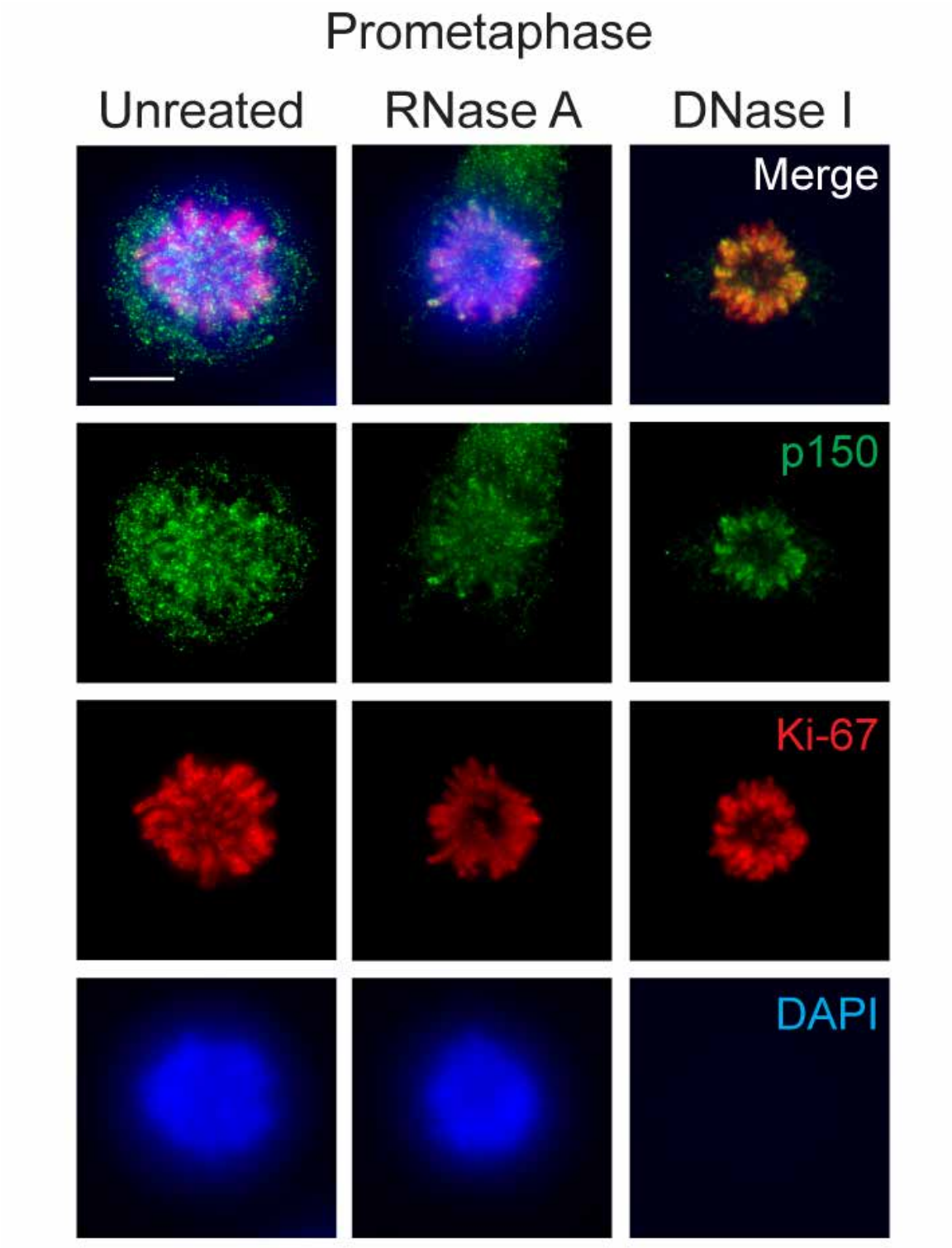


Figure 3.3: A subset of p150 localizes to the PCL during metaphase

RPE1-hTERT cells in metaphase were either untreated or digested with RNase A or DNase I as indicated, and then high-salt extracted. Cells were stained with DAPI to detect DNA (blue), and with antibodies recognizing p150 (green), and Ki-67 (red). Note the DNase I-treated cells lack DAPI staining. Scale bar is 10 µm.

Figure 3.3: A subset of p150 localizes to the PCL during metaphase

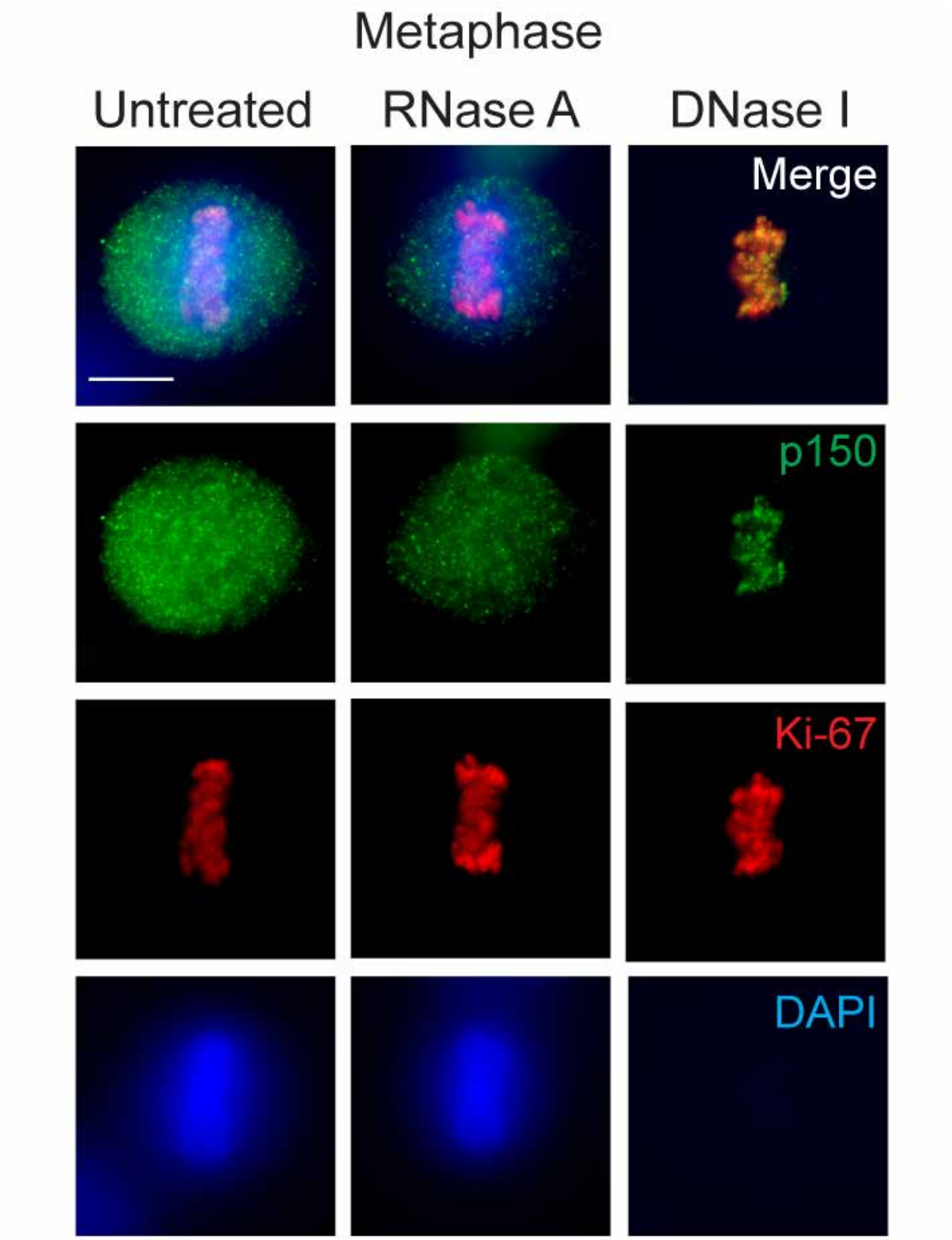


Figure 3.4: A subset of p150 localizes to the PCL during anaphase

RPE1-hTERT cells in anaphase were either untreated or digested with RNase A or DNase I as indicated, and then high-salt extracted. Cells were stained with DAPI to detect DNA (blue), and with antibodies recognizing p150 (green), and Ki-67 (red). Note the DNase I-treated cells lack DAPI staining. Scale bar is 10 µm.

Figure 3.4: A subset of p150 localizes to the PCL during anaphase

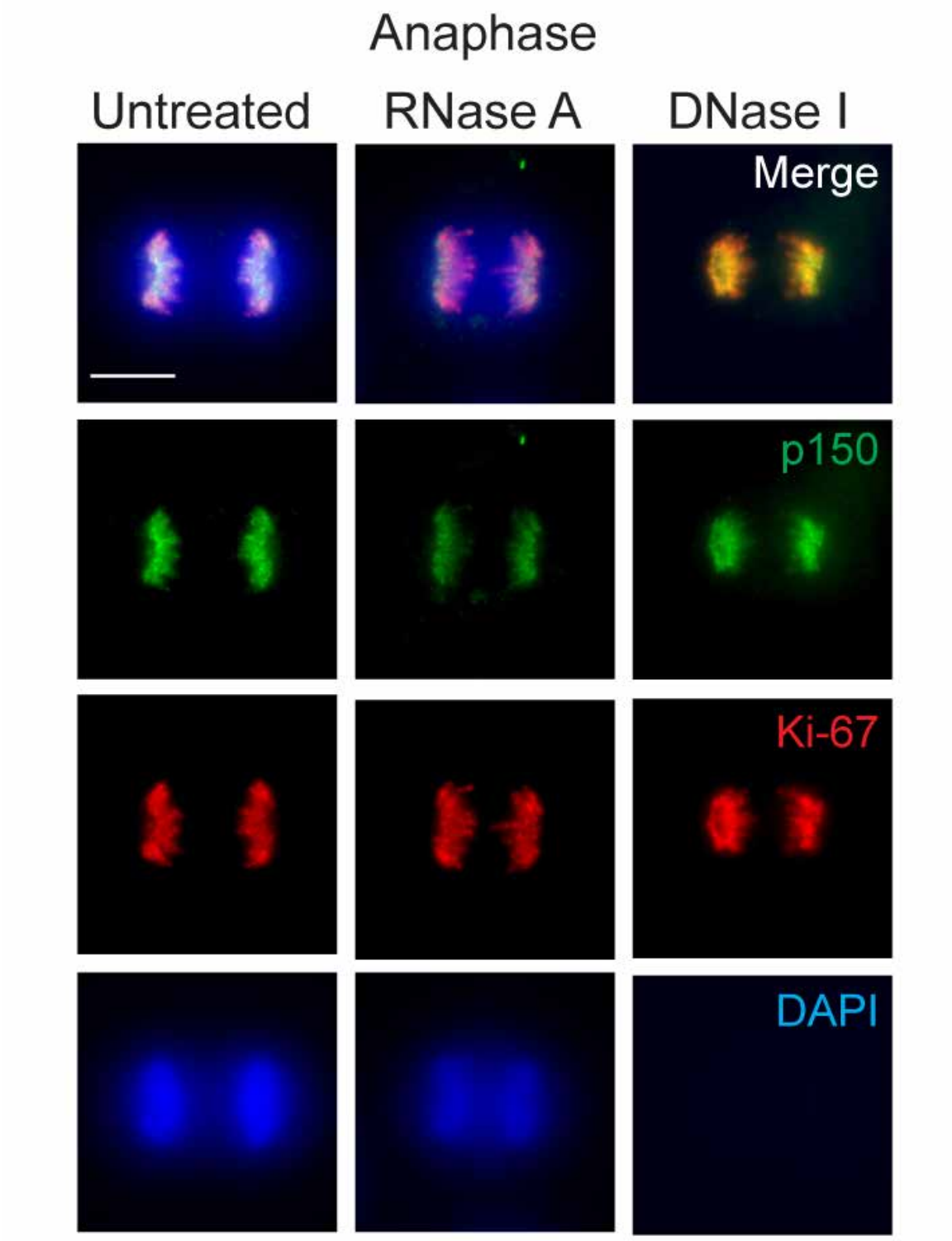


Figure 3.5: RNase A mediated degradation and western blot of DNase I treated PCL preparation.

(A): Positive control for RNase A treatment. RNA from untreated and RNase A-treated cells analyzed in Figures 3.2, 3.3, 3.4, and 3.6 were purified using Trizol reagent and analyzed on a 1% agarose gel. (B): Western blot of mitotic HeLa S3 cells (Input lane, 20 µg) or mitotic HeLa S3 cells digested with DNase I and salt extracted as in Figure 3.2 (2 µg, 4 µg, 8 µg, 16 µg as indicated). Blot was probed with antibodies recognizing Ki-67 (top) and p150 (bottom). Numbers on the right indicate migration of marker proteins of indicated molecular weight x 10^{-3}..

Figure 3.5: RNase A mediated degradation and western blot of DNase I treated PCL preparation.

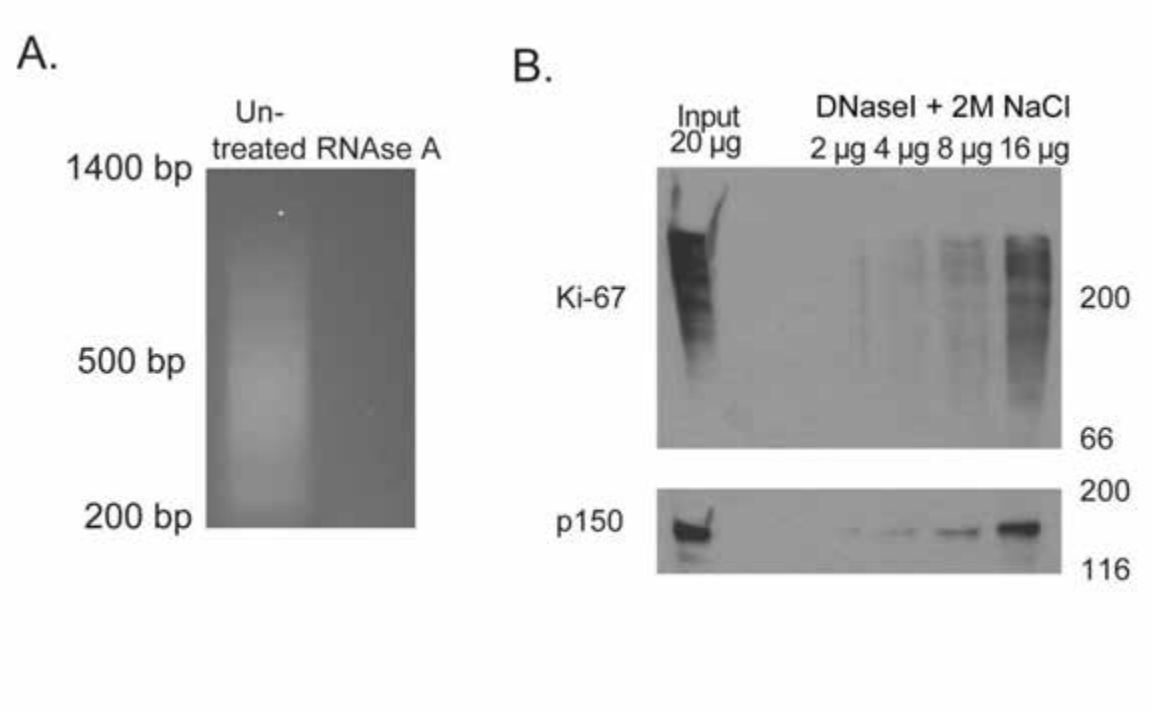
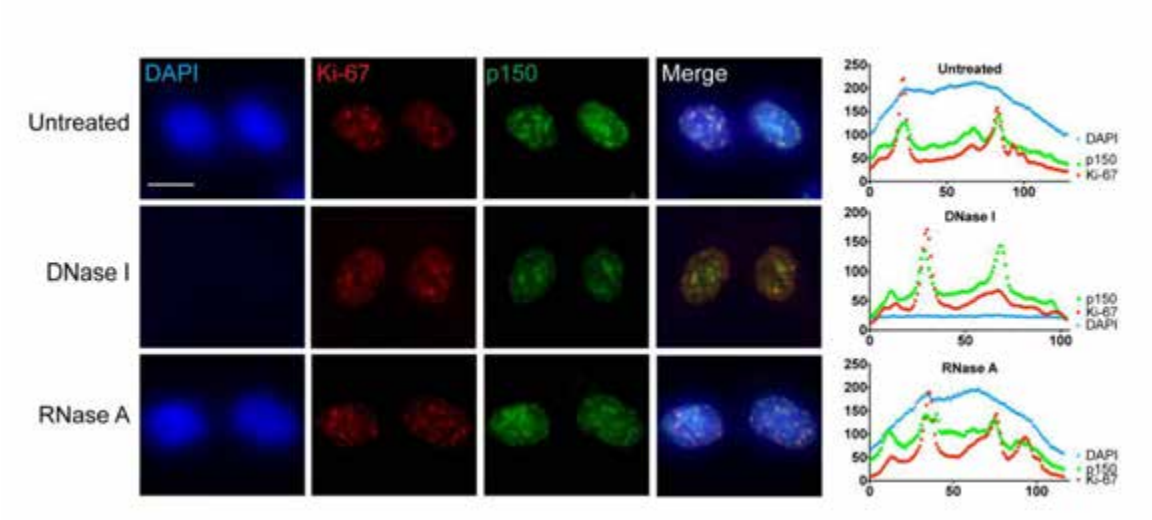


Figure 3.6: A subset of p150 localizes to Ki-67 foci during early G1 of interphase.

RPE1-hTERT cells were either untreated or digested with RNase A or DNase I as indicated, and then high-salt extracted. Cells were stained with DAPI to detect DNA (blue), and with antibodies recognizing p150 (green), and Ki-67 (red). Pairs of recently divided cells featuring hundreds of Ki-67 foci characteristic of early G1 are shown here. Line scans (right-hand panels) of individual cells (yellow triangles in merged images) were used to assess co-localization of p150 with Ki-67 signal. Scale bar is 10 μm.

Figure 3.6: A subset of p150 localizes to Ki-67 foci during early G1 of interphase.



3.3.3: p150 regulates Ki-67 accumulation on the Perichromosomal Layer

Our previous work demonstrated that p150 is required for normal steady-state accumulation of Ki-67 in the nucleolus during interphase (Smith et al., 2014). Because Ki-67 is essential for the formation of the PCL in mitotic cells (Booth et al., 2014; Sobecki et al., 2016), we tested whether p150 also regulated Ki-67 localization during mitosis. Via immunofluorescence, we examined Ki-67 distribution in HeLa S3 cells expressing an inducible shRNA directed against either luciferase (Luc) or p150 (Figure 3.7, A). As expected, we found Ki-67 robustly associated with the PCL during all phases of mitosis in the negative control cells expressing sh-Luc. In contrast, cells expressing sh-p150 displayed less Ki-67 staining on the PCL, as demonstrated in the exposure times matched with the sh-Luc samples. When exposure times were increased, Ki-67 was detected on the PCL, indicating that the PCL was not entirely disassembled upon p150 depletion. When the Ki-67 fluorescence was quantified in prometaphase cells from three biological replicates, cells expressing sh-p150 displayed, on average, a 3.5-fold decrease in fluorescence intensity compared to the control cells expressing sh-Luc (Figure 3.7, B). To test whether this effect of p150 depletion could result from global masking of epitopes on the PCL, we co-stained some samples with an antibody recognizing the mitotic histone modification H3-S28ph (Goto et al., 1999; Goto et al., 2002). As shown in the prometaphase cell in Figure 3A, this antibody stained cells expressing sh-Luc or sh-p150 equally

well, suggesting that p150 regulates Ki-67 accumulation on the PCL rather than affecting overall epitope accessibility on mitotic chromosomes.

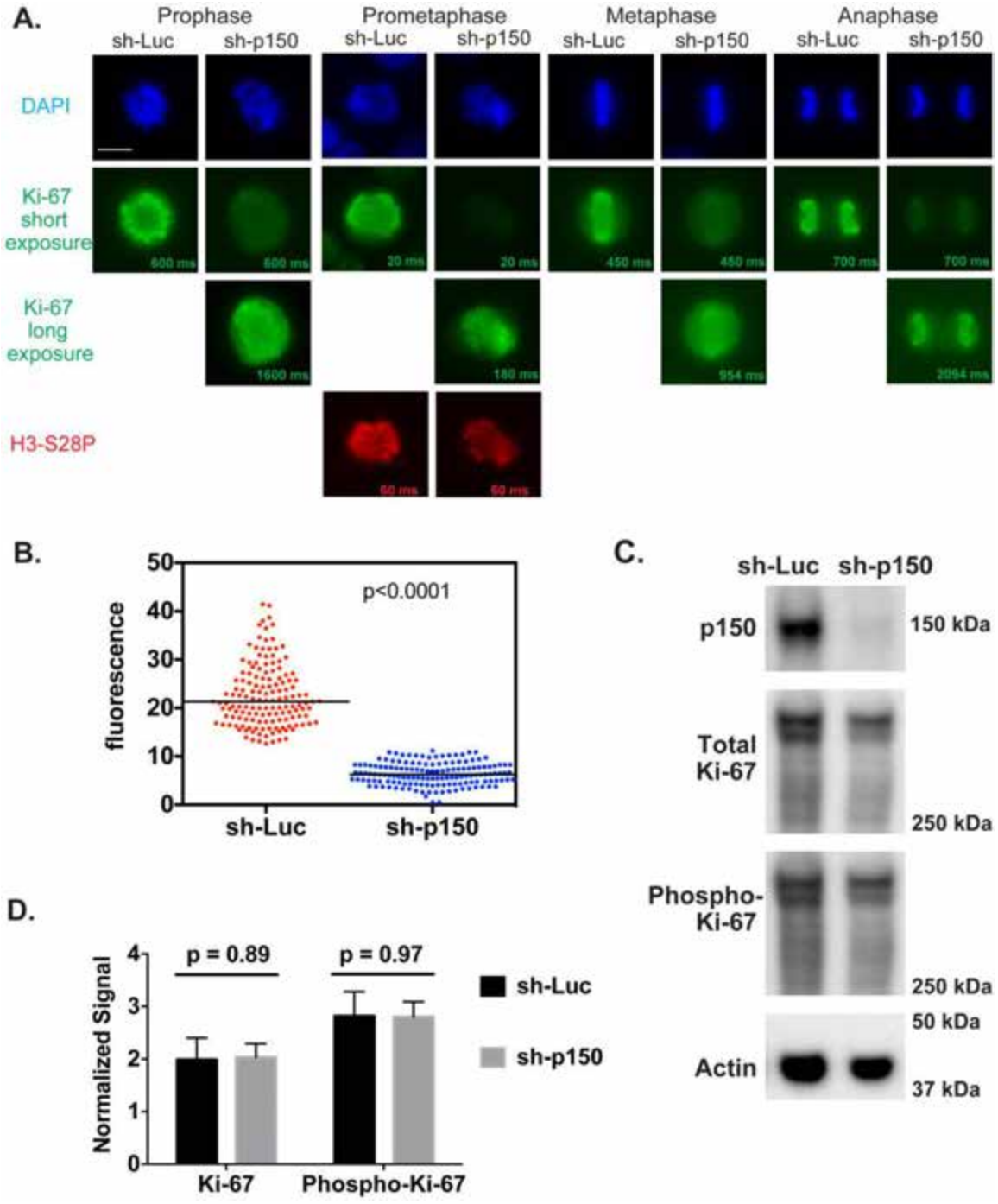
To explore how p150 may be regulating Ki-67 localization, we tested whether p150 is required for maintaining steady-state levels of Ki-67. Our previous work demonstrated that Ki-67 steady-state levels were not affected upon p150 depletion in asynchronous cells (Smith et al., 2014). To distinguish whether p150 regulates the steady-state protein levels of Ki-67 during mitosis, extracts from mitotic-arrested cells expressing sh-Luc or sh-p150 were collected and analyzed by immunoblotting (Smith et al., 2014) (Figure 3.7, C and D). Total levels of Ki-67 in mitotic samples normalized to actin signals were not significantly changed upon p150 depletion (Figure 3.7, C and D), indicating that p150 is not required for maintaining steady-state levels of Ki-67 during mitosis. At the beginning of mitosis, Ki-67 localization to the PCL occurs in conjunction with hyperphosphorylation of the Ki-67 protein (Endl and Gerdes, 2000; MacCallum and Hall, 1999; Takagi et al., 2014a). These phosphorylations are important for PCL localization, as treatment of mitotic cells with protein kinase inhibitors results in dephosphorylation of Ki-67 and relocalization of Ki-67 away from the PCL to distinct nuclear foci (MacCallum and Hall, 1999). Therefore, we tested whether p150 regulates Ki-67's mitotic phosphorylation status by reprobing the immunoblots of mitotically-arrested cell extracts with antibodies that specifically recognize Ki-67 phosphorylated on Cdk consensus sites within the Ki-67 internal repeat structure (Takagi et al., 2014). However, we detected no statistically

significant changes upon p150 depletion (Figure 3.7, C and D). Therefore, p150 does not appear to regulate the steady-state levels or phosphorylation of Ki-67 during mitosis.

Figure 3.7: p150 regulates Ki-67 localization during mitosis

(A): HeLa S3 cells from the indicated cell cycle stages expressed an shRNA directed against luciferase (sh-Luc) or p150 (sh-p150) for 72 hours and were stained with DAPI to visualize DNA (blue) and antibodies against Ki-67 (green). Exposure times for Ki67 are indicated on each image, and in the sh-p150 expressing cells different exposure times are shown to illustrate reduced Ki-67 accumulation on the PCL. As a positive control for antibody accessibility, cells in prometaphase were also stained with antibodies recognizing the mitotic marker histone H3-S28-phosphate (red). Scale bar is 10 μm. (B): Quantified corrected total cellular fluorescence of cells from three biological replicate experiments of cells expressing sh-luc (red, N=150) or sh-p150 (blue, N=147). (C): Immunoblot analysis of extracts from shRNA-expressing cells described in (A) arrested in mitosis (12 hours in 100 ng/mL nocodazole followed by shaking off mitotic cells). Blots were probed with antibodies recognizing p150 (top), Ki-67 (upper middle), phospho-Ki-67 (lower middle), and actin (loading control, bottom). Numbers on the right indicate migration of marker proteins, in kDa. (D): Quantification of the Ki-67 and phospho-Ki-67 blots from (C), normalized to actin signal (N=3). Quantification was performed using the BioRad ChemiDoc system.

Figure 3.7 p150 regulates Ki-67 localization during mitosis



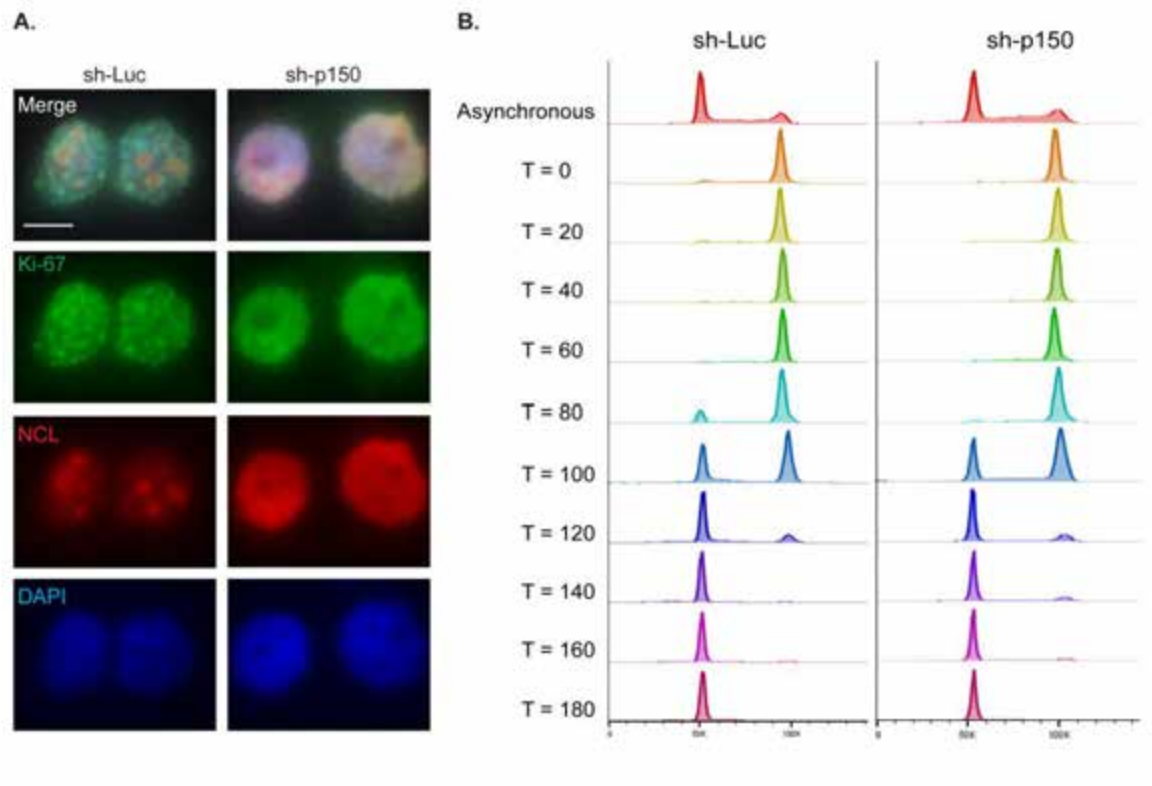
3.3.4: p150 regulates the formation of Ki-67 foci in early G1 phase

Because p150 regulates the localization of Ki-67 to the nucleolus during interphase (Smith et al., 2014) and to the PCL during mitosis (Figure 3.7, A), we wanted to examine whether p150 is also required for the formation of the punctate Ki-67 foci seen at the beginning of G1 phase. To answer this question, we induced expression of sh-Luc or sh-p150 for 60 hours, and then synchronized cells by adding 100 ng/mL nocodazole for the final 12 hours of shRNA expression. After vigorously shaking mitotic cells off the plate, cells were washed three times in PBS and released into nocodazole-free media. Based on FACS of a time course after release (Figure 3.8, B), G1 cells were collected at 120 minutes post release, and stained with antibodies directed against Ki-67 and NCL (Figure 3.8, A). In the sh-Luc samples, hundreds of punctate Ki-67 foci were visible, while NCL was detected within the newly reformed nucleoli. In contrast, sh-p150 samples featured disrupted NCL localization, and dispersal of Ki-67 foci. Together, our data suggest that the contribution of p150N to interphase Ki-67 and NCL localization (Smith et al. 2014) results from events that begin in M and/or G1 phase. In this manner, p150 regulates Ki-67 localization throughout the cell cycle.

Figure 3.8: p150 regulates Ki-67 localization during early G1 phase of interphase

(A): HeLa S3 cells that expressed an shRNA directed against luciferase (sh-Luc) or p150 (sh-p150) for 72 hours were synchronized in mitotsis (12 hours in 100 ng/mL nocodazole followed by shaking off), and released into drug-free media for two hours to enrich for early G1 cells. Cells were stained with DAPI to visualize DNA (blue) and antibodies against Ki-67 (green) and NCL (red). Scale bar is 10 µm. (B): FACS histograms showing cell-cycle profiles of propdium-iodide stained HeLa S3 samples from Figure 3.8, E. Hela S3 cells expressed sh-Luc or sh-p150 for 60 hours before treatment with 100 ng/mL nocodazole for 12 hours. Mitotic cells were then shaken off, washed three times with PBS, and released into media. Time points were taken every 20 minutes for 3 hours, and histograms generated using FlowJo V10.2.

Figure 3.8: p150 regulates Ki-67 localization during early G1 phase of interphase



3.3.5: The SIM within the N-terminus of p150 is required for Ki-67 localization to the PCL

To map p150 domains required for regulating Ki-67 accumulation on the PCL, we utilized previously published HeLa cell lines stably expressing V5-epitope tagged, sh-RNA resistant, p150-derived transgenes (Smith et al., 2014). These V5-transgene cell lines were acutely depleted of endogenously-encoded p150 via lentiviral expression of sh-p150 for 72 hours prior to immunofluorescence analysis of Ki-67. The C-terminal two-thirds of p150 serves as the scaffold for binding the other two subunits of the CAF-1 complex, and thereby is essential for CAF-1's nucleosome assembly activity (Kaufman et al., 1995; Takami et al., 2007). In contrast, p150's N-terminus is dispensable for nucleosome assembly (Kaufman et al., 1995) but is necessary and sufficient to maintain Ki-67 localization to the nucleolus during interphase (Smith et al., 2014). We found that depletion of p150 in HeLa cells expressing either Luciferase or a p150 transgene encoding the C-terminus (amino acids 311-938) displayed reduced Ki-67 localization to the PCL (Figure 3.9, A). In contrast, cells expressing either full-length p150 (aa 1-938) or only the N-terminus (p150N, aa 1-310) maintained normal amounts of Ki-67 on the PCL (Figure 3.9, A). Therefore, the p150 N-terminus regulates mitotic Ki-67 abundance in a manner independent of the chromatin assembly activity of the CAF-1 complex.

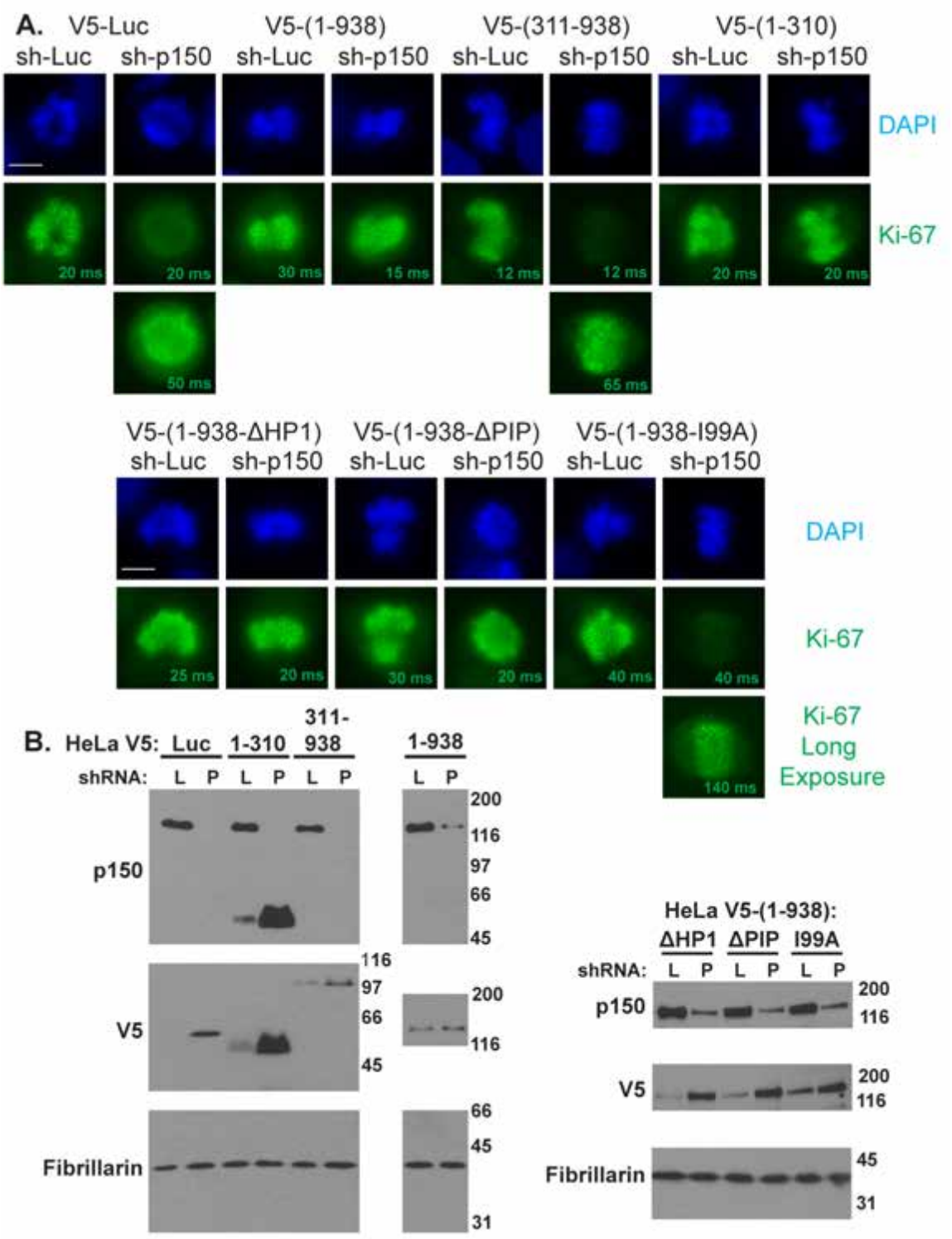
p150N contains several known interaction motifs, including a non-canonical PCNA-interacting peptide (PIP) (Moggs et al., 2000; Rolef Ben-Shahar et al.,

2009), a heterochromatin protein 1-binding domain (Murzina et al., 1999), and a sumoylation-interacting motif (SIM) (Sun and Hunter, 2012; Uwada et al., 2010). Notably, the SIM in p150N is required for normal Ki-67 localization to the nucleolus during interphase (Smith et al., 2014). We therefore determined if transgenes encoding full-length p150 with mutations in the three motifs described above supported normal Ki-67 accumulation during mitosis. The cell lines expressing p150 transgenes with mutations in the PIP and HP1 domains maintained normal Ki-67 levels on the PCL. However, cells expressing a p150 transgene with a single amino acid mutation (I99A) that disrupts the SUMO-binding activity of the SIM (Uwada et al., 2010) displayed reduced levels of Ki-67 on the PCL (Figure 3.9, A). Together, our data indicate that the SIM motif within the N-terminus of p150 is required for the normal accumulation of Ki67 on the PCL during mitosis.

Figure 3.9: The SIM within the N-terminal domain of p150 is sufficient to maintain Ki-67 localization to the PCL

(A): HeLa cells in prometaphase expressing the indicated shRNA-resistant p150 transgene were infected with lentiviruses encoding the indicated shRNAs (sh-Luc or sh-p150) for 72 hours, and then stained with DAPI to visualize DNA (blue) and antibodies against Ki-67 (green). Note that upon expression of sh-p150, cells expressing luciferase (V5-Luc), the p150 C-terminus (V5-(p150-311-938)), or p150 with a I99A point mutation in the SIM motif required longer exposure times to detect Ki-67 on the PCL. Scale bar is 10 μm. (B): Immunoblots of cell extracts described in (A), expressing either sh-Luc (L) or ph-p150 (P). Blots were probed with antibodies recognizing p150 (top), V5 transgenes (middle), and fibrillarin (loading control, bottom). Note the depletion of endogenous p150 in sh-p150 lanes, and that V5-tagged transgene expression often increased in these lanes, as we had observed previously (Smith et al., 2014).

Figure 3.9: The SIM within the N-terminal domain of p150 is sufficient to maintain Ki-67 localization to the PCL



3.4: Discussion

These data and our previous studies suggest a hierarchical relationship between p150N and Ki-67 in regulating nuclear architecture across the cell cycle (Figure 3.10). p150 and Ki-67 both co-localize during mitosis and interphase (Figures 3.2-3.4, and 3.6; (Smith et al., 2014)), regulate NAD localization (Figure 3.1; (Booth et al., 2014; Smith et al., 2014; Sobecki et al., 2016), and have established roles in regulating heterochromatin (Quivy et al., 2008; Sobecki et al., 2016). It is noteworthy that p150 is required for the formation of punctate Ki-67 foci in early G1 of the cell cycle, as previous studies have demonstrated that these foci co-localize with heterochromatic satellite repeats typically enriched within NADs (Bridger et al., 1998). Because ablation of these foci results in mislocalization of NAD elements, we hypothesize that the function of these foci may be to guide heterochromatin-rich NADs back to the nucleolar periphery. However, additional evidence, such as the deep-sequencing of the DNA elements contained within these foci, is required to further support this hypothesis.

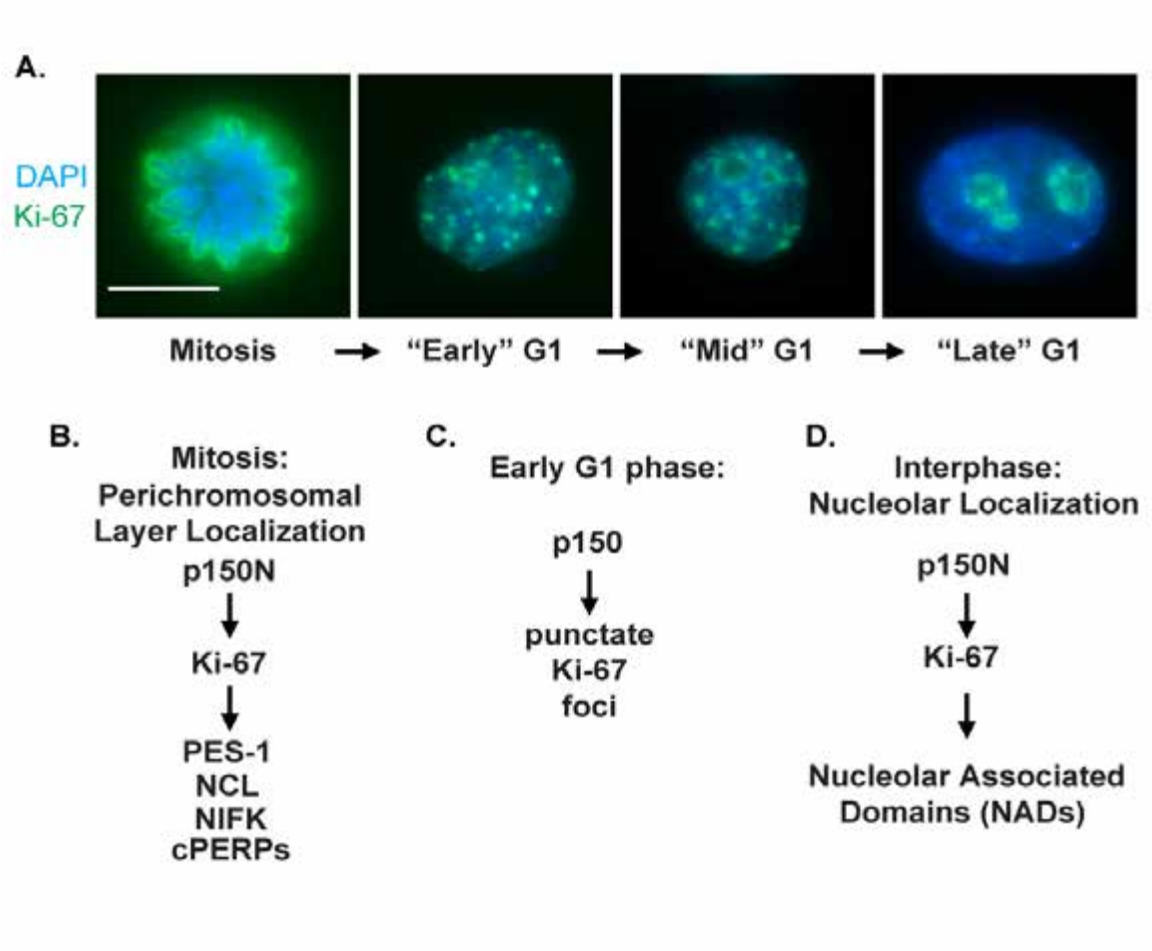
p150N appears to function upstream of Ki-67 in this hierarchy, as p150N is required for efficient Ki-67 association with the PCL during mitosis (Figure 3.7) and with the nucleolus during interphase (Smith et al., 2014). p150N is dispensable for nucleosome assembly by CAF-1, indicating that p150's role in regulating Ki-67 localization is independent of histone deposition. During both mitosis and interphase, the SIM within p150N is required for Ki-67 localization

(Figure 3.9;(Smith et al., 2014)), suggesting that this action involves an as yet unidentified sumoylated protein. These data suggest that future studies should explore the contributions of the p150N domain and its putative sumoylated binding partners to the relationship between Ki-67 and p150 in regulating mitotic and interphase nuclear structure.

Figure 3.10: p150 regulates Ki-67 localization throughout the cell cycle: a summary of dependency relationships

(A): HeLa S3 cells were stained with DAPI to visualize DNA (blue) and antibodies against Ki-67 (green) to demonstrate Ki-67 staining patterns throughout the cell cycle. (B): Hierarchy of known proteins controlling localization to the perichromosomal layer during mitosis. Proteins dependent on Ki-67 include pescadillo (PES-1; Sobecki et al. 2016), as well as nucleolin (NCL), NIFK, and the cPERPs (Booth et al., 2014). (C): p150 is required for Ki-67 localization to punctate foci during early G1 (Figure 3.8). (D): p150N is required for localization of the Ki-67 protein and NAD loci to nucleoli during interphase (Smith et al., 2014).

Figure 3.10: p150 regulates Ki-67 localization throughout the cell cycle: a summary of dependency relationships



3.5: Materials and Methods

3.5.1: Cell culture

HeLa S3 cells containing the Trex CMV/TO promoters driving either sh-Luc or sh-p150 expression (Campeau et al., 2009) were maintained in RPMI media with 5% tetracycline-free fetal bovine serum (FBS), 2 mM L-glutamine, and antibiotic/antimycotic solution (Life Technologies). shRNA expression was induced by supplementing media with 2 µg/mL doxycycline for 72 hours prior to fixation or processing. Mitotic cells were enriched by adding 100 ng/mL nocodazole for 12 hours (hours 60-72 of the doxycycline treatment) and then freed from the cell culture flask surface by vigorous shaking. To enrich for early G1 cells, shaken mitotic cells were washed three times with PBS, plated onto poly-lysine coated cover slips in drug-free media, and samples were taken at specified time points. HeLa cells continuously expressing the V5-tagged p150 transgenes (Smith et al., 2014) were maintained in DMEM and supplemented with 10% FBS, 2 mM L-glutamine, and antibiotic/antimycotic solution (Life Technologies). RPE1-hTERT cells (a generous gift from Judith Sharp) were maintained in 50:50 DMEM-F12 media supplemented with 10% FBS, 7.5% sodium bicarbonate, 2 mM L-glutamine, and antibiotic/antimycotic solution (Life Technologies).

3.5.2: Depletion Reagents

For lentiviral depletion (Smith et al., 2014), cells were infected at MOI = 7.5 with 6 µg /mL polybrene for 72 hours. Lentivirus reagents were synthesized as previously described (Campeau et al., 2009; Smith et al., 2014). esiRNA reagents were generated as previously described (Fazzio et al., 2008; Smith et al., 2014), using primers listed in Table 2 to generate dsRNA. For esiRNA transfection, 500 ng of siRNAs were transfected in 1 ml Opti-MEM (Life Technologies) with 6 µl of Oligofectamine (Life Technologies). After 6.5 h, 2.5 ml of media was added on top of the transfection cocktail and cells were processed after 72 hours. For synthetic siRNA transfection, 10 µL of 5 µM scramble (Ambion, AM4611) or Ki-67 (Ambion, Catalog #4392420-s8796) siRNAs were diluted in 400 µL Opti- MEM (Life Technologies) with 5 µL RNAiMAX (Invitrogen) and incubated at room temperature for 10 minutes. The siRNA cocktail was then slowly added to 6-well dishes containing 800 µL Opti-MEM, and 6 hours later 2.5 mL of appropriate media (lacking antibiotics) was added. Note that the esiRNA directed against Ki-67 targets the Ki-67 repeat region within exon 13 while the synthetic siRNA targets nucleotides 559-577 (CGUCGUGUCUCAAGAUCUAtt) within exon 6.

Table 3.1: Primers for esiRNA synthesis

This table shows the forward and reverse primers used for generating PCR fragments to particular targets used in Chapter III. These amplified targets were eventually *in vitro* transcribed and digested using RNAse III in order to make esiRNA depletion reagents.

Table 3.1: Primers for esiRNA synthesis

Target	Forward Primer	Reverse Primer
Luciferase	gcgtaatacgactcactataggAACAATTGCTTTTACAGATGC	gcgtaatacgactcactataggAGGCAGACCAGTAGATCC
NCL	gcgtaatacgactcactataggGCGACGAAGATGATGAAGATGA	gcgtaatacgactcactataggGTGAGTTCCAACGCTTTCTCC
Ki-67	gcgtaatacgactcactataggGTGCTGCCGGTTAAGTTCTCT	gcgtaatacgactcactataggGCTCCAACAAGCACAAAGCAA

3.5.3: Immunofluorescence and Immuno-FISH

Cells were plated on poly-lysine (Sigma) coated coverslips for 24 hours prior to manipulation. For immunofluorescence experiments, fixation and permeabilization was performed in 6-well tissue culture dishes to minimize displacement of mitotic cells. After aspiration of media, cells were immediately fixed with 4% paraformaldehyde/PBS for 10 minutes at room temperature. Cells were then gently washed with ice-cold PBS and permeabilized with 0.5% Triton TX-100/PBS on ice for 5 minutes. Cells were then washed twice with room temperature PBS and then incubated in blocking buffer (1% BSA/PBS) for 5-30 minutes in a 37 °C humid chamber. After blocking, cells were incubated with primary antibody in blocking buffer for 2 hours in a 37 °C humid chamber. Coverslips were then transferred to Coplin jars and washed three times with PBS on a rotating platform for 10 minutes at room temperature. After washing, cells were incubated with secondary antibody in blocking buffer for 1 hour in a 37°C humid chamber. Coverslips were then transferred to Coplin jars and washed three times with PBS on a rotating platform for 10 minutes at room temperature. After the final washing step, cells were transferred to a Coplin jar containing DAPI (50 ng/mL) in PBS for 2 minutes. Coverslips were mounted with Vecta Shield (Vector Labs) and images were taken on a Zeiss Axioplan2 microscope with a 63x objective. Corrected Total Cell Fluorescence (CTCF) was quantified using the Image J “measure” feature and background subtracted from an area of the image without a cell. Images were all captured using the same exposure

time across 3 biological replicates, and the unpaired Student's t-test was used to generate p-values. Immuno-FISH was performed as previously reported (Smith et al., 2014). Association percentages for each of the three biological replicates were transformed into arcsine units and the unpaired Student's t-test was used (with Welch's correction) to generate p-values. P-values < 0.05 were considered statistically significant. All statistical analysis was performed using Graphpad Prism 6.

Table 3.2: Antibodies used for immunofluorescence and western blotting

This table shows the origin and dilution of every antibody used in Chapter III. Note that the dilution is dependent on the application of the antibody, and that western blot dilutions are greater than that of immunofluorescence.

Table 3.2: Antibodies used for immunofluorescence and western blotting

Epitope	Species	Manufacturer	Catalog #	Immunofluorescence Dilution	Western Blot Dilution
Fibrillarin	Rabbit	Abcam	Ab5821	1:500	1:2000
H3S28ph	Mouse (Clone HTA28)	Sigma	H9908	1:100	
Ki-67	Rabbit	Abcam	Ab66155	1:500	1:2000
NCL	Mouse (Clone 364-5)	Abcam	Ab136649	1:250	1:1000
p150	Rabbit	(Campeau et al., 2009)			1:2000
p150	Mouse (ss1)	(Smith and Stillman, 1991)		1:500	
p150	Mouse (ss48)	(Smith and Stillman, 1991)		1:500	
Phospho-Ki-67	Rabbit	(Takagi et al., 2014)			1:5000
V5	Mouse	Thermo	R960-25	1:1000	1:2000

3.5.4: Nuclease Digestion

RPE1-hTERT cells were utilized for these experiments rather than HeLa cells because they are sufficiently adherent during detergent permeabilization/ nuclease digestion/ high salt extraction. Nuclease digestion was performed as previously reported (Sheval and Polyakov, 2008), with some modification. Cells were plated onto poly-lysine coated coverslips in 6-well dishes at least 24 hours before manipulation, and all subsequent steps were performed with solutions containing 100 μM PMSF. Cells were washed once with Digestion buffer (10 mM Tris-HCl, pH 7.6, 5 mM $MgCl_2$, 1 mM $CuSO_4$), then incubated in 1% Triton TX-100/ Digestion buffer for 10 minutes at 4 °C. Cells were then gently washed with digestion buffer and incubated in 100 μg/ml DNase I/ Digestion buffer, 100 μg/ml RNAse A/ Digestion buffer, or mock digested ("untreated") in Digestion buffer in a 37°C humid chamber for 30 minutes. Proteins were then extracted by incubating for 10 minutes in Extraction buffer (2M NaCl, 10 mM EDTA, 20 mM Tris-HCl, pH 7.6) at 4°C. Cells on coverslips were immediately fixed as described above, or RNA samples were processed using Trizol (Invitrogen). Briefly, 1 mL Trizol was added directly to the plate and cells were homogenized by pipetting. After incubating for 5 minutes at room temperature, samples were stored at -80 °C until further processing. After thawing, 200 μL Chloroform was added and samples were shaken vigorously for 15 seconds before incubation at room temperature for 2 minutes. Samples were then centrifuged at 13000 x g for 15 minutes at 4 °C. The aqueous phase was transferred to a fresh tube and 1

volume of isopropanol was added and mixed well by vigorous shaking. Samples were then incubated at room temperature for 10 minutes before centrifugation at 13000 x g for 15 minutes at 4 °C. Samples were then washed with 75% ethanol and resuspended with nuclease-free water. 10% of recovered samples were run on a 1% agarose gel to compare RNA digestion efficiency. Early G1 cells were selected by choosing pairs of cells which appeared significantly smaller than surrounding cells and featured hundreds of Ki-67 foci (Croft et al., 1999; Isola et al., 1990; du Manoir et al., 1991). Line scans were performed using the RGB Profiles Tool plugin for Image J.

3.5.5: Western blotting

15 µg of protein were loaded and run through a either Tris-HCl polyacrylamide gradient gel (20-5%) for asynchronous samples, or through a NuPAGE™ Novex™ 3-8% Tris-Acetate Protein Gel (Thermo Fischer) for mitotically-arrested samples. Protein samples were then transferred to a PVDF membrane at 20 volts for 17 hours at 4°C in order to maximize the transfer of high molecular weight Ki-67. Chemiluminescence was acquired using the Biorad ChemiDoc system, and quantified using Biorad Image Lab V 5.2.1

CHAPTER IV: UTILIZATION OF CRISPR/CAS9 GENE EDITING TECHNOLOGY TO GENERATE CELL LINES EXPRESSING ENDOGENOUS, EPITOPE-TAGGED KI-67 FOR FUTURE STUDIES

4.1: Abstract

CAF-1 p150 and Ki-67 both regulate the structure of the human nucleus throughout the cell cycle. Both proteins regulate the localization of heterochromatic satellite repeats to the periphery of the nucleolus during interphase, and the structure of the PCL during mitosis. Despite extensive research exploring the nature of each protein, no study has yet explored the genome-scale localization of p150 or Ki-67 in a cell-cycle dependent manner. In the case of Ki-67, several obstacles exist in mapping genome-scale enrichment, notably the lack of commercially available antibodies able to IP the Ki-67 protein. In this Chapter we will describe the use of CRISPR/Cas9 genome editing technology to integrate a fluorescent protein and epitope into the endogenous Ki-67 locus. This insertion does not perturb the localization of Ki-67 throughout the cell cycle, and allows for the quantitative IP of the endogenous protein. This cell line will be a valuable tool in studying Ki-67 genome-wide enrichment in the future, and demonstrates that CRISPR/Cas9 technology can be used to

overcome obstacles that have traditionally hindered progress in performing molecular biology research.

4.2: Introduction

Chapters II and III demonstrated that p150 and Ki-67 are required for the localization of some NAD elements to the nucleolar periphery (Matheson and Kaufman, 2016; Smith et al., 2014). In order to better understand the full extent of each protein's role in regulating nuclear structure, chromatin immunoprecipitation coupled with high throughput next generation deep sequencing (ChIP-seq) should be performed to identify the precise genomic localizations of each protein during the cell cycle. In addition to possibly opening new avenues of exploration involving these proteins, these experiments will also help to confirm several previously proposed hypotheses. For example, in Chapter III we provided evidence that p150 co-localizes with hundreds of punctate Ki-67 foci early in G1 of the cell cycle (Matheson and Kaufman, 2017). We hypothesized that these foci are bound to heterochromatic satellite repeats in early G1, and that p150 and Ki-67 guide these elements to the nucleolar periphery in order to reestablish heterochromatin domains after cellular division. p150 already has a well-established role in regulating heterochromatin structure, including localizing HP1 (Houlard et al., 2006; Huang et al., 2010; Murzina et al., 1999; Quivy et al., 2004, 2008; Roelens et al., 2016) and replicating H3K9me3

(Loyola et al., 2009; Sarraf and Stancheva, 2004; Uchimura et al., 2006), and therefore may play a role in localizing heterochromatin domains within the nucleus. In support of this hypothesis, previous studies have shown that early G1 foci of Ki-67 co-localize with satellite repeats, such as centromeric alpha satellite, telomeric repeats, and Sat III (Bridger et al., 1998), all of which are highly enriched within mapped NAD data sets (Dillinger et al., 2016; van Koningsbruggen et al., 2010; Németh and Längst, 2011; Németh et al., 2010). If we were able to perform ChIP-seq for Ki-67 in cells synchronized in early G1, late G1, and G2, we could directly test this hypothesis by comparing the overlap between data sets.

However, difficulties in performing ChIP-seq with Ki-67 arise due to the lack of high quality, commercially available Ki-67 antibodies suitable for IP. This may be due in part to the large size of the Ki-67 protein isoforms (345 and 395 kDa) (Figure 4.1) and their notable sensitivity to proteolysis (Schluter et al., 1993). One study reported the ChIP of Ki-67 using an monoclonal antibody they developed to target the 9th exon of Ki-67 (Bullwinkel et al., 2006). While this study successfully showed enrichment of Ki-67 on areas within the rDNA, the enrichment was relatively poor (0.008% IP vs. 0.002% nonspecific) and only examined a few repetitive elements. However, with the development of CRISPR/Cas9 genome editing technology, we now have the ability to engineer the insertion of a ChIP-compatible epitope within the endogenous Ki-67 gene.

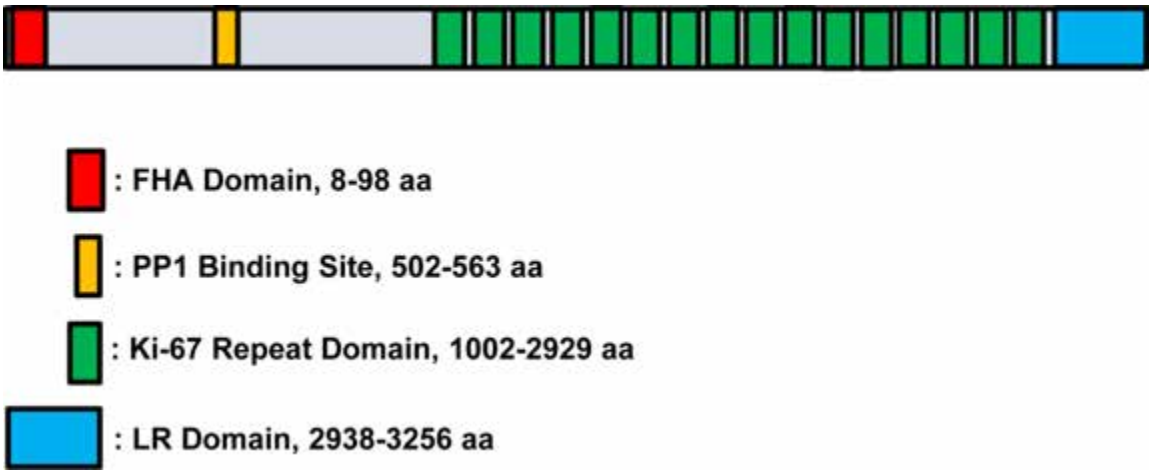
Clustered regularly interspaced short palindromic repeats (CRISPRs) and CRISPR associated proteins (Cas) have been mapped to the genomes of hundreds of different archaea and bacteria species. In 2005, three separate groups discovered these sequences were also present in the genomes of bacteriophages (Bolotin et al., 2005; Mojica et al., 2005; Pourcel et al., 2005), leading to the hypothesis that CRISPRs were part of a bacterial adaptive immune system. While three different versions of this immune system have so far been described (reviewed in (Bhaya et al., 2011)), type II has been adapted to selectively edit the genomes of organisms from yeast to humans (reviewed in (Singh et al., 2017)). The CRISPR type II system has been widely adopted due to its simplicity, requiring only a 20 nucleotide short guide RNA (sgRNA) and the sgRNA-directed endonuclease Cas9 in order to induce double stranded breaks (DSBs) at target DNA sequences (Cong et al., 2013; Garneau et al., 2010; Gasiunas et al., 2012; Jinek et al., 2012; Mali et al., 2013). The sgRNA directs homology-dependent dsDNA cleavage by Cas9 at 3 nucleotides from the terminal end of the protospacer associated motif (PAM) (Gasiunas et al., 2012). In order to selectively edit the endogenous genome, a repair template is introduced with homology to the genome and mutations where desired. After cleavage near the PAM sequence occurs, the DSB is repaired using either the non-homologous end joining (NHEJ) or homology-directed repair (HDR) pathways. In the event that HDR is used to resolve the DSB, the mutated repair template may be utilized, resulting in the incorporation of the desired mutations

directly into the genome. Through CRISPR/cas9 genome editing technology, we proposed to incorporate a ChIP-compatible epitope into the endogenous Ki-67 gene in order to facilitate further study of this protein.

Figure 4.1: Diagram of isoform 1 (395 kDa) of Ki-67

Ki-67 contains an FHA domain near its N-terminus (red), a PP1 binding site (orange), 16 different Ki-67 canonical repeat domains (green), and a C-terminal LR domain. Amino acid (aa) locations for each domain are given for Ki-67 isoform 1, however isoform 2 also contains all of the domains described within the diagram. (Schluter et al., 1993)

Figure 4.1: Diagram of isoform 1 (395 kDa) of Ki-67



4.3: Results

4.3.1: Design of repair template

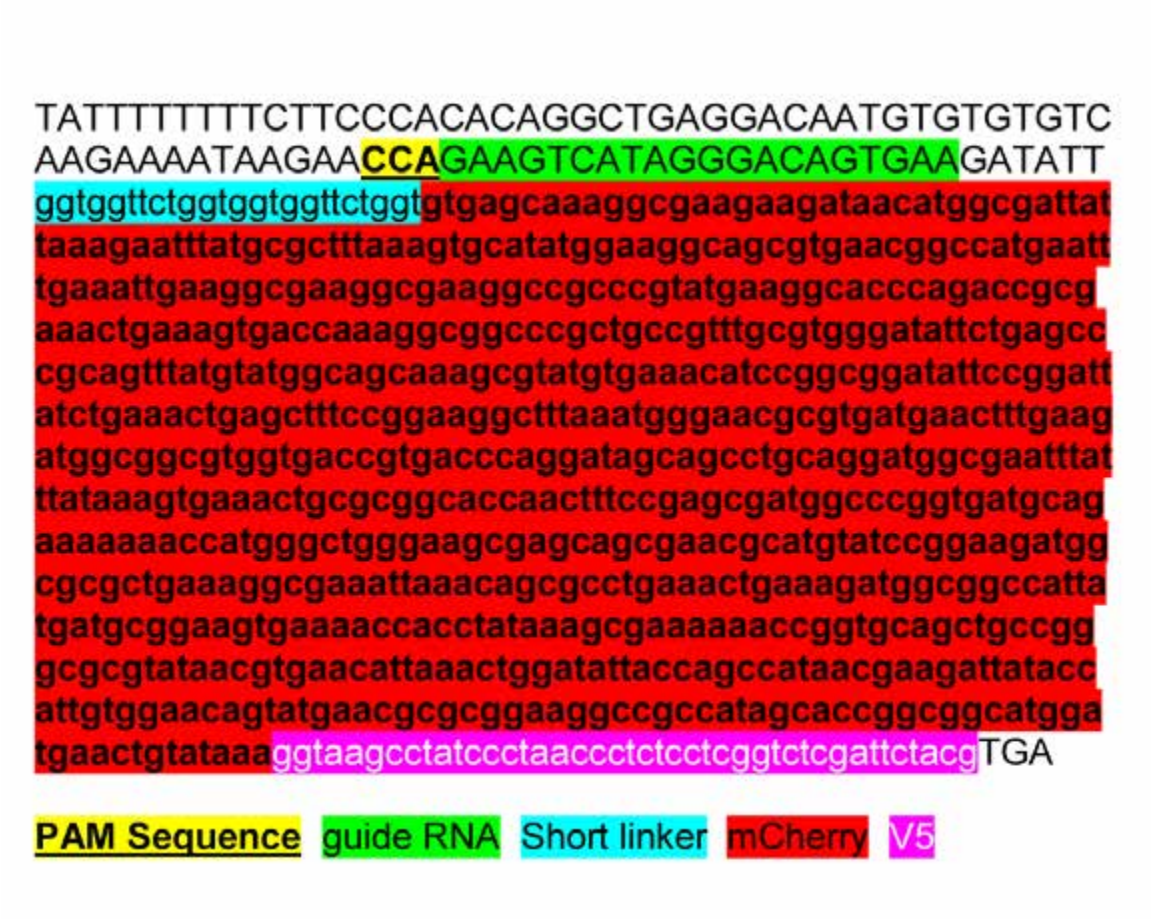
We first decided to edit the genome of the HeLa S3 cell because many of our previous studies regarding Ki-67 and p150 have been performed in this line (Matheson and Kaufman, 2016; Smith et al., 2014). We chose to use the epitope 3xV5 (henceforth referred to as V5) because we have successfully used this epitope previously for both IP and IF. A gene encoding a fluorescent molecule was also added to the repair template, in order to facilitate future microscopy studies, and to allow for FACS-mediated isolation of tagged clones. The fluorescent protein mCherry was selected due to its photostability compared to other monomeric fluorescent proteins (Shaner et al., 2004). However, due to the repetitive nature of the DNA sequence encoding mCherry, several silent mutations were introduced across the gene in order to decrease the overall repetition of the repair template, as repetitive elements can hinder synthesis. A short (Gly-Gly-Ser-Gly)x2 linker between the Ki-67 protein and the mCherry-V5 insert was used in order to decrease the probability of interfering with Ki-67 function. The C-terminal LR domain is required but not sufficient for localization to both nucleolar chromatin and the PCL (Cuylen et al., 2016; Saiwaki et al., 2005) and so we decided to insert the mCherry_V5 tag at the C-terminal end of the protein before the stop codon (Figure 4.2). We used the Zhang lab (MIT) optimized guide RNA CRISPR design algorithm (http://crispr.mit.edu/) (Xu et al.,

2015) to identify several potential guide RNAs near the beginning of the 3'UTR of Ki-67. Once sgRNAs were chosen, silent mutations were made within the repair template at the PAM sequence and sgRNA region in order to decrease continued Cas9 cleavage after successful integration of the repair template.

Figure 4.2: Diagram of mCherry_V5 insert

This Diagram shows part of the repair template used to edit the C-terminus of Ki-67. The endogenous protein-coding region appears in capital letters, the PAM sequence is underlined and highlighted in yellow, the rest of the guide RNA is highlighted in green, the short (Gly-Gly-Ser-Gly)x2 linker is highlighted in light blue, the modified mCherry is highlighted in red, and the V5 epitope is highlighted in magenta. Note that the endogenous stop TGA codon was moved to the end of the C-terminal insert.

Figure 4.2: Diagram of repair template



4.3.2: Isolation and confirmation of homozygous insert clones

HeLa S3 cells were transfected with plasmids containing Cas9, the C-terminal targeting sgRNA, and the repair template described in the previous section. After two days of puromycin selection in order to remove non-transfected cells, mCherry-positive single cells were sorted into a 96-well plate. These cells were expanded until enough cells could be used for IF screening. Cells were plated onto lysine-coated coverslips in order to maintain attachment of mitotic cells, fixed, permeabilized, and then stained with an antibody directed against the V5 epitope. The 11 fastest growing clones were screened first in order to gauge the localization of the mCherry and V5 signal. Out of the 11 clones, 3 showed mCherry/V5 signal within the cytosol, and 1 clone showed mCherry/V5 signal within the nucleus, suggesting random insertion of the repair template. The remaining 7 clones all showed mCherry and V5 co-localization within the nucleolus, suggesting successful insertion of the repair template into the C-terminal region of Ki-67.

The brightest of these clones (Figure 4.3, A.) also showed that the repair template was homozygously inserted when the clone genomic DNA was examined via PCR (Figure 4.3, B.). When screening by PCR, ideally primers should be positioned outside of the repair template. This is to ensure that the PCR product does not originate from a random insertion of the repair template somewhere within the genome. However, due to the large size of the mCherry-

V5 repair template (2 kb), PCR primers were designed to flank the C-terminal stop codon of Ki-67. Although a PCR product of these primers could yield an amplification product from a non-specific insertion event, these primers would allow for the examination of the endogenous locus. In lane 1 of the agarose gel in Figure 4.3 B., the parental line shows a single PCR product at 286 bp. The PCR product in lane 2 appears to be around 1057 bp, the size of the expected amplification product of the locus with the mCherry-V5 insert. Due to the lack of a 286 bp product in this lane, we can conclude that all endogenous Ki-67 loci underwent HDR. When mitotic cells from this clone were observed in prometaphase, metaphase, and anaphase (Figure 4.4), the V5 and mCherry signal also co-localized at the PCL. Together, these data indicate that this clone contains a homozygous insert of the repair template at all Ki-67 loci, and that the tagged Ki-67 localizes to its appropriate cell-cycle specific destinations.

Figure 4.3: Isolation and validation of homozygously repaired clone

(A): Fluorescent microscopy images of a tagged (Ki-67_mCherry_V5) and untagged HeLa cell both in interphase. These cells were stained with an antibody directed against V5 (green) and DAPI to detect DNA. Note that in the HeLa (Ki-67_mCherry_V5) images the mCherry (red) and V5 signals co-localize at the nucleolus, while the untagged control images show no specific mCherry or V5 signal. Matched exposure times were used for each cell line. Scale bar is 10 µm. (B): 2% Agarose gel showing PCR products from a reaction using primers flanking the insertion site of the repair template. Untagged wild type DNA should result in a 286 bp product, while the (Ki-67_mCherry_V5) insert should yield a product of 1057 bp. Note that the (Ki-67_mCherry_V5) lane has only PCR products around the 1057 size, suggesting that this clone features a homozygous insert of the repair template at all three Ki-67 gene loci.

Figure 4.3: Isolation and validation of homozygously repaired clone

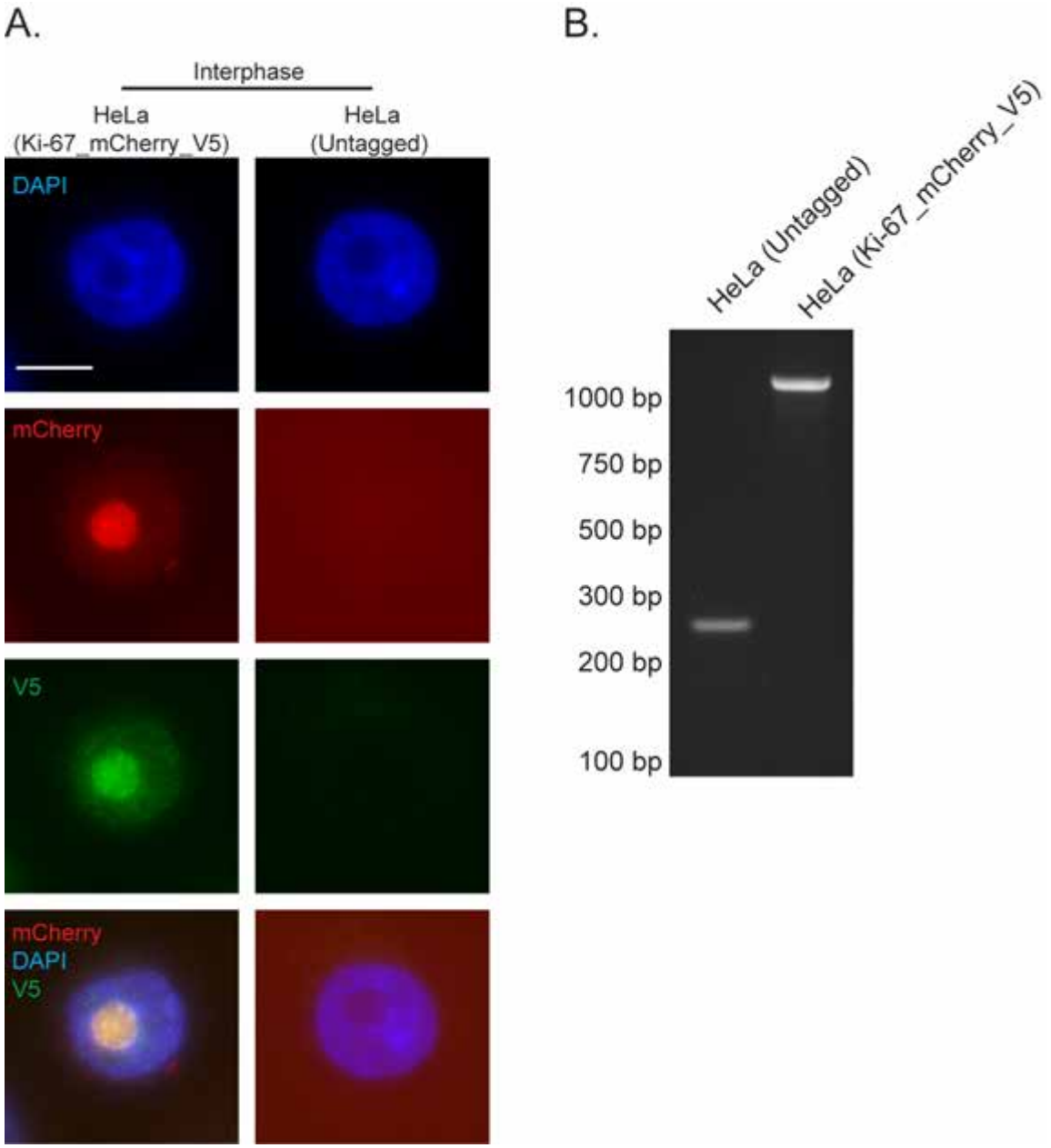
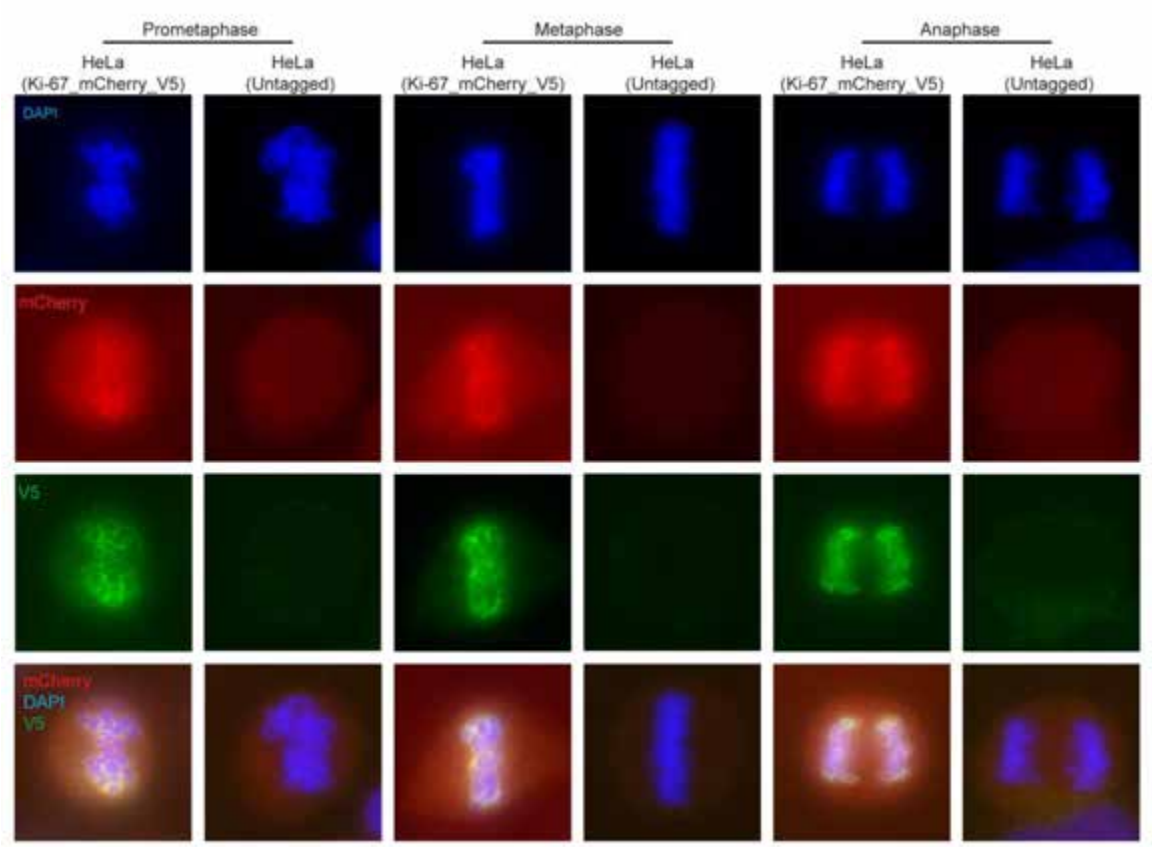


Figure 4.4: Ki-67_mCherry_V5 localizes to the PCL during mitosis

Immunofluorescent images of mitotic untagged HeLa cells and the HeLa (Ki-67_mCherry_V5) clone from Figure 4.3. These cells were stained with an antibody directed against V5 (green) and DAPI to detect DNA. Note that in the HeLa (Ki-67_mCherry_V5) images the mCherry (red) and V5 signals co-localize at the mitotic chromosomal periphery (presumably at the PCL), while the untagged control images show no specific mCherry or V5 signal localization. Matched exposure times were used for each cell line.

Figure 4.4: Ki-67_mCherry_V5 localizes to the PCL during mitosis



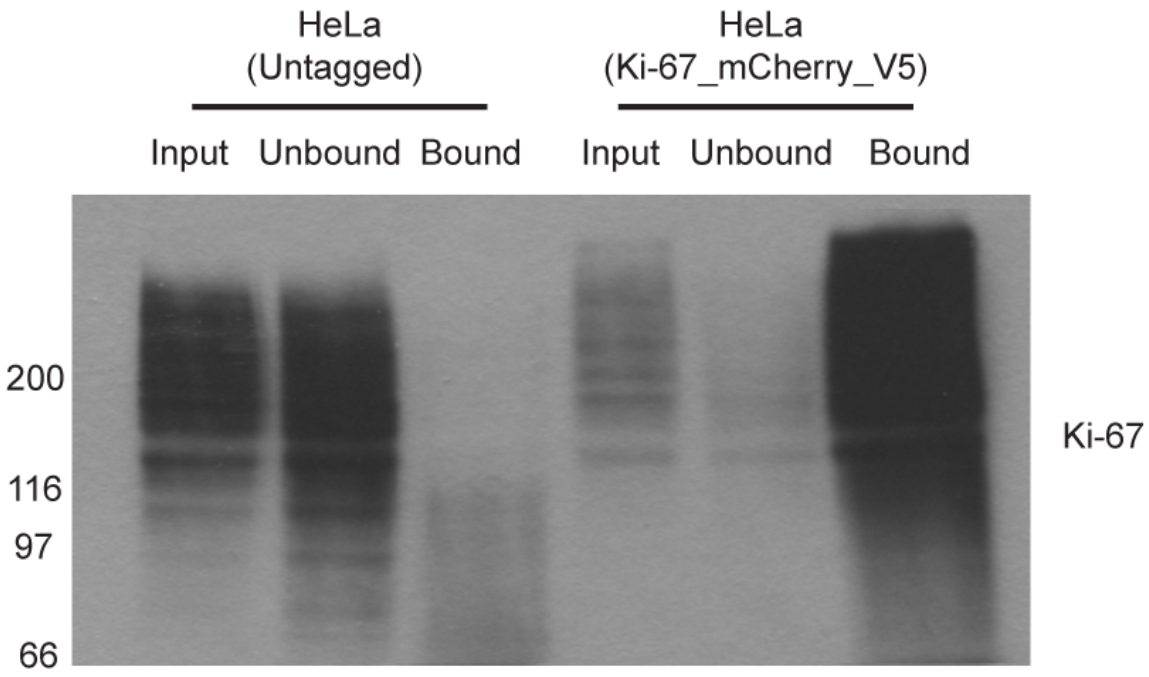
4.3.3: Immunoprecipitation of Ki-67 using the V5 epitope

The homozygous-insert confirmed clone was next used to perform IP using an antibody directed against the V5 epitope. 400 µg of nuclear extract from the untagged parental cell line and the mCherry_V5 line were pre-cleared with beads, and then incubated with 2 µl of monoclonal anti-V5 antibody for 18 hours. After successive washing steps, bound protein was boiled off the beads in SDS-lysis buffer and run on a 20-5% gradient Tris-HCl gel. In order to transfer the maximum amount of high molecular weight Ki-67 protein, the gel was transferred to a PVDF membrane at 20 volts for 17 hours at 4 °C. When the blots were probed with a rabbit anti-Ki-67 antibody, high molecular weight Ki-67 can be observed in both the input lanes for the untagged and tagged samples (Figure 4.5). The untagged samples show robust signal in the unbound lane and virtually no high molecular Ki-67 signal in the bound lane, suggesting that the antibody does not IP untagged Ki-67. The opposite is observed in the tagged samples: the unbound lane shows some Ki-67 signal, however the signal in the bound lane is saturated. This demonstrates that the anti-V5 antibody is sufficient to quantitatively IP endogenous Ki-67 protein in the mCherry_V5 cell line. Future studies should next explore whether this cell line would be suitable for ChIP experiments, in order to determine the genomic enrichment of Ki-67 in a cell-cycle specific manner.

Figure 4.5: Immunopurification of Ki-67_mCherry_V5

Western blot of the input (4%), unbound (4%), and bound (100%) fractions of an immunoprecipitation experiment performed with untagged HeLa cells and the (Ki-67_mCherry_V6) clone shown in Figures 4.3 and 4.4. Immunoprecipitation was performed using a V5 antibody (Thermo) and western blots probed with antibodies directed against Ki-67. Note that the unbound fraction of the untagged cells features high molecular weight Ki-67 and no detectable Ki-67 enrichment in the bound lane. In contrast, the (Ki-67_mCherry_V5) unbound lane shows a depletion of Ki-67 signal and a saturation of high molecular weight Ki-67 signal in the bound lane.

Figure 4.5: Immunopurification of Ki-67_mCherry_V5



4.4: Discussion

We have successfully used CRISPR/cas9 gene editing technology to introduce a mCherry_V5 epitope into the C-terminus of all endogenous Ki-67 loci in a cloned HeLa S3 cell line. This insertion does not interfere with the endogenous localization of Ki-67 to the nucleolus during interphase, nor to the PCL during mitosis. Further, the V5 epitope is sufficient to quantitatively IP endogenously-encoded Ki-67 protein, and future studies should focus on using this cell line to perform ChIP-seq in a cell-cycle dependent manner.

During mitosis Ki-67 and p150 both localize to the PCL (Matheson and Kaufman, 2017; Verheijen et al., 1989b), a characteristic which could prove to be a valuable tool in further examining the structure of the condensed mitotic chromosomes. Many labs have long explored the organization of the mitotic chromosomes (Bak et al., 1977; DuPraw, 1966; Marsden and Laemmli, 1979). However, it was not until the recent development of chromosome conformation capture coupled with high throughput next generation deep sequencing (Hi-C) (Belton et al., 2012; Lieberman-Aiden et al., 2009) that progress was made in mapping mitotic chromosome organization. The Dekker lab performed Hi-C studies with HeLa cells arrested in metaphase and found that topologically associating domains (TADs) were not present within the condensed chromosomes (Naumova et al., 2013). Through polymer model simulations, the Dekker lab hypothesized that the mitotic chromosomes are organized as a linear,

longitudinally compressed array of consecutive chromatin loops (Naumova et al., 2013). While this study revealed much about the macrostructure of the mitotic chromosome, there are still many questions to be answered. One of these questions may be answered by performing ChIP-seq on Ki-67_mCherry_V5 in order to determine the loci frequently associated with the exterior of the condensed mitotic chromosomes. We hypothesize that the exterior domains of the mitotic chromosomes are enriched for heterochromatic satellite elements that will eventually reassociate with the periphery of the nucleolus as NADs. Studies have shown that both p150 and Ki-67 have minimal DNA-binding activity during prophase and metaphase due to hyperphosphorylation, but regain DNA-binding ability at the beginning of anaphase (Endl and Gerdes, 2000; MacCallum and Hall, 1999, 2000; Marheineke and Krude, 1998). This process is better described for Ki-67: at the beginning of anaphase, Ki-67 recruits PP1γ to facilitate dephosphorylation, coinciding with a shift to an immobile state, and a reestablishment of DNA binding activity (Endl and Gerdes, 2000; MacCallum and Hall, 1999; Saiwaki et al., 2005; Takagi et al., 2014b). Therefore, synchronization protocols should be utilized to arrest cells in anaphase in order to capture chromatin interactions with Ki-67_mCherry_V5.

Future studies should also use the reagents described within this chapter to tag endogenous Ki-67 in other cell lines, further exploring the role Ki-67 in regulating nuclear structure in noncancerous cells. This chapter also demonstrates that CRISPR/cas9 technology can be used to overcome hurdles

which have traditionally hindered progress in studying the molecular functions of various proteins. Future studies should continue to utilize CRISPR/cas9 to selectively mutate specific subdomains within Ki-67. For example, Ki-67 contains an HP1 binding motif within its LR domain in the C-terminus (Kametaka et al., 2002). Since the NADs are enriched for heterochromatic satellite repeats, CRISPR/cas9 technology could be utilized to disrupt the HP1 binding motif and in order to determine if it is required for the localization of the NADs. The speed, ease of use, and low cost of CRISPR/cas9 technology will allow future studies to rapidly investigate the molecular nature of Ki-67 and elucidate its role in regulating human nuclear structure.

4.5: Materials and Methods

4.5.1: CRISPR/cas9 design and reagents

sgRNAs were designed using the Zhang lab (MIT) optimized guide RNA CRISPR design algorithm (http://crispr.mit.edu/) (Xu et al., 2015) and cloned in to the pX330_Puro plasmid (a gift from T. Fazzio) (Pyzocha et al., 2014).The sgRNA oligos were 5'-CACCGTTCACTGTCCCTATGACTTC-3' and 5'-AAACGAAGTCATAGGGACAGTGAAC-3'. The repair template was purchased as a gBlock (Integrated DNA Technologies) and cloned into pCR2.1 (Thermo). The gBlock contained 774 bp coding the (mCherry_V5 insert), and 613 bp of

DNA homologous to the regions flanking either side of the Ki-67 stop codon

(Figure 4.2). The entire 2000 bp repair template is as follows:

TCGGTAGTCCTAGAAAATGCATATATAAGATAGATTTTTTCCAGTAAGAAGCT
TGTAGCCATGCTTTTCACCATGGTTCCTCTCCCTTAGCCAAGGGGTGAGAAC
TACTGCAAGAGTAAAGGCCAAGGCAGGTCTCCTGCATGCAAGTTGGGCATG
CTTCTGTCTACAGGGGTTCCTTGGTTTAGGAGACCCAAAAGACTTAATCCTG
GTTGGATTCACTTTTTCTGAGTGACATTTTTTAGTTTGTGAAAATGTGTGCAT
CGATGAAGAAATTTTATTATGAATTAGCTTAAAAATGCATTAGGAACTTCTGT
ATGAAAAGATCACATTATTTAAGTGTAAAAAAACTGCATAATAAAAGCAGTTC
AAGTCAAGAAAAACAATGTTAATGGAATATATTTTAAAACTTATTTCCAACCT
CAAAATTAATTTTCTGCAACTAAGGACCTGCATAATACCTAGTAAGCCTTTGG
GGTTTTGCAGAGGAGGTCGATTCTAAAAATGGGTGTTTAAATTACTTAAGAG
TTCTATTTTTTTTCTTCCCACACAGGCTGAGGACAATGTGTGTGTCAAGAAAA
TAAGAACAAGGAGCCACAGAGATAGCGAGGATATTGGTGGTTCTGGTGGTG
GTTCTGGTGTGAGCAAAGGCGAAGAAGATAACATGGCGATTATTAAAGAATT
TATGCGCTTTAAAGTGCATATGGAAGGCAGCGTGAACGGCCATGAATTTGA
AATTGAAGGCGAAGGCGAAGGCCGCCCGTATGAAGGCACCCAGACCGCGA
AACTGAAAGTGACCAAAGGCGGCCCGCTGCCGTTTGCGTGGGATATTCTGA
GCCCGCAGTTTATGTATGGCAGCAAAGCGTATGTGAAACATCCGGCGGATA
TTCCGGATTATCTGAAACTGAGCTTTCCGGAAGGCTTTAAATGGGAACGCGT
GATGAACTTTGAAGATGGCGGCGTGGTGACCGTGACCCAGGATAGCAGCC
TGCAGGATGGCGAATTTATTTATAAAGTGAAACTGCGCGGCACCAACTTTCC
GAGCGATGGCCCGGTGATGCAGAAAAAAACCATGGGCTGGGAAGCGAGCA
GCGAACGCATGTATCCGGAAGATGGCGCGCTGAAAGGCGAAATTAAACAG
CGCCTGAAACTGAAAGATGGCGGCCATTATGATGCGGAAGTGAAAACCACC
TATAAAGCGAAAAAACCGGTGCAGCTGCCGGGCGCGTATAACGTGAACATT
AAACTGGATATTACCAGCCATAACGAAGATTATACCATTGTGGAACAGTATG
AACGCGCGGAAGGCCGCCATAGCACCGGCGGCATGGATGAACTGTATAAA
GGTAAGCCTATCCCTAACCCTCTCCTCGGTCTCGATTCTACGTGACAGAAAA
ATCGAACTGTTAAAAATATAATAAAGTTAGTTTTGTGATAAGTTCTAGTGCAG
TTTTTGTCATAAATTACAAGTGAATTCTGTAAGTAAGGCTGTCAGTCTGCTTA
AGGGAAGAAAACTTTGGATTTGCTGGGTCTGAATCGGCTTCATAAACTCCAC
TGGGAGCACTGCTGGGCTCCTGGACTGAGAATAGTTGAACACCGGGGGCT
TTGTGAAGGAGTCTGGGCCAAGGTTTGCCCTCAGCTTTGCAGAATGAAGCC
TTGAGGTCTGTCACCACCCACAGCCACCCTACAGCAGCCTTAACTGTGACA
CTTGCCACACTGTGTCGTCGTTTGTTTGCCTATGTCCTCCAGGGCACGGTG
GCAGGAACAACTATCCTCGTCTGTCCCAACACTGAGCAGGCACTCGGTAAA
CACGAATGAATGGATGAGCGCACGGATGAATGGAGCTTACAAGATCTGTCT
TTCCAATGGCCGGGGGCATTTGGTCCCCAAATTAAGGCTATTGGACATCTG
CACAGGACAGTCCTATTTTTGATGTCCTTTCCTTTCTGAAAATAAAGTTTTGT
GCTTTGGAGAATGACTCGTGAGCACATCTTTAGGGACCA

4.5.1: Cell culture

HeLa S3 cells were maintained in RPMI medium (Gibco) with 10% fetal bovine serum (FBS), 2 mM L-glutamine, and antibiotic/antimycotic solution (Life Technologies). CRISPR/cas9 transfection protocol adapted from (Hainer et al., 2016). 24 hours before transfection, 200,000 cells were plated into 6 well dishes. Two to four hours prior to transfection, medium was aspirated, cells were washed twice with PBS, and 1 mL antibiotic-free medium was pipetted over the cells. During transfection 3 µg pX330_Puro containing a sgRNA, 3 µg of pCR2.1 containing the repair template, and 24 µl Fugene HD (Promega) was added to 100 µl OptiMEM (Gibco) and incubated at room temperature for 10 minutes prior to slowly pipetting on top of the cells. 14-16 hours post transfection, cells were trypsinized and plated onto a 10-cm dish with serum-containing media. 48 hours post transfection, cells were washed twice with PBS and media containing 0.5 µg/mL puromycin (Thermo) was pipetted over cells. Cells were incubated in puromycin for an additional 48 hours, before being trypsinized and sorted by a BD FACSAria II Cell Sorter. mCherry-positive single cells were sorted into 96-well dishes in standard media, and expanded until enough cells could be used to screen via immunofluorescence.

4.5.2: Immunofluorescence and microscopy

Cells were plated on poly-lysine (Sigma) coated coverslips for 24 hours prior to manipulation. For immunofluorescence experiments, fixation and permeabilization was performed in 6-well tissue culture dishes to minimize displacement of mitotic cells. After aspiration of media, cells were immediately fixed with 4% paraformaldehyde/PBS for 10 minutes at room temperature in the dark. All subsequent steps were performed in the dark as much as possible in order to avoid bleaching the mCherry signal. Cells were then gently washed with ice-cold PBS and permeabilized with 0.5% Triton TX-100/PBS on ice for 5 minutes. Cells were then washed twice with room temperature PBS and then incubated in blocking buffer (1% BSA/PBS) for 5-30 minutes in a 37 °C humid chamber. After blocking, cells were incubated with mouse anti-V5 antibody (1:1000 dilution, Thermo) in blocking buffer in a 37 °C humid chamber for 60 minutes. Coverslips were then transferred to coplin jars and washed three times with PBS on a rotating platform for 10 minutes at room temperature. After washing, cells were incubated with donkey anti-mouse Alexa 488 secondary antibody in blocking buffer for 1 hour in a 37°C humid chamber. Coverslips were then transferred to Coplin jars and washed three times with PBS on a rotating platform for 10 minutes at room temperature. After the final washing step, cells were transferred to a Coplin jar containing DAPI (50 ng/mL) in PBS for 2 minutes.

Coverslips were mounted with Vecta Shield (Vector Labs) and images were taken on a Zeiss Axioplan2 microscope with a 63x objective

4.5.3: Isolation of genomic DNA and PCR

In order to harvest genomic DNA for further PCR analysis, FACS-sorted clones in 96-well dishes were grown to approximately 75% confluency, before passaging and transferring three-quarters of the cells into a 24-well dish. The remaining cells in the 96 well plate allowed to grow back to confluency, before trypsinization and transfer to a 1.5 ml eppendorf tube. Cells were then centrifuged at 500 x g for 5 minutes at 4°C and resuspended in ice cold PBS. Cells were then centrifuged again before being resuspended in 200 µl in freshly made DNA digest buffer (100 mM Tris HCl pH = 8.0, 250 mM NaCl, 25 mM EDTA, 0.5% SDS, 1 mg/mL Proteinase K). After thoroughly mixing the cells in the buffer, the Eppendorf tubes were placed in a 50 °C rotating chamber and left overnight. The next morning, 200 µl of TE buffer was added to the Eppendorf tubes, before the addition of 400 µl of Phenol Chloroform isoamyl alcohol in a 25:24:1 ratio (Thermo). The cells were vortexed for 10 seconds before being centrifuged at 3000 x g for 10 minutes at room temperature. The aqueous layer was then precipitated with 1/25 volume 5 M NaCl, 1.5 µl glycogen (Sigma, 20 mg/mL), and 2.5 volumes of ethanol. After 60 minutes at -20°C, the Eppendorf tubes were centrifuged at maximum speed for 20 minutes at 4°C. The genomic DNA pellet was washed once with 80% ethanol before being briefly dried and

resuspended in 15 µl buffer TE. Approximately 200 ng of genomic DNA was used per PCR reaction with primers 5'-TTGCAGAGGAGGTCGATTCT-3' and 5'-ATTCAGACCCAGCAAATCCA-3' to amplify a fragment flanking the stop codon of Ki-67.

4.6.3: Immunoprecipitation

5 x10^6 untagged or (Ki-67_mCherry_V5) tagged HeLa cells were plated onto three 15-cm tissue culture plates. The next day, cells were trypsinized, transferred to 50 ml conical tubes, and centrifuged at 1000 x g for 5 minutes at 4°C. Cells were successively washed with cold PBS and 5 mL hypotonic buffer (20 mM Hepes-KOH, pH 8.0, 5 mM KCl, 1.5 mM MgCl2) with 10 mM Iodoacetamide (IAA, Sigma). Cells were then resuspended in 1 mL hypotonic buffer and transferred to a Cells were disrupted by 28 strokes of a B pestle (Wheaton, loose) by dounce homogenization. Nuclei were pelleted by centrifugation for 5 minutes at 1000 x g and washed with nuclei wash buffer (10 mM NaCO3, 150 mM NaCl). The pellet was then incubated in nuclei with extraction buffer (15 mM Tris-HCl, pH 7.8, 1 mM EDTA, 400 mM NaCl, 10% sucrose, 0.1 mM PMSF, 1 mM DTT) for 30 mins in a rotating platform at 4 °C. Extracts were then clarified by ultracentrifugation at 100,000 x g for 60 minutes, and Bradford (BioRad) assays were performed to determine the protein

concentration of the nuclear extract. Nuclear extracts were aliquoted into 500 µg and flash frozen in liquid nitrogen before storage at -80 °C.

For immunoprecipitation, 50 µl of protein A magnetic beads (NEB) were used per 400 µg of nuclear extract. The beads were first transferred to a lobind tube (Eppendorf) and washed three times with A_{200} buffer (25 mM Tris pH 7.5, 1 mM EDTA, 200 mM NaCl, 0.01% NP-40, 10 mM IAA, 0.1 mM PMSF). During the washing steps, a vial of aliquoted nuclear extract was thawed on ice, and then 10% (50 µg) was set aside to serve as an input sample. A_{200} and A_0 (25 mM Tris pH 7.5, 1 mM EDTA, 0 mM NaCl, 0.01% NP-40, 10 mM IAA, 0.1 mM PMSF) was added to 400 µg of nuclear extract until a final concentration of 200 mM NaCl was achieved. This diluted nuclear extract solution was then transferred to a Lobind tube containing half of the beads (25 µl) and rotated for 30 minutes at 4 °C in order to pre-clear the solution. The pre-cleared solution was then transferred to the remaining 25 µl of beads with 2 µl mouse anti-V5 antibody (Thermo) and rotated overnight at 4 °C. The next morning, 10% of the solution was reserved to serve as the “unbound” sample. The beads were washed six times with A_{200} buffer for 5 minutes at 4 °C. After the sixth wash, the beads were resuspended in 25 µl 2X SDS lysis buffer (100 uM Tris HCl pH 6.8, 4% SDS, 12% glycerol, 2% 2-mercaptoethanol, 0.008 bromophenol blue) and boiled for 5 minutes. 4% of the input samples, 4% of the unbound, and 100% of the bound samples were loaded onto a Tris-HCl polyacrylamide gradient gel (20-5%). Protein samples were then transferred to a PVDF membrane at 20 volts for

17 hours at 4°C in order to maximize the transfer of high molecular weight Ki-67, and were sequentially blotted for Ki-67 (Abcam, Ab66155, 1:2000 dilution) and p150 ((Campeau et al., 2009), 1:2000 dilution).

CHAPTER V: DISCUSSION

5.1: Scientific Questions Addressed by this Dissertation

This dissertation attempted to answer a fundamental question of cellular biology: how is nuclear structure reestablished after cellular division? At the beginning of mitosis, nuclear structure is dramatically altered as chromatin is condensed in order to facilitate equal distribution of genetic material to daughter cells. At the beginning of telophase, chromatin decondensation is initiated and the nucleus begins the process of reestablishing interphase nuclear structure. One critical sub-nuclear structure which is disassembled during mitosis and reassembled *de novo* after cytokinesis is the nucleolus (reviewed in (Hernandez-Verdun, 2011). The nucleolus is comprised of thousands of different proteins and RNAs organized around the nucleolus organizer regions (NORs) of the five acrocentric chromosomes in human (reviewed in (Pederson, 2011; Sirri et al., 2008)). In addition to the NORs, thousands of distinct regions within the genome make contact with the nucleolar periphery and are called nucleolar associated domains (NADs) (Dillinger et al., 2016; van Koningsbruggen et al., 2010; Németh et al., 2010; Pontvianne et al., 2016). The NADs are enriched for satellite heterochromatin and the purpose of their localization to the perinucleolar (PN) region is hypothesized to maintain the transcriptionally silenced state within these loci (reviewed in (Matheson and Kaufman, 2015; Padeken and Heun, 2014)).

This dissertation specifically explored how heterochromatin-rich NAD loci are localized to the PN region at the beginning of a new cell cycle. In the

process of trying to answer this question, I discovered that proteins p150 and Ki-67 play a critical role in regulating the localization of some NADs. This discovery yielded many more questions: Where does p150 localize throughout the cell cycle? Do p150 and Ki-67 co-localize at specific phases of the cell cycle? Which domains within the p150 protein regulate NAD and Ki-67 localization? In the following chapter I will discuss experimental results which may answer these and other questions, put these results in the context the published literature, and discuss how future studies can build upon these results.

5.2: Summary of Major Results and Conclusions

5.2.1: p150 regulates the localization of some NADs

Immunoprecipitation of p150 and identification of novel binding partners via mass spectrometry (Co-IP-MS) revealed that p150 interacts with several nucleolar proteins (Table 2.1). Since many of these proteins are responsible for shuttling protein and RNA across the nucleolar border, it was hypothesized that p150 may also be responsible for nucleolar protein localization. As predicted, upon depletion of p150 in some cancer cell lines, several p150-interacting nucleolar proteins are mislocalized to the nucleoplasm (Figure 2.3 and 2.4). However, p150 is not required for the nucleolar localization of every novel binding partner, as p150 depletion fails to mislocalize the pre-ribosomal rRNA processing protein FBL (Figure 2.3 and 2.4). Additionally, the localization of the rDNA arrays within the NORs do not appear to change upon p150 depletion,

suggesting that the macrostructure of the nucleolus remains stable upon p150 depletion (Videos 1.1 and 1.2). In order to determine if NAD localization is regulated by p150, DNA FISH-IF was utilized to examine the localization of several NAD elements in relation to the nucleolus as marked by FBL staining. The NADs examined included the 5S rDNA array on chromosome 1, the D4Z4 macrosatellite array on chromosome 10, and the centromeric alpha satellite region of chromosome 17. The localization of each NAD decreased by approximately 50% upon depletion of p150, while a control region on chromosome 10 previously reported to have little association with the nucleolus showed no change in association (Figure 2.14).

There are several possibilities as to how p150 regulates NAD localization. The first is that p150 regulates NAD localization in conjunction with replication of heterochromatin during mid and late S-phase of the cell cycle. The NADs are highly enriched for heterochromatin silencing marks, including H3K9me3 (van Koningsbruggen et al., 2010; Németh et al., 2010), of which p150 also has a well-established role in replicating during chromatin assembly (Loyola et al., 2009; Reese et al., 2003; Sarraf and Stancheva, 2004). It is possible that depletion of p150 interferes with replication of heterochromatin silencing marks within the NADs, resulting in mislocalization of NAD loci away from the PN region. However, domain-analysis of p150 showed that the N-terminal 310 amino acids (p150N) is necessary and sufficient to maintain normal rates of NAD association (Figure 2.15). p150N is dispensable for chromatin assembly, as the

C-terminal region of the protein acts as the scaffold for p60 and p48 interaction (Kaufman et al., 1995). It is therefore probable that p150 regulates NAD localization outside the context of chromatin assembly, but there are several caveats to consider before drawing such a conclusion. Although p150N cannot perform chromatin assembly independently, we currently have no evidence that it cannot participate in chromatin assembly. It is possible that the N-terminus can still associate with replication foci during S-phase, as it contains a PCNA interacting peptide (PIP) (Rolef Ben-Shahar et al., 2009). Another caveat to consider is that these experiments occur in a depletion setting of p150, meaning there are still residual p150-containing CAF-1 complexes within the cells. This baseline amount of p150-containing CAF-1 is enough to maintain relatively normal cell growth rates, including chromatin assembly, in cancer cell lines. This may also allow p150N to associate with CAF-1 containing replication foci during S-phase and successfully replicate heterochromatin marks within the NAD elements. In order to rule out this possibility, experiments should be performed to determine if p150N can independently localize to replication forks during S-phase. If p150N can independently localize the replication forks, new cells lines will need to be generated using CRISPR/cas9 in order to mutate endogenous regions within p150. Another possible mechanism is that p150 may act as a shuttle of NAD elements to the nucleolar periphery at the beginning of the cell cycle. If p150N cannot localize to replication-foci during S-phase, then this mechanism seems plausible and likely.

5.2.2: The SIM within p150N regulates NAD localization

In order to determine which domains within p150N are important for regulating NAD localization, HeLa cells expressing full length transgenes of p150 were generated with mutations within three distinct motifs within the N-terminus. These mutations disrupted a HP1 binding domain, a PIP box, and a sumoylation interacting motif (SIM). Only the cell line expressing the SIM mutation failed to rescue NAD localization upon depletion of endogenous p150, suggesting that the SIM is required for regulating the localization of NADs (Figure 2.16). Additionally, depletion of SUMO2 or the SUMO E2 ligase UBC9 disrupted NAD localization, suggesting that the interaction of p150 with a sumoylated protein may facilitate NAD localization.

Two questions remain to be answered in order to further our knowledge of this mechanism: what is the identity of the sumoylated protein or proteins interacting with p150, and when do these interactions occur? The process of identifying the sumoylated binding partners of p150 can be accomplished by performing Co-IP-MS in cell lines in which the SIM has been mutated using CRISPR/cas9 genome editing, and comparing it to a control cell line which lacks these mutations. Novel binding partners bound to the control line, but not the SIM mutant line, could be further analyzed to confirm that the interaction is facilitated through interaction of SUMO with the SIM within p150N. These experiments should be performed in the presence of cysteine protease inhibitors

in order to inhibit the action of SUMO specific proteases (SENPs), which can often catalyze de-conjugation of SUMO proteins during cell lysis (reviewed in (Kumar and Zhang, 2015)). Since the original Co-IP-MS experiment which identified novel p150-interacting proteins failed to include cysteine protease inhibitors (Table 2.1), the possibility remains that the sumoylated p150-interacting protein or proteins may not be included within these results.

Several studies have shown that the SIM within p150N has an important role during S-phase of the cell cycle. One study demonstrated that p150 depletion or ablation of the p150N SIM inhibits recruitment of SUMO2/3-conjugated proteins to replication foci (Uwada et al., 2010). Another showed that p150 directly interacts with sumoylated MBD1, and that this interaction is required for the replication of heterochromatin silencing marks and localization of HP1 (Uchimura et al., 2006). Since MBD1 is the only known sumoylated protein which directly interacts with p150, studies should examine whether MBD1 depletion can reproduce NAD mislocalization. It is crucial to identify when sumoylated proteins interact with p150 in regulating NAD localization in order to determine if this mechanism is directly tied to chromatin assembly during S-phase. If the sumoylated p150-interacting protein has been identified through MS, a straightforward method would be to synchronize cells at various phases of the cell cycle and probe whole cell lysates to determine when the p150-interacting protein is sumoylated. The possibility also remains that this

interaction could occur at several points during the cell cycle, and so further experiments described in the following sections would be required.

5.2.3: Ki-67 regulates NAD localization

In order to discover other proteins involved in p150-mediated regulation of NAD localization, novel p150-interacting proteins identified in the IP-MS experiments were further analyzed (Table 2.1). These proteins were depleted in HeLa cells and then the association rates of the alpha satellite on chromosome 17 with the nucleolus were compared to control cells (Figure 3.1). Depletion of the most abundant protein discovered in the Co-IP-MS experiments, Ki-67, was also found to reduce the association of the alpha satellite NAD in a manner similar to that of p150 depletion (Figure 3.1, A and B). Conversely, upon NCL depletion the association of the NAD increased. In addition, the morphology of the nucleolus was altered upon NCL depletion: FBL signal became more dispersed, but still maintained a clear and distinct boundary with the nucleoplasm (Figure 3.1, A and B). This suggests that disruption of nucleolar macrostructure cannot recapitulate the decrease NAD association observed during p150 and Ki-67 depletion, and that an increase in nucleolar surface area may correlate with an increase in NAD localization. Of note, both Ki-67 and NCL nucleolar localizations are also regulated by p150 (Figures 2.3 and 2.4). The SIM within p150N is specifically required for the nucleolar localization of Ki-67 (Figures 2.6,

2.8, and 2.9), suggesting that p150 may be acting upstream of Ki-67 in regulating NAD localization.

Like p150, Ki-67 has a well-established role in regulating heterochromatin structure, but the mechanism of this regulation is ill-defined. Ki-67 directly interacts with HP1 within its C-terminus LR domain (Figure 4.1) (Kametaka et al., 2002), and overexpression of Ki-67 homologs in human cells induces the formation of dense ectopic heterochromatin regions (Sobecki et al., 2016; Takagi et al., 1999). Depletion of Ki-67 results in the relocalization of H3K9me3 heterochromatin domains within the nucleus, and the disruption of centromere and rDNA NOR localization with the nucleolus (Booth et al., 2014; Sobecki et al., 2016). Several classes of genes enriched within the NADs show increased expression after Ki-67 depletion, further suggesting that Ki-67 may regulate both the localization and transcriptional silencing of NAD elements (Sobecki et al., 2016). While Ki-67 may be a prime suspect as the sumoylated p150-interacting protein, only one study has also shown that Ki-67 is sumoylated at lysine 1517 in response to heat shock (Golebiowski et al., 2009). Future studies should attempt to Co-IP p150 and Ki-67, with and without SENP digestion in order to gauge the importance of sumoylation in facilitating this interaction. If Ki-67 is confirmed to be the sumoylated protein interacting with p150 in facilitating NAD localization, future studies should also attempt to identify the precise sumoylation site, and the phase of the cell cycle during which this interaction occurs. CRISPR/cas9

could be utilized to mutate these endogenous sites in order to gauge nucleolar localization of Ki-67, as well as localization of NAD elements.

5.2.4: p150 localizes to distinct Ki-67 foci during early G1 of the cell cycle

After cytokinesis and early in G1, Ki-67 localizes to hundreds of distinct foci (Verheijen et al., 1989a) which co-localize with heterochromatin satellite repeat elements typically enriched within NADs (Bridger et al., 1998). Based on this co-localization and observations that these foci migrate to reforming nucleoli (Saiwaki et al., 2005), I hypothesized that Ki-67 acts to guide heterochromatin to the nucleolar periphery as a mechanism to re-establish NAD structure after mitosis. Since I previously predicted that p150 may also be serving as a shuttle for these heterochromatin domains, I wanted to determine if a subset of p150 co-localized with Ki-67 loci. To address this prediction, cells were stained for both Ki-67 and p150, and early G1 cells were observed based on their Ki-67 morphology. A clear subset of p150 formed punctate foci which co-localized with Ki-67 foci (Figure 3.6), however the majority of p150 signal still remained in the nucleoplasm. When these cells were digested with either RNAse A or DNAse I, the Ki-67 and p150 foci remained intact (Figure 3.6). This suggests that the structural integrity of these foci is not reliant upon the presence of either RNA or genomic DNA. While it would be expected that removal of RNA from transcriptionally silent heterochromatin may not interfere with the structure of these foci, removal of genomic DNA perhaps contradicts the hypothesis that

these foci directly interact with heterochromatin in order to shuttle their localization back to the nucleolus. This does not rule out the possibility that RNA and/or DNA are required for the establishment and not the maintenance of these foci. Since the presence of Ki-67 foci was used as a marker for cells in early G1, early ablation of these foci would not be readily detectable within this assay. In order to determine if the establishment of these foci is dependent upon RNA or DNA, cells should first be synchronized in mitosis, released, digested with the appropriate nuclease, and then stained for p150 and Ki-67. While this experiment may be difficult to perform, as mitotic arrested cells lacking genomic DNA may not proceed through cytokinesis and enter the next cell cycle, these results could prove enlightening and confirm one of my major hypotheses. I predict that this experiment would show a distinct lack of Ki-67/p150 foci after DNAse I digestion, as the association of Ki-67 and p150 to heterochromatin after telophase may be a critical step in establishing Ki-67/p150 foci. However, if the Ki-67/p150 foci remain intact despite mitotic DNAse I digestion, this would provide evidence that Ki-67 and p150 may not be shuttling heterochromatin to the PN region.

Since very little is known of about these foci, multiple experiments should be carried out in order to determine both the function and composition of Ki-67/p150 foci. First, ChIP-seq experiments should be performed in early G1-arrested cells by IP of Ki-67 in order to identify the regions within the genome enriched within these foci. ChIP-seq by IP of p150 may also yield interesting

results, but as the bulk of p150 resides outside of Ki-67 foci, these results may not be helpful in elucidating foci function. I would predict that the Ki-67 ChIP-seq results would show enrichment on heterochromatin and other domains highly enriched within the NAD data sets. It is possible, however, that these foci do not directly interact with chromatin, and that their function could be completely unrelated to regulating NAD localization. Since these foci have been observed to translocate to the nucleolus (Saiwaki et al., 2005), perhaps their function is related to regulating the nucleolar accumulation of proteins and/or RNAs after mitosis. To test this possibility, Co-IP-MS and RIP-seq studies should be carried out to identify other protein and RNA components of these foci.

5.2.5: p150 localizes to the PCL

During mitosis, Ki-67 localizes with many other nucleolar proteins to the periphery of the condensed chromosomes in a structure known as the perichromosomal layer (PCL) (reviewed in (Van Hooser et al., 2005). This layer is hypothesized to ensure equal distribution of nucleolar proteins to daughter cells and to facilitate rebuilding of the nucleoli after cytokinesis (Booth et al., 2014; Sobecki et al., 2016). One study also demonstrated that Ki-67 acts as a surfactant to ensure separation of condensed chromosomes during mitosis (Cuylen et al., 2016). Due to observations that Ki-67 and p150 colocalize at the nucleoli and within early G1 foci, I also predicted that a subset of p150 would localize to the PCL during mitosis. Previous work has shown that subunits of the

CAF-1 complex are hyperphosphorylated at the beginning of mitosis, corresponding with ejection of CAF-1 from chromatin and a loss of chromatin assembly function (Marheineke and Krude, 1998). At the beginning of anaphase, CAF-1 subunits are dephosphorylated, coinciding with re-association with mitotic chromosomes and acquisition of chromatin assembly function (Marheineke and Krude, 1998). As expected, when cells were stained with p150 and Ki-67, p150 co-localized with Ki-67 during anaphase (Figure 3.4). However, prometaphase and metaphase cells featured the majority of p150 signal in the nucleoplasm (Figures 3.2 and 3.3), making it difficult to determine if a subset of p150 localized to the PCL during these phases. In order to remove this background, cells were digested with RNAse A or DNAse I, and then soluble proteins extracted with a high salt solution. While digestion with RNAse A did remove some p150 in the nucleoplasm, digestion of the genome with DNAse I clearly showed that a subset of p150 co-localizes with Ki-67 at the PCL during early mitosis (Figures 3.2-3.4). Because this localization occurs independently of the presence of genomic DNA, we can be sure that p150 is localizing to the PCL and is not associating with chromatin.

The function of bulk p150 localization to the PCL during anaphase may be linked to ensuring an equal distribution of CAF-1 molecules to each daughter cell after cytokinesis. The function of p150 localization to the PCL in early mitosis remains speculative at this point. During early mitotic phases, the majority of CAF-1 has been ejected from the condensed chromosomes and has lost

chromatin assembly functionality. This means that the function of early mitotic p150 localization to the PCL most likely occurs outside of a chromatin assembly context. Future studies should try to confirm this by mapping the domains within p150 which are required for early mitotic PCL localization. The localization of p60 during early mitotic phases should also be examined in order to determine if a subset of the entire CAF-1 complex also localizes to the PCL. One possible function for this localization could be that a subset of p150 is required to associate with the PCL in order to facilitate gross association of reactivated CAF-1 complex at the beginning of anaphase. While this hypothesized function is difficult to test, future sections within this chapter will show evidence that early mitotic p150 localization may be linked to regulating the structure of the PCL.

5.2.6: p150 regulates the formation of Ki-67 foci in early G1 of the cell cycle

Since p150 depletion regulates the localization of Ki-67 to the nucleolus, I hypothesized that p150 may also be required for the localization of Ki-67 to punctate foci during early G1 of the cell cycle. This was a difficult hypothesis to test, as Ki-67 and p150 are the only known protein constituent of the early G1 foci and thus the only markers to visualize this sub-nuclear structure. To overcome this, cells were synchronized in mitosis and released, and an enriched population of cells depleted of p150 were compared to control cells expressing a shRNA directed against luciferase. All control cells appeared as two small cells in close proximity to one another, with NCL signal localized primarily to the

nucleolus, and Ki-67 signal appearing as hundreds of punctate foci. In contrast, cells depleted of p150 also appeared in groups of two small cells, but showed dispersed NCL and Ki-67 signal within the nucleoplasm (Figure 3.8). This suggests that p150 does regulate the formation of Ki-67 foci in early G1 of the cell cycle.

There are many possibilities as to how p150 regulates the formation of early G1 foci. For example, CAF-1 re-association with chromatin during anaphase may facilitate p150-mediated Ki-67 recruitment and the establishment of these foci at the beginning of the next cell cycle. Another possibility is that Ki-67 may actually recruit p150 to the early G1 foci, and that both proteins may be required to maintain foci structural integrity. To test this possibility, depletion of Ki-67 should be performed while monitoring the presence of p150-foci in early G1-synchronized cells. Future studies should also map the domains within p150 required to maintain Ki-67 foci formation in order to determine if this function is linked to chromatin assembly. Since Ki-67 nucleolar localization requires the SIM with p150N, I would also predict that the SIM is required for Ki-67 foci formation. If this proves to be true, IF should be utilized to determine if SUMO proteins reside within the early G1 foci, and western blotting should be used to determine if Ki-67 is sumoylated at this point in the cell cycle. Additionally, depletion of sumo proteins and UBC9 should be used to explore whether sumoylation is required to maintain the formation of these foci.

5.2.7: p150 regulates Ki-67 localization to the PCL during mitosis

Since p150 depletion affects the localization of Ki-67 to the nucleolus and to foci during early G1 of the cell cycle, I hypothesized that p150 may also be required for Ki-67 localization to the PCL during mitosis. Upon depletion of p150 in HeLa S3 cells, Ki-67 localization to the PCL dramatically decreased compared to control cells with matched mitotic phase and exposure time (Figure 3.7, A). When the Ki-67 fluorescence of 297 prometaphase cells across three biological replicates were quantified, the p150 depleted cells featured a 3.5 fold decrease in Ki-67 fluorescence intensity (Figure 3.7, B). This result is different than previous Ki-67 mislocalization upon p150 depletion in that mitotic Ki-67 mislocalization is partial. However, this still demonstrates that p150 is required for normal levels of Ki-67 localization to the PCL, supporting the hypothesis that early mitotic p150 localization to the PCL may be linked to regulating PCL structure.

Why would a histone chaperone with chromatin assembly function regulate a mitotic structure? Previous studies have demonstrated that the majority of CAF-1 loses chromatin assembly functionality during mitosis (Marheineke and Krude, 1998). This observation supports the hypothesis that p150 regulation of PCL structure may occur independently of chromatin assembly, and evidence of this will be discussed in the following section. Yet another possibility is that, while the majority of CAF-1 is hyperphosphorylated and unable of performing chromatin assembly, a subpopulation of CAF-1 may escapes phosphorylation and localizes to the PCL with chromatin assembly

function intact. In order to test this hypothesis, antibodies which detect the hyperphosphorylated form of p150 should be developed. These antibodies should then be utilized to determine if the p150 subpopulation localized to the PCL are hyperphosphorylated. These studies could be performed by using IF or by isolating purified PCL structures and probing for the presence of phosphorylated p150 via western blotting (Figure 3.5). If the PCL-localized p150 lacks hyperphosphorylation, purified PCL should be analyzed to determine if the bound p150 retains *in vitro* chromatin assembly function. Mitotic chromatin undergoes many changes throughout mitosis (reviewed in (Antonin and Neumann, 2016)), and the prospected that a subset of CAF-1 retains chromatin assembly function in order to modify the periphery of the mitotic chromosomes and recruit PCL proteins is not out of the realm of possibility.

5.2.8: The SIM within p150N is required for normal Ki-67 localization to the PCL

In order to determine if p150 regulates PCL structure through chromatin assembly, I performed experiments to map the domains within p150 required for localizing Ki-67 to the PCL. It was found that the N-terminal 310 amino acids, which is incapable of facilitating chromatin assembly, was also critical in regulating Ki-67 localization to the PCL (Figure 3.9, A). Moreover, the SIM within the N-terminus is also important for regulating PCL structure (Figure 3.9, A), and

therefore the p150N SIM is important for regulating Ki-67 localization throughout the cell cycle.

As discussed in previous sections, experiments should be carried out to determine if p150N can associate with residual CAF-1 capable of chromatin assembly function during mitosis. Additionally, experiments should examine the sumoylation status of Ki-67 during mitosis to determine if the SIM within p150N directly interacts with sumoylated Ki-67. Ki-67 can be sumoylated at Lys1517(Golebiowski et al., 2009), but the functionality of this modification or others with regards to Ki-67 activity remains unknown. If Ki-67 is sumoylated during mitosis and directly interacts with the p150N SIM, this interaction may yield clues as to the mechanism which regulate Ki-67 localization. For example, unbound SUMO modifications can serve as a signal for polyubiquitylation mediated proteasome degradation(Sun et al., 2007; Uzunova et al., 2007). While my experiments show that depletion of p150 does not affect the expression level or phosphorylation of Ki-67 (Figure 3.7, C and D), an unbound SUMO conjugate within Ki-67 may interact with other proteins to induce mislocalization.

5.3: Future Directions

5.3.1: Further investigation into NAD structure and function

This dissertation has demonstrated that 3 different NADs are regulated by p150, and that one of these NADs is also regulated by Ki-67. Other studies have shown that Ki-67 regulates the localization of a NAD proximal to the rDNA repeat

array on chromosome 13 and centromere association with the nucleoli (Booth et al., 2014; Sobecki et al., 2016). While this dissertation and these studies suggest that p150 and Ki-67 may regulate overall NAD localization, future studies should seek to map the precise loci subject to p150 and Ki-67 regulation. This dissertation hypothesizes that p150 and Ki-67 are within the same pathway in regulating NAD localization, as depletion of p150 regulates the nucleolar localization of both Ki-67 and NADs. However, it is possible that p150 and Ki-67 may regulate NAD localization through independent mechanisms. One way to test this hypothesis would be to perform NAD-seq in cells depleted of p150 or Ki-67. We could then compare these data sets to determine which NADs are specifically regulated by p150 or Ki-67, and further study where differences occur. If there are significant differences between the changes in NAD composition after p150 or Ki-67 depletion, these proteins may be acting in different pathways. In this case, Co-depletion of both proteins followed by NAD-seq should be utilized in order to determine if one protein is dominant over the other, or if there is a synergistic effect in regulating NAD structure.

These experiments would also allow us to determine if p150 and Ki-67 regulate all NAD localizations, or just a subset. Both proteins have well established roles in regulating heterochromatin structure, and the NADs are highly enriched for heterochromatin associated silencing marks. However, there are several classes of genes within the NAD data sets that are not typically associated with heterochromatin. In HeLa cells, these include zinc finger,

olfactory receptor, and defensin genes (Németh et al., 2010). While these genes are typically silenced in HeLa cells, their localization to the PN region may be regulated by a different mechanism responsible for lineage-specific nuclear organization.

In a recent study Ki-67-depleted cells showed an increase in expression of many genes enriched within the NAD data sets (Sobecki et al., 2016). This supports the hypothesis that mislocalization of NAD elements corresponds with a loss of transcriptional silencing. This further bolsters the idea that the PN region acts as an organizational hub to maintain transcriptional silencing of heterochromatin (reviewed in (Matheson and Kaufman, 2015; Padeken and Heun, 2014)). While many recent studies have focused on studying the PN region and NADs, it is still unknown whether NAD localization induces heterochromatin formation, or vice versa. One study showed that insertion of a 5S rDNA array proximal to a reporter gene was sufficient to target the reporter gene to the PN region and induce silencing (Fedoriw et al., 2012a). However, since most 5S rDNA repeats are transcriptionally silenced, it is unknown whether the silencing of the reporter gene was a consequence of PN localization or proximity to a 5S rDNA repeat. Several groups studying lamina associated domain (LAD) targeting and heterochromatin formation have reported that ectopic localization of reporter genes to the nuclear lamina (NL) resulted in a decrease in reporter expression. This was accomplished through inserting a LacO array proximal to a reporter gene, and fusing LacI with an inner NL protein

(Dialynas et al., 2010; Finlan et al., 2008; Reddy et al., 2008). Ectopic targeting of a reporter gene to the PN region may prove more difficult, as the nucleolus is not bound by a solid structure or membrane. Future investigators may choose to utilize CRISPR/cas9 technology to explore how PN targeting affects heterochromatin formation. For example, a fluorescently-tagged and catalytically inactive Cas9 exonuclease could be fused to a protein which localizes to the PN region, such as NCL or NPM. These cells could then be transfected with guide RNAs that target any locus within the genome. This method would bypasses the need to mutate endogenous loci with PN targeting sequences like the 5S rDNA, and would allow for quick screening of many distinct loci. Highly transcribed loci could then be targeted to the PN region, and RT-qPCR and ChIP-qPCR could be used to monitor gene expression and heterochromatin silencing mark occupancy. However, in the event that this methodology does not robustly target DNA to the PN region, utilization of LacO arrays and LacI fusion proteins may be attempted.

5.3.2: When does p150 regulate Ki-67 localization during the cell cycle?

We can now conclude that a subset of p150 colocalizes with and regulates the localization of Ki-67 throughout the cell cycle. There are several possibilities as to when this regulation occurs: p150 may regulate Ki-67 localization to the PCL during mitosis, to foci during early G1, to the nucleoli during late G1, or some combination of these possibilities. Determining the precise phase at which this regulation occurs will be difficult, as the localization during one phase of the

cell cycle may affect the localization at other phases. For example, let's assume that p150 specifically regulates Ki-67 localization to early G1 foci. Mislocalization of early G1 Ki-67 foci upon p150 depletion could result in the mislocalization of Ki-67 to the nucleoli, as G1 foci localization may be a prerequisite for nucleoli localization later in the cell cycle. This in turn could result in mislocalization of Ki-67 to the PCL during mitosis, as nucleolar localization may be required for PCL localization during prophase. This "chicken or egg" causality dilemma will make determining the exact point of regulation difficult to determine, however there are several ways to infer when the regulation may be occurring. For example, if Ki-67 is the sumoylated protein directly interacting with the SIM of p150N, probing cells arrested in mitosis, early G1, and late G1 for Ki-67 sumoylation may reveal when this interaction occurs. However, this assumes that Ki-67 is only sumoylated at specific points during the cell cycle, and that interaction with p150 occurs concurrently with the regulation of Ki-67 localization.

Regardless of when p150-mediated regulation of Ki-67 localization occurs, it will be difficult to explore this question using the current shRNA system. This system requires the depletion of p150 to occur over at least 48 hours, and all experiments shown in this dissertation take place over 72 hours to ensure maximum knockdown. During this depletion, the cells divide 2-4 times, meaning that little could be gained by arresting cells at particular phases of the cell cycle and asking about localization. One technology that could be employed to overcome these obstacles involves using CRISPR/cas9 genome editing to

homozygously insert a sequence encoding an auxin inducible degron (AID) to a terminus of the p150 gene (see methods in (Natsume et al., 2016)). Upon addition of auxin to this cell line, p150 could be rapidly depleted over the course of a few hours. These cells could first be arrested at specific points of the cell cycle, and then p150 degradation induced in order to gauge the effect on Ki-67 localization. Another method could include using a cell line with a fluorescently tagged Ki-67 gene, and utilizing live cell imaging to gauge Ki-67 localization in real time as p150 is degraded. AID systems currently stand at the best possible method for determining when p150 regulates the localization of Ki-67 during the cell cycle.

Although I have no experimental evidence to support this hypothesis, I predict that p150 regulates Ki-67 localization at the beginning of prophase or anaphase. During mitosis, both p150 and Ki-67 are hyperphosphorylated, corresponding to changes in their molecular functionality. At the beginning of prophase, p150 hyperphosphorylation corresponds with ejection from mitotic chromatin and a loss of chromatin assembly function (Marheineke and Krude, 1998). Ki-67 remains bound to the nucleoli despite the condensation of all chromosomes at the beginning of prophase. Upon hyperphosphorylation by cdc2/cylin B and protein kinase C, Ki-67 loses DNA binding ability and relocalizes to the PCL (Endl and Gerdes, 2000; MacCallum and Hall, 1999, 2000; Saiwaki et al., 2005). It is possible that the subset of PCL-localized p150 recruits the mobile, phosphorylated Ki-67 during prophase, and depletion of p150 inhibits this

recruitment. At the beginning of anaphase, both proteins are dephosphorylated and regain some of their lost functionality. For p150, this corresponds with a regain of chromatin assembly activity and bulk association to the PCL and mitotic chromatin (Marheineke and Krude, 1998). Ki-67 recruits PP1γ to facilitate dephosphorylation, coinciding with a shift to an immobile state, and reestablishment of DNA binding activity (Endl and Gerdes, 2000; MacCallum and Hall, 1999, 2000; Saiwaki et al., 2005; Takagi et al., 2014a). It is also possible that bulk reassociation of p150 to the PCL and chromatin is required to maintain Ki-67 localization to the PCL, or to re-establish Ki-67 binding of chromatin. While it is also possible that p150 regulates Ki-67 localization at other points in the cell cycle, mitosis is an appealing phase to investigate due to the post translational modifications of both proteins corresponding to loss of function and relocalization.

5.4: Concluding Remarks

This dissertation has established that Ki-67 and p150 both regulate NAD localization to the PN region. In addition, p150 co-localizes with Ki-67 throughout the cell cycle, and p150 regulates Ki-67 localization to the PCL, early G1 foci, and to the nucleolus. These novel regulatory functions of p150 have been mapped to the SIM within the N-terminus of p150. This suggests that p150 interacts with a sumoylated protein or proteins in mediating NAD and Ki-67 localization, however the identity of these proteins are currently unknown. Future

studies should strive to identify these sumoylated proteins, as well as the phases within the cell cycle that p150 actively regulates Ki-67 localization. Future studies should also explore the structure and function of the NADs in relation to p150 and Ki-67 mediated regulation. The PN region serves as an organizational hub of heterochromatin that is successfully constructed *de novo* after every cellular division. A better understanding of the regulation of this sub-nuclear structure will provide greater insight into how nuclear structure is reestablished after cellular division.

BIBLIOGRAPHY

Ahmad, K., and Henikoff, S. (2002). The histone variant H3.3 marks active chromatin by replication-independent nucleosome assembly. Mol. Cell *9*, 1191–1200.

Ahmad, Y., Boisvert, F.M., Gregor, P., Cobley, A., and Lamond, A.I. (2009). NOPdb: Nucleolar proteome database - 2008 Update. Nucleic Acids Res. *37*, 181–184.

Anderson, A.E., Karandikar, U.C., Pepple, K.L., Chen, Z., Bergmann, A., Mardon, G., Ambrus, A.M., Rasheva, V.I., Nicolay, B.N., Frolov, M. V., et al. (2011). The enhancer of trithorax and polycomb gene Caf1/p55 is essential for cell survival and patterning in Drosophila development. Development *138*, 1957–1966.

Angelov, D., Bondarenko, V. a, Almagro, S., Menoni, H., Mongélard, F., Hans, F., Mietton, F., Studitsky, V.M., Hamiche, A., Dimitrov, S., et al. (2006). Nucleolin is a histone chaperone with FACT-like activity and assists remodeling of nucleosomes. EMBO J. *25*, 1669–1679.

Antonin, W., and Neumann, H. (2016). Chromosome condensation and decondensation during mitosis. Curr. Opin. Cell Biol. *40*, 15–22.

Bak, A.L., Zeuthen, J., and Crick, F.H. (1977). Higher-order structure of human mitotic chromosomes. Proc. Natl. Acad. Sci. U. S. A. *74*, 1595–1599.

Baldeyron, C., Soria, G., Roche, D., Cook, A.J.L., and Almouzni, G. (2011). HP1alpha recruitment to DNA damage by p150CAF-1 promotes homologous recombination repair. J. Cell Biol. *193*, 81–95.

Barr, M.L., and Bertram, E.G. (1949). A morphological distinction between neurones of the male and female, and the behaviour of the nucleolar satellite during accelerated nucleoprotein synthesis. Nature *163*, 676.

Barski, A., Cuddapah, S., Cui, K., Roh, T.-Y., Schones, D.E., Wang, Z., Wei, G., Chepelev, I., and Zhao, K. (2007). High-resolution profiling of histone methylations in the human genome. Cell *129*, 823–837.

Barton, D.E., David, F.N., and Merrington, M. (1965). The relative positions of the chromosomes in the human cell in mitosis. Ann. Hum. Genet. *29*, 139–146.

Bell, S.P., Learned, R.M., Jantzen, H.M., and Tjian, R. (1988). Functional cooperativity between transcription factors UBF1 and SL1 mediates human ribosomal RNA synthesis. Science *241*, 1192–1197.

Belton, J.-M., McCord, R.P., Gibcus, J.H., Naumova, N., Zhan, Y., and Dekker, J. (2012). Hi-C: a comprehensive technique to capture the conformation of genomes. Methods *58*, 268–276.

Benanti, J.A., and Galloway, D.A. (2004). Normal human fibroblasts are resistant to RAS-induced senescence. Mol. Cell. Biol. *24*, 2842–2852.

Bhaya, D., Davison, M., and Barrangou, R. (2011). CRISPR-Cas systems

in bacteria and archaea: versatile small RNAs for adaptive defense and regulation. Annu. Rev. Genet. *45*, 273–297.

Boisvert, F., van Koningsbruggen, S., Navascués, J., and Lamond, A.I. (2007). The multifunctional nucleolus. Nat. Rev. Mol. Cell Biol. *8*, 574–585.

Bolotin, A., Quinquis, B., Sorokin, A., and Dusko Ehrlich, S. (2005). Clustered regularly interspaced short palindrome repeats (CRISPRs) have spacers of extrachromosomal origin. Microbiology *151*, 2551–2561.

Booth, D.G., Takagi, M., Sanchez-Pulido, L., Petfalski, E., Vargiu, G., Samejima, K., Imamoto, N., Ponting, C.P., Tollervey, D., Earnshaw, W.C., et al. (2014). Ki-67 is a PP1-interacting protein that organises the mitotic chromosome periphery. Elife *3*, e01641.

Bourgeois, C. a., Laquerriere, F., Hemon, D., Hubert, J., and Bouteille, M. (1985). New data on the in situ position of the inactive X chromosome in the interphase nucleus of human fibroblasts. Hum. Genet. *69*, 122–129.

Boyne, J.R., and Whitehouse, A. (2006). Nucleolar trafficking is essential for nuclear export of intronless herpesvirus mRNA. Proc. Natl. Acad. Sci. U. S. A. *103*, 15190–15195.

Bridger, J.M., Kill, I.R., and Lichter, P. (1998). Association of pKi-67 with satellite DNA of the human genome in early G1 cells. Chromosom. Res. *6*, 13–24.

Brown, C.J., Ballabio, a, Rupert, J.L., Lafreniere, R.G., Grompe, M., Tonlorenzi, R., and Willard, H.F. (1991). A gene from the region of the human X inactivation centre is expressed exclusively from the inactive X chromosome. Nature *349*, 38–44.

Bugler, B., Caizergues-Ferrer, M., Bouche, G., Bourbon, H., and Amalric, F. (1982). Detection and localization of a class of proteins immunologically related to a 100-kDa nucleolar protein. Eur. J. Biochem. *128*, 475–480.

Bullwinkel, J., Baron-Lühr, B., Lüdemann, A., Wohlenberg, C., Gerdes, J., and Scholzen, T. (2006). Ki-67 protein is associated with ribosomal RNA transcription in quiescent and proliferating cells. J. Cell. Physiol. *206*, 624–635.

Byron, M., Hall, L.L., and Lawrence, J.B. (2013). A multifaceted FISH approach to study endogenous RNAs and DNAs in native nuclear and cell structures. Curr. Protoc. Hum. Genet. 1–28.

Campeau, E., Ruhl, V.E., Rodier, F., Smith, C.L., Rahmberg, B.L., Fuss, J.O., Campisi, J., Yaswen, P., Cooper, P.K., and Kaufman, P.D. (2009). A versatile viral system for expression and depletion of proteins in mammalian cells. PLoS One *4*, e6529.

Cesarini, E., D'Alfonso, a., and Camilloni, G. (2012). H4K16 acetylation affects recombination and ncRNA transcription at rDNA in Saccharomyces cerevisiae. Mol. Biol. Cell *23*, 2770–2781.

Chamousset, D., De Wever, V., Moorhead, G.B., Chen, Y., Boisvert, F.-M., Lamond, A.I., and Trinkle-Mulcahy, L. (2010). RRP1B targets PP1 to mammalian cell nucleoli and is associated with Pre-60S ribosomal subunits. Mol. Biol. Cell *21*, 4212–4226.

Cheloufi, S., Elling, U., Hopfgartner, B., Jung, Y.L., Murn, J., Ninova, M., Hubmann, M., Badeaux, A.I., Euong Ang, C., Tenen, D., et al. (2015). The histone chaperone CAF-1 safeguards somatic cell identity. Nature *528*, 218–224.

Chen, C.-C., Greene, E., Bowers, S.R., and Mellone, B.G. (2012a). A role for the CAL1-partner Modulo in centromere integrity and accurate chromosome segregation in Drosophila. PLoS One *7*, e45094.

Chen, H., Tian, Y., Shu, W., Bo, X., and Wang, S. (2012b). Comprehensive identification and annotation of cell type-specific and ubiquitous CTCF-binding sites in the human genome. PLoS One *7*.

Chen, X., Xu, H., Yuan, P., Fang, F., Huss, M., Vega, V.B., Wong, E., Orlov, Y.L., Zhang, W., Jiang, J., et al. (2008). Integration of external signaling pathways with the core transcriptional network in embryonic stem cells. Cell *133*, 1106–1117.

Cheutin, T., O'Donohue, M.-F., Beorchia, A., Klein, C., Kaplan, H., and Ploton, D. (2003). Three-dimensional organization of pKi-67: a comparative fluorescence and electron tomography study using FluoroNanogold. J. Histochem. Cytochem. *51*, 1411–1423.

Chu, C., Zhang, Q.C., da Rocha, S.T., Flynn, R.A., Bharadwaj, M., Calabrese, J.M., Magnuson, T., Heard, E., and Chang, H.Y. (2015). Systematic discovery of xist RNA binding proteins. Cell *161*, 404–416.

Ciccia, A., and Elledge, S.J. (2010). The DNA damage response: making it safe to play with knives. Mol. Cell *40*, 179–204.

Ciufo, L.F., and Brown, J.D. (2000). Nuclear export of yeast signal recognition particle lacking Srp54p by the Xpo1p/Crm1p NES-dependent pathway. Curr. Biol. *10*, 1256–1264.

Clemson, C.M., McNeil, J. a., Willard, H.F., and Lawrence, J.B. (1996). XIST RNA paints the inactive X chromosome at interphase: Evidence for a novel RNA involved in nuclear/chromosome structure. J. Cell Biol. *132*, 259–275.

Cohet, N., Stewart, K.M., Mudhasani, R., Asirvatham, A.J., Mallappa, C., Imbalzano, K.M., Weaver, V.M., Imbalzano, A.N., and Nickerson, J. a (2010). SWI/SNF chromatin remodeling enzyme ATPases promote cell proliferation in normal mammary epithelial cells. J. Cell. Physiol. *223*, 667–678.

Cong, L., Ran, F.A., Cox, D., Lin, S., Barretto, R., Habib, N., Hsu, P.D., Wu, X., Jiang, W., Marraffini, L.A., et al. (2013). Multiplex genome engineering using CRISPR/Cas systems. Science *339*, 819–823.

Cong, R., Das, S., Ugrinova, I., Kumar, S., Mongelard, F., Wong, J., and Bouvet, P. (2012). Interaction of nucleolin with ribosomal RNA genes and its role in RNA polymerase I transcription. Nucleic Acids Res. *40*, 9441–9454.

Crawford, N.P.S., Qian, X., Ziogas, A., Papageorge, A.G., Boersma, B.J., Walker, R.C., Lukes, L., Rowe, W.L., Zhang, J., Ambs, S., et al. (2007). Rrp1b, a new candidate susceptibility gene for breast cancer progression and metastasis. PLoS Genet. *3*, 2296–2311.

Crawford, N.P.S., Yang, H., Mattaini, K.R., and Hunter, K.W. (2009). The metastasis efficiency modifier ribosomal RNA processing 1 homolog B (RRP1B)

is a chromatin-associated factor. J. Biol. Chem. *284*, 28660–28673.

Croft, J.A., Bridger, J.M., Boyle, S., Perry, P., Teague, P., and Bickmore, W.A. (1999). Differences in the localization and morphology of chromosomes in the human nucleus. J. Cell Biol. *145*, 1119–1131.

Csankovszki, G., Nagy, A., and Jaenisch, R. (2001). Synergism of Xist RNA, DNA methylation, and histone hypoacetylation in Maintaining X Chromosome Inactivation. J. Cell Biol. *153*, 773–783.

Cuddapah, S., Jothi, R., Schones, D.E., Roh, T.Y., Cui, K., and Zhao, K. (2009). Global analysis of the insulator binding protein CTCF in chromatin barrier regions reveals demarcation of active and repressive domains. Genome Res. *19*, 24–32.

Cuylen, S., Blaukopf, C., Politi, A.Z., Müller-Reichert, T., Neumann, B., Poser, I., Ellenberg, J., Hyman, A.A., and Gerlich, D.W. (2016). Ki-67 acts as a biological surfactant to disperse mitotic chromosomes. Nature *535*, 308–312.

DeMare, L.E., Leng, J., Cotney, J., Reilly, S.K., Yin, J., Sarro, R., and Noonan, J.P. (2013). The genomic landscape of cohesin-Associated chromatin interactions. Genome Res. *23*, 1224–1234.

Dialynas, G., Speese, S., Budnik, V., Geyer, P.K., and Wallrath, L.L. (2010). The role of Drosophila Lamin C in muscle function and gene expression. Development *137*, 3067–3077.

Dillinger, S., Straub, T., and Nemeth, A. (2016). Nucleolus association of chromosomal domains is largely maintained in cellular senescence despite massive nuclear reorganisation. bioRxiv.

Dohke, K., Miyazaki, S., Tanaka, K., Urano, T., Grewal, S.I.S., and Murakami, Y. (2008). Fission yeast chromatin assembly factor 1 assists in the replication-coupled maintenance of heterochromatin. Genes Cells *13*, 1027–1043.

Doyen, C.M., Moshkin, Y.M., Chalkley, G.E., Bezstarosti, K., Demmers, J.A.A., Rathke, C., Renkawitz-Pohl, R., and Verrijzer, C.P. (2013). Subunits of the Histone Chaperone CAF1 Also Mediate Assembly of Protamine-Based Chromatin. Cell Rep. *4*, 59–65.

DuPraw, E.J. (1966). Evidence for a “folded-fibre” organization in human chromosomes. Nature *209*, 577–581.

Duriez, P.J., and Shah, G.M. (1997). Cleavage of poly(ADP-ribose) polymerase: a sensitive parameter to study cell death. Biochem. Cell Biol. *75*, 337–349.

Emmott, E., and Hiscox, J.A. (2009). Nucleolar targeting: the hub of the matter. EMBO Rep. *10*, 231–238.

Endl, E., and Gerdes, J. (2000). Posttranslational modifications of the Ki-67 protein coincide with two major checkpoints during mitosis. J. Cell. Physiol. *182*, 371–380.

Eng, J.K., McCormack, A.L., and Yates, J.R. (1994). An approach to correlate tandem mass spectral data of peptides with amino acid sequences in a protein database. J. Am. Soc. Mass Spectrom. *5*, 976–989.

Enomoto, S., McCune-Zierath, P.D., Gerami-Nejad, M., Sanders, M.A., and Berman, J. (1997). RLF2, a subunit of yeast chromatin assembly factor-I, is required for telomeric chromatin function in vivo. Genes Dev. *11*, 358–370.

Escande, M.L., Gas, N., and Stevens, B.J. (1985). Immunolocalization of the 100 K nucleolar protein in CHO cells. Biol. Cell *53*, 99–109.

Espada, J., Ballestar, E., Santoro, R., Fraga, M.F., Villar-Garea, A., Németh, A., Lopez-Serra, L., Ropero, S., Aranda, A., Orozco, H., et al. (2007). Epigenetic disruption of ribosomal RNA genes and nucleolar architecture in DNA methyltransferase 1 (Dnmt1) deficient cells. Nucleic Acids Res. *35*, 2191–2198.

Evan, G.I., and Vousden, K.H. (2001). Proliferation, cell cycle and apoptosis in cancer. Nature *411*, 342–348.

Fazzio, T.G., Huff, J.T., and Panning, B. (2008). An RNAi screen of chromatin proteins identifies Tip60-p400 as a regulator of embryonic stem cell identity. Cell *134*, 162–174.

Fedoriw, A.M., Starmer, J., Yee, D., and Magnuson, T. (2012a). Nucleolar association and transcriptional inhibition through 5S rDNA in mammals. PLoS Genet. *8*.

Fedoriw, A.M., Calabrese, J.M., Mu, W., Yee, D., and Magnuson, T. (2012b). Differentiation-driven nucleolar association of the mouse imprinted Kcnq1 locus. G3 (Bethesda). *2*, 1521–1528.

Finkbeiner, E., Haindl, M., and Muller, S. (2011). The SUMO system controls nucleolar partitioning of a novel mammalian ribosome biogenesis complex. EMBO J. *30*, 1067–1078.

Finlan, L.E., Sproul, D., Thomson, I., Boyle, S., Kerr, E., Perry, P., Ylstra, B., Chubb, J.R., and Bickmore, W. a (2008). Recruitment to the nuclear periphery can alter expression of genes in human cells. PLoS Genet. *4*, e1000039.

Fischer, S., Prykhozhij, S., Rau, M.J., and Neumann, C.J. (2007). Mutation of zebrafish caf-1b results in S phase arrest, defective differentiation and p53-mediated apoptosis during organogenesis. Cell Cycle *6*, 2962–2969.

Fitzpatrick, G. V, Soloway, P.D., and Higgins, M.J. (2002). Regional loss of imprinting and growth deficiency in mice with a targeted deletion of KvDMR1. Nat. Genet. *32*, 426–431.

Foltz, D.R., Jansen, L.E.T., Black, B.E., Bailey, A.O., Yates, J.R., and Cleveland, D.W. (2006). The human CENP-A centromeric nucleosome-associated complex. Nat. Cell Biol. *8*, 458–469.

Franklin, S.G., and Zweidler, A. (1977). Non-allelic variants of histones 2a, 2b and 3 in mammals. Nature *266*, 273–275.

Gaillard, P.H., Martini, E.M., Kaufman, P.D., Stillman, B., Moustacchi, E., and Almouzni, G. (1996). Chromatin assembly coupled to DNA repair: a new role for chromatin assembly factor I. Cell *86*, 887–896.

Garneau, J.E., Dupuis, M.E., Villion, M., Romero, D.A., Barrangou, R., Boyaval, P., Fremaux, C., Horvath, P., Magadan, A.H., and Moineau, S. (2010). The CRISPR/Cas bacterial immune system cleaves bacteriophage and plasmid DNA. Nature *468*, 67–71.

Gasiunas, G., Barrangou, R., Horvath, P., and Siksnys, V. (2012). Cas9-crRNA ribonucleoprotein complex mediates specific DNA cleavage for adaptive immunity in bacteria. Proc. Natl. Acad. Sci. U. S. A. *109*, E2579-86.

Gerdes, J., Schwab, U., Lemke, H., and Stein, H. (1983). Production of a mouse monoclonal antibody reactive with a human nuclear antigen associated with cell proliferation. Int. J. Cancer *31*, 13–20.

Gerdes, J., Lemke, H., Baisch, H., Wacker, H.H., Schwab, U., and Stein, H. (1984). Cell cycle analysis of a cell proliferation-associated human nuclear antigen defined by the monoclonal antibody Ki-67. J. Immunol. *133*, 1710–1715.

Ghetti, a, Piñol-Roma, S., Michael, W.M., Morandi, C., and Dreyfuss, G. (1992). hnRNP I, the polypyrimidine tract-binding protein: distinct nuclear localization and association with hnRNAs. Nucleic Acids Res. *20*, 3671–3678.

Ginisty, H., Amalric, F., and Bouvet, P. (1998). Nucleolin functions in the first step of ribosomal RNA processing. EMBO J. *17*, 1476–1486.

Ginisty, H., Sicard, H., Roger, B., and Bouvet, P. (1999). Structure and functions of nucleolin. J. Cell Sci. *112 (6)*, 761–772.

Golebiowski, F., Matic, I., Tatham, M.H., Cole, C., Yin, Y., Nakamura, A., Cox, J., Barton, G.J., Mann, M., and Hay, R.T. (2009). System-wide changes to SUMO modifications in response to heat shock. Sci. Signal. *2*, ra24.

Goto, H., Tomono, Y., Ajiro, K., Kosako, H., Fujita, M., Sakurai, M., Okawa, K., Iwamatsu, A., Okigaki, T., Takahashi, T., et al. (1999). Identification of a novel phosphorylation site on histone H3 coupled with mitotic chromosome condensation. J. Biol. Chem. *274*, 25543–25549.

Goto, H., Yasui, Y., Nigg, E.A., and Inagaki, M. (2002). Aurora-B phosphorylates Histone H3 at serine28 with regard to the mitotic chromosome condensation. Genes to Cells *7*, 11–17.

Green, C.M., and Almouzni, G. (2003). Local action of the chromatin assembly factor CAF-1 at sites of nucleotide excision repair in vivo. EMBO J. *22*, 5163–5174.

Grosshans, H., Deinert, K., Hurt, E., and Simos, G. (2001). Biogenesis of the signal recognition particle (SRP) involves import of SRP proteins into the nucleolus, assembly with the SRP-RNA, and Xpo1p-mediated export. J. Cell Biol. *153*, 745–762.

Guelen, L., Pagie, L., Brasset, E., Meuleman, W., Faza, M.B., Talhout, W., Eussen, B.H., de Klein, A., Wessels, L., de Laat, W., et al. (2008). Domain organization of human chromosomes revealed by mapping of nuclear lamina interactions. Nature *453*, 948–951.

Hacisuleyman, E., Goff, L. a, Trapnell, C., Williams, A., Henao-Mejia, J., Sun, L., McClanahan, P., Hendrickson, D.G., Sauvageau, M., Kelley, D.R., et al. (2014). Topological organization of multichromosomal regions by the long intergenic noncoding RNA Firre. Nat. Struct. Mol. Biol. *21*, 198–206.

Haeusler, R. a, and Engelke, D.R. (2006). Spatial organization of transcription by RNA polymerase III. Nucleic Acids Res. *34*, 4826–4836.

Hainer, S.J., McCannell, K.N., Yu, J., Ee, L.-S., Zhu, L.J., Rando, O.J.,

and Fazzio, T.G. (2016). DNA methylation directs genomic localization of Mbd2 and Mbd3 in embryonic stem cells. Elife *5*, 1–24.

Hall, M.P., Huang, S., and Black, D.L. (2004). Differentiation-induced colocalization of the KH-type splicing regulatory protein with polypyrimidine tract binding protein and the c-src pre-mRNA. Mol. Biol. Cell *15*, 774–786.

Hatanaka, Y., Inoue, K., Oikawa, M., Kamimura, S., Ogonuki, N., Kodama, E.N., Ohkawa, Y., Tsukada, Y., and Ogura, A. (2015). Histone chaperone CAF-1 mediates repressive histone modifications to protect preimplantation mouse embryos from endogenous retrotransposons. Proc. Natl. Acad. Sci. U. S. A. *112*, 14641–14646.

Heitz, E. (1931). Nukleolar und chromosomen in der gattung. Vicia Planta *15*, 495–505.

Hernandez-Verdun, D. (2011). Assembly and disassembly of the nucleolus during the cell cycle. Nucleus *2*, 189–194.

Herrera, J.E., Savkur, R., and Olson, M.O. (1995). The ribonuclease activity of nucleolar protein B23. Nucleic Acids Res. *23*, 3974–3979.

Hoek, M., and Stillman, B. (2003). Chromatin assembly factor 1 is essential and couples chromatin assembly to DNA replication in vivo. Proc Natl Acad Sci U S A *100*, 12183–12188.

Hoek, M., Myers, M.P., and Stillman, B. (2011). An analysis of CAF-1-interacting proteins reveals dynamic and direct interactions with the KU complex and 14-3-3 proteins. J. Biol. Chem. *286*, 10876–10887.

Van Hooser, A. a, Yuh, P., and Heald, R. (2005). The perichromosomal layer. Chromosoma *114*, 377–388.

Houlard, M., Berlivet, S., Probst, A. V., Quivy, J.-P., Héry, P., Almouzni, G., and Gérard, M. (2006). CAF-1 is essential for heterochromatin organization in pluripotent embryonic cells. PLoS Genet. *2*, e181.

Huang, H., Yu, Z., Zhang, S., Liang, X., Chen, J., Li, C., Ma, J., and Jiao, R. (2010). Drosophila CAF-1 regulates HP1-mediated epigenetic silencing and pericentric heterochromatin stability. J. Cell Sci. *123*, 2853–2861.

Huang, K., Jia, J., Wu, C., Yao, M., Li, M., Jin, J., Jiang, C., Cai, Y., Pei, D., Pan, G., et al. (2013). Ribosomal RNA gene transcription mediated by the master genome regulator protein CCCTC-binding factor (CTCF) is negatively regulated by the condensin complex. J. Biol. Chem. *288*, 26067–26077.

Huang, S., Deerinck, T.J., Ellisman, M.H., and Spector, D.L. (1997). The dynamic organization of the perinucleolar compartment in the cell nucleus. J. Cell Biol. *137*, 965–974.

Huang, S., Zhou, H., Tarara, J., and Zhang, Z. (2007). A novel role for histone chaperones CAF-1 and Rtt106p in heterochromatin silencing. EMBO J. *26*, 2274–2283.

Ide, S., Saka, K., and Kobayashi, T. (2013). Rtt109 Prevents Hyper-Amplification of Ribosomal RNA Genes through Histone Modification in Budding Yeast. PLoS Genet. *9*.

Isaac, C., Yang, Y., and Meier, U.T. (1998). Nopp 140 functions as a

molecular link between the nucleolus and the coiled bodies. J. Cell Biol. *142*, 319–329.

Ishiuchi, T., Enriquez-Gasca, R., Mizutani, E., Bošković, A., Ziegler-Birling, C., Rodriguez-Terrones, D., Wakayama, T., Vaquerizas, J.M., and Torres-Padilla, M.-E. (2015). Early embryonic-like cells are induced by downregulating replication-dependent chromatin assembly. Nat. Struct. Mol. Biol. *22*, 662–671.

Isola, J., Helin, H., and Kallioniemi, O.P. (1990). Immunoelectron-microscopic localization of a proliferation-associated antigen Ki-67 in MCF-7 cells. Histochem. J. *22*, 498–506.

Jacobson, M.R., and Pederson, T. (1998). Localization of signal recognition particle RNA in the nucleolus of mammalian cells. Proc. Natl. Acad. Sci. U. S. A. *95*, 7981–7986.

Jalal, C., Uhlmann-Schiffler, H., and Stahl, H. (2007). Redundant role of DEAD box proteins p68 (Ddx5) and p72/p82 (Ddx17) in ribosome biogenesis and cell proliferation. Nucleic Acids Res. *35*, 3590–3601.

Jentsch, S., and Psakhye, I. (2013). Control of nuclear activities by substrate-selective and protein-group SUMOylation. Annu. Rev. Genet. *47*, 167–186.

Jinek, M., Chylinski, K., Fonfara, I., Hauer, M., Doudna, J.A., and Charpentier, E. (2012). A programmable dual-RNA-guided DNA endonuclease in adaptive bacterial immunity. Science *337*, 816–821.

Kamath, R. V., Thor, A.D., Wang, C., Edgerton, S.M., Slusarczyk, A., Leary, D.J., Wang, J., Wiley, E.L., Jovanovic, B., Wu, Q., et al. (2005). Perinucleolar compartment prevalence has an independent prognostic value for breast cancer. Cancer Res. *65*, 246–253.

Kametaka, A., Takagi, M., Hayakawa, T., Haraguchi, T., Hiraoka, Y., and Yoneda, Y. (2002). Interaction of the chromatin compaction-inducing domain (LR domain) of Ki-67 antigen with HP1 proteins. Genes Cells *7*, 1231–1242.

Kaufman, P.D., Kobayashi, R., Kessler, N., and Stillman, B. (1995). The p150 and p60 subunits of chromatin assembly factor I: a molecular link between newly synthesized histones and DNA replication. Cell *81*, 1105–1114.

Kaufman, P.D., Kobayashi, R., and Stillman, B. (1997). Ultraviolet radiation sensitivity and reduction of telomeric silencing in Saccharomyces cerevisiae cells lacking chromatin assembly factor-I. Genes Dev. *11*, 345–357.

Kaya, H., Shibahara, K. ichi, Taoka, K. ichiro, Iwabuchi, M., Stillman, B., and Araki, T. (2001). FASCIATA genes for chromatin assembly factor-1 in Arabidopsis maintain the cellular organization of apical meristems. Cell *104*, 131–142.

Keller, C., and Krude, T. (2000). Requirement of cyclin/Cdk2 and protein phosphatase 1 activity for chromatin assembly factor 1-dependent chromatin assembly during DNA synthesis. J. Biol. Chem. *275*, 35512–35521.

Kill, I.R. (1996). Localisation of the Ki-67 antigen within the nucleolus. Evidence for a fibrillarin-deficient region of the dense fibrillar component. J. Cell Sci. *109 (Pt 6*, 1253–1263.

Kim, T.H., Abdullaev, Z.K., Smith, A.D., Ching, K. a., Loukinov, D.I., Green, R.D., Zhang, M.Q., Lobanenkov, V. V., and Ren, B. (2007). Analysis of the vertebrate insulator protein CTCF-binding sites in the human genome. Cell *128*, 1231–1245.

Kind, J., and van Steensel, B. (2010). Genome-nuclear lamina interactions and gene regulation. Curr. Opin. Cell Biol. *22*, 320–325.

Kind, J., Pagie, L., Ortabozkoyun, H., Boyle, S., de Vries, S.S., Janssen, H., Amendola, M., Nolen, L.D., Bickmore, W. a, and van Steensel, B. (2013). Single-cell dynamics of genome-nuclear lamina interactions. Cell *153*, 178–192.

Kittur, N., Zapantis, G., Aubuchon, M., Santoro, N., Bazett-Jones, D.P., and Meier, U.T. (2007). The nucleolar channel system of human endometrium is related to endoplasmic reticulum and R-rings. Mol. Biol. Cell *18*, 2296–2304.

Klapholz, B., Dietrich, B.H., Schaffner, C., Hérédia, F., Quivy, J.P., Almouzni, G., and Dostatni, N. (2009). CAF-1 is required for efficient replication of euchromatic DNA in Drosophila larval endocycling cells. Chromosoma *118*, 235–248.

van Koningsbruggen, S., Gierlinski, M., Schofield, P., Martin, D., Barton, G.J., Ariyurek, Y., den Dunnen, J.T., and Lamond, A.I. (2010). High-resolution whole-genome sequencing reveals that specific chromatin domains from most human chromosomes associate with nucleoli. Mol. Biol. Cell *21*, 3735–3748.

Korgaonkar, C., Hagen, J., Tompkins, V., Frazier, A.A., Allamargot, C., Quelle, F.W., and Quelle, D.E. (2005). Nucleophosmin (B23) targets ARF to nucleoli and inhibits its function. Mol. Cell. Biol. *25*, 1258–1271.

Krude, T. (1995). Chromatin assembly factor 1 (CAF-1) colocalizes with replication foci in HeLa cell nuclei. Exp. Cell Res. *220*, 304–311.

Kumar, A., and Zhang, K.Y.J. (2015). Advances in the development of SUMO specific protease (SENP) inhibitors. Comput. Struct. Biotechnol. J. *13*, 204–211.

Kuzmichev, A., Nishioka, K., Erdjument-Bromage, H., Tempst, P., and Reinberg, D. (2002). Histone methyltransferase activity associated with a human multiprotein complex containing the Enhancer of Zeste protein. Genes Dev. *16*, 2893–2905.

Lai, J.S., and Herr, W. (1992). Ethidium bromide provides a simple tool for identifying genuine DNA-independent protein associations. Proc. Natl. Acad. Sci. *89*, 6958–6962.

Längst, G., Blank, T.A., Becker, P.B., and Grummt, I. (1997). RNA polymerase I transcription on nucleosomal templates: The transcription termination factor TTF-I induces chromatin remodeling and relieves transcriptional repression. EMBO J. *16*, 760–768.

Latreille, D., Bluy, L., Benkirane, M., and Kiernan, R.E. (2014). Identification of histone 3 variant 2 interacting factors. Nucleic Acids Res. *42*, 3542–3550.

Lee, J.T. (2012). Epigenetic Regulation by Long Noncoding RNAs. Sci. (Washington, DC, U. S.) *338*, 1435–1439.

Lee, S.-B., Ou, D.S.-C., Lee, C.-F., and Juan, L.-J. (2009). Gene-specific transcriptional activation mediated by the p150 subunit of the chromatin assembly factor 1. J. Biol. Chem. *284*, 14040–14049.

Li, Y.P. (1997). Protein B23 is an important human factor for the nucleolar localization of the human immunodeficiency virus protein Tat. J. Virol. *71*, 4098–4102.

Li, Z., and Hann, S.R. (2013). Nucleophosmin is essential for c-Myc nucleolar localization and c-Myc-mediated rDNA transcription. Oncogene *32*, 1988–1994.

Lieberman-Aiden, E., van Berkum, N.L., Williams, L., Imakaev, M., Ragoczy, T., Telling, A., Amit, I., Lajoie, B.R., Sabo, P.J., Dorschner, M.O., et al. (2009). Comprehensive mapping of long-range interactions reveals folding principles of the human genome. Science *326*, 289–293.

Lindstrom, D.L., Leverich, C.K., Henderson, K. a., and Gottschling, D.E. (2011). Replicative age induces mitotic recombination in the ribosomal RNA gene cluster of Saccharomyces cerevisiae. PLoS Genet. *7*.

Lindström, M.S., and Zhang, Y. (2008). Ribosomal protein S9 is a novel B23/NPM-binding protein required for normal cell proliferation. J. Biol. Chem. *283*, 15568–15576.

Lischwe, M. a, Richards, R.L., Busch, R.K., and Busch, H. (1981). Localization of phosphoprotein C23 to nucleolar structures and to the nucleolus organizer regions. Exp. Cell Res. *136*, 101–109.

Loyola, A., Bonaldi, T., Roche, D., Imhof, A., and Almouzni, G. (2006). PTMs on H3 variants before chromatin assembly potentiate their final epigenetic state. Mol. Cell *24*, 309–316.

Loyola, A., Tagami, H., Bonaldi, T., Roche, D., Quivy, J.P., Imhof, A., Nakatani, Y., Dent, S.Y.R., and Almouzni, G. (2009). The HP1alpha-CAF1-SetDB1-containing complex provides H3K9me1 for Suv39-mediated K9me3 in pericentric heterochromatin. EMBO Rep. *10*, 769–775.

Lucchesi, J.C., Kelly, W.G., and Panning, B. (2005). Chromatin remodeling in dosage compensation. Annu. Rev. Genet. *39*, 615–651.

Luger, K., Mäder, A.W., Richmond, R.K., Sargent, D.F., and Richmond, T.J. (1997). Crystal structure of the nucleosome core particle at 2.8 A resolution. Nature *389*, 251–260.

Lukášová, E., Kozubek, S., Kozubek, M., Kjeronská, J., Rýznar, L., Horákova, J., Krahulcová, E., and Horneck, G. (1997). Localisation and distance between ABL and BCR genes in interphase nuclei of bone marrow cells of control donors and patients with chronic myeloid leukaemia. Hum. Genet. *100*, 525–535.

Luo, Y., Ren, F., Liu, Y., Shi, Z., Tan, Z., Xiong, H., Dang, Y., and Chen, G. (2015). Clinicopathological and prognostic significance of high Ki-67 labeling index in hepatocellular carcinoma patients: a meta-analysis. Int. J. Clin. Exp. Med. *8*, 10235–10247.

Lyon, M. (1961). Gene action in the X-chromosome of the mouse (Mus

musculus L.). Nature *190*, 372–373.

Ma, N., Matsunaga, S., Takata, H., Ono-Maniwa, R., Uchiyama, S., and Fukui, K. (2007). Nucleolin functions in nucleolus formation and chromosome congression. J. Cell Sci. *120*, 2091–2105.

MacCallum, D.E., and Hall, P.A. (1999). Biochemical characterization of pKi67 with the identification of a mitotic-specific form associated with hyperphosphorylation and altered DNA binding. Exp. Cell Res. *252*, 186–198.

MacCallum, D.E., and Hall, P. a. (2000). The biochemical characterization of the DNA binding activity of pKi67. J. Pathol. *191*, 286–298.

Maeso, I., Acemel, R.D., and Gómez-Skarmeta, J.L. (2016). Cis-regulatory landscapes in development and evolution. Curr. Opin. Genet. Dev. *43*, 17–22.

Maggi, L.B., and Weber, J.D. (2005). Nucleolar adaptation in human cancer. Cancer Invest. *23*, 599–608.

Maggi, L.B., Kuchenruether, M., Dadey, D.Y. a, Schwope, R.M., Grisendi, S., Townsend, R.R., Pandolfi, P.P., and Weber, J.D. (2008). Nucleophosmin serves as a rate-limiting nuclear export chaperone for the Mammalian ribosome. Mol. Cell. Biol. *28*, 7050–7065.

Mali, P., Yang, L., Esvelt, K.M., Aach, J., Guell, M., DiCarlo, J.E., Norville, J.E., and Church, G.M. (2013). RNA-Guided Human Genome Engineering via Cas9 Prashant. Science (80-.). *339*, 823–826.

Mancini-DiNardo, D., Steele, S.J.S., Levorse, J.M., Ingram, R.S., and Tilghman, S.M. (2006). Elongation of the Kcnq1ot1 transcript is required for genomic imprinting of neighboring genes. Genes Dev. *20*, 1268–1282.

du Manoir, S., Guillaud, P., Camus, E., Seigneurin, D., and Brugal, G. (1991). Ki-67 labeling in postmitotic cells defines different Ki-67 pathways within the 2c compartment. Cytometry *12*, 455–463.

Marheineke, K., and Krude, T. (1998). Nucleosome assembly activity and intracellular localization of human CAF-1 changes during the cell division cycle. J. Biol. Chem. *273*, 15279–15286.

Marsden, M.P.F., and Laemmli, U.K. (1979). Metaphase chromosome structure: Evidence for a radial loop model. Cell *17*, 849–858.

Martindill, D.M.J., Risebro, C. a, Smart, N., Franco-Viseras, M.D.M., Rosario, C.O., Swallow, C.J., Dennis, J.W., and Riley, P.R. (2007). Nucleolar release of Hand1 acts as a molecular switch to determine cell fate. Nat. Cell Biol. *9*, 1131–1141.

Martínez-Balbás, M.A., Tsukiyama, T., Gdula, D., and Wu, C. (1998). Drosophila NURF-55, a WD repeat protein involved in histone metabolism. Proc. Natl. Acad. Sci. U. S. A. *95*, 132–137.

Mascolo, M., Vecchione, M.L., Ilardi, G., Scalvenzi, M., Molea, G., Di Benedetto, M., Nugnes, L., Siano, M., De Rosa, G., and Staibano, S. (2010). Overexpression of Chromatin Assembly Factor-1/p60 helps to predict the prognosis of melanoma patients. BMC Cancer *10*, 63.

Mascolo, M., Ilardi, G., Romano, M.F., Celetti, A., Siano, M., Romano, S.,

Luise, C., Merolla, F., Rocco, A., Vecchione, M.L., et al. (2012a). Overexpression of chromatin assembly factor-1 p60, poly(ADP-ribose) polymerase 1 and nestin predicts metastasizing behaviour of oral cancer. Histopathology *61*, 1089–1105.

Mascolo, M., Ilardi, G., Merolla, F., Russo, D., Vecchione, M.L., de Rosa, G., and Staibano, S. (2012b). Tissue microarray-based evaluation of chromatin assembly factor-1 (CAF-1)/p60 as tumour prognostic marker. Int. J. Mol. Sci. *13*, 11044–11062.

Matera, A.G., Frey, M.R., Margelot, K., and Wolin, S.L. (1995). A perinucleolar compartment contains several RNA polymerase III transcripts as well as the polypyrimidine tract-binding protein, hnRNP I. J. Cell Biol. *129*, 1181–1193.

Matheson, T.D., and Kaufman, P.D. (2015). Grabbing the genome by the NADs. Chromosoma *125*, 361–371.

Matheson, T.D., and Kaufman, P.D. (2017). The p150N domain of chromatin assembly factor-1 regulates Ki-67 accumulation on the mitotic perichromosomal layer. Mol. Biol. Cell *28*, 21–29.

Matsumoto-Taniura, N., Pirollet, F., Monroe, R., Gerace, L., and Westendorf, J.M. (1996). Identification of novel M phase phosphoproteins by expression cloning. Mol. Biol. Cell *7*, 1455–1469.

Mayer, C., Stefanovsky, V., Driel, M. Van, Grummt, I., Denissov, S., Moss, T., and Stunnenberg, H.G. (2011). Amodel for the topology of active ribosomal RNA genes. *12*, 1–7.

McClintock, B. (1934). The relationship of a particular chro-mosomal element to the development of the nucleoli in Zea mays. Z. ZellforschMikrosk *21*, 294–398.

McDonald, W.H., Tabb, D.L., Sadygov, R.G., MacCoss, M.J., Venable, J., Graumann, J., Johnson, J.R., Cociorva, D., and Yates, J.R. (2004). MS1, MS2, and SQT-three unified, compact, and easily parsed file formats for the storage of shotgun proteomic spectra and identifications. Rapid Commun. Mass Spectrom. *18*, 2162–2168.

McHugh, C. a., Chen, C.-K., Chow, A., Surka, C.F., Tran, C., McDonel, P., Pandya-Jones, A., Blanco, M., Burghard, C., Moradian, A., et al. (2015). The Xist lncRNA interacts directly with SHARP to silence transcription through HDAC3. Nature.

McStay, B., and Grummt, I. (2008). The epigenetics of rRNA genes: from molecular to chromosome biology. Annu. Rev. Cell Dev. Biol. *24*, 131–157.

Mello, J.A., Silljé, H.H.W., Roche, D.M.J., Kirschner, D.B., Nigg, E.A., and Almouzni, G. (2002). Human Asf1 and CAF-1 interact and synergize in a repair-coupled nucleosome assembly pathway. EMBO Rep. *3*, 329–334.

Michalik, J., Yeoman, L.C., and Busch, H. (1981). Nucleolar localization of protein B23 (37/5.1) by immunocytochemical techniques. Life Sci. *28*, 1371–1379.

Misteli, T. (2010). Higher-order genome organization in human disease. Cold Spring Harb. Perspect. Biol. *2*, 85–92.

Moggs, J.G., Grandi, P., Quivy, J.P., Jónsson, Z.O., Hübscher, U., Becker, P.B., and Almouzni, G. (2000). A CAF-1-PCNA-mediated chromatin assembly pathway triggered by sensing DNA damage. Mol. Cell. Biol. *20*, 1206–1218.

Mohammad, F., Pandey, R.R., Nagano, T., Chakalova, L., Mondal, T., Fraser, P., and Kanduri, C. (2008). Kcnq1ot1/Lit1 noncoding RNA mediates transcriptional silencing by targeting to the perinucleolar region. Mol. Cell. Biol. *28*, 3713–3728.

Mojica, F.J.M., Díez-Villaseñor, C., García-Martínez, J., and Soria, E. (2005). Intervening sequences of regularly spaced prokaryotic repeats derive from foreign genetic elements. J. Mol. Evol. *60*, 174–182.

Moldovan, G.-L., Pfander, B., and Jentsch, S. (2007). PCNA, the maestro of the replication fork. Cell *129*, 665–679.

Murano, K., Okuwaki, M., Hisaoka, M., and Nagata, K. (2008). Transcription regulation of the rRNA gene by a multifunctional nucleolar protein, B23/nucleophosmin, through its histone chaperone activity. Mol. Cell. Biol. *28*, 3114–3126.

Murayama, A., Ohmori, K., Fujimura, A., Minami, H., Yasuzawa-Tanaka, K., Kuroda, T., Oie, S., Daitoku, H., Okuwaki, M., Nagata, K., et al. (2008). Epigenetic control of rDNA loci in response to intracellular energy status. Cell *133*, 627–639.

Murzina, N., Verreault, a, Laue, E., and Stillman, B. (1999). Heterochromatin dynamics in mouse cells: interaction between chromatin assembly factor 1 and HP1 proteins. Mol. Cell *4*, 529–540.

Murzina, N. V., Pei, X.-Y., Zhang, W., Sparkes, M., Vicente-Garcia, J., Pratap, J.V., McLaughlin, S.H., Ben-Shahar, T.R., Verreault, A., Luisi, B.F., et al. (2008). Structural basis for the recognition of histone H4 by the histone-chaperone RbAp46. Structure *16*, 1077–1085.

Natsume, T., Kiyomitsu, T., Saga, Y., and Kanemaki, M.T. (2016). Rapid Protein Depletion in Human Cells by Auxin-Inducible Degron Tagging with Short Homology Donors. Cell Rep. *15*, 210–218.

Naumova, N., Imakaev, M., Fudenberg, G., Zhan, Y., Lajoie, B.R., Mirny, L. a, and Dekker, J. (2013). Organization of the mitotic chromosome. Science *342*, 948–953.

Németh, A., and Längst, G. (2011). Genome organization in and around the nucleolus. Trends Genet. *27*, 149–156.

Németh, A., Guibert, S., Tiwari, V.K., Ohlsson, R., Längst, G., Brock, G., Bird, A., Laat, W. de, Grosveld, F., Dekker, J., et al. (2008). Epigenetic regulation of TTF-I-mediated promoter–terminator interactions of rRNA genes. EMBO J. *27*, 1255–1265.

Németh, A., Conesa, A., Santoyo-Lopez, J., Medina, I., Montaner, D., Péterfia, B., Solovei, I., Cremer, T., Dopazo, J., and Längst, G. (2010). Initial genomics of the human nucleolus. PLoS Genet. *6*, e1000889.

Neves, H., Ramos, C., da Silva, M.G., Parreira, a, and Parreira, L. (1999). The nuclear topography of ABL, BCR, PML, and RARalpha genes: evidence for

gene proximity in specific phases of the cell cycle and stages of hematopoietic differentiation. Blood *93*, 1197–1207.

van de Nobelen, S., Rosa-Garrido, M., Leers, J., Heath, H., Soochit, W., Joosen, L., Jonkers, I., Demmers, J., van der Reijden, M., Torrano, V., et al. (2010). CTCF regulates the local epigenetic state of ribosomal DNA repeats. Epigenetics Chromatin *3*, 19.

Norton, J.T., Pollock, C.B., Wang, C., Schink, J.C., Kim, J.J., and Huang, S. (2008). Perinucleolar compartment prevalence is a phenotypic pancancer marker of malignancy. Cancer *113*, 861–869.

Ochs, R.L., and Press, R.I. (1992). Centromere autoantigens are associated with the nucleolus. Exp. Cell Res. *200*, 339–350.

Ohta, S., Bukowski-Wills, J.-C., Sanchez-Pulido, L., Alves, F.D.L., Wood, L., Chen, Z. a., Platani, M., Fischer, L., Hudson, D.F., Ponting, C.P., et al. (2010). The protein composition of mitotic chromosomes determined using multiclassifier combinatorial proteomics. Cell *142*, 810–821.

Padeken, J., and Heun, P. (2014). Nucleolus and nuclear periphery: Velcro for heterochromatin. Curr. Opin. Cell Biol. *28C*, 54–60.

Padeken, J., Mendiburo, M.J., Chlamydas, S., Schwarz, H.-J., Kremmer, E., and Heun, P. (2013). The nucleoplasmin homolog NLP mediates centromere clustering and anchoring to the nucleolus. Mol. Cell *50*, 236–249.

Pandey, R.R., Ceribelli, M., Singh, P.B., Ericsson, J., Mantovani, R., and Kanduri, C. (2004). NF-Y regulates the antisense promoter, bidirectional silencing, and differential epigenetic marks of the Kcnq1 imprinting control region. J. Biol. Chem. *279*, 52685–52693.

Pandey, R.R., Mondal, T., Mohammad, F., Enroth, S., Redrup, L., Komorowski, J., Nagano, T., Mancini-Dinardo, D., and Kanduri, C. (2008). Kcnq1ot1 antisense noncoding RNA mediates lineage-specific transcriptional silencing through chromatin-level regulation. Mol. Cell *32*, 232–246.

Pederson, T. (2011). The nucleolus. Cold Spring Harb. Perspect. Biol. *3*, 1–15.

Pederson, T., and Politz, J.C. (2000). The nucleolus and the four ribonucleoproteins of translation. J. Cell Biol. *148*, 1091–1095.

Peng, J.C., and Karpen, G.H. (2007). H3K9 methylation and RNA interference regulate nucleolar organization and repeated DNA stability. Nat. Cell Biol. *9*, 25–35.

Peng, J., Elias, J.E., Thoreen, C.C., Licklider, L.J., and Gygi, S.P. (2003). Evaluation of multidimensional chromatography coupled with tandem mass spectrometry (LC/LC-MS/MS) for large-scale protein analysis: the yeast proteome. J. Proteome Res. *2*, 43–50.

Peric-Hupkes, D., Meuleman, W., Pagie, L., Bruggeman, S.W.M., Solovei, I., Brugman, W., Gräf, S., Flicek, P., Kerkhoven, R.M., van Lohuizen, M., et al. (2010). Molecular maps of the reorganization of genome-nuclear lamina interactions during differentiation. Mol. Cell *38*, 603–613.

Pezzilli, R., Partelli, S., Cannizzaro, R., Pagano, N., Crippa, S.,

Pagnanelli, M., and Falconi, M. (2016). Ki-67 prognostic and therapeutic decision driven marker for pancreatic neuroendocrine neoplasms (PNENs): A systematic review. Adv. Med. Sci. *61*, 147–153.

Pickersgill, H., Kalverda, B., de Wit, E., Talhout, W., Fornerod, M., and van Steensel, B. (2006). Characterization of the Drosophila melanogaster genome at the nuclear lamina. Nat. Genet. *38*, 1005–1014.

Plath, K., Fang, J., Mlynarczyk-Evans, S.K., Cao, R., Worringer, K. a, Wang, H., de la Cruz, C.C., Otte, A.P., Panning, B., and Zhang, Y. (2003). Role of histone H3 lysine 27 methylation in X inactivation. Science *300*, 131–135.

Plath, K., Talbot, D., Hamer, K.M., Otte, A.P., Yang, T.P., Jaenisch, R., and Panning, B. (2004). Developmentally regulated alterations in polycomb repressive complex 1 proteins on the inactive X chromosome. J. Cell Biol. *167*, 1025–1035.

Pluta, A.F., and Earnshaw, W.C. (1996). Specific interaction between human kinetochore protein CENP-C and a nucleolar transcriptional regulator. J. Biol. Chem. *271*, 18767–18774.

Politz, J.C., Yarovoi, S., Kilroy, S.M., Gowda, K., Zwieb, C., and Pederson, T. (2000). Signal recognition particle components in the nucleolus. Proc. Natl. Acad. Sci. *97*, 55–60.

Politz, J.C.R., Scalzo, D., and Groudine, M. (2016). The redundancy of the mammalian heterochromatic compartment. Curr. Opin. Genet. Dev. *37*, 1–8.

Pollock, C., and Huang, S. (2010). The perinucleolar compartment. J. Cell. Biochem. *107*, 189–193.

Polo, S.E., Theocharis, S.E., Klijanienko, J., Savignoni, A., Asselain, B., Vielh, P., and Almouzni, G. (2004). Chromatin assembly factor-1, a marker of clinical value to distinguish quiescent from proliferating cells. Cancer Res. *64*, 2371–2381.

Polo, S.E., Roche, D., and Almouzni, G. (2006). New histone incorporation marks sites of UV repair in human cells. Cell *127*, 481–493.

Polo, S.E., Theocharis, S.E., Grandin, L., Gambotti, L., Antoni, G., Savignoni, A., Asselain, B., Patsouris, E., and Almouzni, G. (2010). Clinical significance and prognostic value of chromatin assembly factor-1 overexpression in human solid tumours. Histopathology *57*, 716–724.

Pontvianne, F., Blevins, T., Chandrasekhara, C., Mozgová, I., Hassel, C., Pontes, O.M.F., Tucker, S., Mokroš, P., Muchová, V., Fajkus, J., et al. (2013). Subnuclear partitioning of rRNA genes between the nucleolus and nucleoplasm reflects alternative epiallelic states. Genes Dev. *27*, 1545–1550.

Pontvianne, F., Carpentier, M.-C., Durut, N., Pavlištová, V., Jaške, K., Schořová, Š., Parrinello, H., Rohmer, M., Pikaard, C.S., Fojtová, M., et al. (2016). Identification of nucleolus-associated chromatin domains reveals a role for thenucleolus in 3D organization of the A. thaliana genome. Cell Rep. *16*, 1574–1587.

Pourcel, C., Salvignol, G., and Vergnaud, G. (2005). CRISPR elements in Yersinia pestis acquire new repeats by preferential uptake of bacteriophage

DNA, and provide additional tools for evolutionary studies. Microbiology *151*, 653–663.

Pyo, J.-S., Kang, G., and Sohn, J.H. (2016). Ki-67 labeling index can be used as a prognostic marker in gastrointestinal stromal tumor: a systematic review and meta-analysis. Int. J. Biol. Markers *31*, e204-10.

Pyzocha, N.K., Ran, F.A., Hsu, P.D., and Zhang, F. (2014). RNA-guided genome editing of mammalian cells. Methods Mol. Biol. *1114*, 269–277.

Quivy, J.-P., Roche, D., Kirschner, D., Tagami, H., Nakatani, Y., and Almouzni, G. (2004). A CAF-1 dependent pool of HP1 during heterochromatin duplication. EMBO J. *23*, 3516–3526.

Quivy, J.-P., Gérard, A., Cook, A.J.L., Roche, D., and Almouzni, G. (2008). The HP1-p150/CAF-1 interaction is required for pericentric heterochromatin replication and S-phase progression in mouse cells. Nat. Struct. Mol. Biol. *15*, 972–979.

Quivy, J.P., Grandi, P., and Almouzni, G. (2001). Dimerization of the largest subunit of chromatin assembly factor 1: importance in vitro and during Xenopus early development. EMBO J. *20*, 2015–2027.

Ragoczy, T., Telling, A., Scalzo, D., Kooperberg, C., and Groudine, M. (2015). Functional redundancy in the nuclear compartmentalization of the late-replicating genome. Nucleus *5*, 626–635.

Rahmanzadeh, R., Hüttmann, G., Gerdes, J., and Scholzen, T. (2007). Chromophore-assisted light inactivation of pKi-67 leads to inhibition of ribosomal RNA synthesis. Cell Prolif. *40*, 422–430.

Ransom, M., Dennehey, B.K., and Tyler, J.K. (2010). Chaperoning histones during DNA replication and repair. Cell *140*, 183–195.

Reddy, K.L., Zullo, J.M., Bertolino, E., and Singh, H. (2008). Transcriptional repression mediated by repositioning of genes to the nuclear lamina. Nature *452*, 243–247.

Reese, B.E., Bachman, K.E., Baylin, S.B., and Rountree, M.R. (2003). The methyl-CpG binding protein MBD1 interacts with the p150 subunit of chromatin assembly factor 1. Mol. Cell. Biol. *23*, 3226–3236.

Reichow, S.L., Hamma, T., Ferré-D'Amaré, A.R., and Varani, G. (2007). The structure and function of small nucleolar ribonucleoproteins. Nucleic Acids Res. *35*, 1452–1464.

Richards-Taylor, S., Ewings, S.M., Jaynes, E., Tilley, C., Ellis, S.G., Armstrong, T., Pearce, N., and Cave, J. (2016). The assessment of Ki-67 as a prognostic marker in neuroendocrine tumours: a systematic review and meta-analysis. J. Clin. Pathol. *69*, 612–618.

Rickards, B., Flint, S.J., Cole, M.D., and LeRoy, G. (2007). Nucleolin is required for RNA polymerase I transcription in vivo. Mol. Cell. Biol. *27*, 937–948.

Roelens, B., Clémot, M., Leroux-Coyau, M., Klapholz, B., and Dostatni, N. (2016). Maintenance of Heterochromatin by the Large Subunit of the Replication-Coupled Histone Chaperone CAF-1 Requires Its Interaction with HP1a Through a Conserved Motif. Genetics.

Roger, B., Moisand, A., Amalric, F., and Bouvet, P. (2002). Repression of RNA polymerase I transcription by nucleolin is independent of the RNA sequence that is transcribed. J. Biol. Chem. *277*, 10209–10219.

Rogers, S., Wells, R., and Rechsteiner, M. (1986). Amino acid sequences common to rapidly degraded proteins: the PEST hypothesis. Science *234*, 364–368.

Rolef Ben-Shahar, T., Castillo, A.G., Osborne, M.J., Borden, K.L.B., Kornblatt, J., and Verreault, A. (2009). Two fundamentally distinct PCNA interaction peptides contribute to chromatin assembly factor 1 function. Mol. Cell. Biol. *29*, 6353–6365.

Sáez-Vasquez, J., Caparros-Ruiz, D., Barneche, F., and Echeverría, M. (2004). A plant snoRNP complex containing snoRNAs, fibrillarin, and nucleolin-like proteins is competent for both rRNA gene binding and pre-rRNA processing in vitro. Mol. Cell. Biol. *24*, 7284–7297.

Saiwaki, T., Kotera, I., Sasaki, M., Takagi, M., and Yoneda, Y. (2005). In vivo dynamics and kinetics of pKi-67: transition from a mobile to an immobile form at the onset of anaphase. Exp. Cell Res. *308*, 123–134.

Sanyal, A., Lajoie, B.R., Jain, G., and Dekker, J. (2012). The long-range interaction landscape of gene promoters. Nature *489*, 109–113.

Sarraf, S. a, and Stancheva, I. (2004). Methyl-CpG binding protein MBD1 couples histone H3 methylation at lysine 9 by SETDB1 to DNA replication and chromatin assembly. Mol. Cell *15*, 595–605.

Savkur, R.S., and Olson, M.O.J. (1998). Preferential cleavage in pre-ribosomal RNA by protein B23 endoribonuclease. Nucleic Acids Res. *26*, 4508–4515.

Schluter, C., Duchrow, M., Wohlenberg, C., Becker, M.H.G., Key, G., Flad -, H.D., and Gerdes, J. (1993). The cell proliferation-associated antigen of antibody Ki-67: A very large, ubiquitous nuclear protein with numerous repeated elements, representing a new kind of cell cycle-maintaining proteins. J. Cell Biol. *123*, 513–522.

Shaner, N.C., Campbell, R.E., Steinbach, P.A., Giepmans, B.N.G., Palmer, A.E., and Tsien, R.Y. (2004). Improved monomeric red, orange and yellow fluorescent proteins derived from Discosoma sp. red fluorescent protein. Nat. Biotechnol. *22*, 1567–1572.

Sharp, J.A., Fouts, E.T., Krawitz, D.C., and Kaufman, P.D. (2001). Yeast histone deposition protein Asf1p requires Hir proteins and PCNA for heterochromatic silencing. Curr. Biol. *11*, 463–473.

Shen, Y., Yue, F., McCleary, D.F., Ye, Z., Edsall, L., Kuan, S., Wagner, U., Dixon, J., Lee, L., Lobanenkov, V. V., et al. (2012). A map of the cis-regulatory sequences in the mouse genome. Nature *488*, 116–120.

Sheval, E. V, and Polyakov, V.Y. (2008). The peripheral chromosome scaffold, a novel structural component of mitotic chromosomes. Cell Biol. Int. *32*, 708–712.

Shibahara, K., and Stillman, B. (1999). Replication-dependent marking of

DNA by PCNA facilitates CAF-1-coupled inheritance of chromatin. Cell *96*, 575–585.

Singh, V., Braddick, D., and Dhar, P.K. (2017). Exploring the potential of genome editing CRISPR-Cas9 technology. Gene *599*, 1–18.

Sirri, V., Urcuqui-Inchima, S., Roussel, P., and Hernandez-Verdun, D. (2008). Nucleolus: the fascinating nuclear body. Histochem. Cell Biol. *129*, 13–31.

Smith, S., and Stillman, B. (1989a). Purification and characterization of CAF-I, a human cell factor required for chromatin assembly during DNA replication in vitro. Cell *58*, 15–25.

Smith, S., and Stillman, B. (1989b). Purification and characterization of CAF-I, a human cell factor required for chromatin assembly during DNA replication in vitro. Cell *58*, 15–25.

Smith, S., and Stillman, B. (1991). Immunological characterization of chromatin assembly factor I, a human cell factor required for chromatin assembly during DNA replication in vitro. J. Biol. Chem. *266*, 12041–12047.

Smith, C.L., Matheson, T.D., Trombly, D.J., Sun, X., Campeau, E., Han, X., Yates, J.R., and Kaufman, P.D. (2014a). A separable domain of the p150 subunit of human chromatin assembly factor-1 promotes protein and chromosome associations with nucleoli. Mol. Biol. Cell *25*, 2866–2881.

Smith, C.L., Matheson, T.D., Trombly, D.J., Sun, X., Campeau, E., Han, X., Yates, J.R., and Kaufman, P.D. (2014b). A separable domain of the p150 subunit of human chromatin assembly factor-1 promotes protein and chromosome associations with nucleoli. Mol. Biol. Cell *25*, 2866–2881.

Sobecki, M., Mrouj, K., Camasses, A., Parisis, N., Nicolas, E., Llères, D., Gerbe, F., Prieto, S., Krasinska, L., David, A., et al. (2016). The cell proliferation antigen Ki-67 organises heterochromatin. Elife *5*, e13722.

Song, J.J., Garlick, J.D., and Kingston, R.E. (2008). Structural basis of histone H4 recognition by p55. Genes Dev. *22*, 1313–1318.

Song, L., Zhang, Z., Grasfeder, L.L., Boyle, A.P., Giresi, P.G., Lee, B.K., Sheffield, N.C., Gräf, S., Huss, M., Keefe, D., et al. (2011). Open chromatin defined by DNaseI and FAIRE identifies regulatory elements that shape cell-type identity. Genome Res. *21*, 1757–1767.

Song, Y., He, F., Xie, G., Guo, X., Xu, Y., Chen, Y., Liang, X., Stagljar, I., Egli, D., Ma, J., et al. (2007). CAF-1 is essential for Drosophila development and involved in the maintenance of epigenetic memory. Dev. Biol. *311*, 213–222.

Sonntag, F., Schmidt, K., and Kleinschmidt, J.A. (2010). A viral assembly factor promotes AAV2 capsid formation in the nucleolus. Proc. Natl. Acad. Sci. U. S. A. *107*, 10220–10225.

Spector, D.L., Ochs, R.L., and Busch, H. (1984). Silver staining, immunofluorescence, and immunoelectron microscopic localization of nucleolar phosphoproteins B23 and C23. Chromosoma *90*, 139–148.

Staibano, S., and Mascolo, M. (2011). The proliferation marker Chromatin Assembly Factor-1 is of clinical value in predicting the biological behaviour of

salivary gland tumours. Oncol. … 13–22.

Staibano, S., Mignogna, C., Lo Muzio, L., Mascolo, M., Salvatore, G., Di Benedetto, M., Califano, L., Rubini, C., and De Rosa, G. (2007). Chromatin assembly factor-1 (CAF-1)-mediated regulation of cell proliferation and DNA repair: A link with the biological behaviour of squamous cell carcinoma of the tongue? Histopathology *50*, 911–919.

Staibano, S., Mascolo, M., Mancini, F.P., Kisslinger, A., Salvatore, G., Di Benedetto, M., Chieffi, P., Altieri, V., Prezioso, D., Ilardi, G., et al. (2009). Overexpression of chromatin assembly factor-1 (CAF-1) p60 is predictive of adverse behaviour of prostatic cancer. Histopathology *54*, 580–589.

van Steensel, B., and Henikoff, S. (2000). Identification of in vivo DNA targets of chromatin proteins using tethered dam methyltransferase. Nat. Biotechnol. *18*, 424–428.

Steffensen, D.M., Duffey, P., and Prensky, W. (1974). Localisation of 5S ribosomal RNA genes on human chromosome 1. Nature *252*, 741–743.

Stillman, B. (1986). Chromatin assembly during SV40 DNA replication in vitro. Cell *45*, 555–565.

Stults, D.M., Killen, M.W., Pierce, H.H., and Pierce, A.J. (2008). Genomic architecture and inheritance of human ribosomal RNA gene clusters. Genome Res. *18*, 13–18.

Sun, H., and Hunter, T. (2012). Poly-small ubiquitin-like modifier (PolySUMO)-binding proteins identified through a string search. J. Biol. Chem. *287*, 42071–42083.

Sun, H., Leverson, J.D., and Hunter, T. (2007). Conserved function of RNF4 family proteins in eukaryotes: targeting a ubiquitin ligase to SUMOylated proteins. EMBO J. *26*, 4102–4112.

Surendranath, V., Theis, M., Habermann, B.H., and Buchholz, F. (2013). Designing efficient and specific endoribonuclease-prepared siRNAs. Methods Mol. Biol. *942*, 193–204.

Tabb, D.L., McDonald, W.H., and Yates, J.R. (2002). DTASelect and Contrast: tools for assembling and comparing protein identifications from shotgun proteomics. J. Proteome Res. *1*, 21–26.

Tagami, H., Ray-Gallet, D., Almouzni, G., and Nakatani, Y. (2004). Histone H3.1 and H3.3 complexes mediate nucleosome assembly pathways dependent or independent of DNA synthesis. Cell *116*, 51–61.

Takagi, M., Matsuoka, Y., Kurihara, T., and Yoneda, Y. (1999). Chmadrin: a novel Ki-67 antigen-related perichromosomal protein possibly implicated in higher order chromatin structure. J. Cell Sci. *112 (1)*, 2463–2472.

Takagi, M., Sueishi, M., Saiwaki, T., Kametaka, A., and Yoneda, Y. (2001). A novel nucleolar protein, NIFK, interacts with the forkhead associated domain of Ki-67 antigen in mitosis. J. Biol. Chem. *276*, 25386–25391.

Takagi, M., Nishiyama, Y., Taguchi, A., and Imamoto, N. (2014a). Ki67 antigen contributes to the timely accumulation of protein phosphatase 1γ on anaphase chromosomes. J. Biol. Chem. *289*, 22877–22887.

Takagi, M., Nishiyama, Y., Taguchi, A., and Imamoto, N. (2014b). Ki67 antigen contributes to the timely accumulation of protein phosphatase 1γ on anaphase chromosomes. J. Biol. Chem. *289*, 22877–22887.

Takagi, M., Natsume, T., Kanemaki, M.T., and Imamoto, N. (2016). Perichromosomal protein Ki67 supports mitotic chromosome architecture. Genes to Cells 1–12.

Takami, Y., Ono, T., Fukagawa, T., Shibahara, K., and Nakayama, T. (2007). Essential role of chromatin assembly factor-1-mediated rapid nucleosome assembly for DNA replication and cell division in vertebrate cells. Mol. Biol. Cell *18*, 129–141.

Tang, Y., Poustovoitov, M. V, Zhao, K., Garfinkel, M., Canutescu, A., Dunbrack, R., Adams, P.D., and Marmorstein, R. (2006). Structure of a human ASF1a-HIRA complex and insights into specificity of histone chaperone complex assembly. Nat. Struct. Mol. Biol. *13*, 921–929.

Tessarz, P., Santos-Rosa, H., Robson, S.C., Sylvestersen, K.B., Nelson, C.J., Nielsen, M.L., and Kouzarides, T. (2014). Glutamine methylation in histone H2A is an RNA-polymerase-I-dedicated modification. Nature *505*, 564–568.

Thakur, N., Tiwari, V.K., Thomassin, H., Pandey, R.R., Kanduri, M., Göndör, A., Grange, T., Ohlsson, R., and Kanduri, C. (2004). An antisense RNA regulates the bidirectional silencing property of the Kcnq1 imprinting control region. Mol. Cell. Biol. *24*, 7855–7862.

Thompson, M., Haeusler, R.A., Good, P.D., and Engelke, D.R. (2003). Nucleolar clustering of dispersed tRNA genes. Science *302*, 1399–1401.

Thorvaldsen, J.L., Verona, R.I., and Bartolomei, M.S. (2006). X-tra! X-tra! News from the Mouse X Chromosome. Dev. Biol. *298*, 344–353.

Timchenko, L.T., Miller, J.W., Timchenko, N. a., Devore, D.R., Datar, K. V., Lin, L., Roberts, R., Thomas Caskey, C., and Swanson, M.S. (1996). Identification of a (CUG)(n) triplet repeat RNA-binding protein and its expression in myotonic dystrophy. Nucleic Acids Res. *24*, 4407–4414.

Traut, W., Endl, E., Scholzen, T., Gerdes, J., and Winking, H. (2002). The temporal and spatial distribution of the proliferation associated Ki-67 protein during female and male meiosis. Chromosoma *111*, 156–164.

Tyler, J.K., Collins, K.A., Prasad-Sinha, J., Amiott, E., Bulger, M., Harte, P.J., Kobayashi, R., and Kadonaga, J.T. (2001). Interaction between the Drosophila CAF-1 and ASF1 chromatin assembly factors. Mol. Cell. Biol. *21*, 6574–6584.

Uchimura, Y., Ichimura, T., Uwada, J., Tachibana, T., Sugahara, S., Nakao, M., and Saitoh, H. (2006). Involvement of SUMO modification in MBD1- and MCAF1-mediated heterochromatin formation. J. Biol. Chem. *281*, 23180–23190.

Ugrinova, I., Monier, K., Ivaldi, C., Thiry, M., Storck, S., Mongelard, F., and Bouvet, P. (2007). Inactivation of nucleolin leads to nucleolar disruption, cell cycle arrest and defects in centrosome duplication. BMC Mol. Biol. *8*, 66.

Uwada, J., Tanaka, N., Yamaguchi, Y., Uchimura, Y., Shibahara, K.,

Nakao, M., and Saitoh, H. (2010). The p150 subunit of CAF-1 causes association of SUMO2/3 with the DNA replication foci. Biochem. Biophys. Res. Commun. *391*, 407–413.

Uzunova, K., G??ttsche, K., Miteva, M., Weisshaar, S.R., Glanemann, C., Schnellhardt, M., Niessen, M., Scheel, H., Hofmann, K., Johnson, E.S., et al. (2007). Ubiquitin-dependent proteolytic control of SUMO conjugates. J. Biol. Chem. *282*, 34167–34175.

Valentin, G. (1836). Repertorium fur Anatomie und Physiologie. Verlag von Veit Und Comp. Berlin. *1*, 1–293.

Valentin, G. (1839). Repertorium fur Anatomie und Physiologie. Verlag von Veit Und Comp. Berlin. *4*, 1–275.

Verheijen, R., Kuijpers, H.J., Schlingemann, R.O., Boehmer, A.L., van Driel, R., Brakenhoff, G.J., and Ramaekers, F.C. (1989a). Ki-67 detects a nuclear matrix-associated proliferation-related antigen. I. Intracellular localization during interphase. J. Cell Sci. *92 (Pt 1)*, 123–130.

Verheijen, R., Kuijpers, H.J., van Driel, R., Beck, J.L., van Dierendonck, J.H., Brakenhoff, G.J., and Ramaekers, F.C. (1989b). Ki-67 detects a nuclear matrix-associated proliferation-related antigen. II. Localization in mitotic cells and association with chromosomes. J. Cell Sci. *92 (4)*, 531–540.

Verreault, a, Kaufman, P.D., Kobayashi, R., and Stillman, B. (1996). Nucleosome assembly by a complex of CAF-1 and acetylated histones H3/H4. Cell *87*, 95–104.

Volders, P.J., Helsens, K., Wang, X., Menten, B., Martens, L., Gevaert, K., Vandesompele, J., and Mestdagh, P. (2013). LNCipedia: A database for annotated human lncRNA transcript sequences and structures. Nucleic Acids Res. *41*, 246–251.

Volk, A., and Crispino, J.D. (2015). The role of the chromatin assembly complex (CAF-1) and its p60 subunit (CHAF1b) in homeostasis and disease. Biochim. Biophys. Acta *1849*, 979–986.

Wagner, R. (1835). Einige Bemerkungen und Fragen uber das Keimblaschen (vesicular germinativa). Muller's Arch. Anat Physiol Wiss. Med 373–377.

Wang, C., Politz, J.C., Pederson, T., and Huang, S. (2003). RNA polymerase III transcripts and the PTB protein are essential for the integrity of the perinucleolar compartment. Mol. Biol. Cell *14*, 2425–2435.

Warburton, P.E., Greig, G.M., Haaf, T., and Willard, H.F. (1991). PCR amplification of chromosome-specific alpha satellite DNA: definition of centromeric STS markers and polymorphic analysis. Genomics *11*, 324–333.

Weber, J.D., Taylor, L.J., Roussel, M.F., Sherr, C.J., and Bar-Sagi, D. (1999). Nucleolar Arf sequesters Mdm2 and activates p53. Nat. Cell Biol. *1*, 20–26.

Weierich, C., Brero, A., Stein, S., Von Hase, J., Cremer, C., Cremer, T., and Solovei, I. (2003). Three-dimensional arrangements of centromeres and telomeres in nuclei of human and murine lymphocytes. Chromosom. Res. *11*,

485–502.

Westman, B.J., Verheggen, C., Hutten, S., Lam, Y.W., Bertrand, E., and Lamond, A.I. (2010). A proteomic screen for nucleolar SUMO targets shows SUMOylation modulates the function of Nop5/Nop58. Mol. Cell *39*, 618–631.

Whitfield, M.L., Sherlock, G., Saldanha, A.J., Murray, J.I., Ball, C.A., Alexander, K.E., Matese, J.C., Perou, C.M., Hurt, M.M., Brown, P.O., et al. (2002). Identification of genes periodically expressed in the human cell cycle and their expression in tumors. Mol. Biol. Cell *13*, 1977–2000.

Wong, L.H., Brettingham-Moore, K.H., Chan, L., Quach, J.M., Anderson, M.A., Northrop, E.L., Hannan, R., Saffery, R., Shaw, M.L., Williams, E., et al. (2007). Centromere RNA is a key component for the assembly of nucleoproteins at the nucleolus and centromere. Genome Res. *17*, 1146–1160.

Wu, R.S., Tsai, S., and Bonner, W.M. (1982). Patterns of histone variant synthesis can distinguish G0 from G1 cells. Cell *31*, 367–374.

Xu, H., Xiao, T., Chen, C.H., Li, W., Meyer, C.A., Wu, Q., Wu, D., Cong, L., Zhang, F., Liu, J.S., et al. (2015). Sequence determinants of improved CRISPR sgRNA design. Genome Res. *25*, 1147–1157.

Yang, F., Babak, T., Shendure, J., and Disteche, C.M. (2010). Global survey of escape from X inactivation by RNA-sequencing in mouse. Genome Res. *20*, 614–622.

Yang, F., Deng, X., Ma, W., Berletch, J.B., Rabaia, N., Wei, G., Moore, J.M., Filippova, G.N., Xu, J., Liu, Y., et al. (2015). The lncRNA Firre anchors the inactive X chromosome to the nucleolus by binding CTCF and maintains H3K27me3 methylation. Genome Biol. *16*.

Ye, X., Franco, A. a, Santos, H., Nelson, D.M., Kaufman, P.D., and Adams, P.D. (2003). Defective S phase chromatin assembly causes DNA damage, activation of the S phase checkpoint, and S phase arrest. Mol. Cell *11*, 341–351.

Yerushalmi, R., Woods, R., Ravdin, P.M., Hayes, M.M., and Gelmon, K.A. (2010). Ki67 in breast cancer: prognostic and predictive potential. Lancet Oncol. *11*, 174–183.

Yu, Y., Maggi, L.B., Brady, S.N., Apicelli, A.J., Dai, M., Lu, H., and Weber, J.D. (2006). Nucleophosmin is essential for ribosomal protein L5 nuclear export. Mol. Cell. Biol. *26*, 3798–3809.

Yu, Z., Wu, H., Chen, H., Wang, R., Liang, X., Liu, J., Li, C., Deng, W.-M., Jiao, R., Acar, M., et al. (2013). CAF-1 promotes Notch signaling through epigenetic control of target gene expression during Drosophila development. Development *140*, 3635–3644.

Yu, Z., Liu, J., Deng, W.M., and Jiao, R. (2015). Histone chaperone CAF-1: Essential roles in multi-cellular organism development. Cell. Mol. Life Sci. *72*, 327–337.

Yusufzai, T.M., Tagami, H., Nakatani, Y., and Felsenfeld, G. (2004). CTCF tethers an insulator to subnuclear sites, suggesting shared insulator mechanisms across species. Mol. Cell *13*, 291–298.

Zhang, L.-F., Huynh, K.D., and Lee, J.T. (2007). Perinucleolar targeting of the inactive X during S phase: evidence for a role in the maintenance of silencing. Cell *129*, 693–706.

Zhang, Y., Ng, H.H., Erdjument-Bromage, H., Tempst, P., Bird, A., and Reinberg, D. (1999). Analysis of the NuRD subunits reveals a histone deacetylase core complex and a connection with DNA methylation. Genes Dev. *13*, 1924–1935.

Zhang, Y., McCord, R.P., Ho, Y.J., Lajoie, B.R., Hildebrand, D.G., Simon, A.C., Becker, M.S., Alt, F.W., and Dekker, J. (2012). Spatial organization of the mouse genome and its role in recurrent chromosomal translocations. Cell *148*, 908–921.